THE UNIVERSITY
of EDINBURGH

Investigation of Juxtaglomerular Structure and Function

Charlotte Buckley

Centre for Cardiovascular Biology

University of Edinburgh

A thesis submitted for the degree of

PhD

April 2015

Abstract

Renin is the initiator and rate-limiting factor of the renin-angiotensin system, a major mechanism of blood pressure regulation. The synthesis and secretion of this active circulatory enzyme is confined exclusively to the dense core granules of kidney juxtaglomerular (JG) cells where its precursor prorenin is packaged, cleaved to the active form and stored for release on a regulated pathway. Given its importance, surprisingly little is known about this process, in part due to the difficulty in culturing primary JG cells in vitro and the lack of reliable cell lines.

The initial aim of the current work was to investigate renin-containing granule dynamics in live JG cells. To achieve this, I attempted to derive novel cell lines from triple transgenic mouse models comprising immortalised granulated or non-granulated JG cells. Due to the nature of JG cells in culture, the use of these cell lines to investigate granulation was not feasible; therefore the culture of primary JG cell culture was modified and enhanced to visualise granule dynamics in live, primary JG cells for the first time. By isolating cells using a Percoll gradient and plating them on fibronectin-coated dishes, rapid and full adhesion of JG cells was achieved, as well as prolonged expression of renin from 3 days to up to 8 days post-isolation. Using this protocol to isolate JG cells from RenGFP renin reporter mice and

identifying granules using the acidotropic fluorophore Lysotracker, granule dynamics were investigated in primary JG cells. High resolution, rapid image acquisition was performed using widefield and total internal reflection microscopy, showing that dense core granules respond dynamically to the β-adrenergic agonist isoproterenol, a known renin secretory stimulus. Two different pools of granules of varying granule diameters and dynamic parameters were identified optically, suggesting that separate granule pools were being identified.

Mice null for the Ren-1d gene lack renin storage granules in their JG cells, however granulation was restored in Ren1d-null mice carrying a transgene encompassing the human renin (hRen) locus. Therefore in order to investigate the relationship between renin expression and the amount of granulation in JG cells, mice expressing human renin were used. To dissect the granulation phenotype in detail, 2D electron micrographs were taken of JG cells, which were immunogold stained to confirm renin content, and reconstructed in 3D. Female hRen mice showed a significantly higher volume of granulation and an increased granule number compared to males, a finding consistent with the sexually dimorphic expression of the transgene, supporting the hypothesis that granulation in JG cells is dependent on the level of renin expression.

The macula densa (MD) is a critical sensor of flow and salt content in the blood; through extensive tubulo-vascular crosstalk known as tubuloglomerular feedback (TGF), it releases key signalling factors stimulating and inhibit-

ing renin synthesis and secretion from JG cells. Ren-1d$^{-/-}$ mice showed a hypercellular and columnar MD plaque, which was not restored by the introduction of the hRen transgene, indicating that TGF may be impaired in these mice. Using an isolated, perfused juxtaglomerular apparatus model it was shown that high salt- and increased flow-induced TGF functioned effectively in Ren1d$^{-/-}$ and huRen$^{+/-}$Ren1d$^{-/-}$ mice, although animals on a Ren1d$^{-/-}$ background showed decreased sensitivity of glomerular tuft contraction and abnormal calcium signalling within macula densa cells.

In conclusion, an appropriate *in vitro* model was developed for investigating granule dynamics in JG cells, using which granule motion was visualised and quantified for the first time in these cells. Although JG cell granulation is required for normal MD morphology, it was shown to not affect JGA function.

Acknowledgements

I feel slightly intimiated about acknowledging the huge number of people who have helped, supported and made me laugh and smile throughout this PhD.

First and foremost, I must thank my fantastic supervisor, John for all his invaluable help and support. You have given me so, so many fantastic opportunities throughout my PhD, and I can't thank you enough. Linda and Matt also deserve a massive amount of thanks for always being there to help me talk through areas which were troubling me! I must also mention the rest of my PhD advisory committee, Chris and Margarete: without your advice, input and ideas I would not have been able to perform many of the experiments, so thank you. I can not thank Audrey the TC goddess enough for all the help she has given me over the years, in TC, the lab and in life! Thank you to all the fantastic BRR staff (particularly Mike, Sandra, Lorraine and Lee), everyone in flow cytometry (Shona, Fiona and Will), Dawn for her PCR help, Chris and Melanie for your help with embryonic kidney culture, Ania and James for all your help with FACS and TC, and Chris for always being willing to help me with some data analysis, whilst eating a magnificant culinary creation. Ali and Rory, thank you for being so wonderful and suppotive and welcoming me into the lab group at Heriot Watt! I need to specially thank Janos, who was so incredibly kind and welcoming, and who did so much work to help me with this project, and

to everyone who helped me in his lab: Anne, Anush, Jim, Ina, Lisa and Matthias - you are all amazing and I am so lucky to have had the oppotunity to meet you and explore LA with you, we had such a fantastic time. I also need to specially thank Helen Christian for all her work on the electron microscopy and invaluable advice and kindness. Similarly, Armin Kurtz for welcoming me into his lab, to Dominik for his patience in teaching me to do the 3D reconstructions and to Anita for all her work sectioning and imaging samples. Thank you!

To all my friends who have lived the highs and lows with me, you all mean the world to me. Dobs, thank you for being such a truly wonderful person and constantly helping me believe in myself. Todd, thank you for always believing in me and supporting me. And all my wonderful friends from Chad's: Welly, Gorsk, Tim, Lorn, Roo, Kate, Han, Livs, and to the wonderful Papa Joe who will be greatly missed. Rach, thank you for all the bubbles, the bary wraps, the work sessions, the dobble and the chilled times. Kirsten, Barry and Cora: thank you for all the gigs, PVB funtimes, dancing ourselves clean, the runs, there are too many times to count, we've had such a wonderful 4 years. Barry and Catherine, thanks for all the cake and pep talks during the write up, and for sharing the pain! To the Q.M.R.I. girls - Rach, Catherine, JBlo, Iris, Nicole and Yolanda for all our random adventures, holidays, tea catch-ups and wonderful evenings. Nash and Michael - you crazy, wonderful people, thank you for all the fun and cocktails, nights out and nights in! Jivy - your squash, catchats, lifechats, workchats and general wonderfulness was amazing, and Rob for office hilarity and being so easily

persuaded to indulge my tea-making habits. Thanks to Sofia and Adrienne for all the wonderful evenings of culinary adventures, and to Phoebs and Hel and all the wonderful Peter's girlies who have helped me so much and always been there for me.

Finally, I want to thank my incredible family, who have always been there for me and whom I love very much - especially to my grandparents Pat, David, Val and Michael; my brother, Henry and sister Lizzie. Dad, thanks for the printing :) Mum and Dad - thank you so much for always believing in me, for constantly supporting me and for making so many sacrifices to ensure that we all got the best education that we could. It means so much to me, and I can't thank you enough.

Contents

List of Figures

List of Tables

Glossary

Adcy: Adenylyl cyclase

Adrb: Adrenoreceptor B

α-SMA: Alpha smooth muscle actin

AA: Afferent arteriole

ACE: Angiotensin-converting enzyme

AFU: Arbitrary Fluorescence Units

AGT: Angiotensinogen

AGTR2: Angiotensin II receptor type 2

ANGI: Angiotensin I

ANGII: Angiotensin II

ANP: Atiral natriuretic peptide

AR: Adenosine receptor

ARB: Adrenoreceptor blocker

ATP: Adenosine triphosphate

β-Geo: Beta galactosidase

BAC: Bacterial artificial chromosome

BP: Blood pressure

CALM: Calmodulin

cAMP: Cyclic adenosine monophosphate

CCSI: Collected total cell signal intensity

cDNA: Complementary DNA

cGKII: cGMP-regulated protein kinase II

cGMP: Cyclic guanosine monophosphate

CLSM: Confocal light scanning microscopy

COX2: Cyclooxygenase 2

CRE(B): CAMP response element (binding protein)

CRIP1: Cysteine-rich protein 1

cTAL: Cortical thick ascending limb

Cx: Connexin

DAPI: 4',6-diamidino-2-phenylindole

dNTP: Deoxynucleotide

DMEM: Dulbecco's modified eagle medium

DMSO: Dimethyl sulfoxide

DNA: Deoxiribonucleic acid

DRD: Dopamine receptor

EA: Efferent arteriole

ECM: Extracellular matrix

EDTA: Ethylene diamine tetraacetic acid

EGTA: Ethylene glycol tetraacetic acid

EM: Electron microscopy

EMCCD: Electron-multiplying charge coupled device

FACS: Flow activated cell sorting

FCS: Fetal calf serum

FITC: Fluorescein isothiocyanate

FRET: Fluorescence resonant energy transfer

FSC: Forward scatter

GFP: Green fluorescent protein

GFR: Glomerular filtration rate

GNAI: Inhibitory G-protein coupled receptor

GNAS: G-protein coupled receptor

GTP: Guanosine triphosphate

HPRT: Hypoxanthine-guanine phosphoribosyltransferase

IBMX: 3-isobutyl-1-methylxanthine

IFN-γ: Interferon gamma

ITS: Insulin-transferrin-selenite

JG: Juxtaglomerular

JGA: Juxtaglomerular apparatus

LUT: Lookup table

LYST: Lysosomal trafficking regulator

MD: Macula densa

mRNA: Messanger RNA

NaCl: Sodium chloride

NG2: Neural glial antigen 2

NH_4Cl: Ammonium chloride

NKCC2: Sodium-potassium-chlorine cotransporter 2

NMDG: N-methyl-d-glucamine

NO: Nitric oxide

nNOS: Neuronal nitric oxide synthase

OCT: Optimal cutting temperature

PBS: Phosphate-buffered saline

PCR: Polymerase chain reaction

PDE: Phosphodiesterase

PDGFR-β: Platelet-derived growth factor-β receptor

PDL: Poly-D-lysine

Pen/strep: Penicillin/streptomycin

PGE2: Prostaglandin E2

qPCR: Quantitative polymerase chain reaction

PFA: Paraformaldehyde

PRC: Plasma renin concentration

PK-: Protein kinase

PTH: Parathyroid hormone

RAAS: Renin-angiotensin-aldosterone system

REN-: Renin

(R)ER: (Rough) endoplasmic reticulum

RNA: Ribonucleic acid

ROCK inhibitor: Rho Kinase inhibitor

ROI: Region of interest

RT: Reverse transcription

SCID: Severe combined immunodeficiency

SDS: Sodium dodecyl sulphate

S.E.M.: Standard error on the mean

siRNA: Small interfering RNA

SNAP: soluble *N*-ethylmaleimide-sensitive factor attachment protein

SNARE: SNAP receptor

SNR: Signal to noise ratio

SSC: Side scatter

SV40: Simian virus 40

TAE: Tris-acetate-EDTA

TBE: Tris-borate-EDTA

TE: Trypsin-EDTA

TERT: Telomere reverse transcriptase protein

TGF: Tubuloglomerular feedback

TGF-β: Transforming growth factor-β

TIRF(M): Total internal reflection fluorescence (microscopy)

TRITC: Tetramethylrhodamine

UPL: Universal probe library

UUO: Unilateral ureteric obstruction

VAMP: Vesicle associated membrane protein

VEGF: Vascular endothelial growth factor

VSMC: Vascular smooth muscle cell

1

Introduction

1.1 Overview

Control and regulation of blood pressure (BP) critically rests in the kidney, where coordinated physiological systems act to maintain homeostasis. One of the most important of these mechanisms is the renin-angiotensin-aldosterone system (RAAS). Renin, the rate-limiting enzyme in the RAAS, is synthesised within the juxtaglomerular (JG) cells of the kidney and is essential for the formation of circulating angiotensin II (AngII). Manipulation of this system through the systematic administration of renin inhibitors, angiotensin receptor blockers (ARB) and angiotensin converting enzyme inhibitors is routinely employed as part of the treatment for both cardiovascular and renal diseases (1). Although renin is clearly an important factor in both chronic kidney disease and cardiovascular disease, there remain a lot of fundamental unanswered questions regarding the generation and secretion of this enzyme. Determining the mechanisms and factors affecting the regulation of renin synthesis, maturation and secretion may contribute to future therapies.

1.2 The Action of Renin in Blood Pressure Regulation

The kidneys perform key filtration and reabsorption steps in the urinary system whilst maintaining BP and electrolyte homeostasis. The gross structure of the kidney comprises an outer cortex and an inner medulla, all enclosed within a fibrous capsule. Within the inner medulla lie the renal pyramids, sections of cone-shaped tissue containing nephrons which transport filtrate to the renal pelvis and on to the bladder. These are the functional units of the kidney, maintaining plasma osmolality via reabsorption of water and electrolytes. The structure of the nephron is shown in Figure 1.1a.

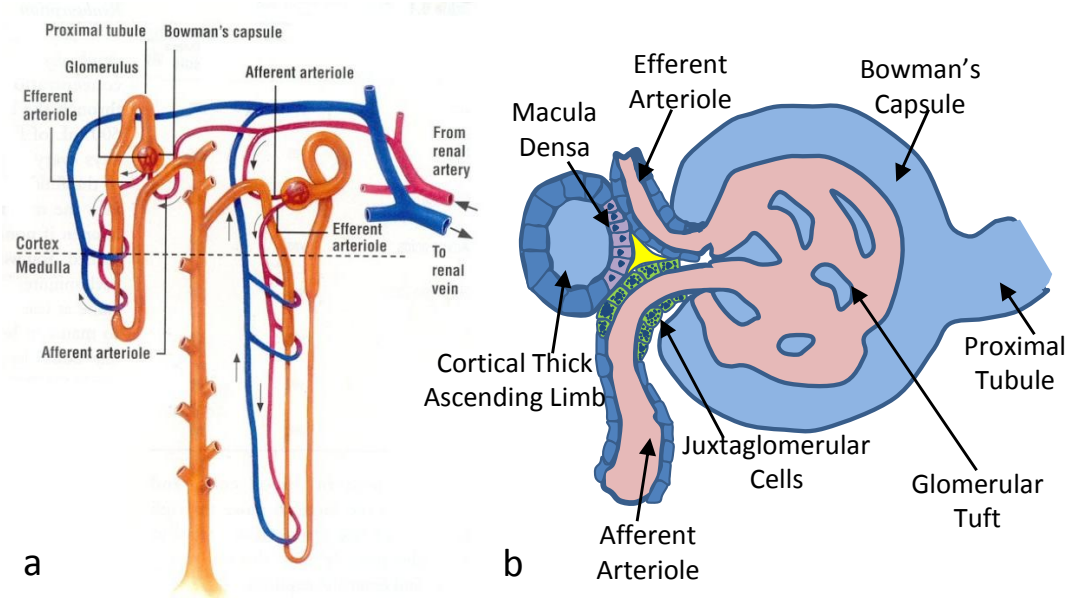

Figure 1.1: Schematic of nephron morphology. - (a) Nephrons comprise a tubule which originates from the closed glomerular capsule at the proximal end and terminates in the collecting tubule distally. The afferent arteriole carries blood to the glomerular tuft where a dense glomerular capillary network resides. It is across the capillary walls that exchange of oxygen and nutrients occur, regulating blood composition and moving the filtrate into the Bowman's capsule and on to the proximal tubule. Figure adapted from http://kidneyadvice.net/kidney%20disorders.html. (b) The juxtaglomerular apparatus. The macula densa cell plaque comprises part of the cortical thick ascending limb wall. Juxtaglomerular cells, localised to the distal end of the afferent arteriole, are separated from macula densa cells by mesangial cells (yellow).

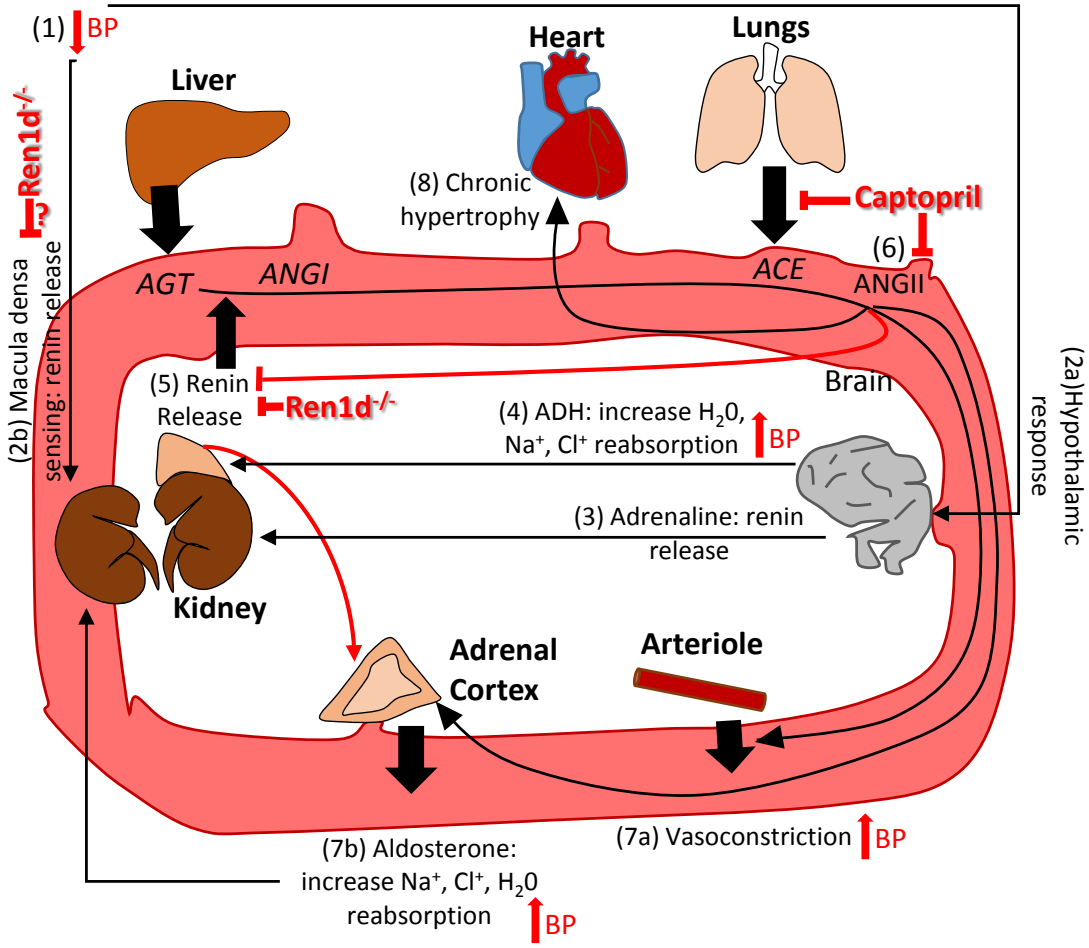

Figure 1.2: Schematic representation of the renin-angiotensin-aldosterone system. - (1) A drop in tubular salt or blood pressure is sensed within the thirst centre of the brain (2a), leading to antidiuretic hormone (ADH) secretion (4) which causes increased tubular water, sodium and chlorine reabsorption and an increase in blood pressure. (3) Adrenaline is also released, causing a release of renin from juxtaglomerular cells. This drop in blood pressure is also sensed within the kidney in the macula densa cells (2b), which signals to release renin (5) which cleaves angiotensinogen (AGT) (generated in the liver) to angiotensin I (ANGI). (6) Angiotensin converting enzyme (ACE) released from the lungs generates the vasoactive peptide angiotensin II (ANGII), which then alters vasoconstriction of blood vessels (7a) and increased tubular sodium and water reabsorption via aldosterone secretion from the adrenal cortex (7b), increasing blood pressure. Chronic ANGII generation also leads to hypertrophy, leading to hypertension. Captopril is an antihypertensive ACE inhibitor drug, and in Ren1d$^{-/-}$ mouse, the Ren-1d gene required for the generation of active renin is inactivated.

Alterations in systemic vascular resistance caused by modulation of blood vessel diameter are also vitally important to BP homeostasis (2). A drop in tubular salt or blood pressure is sensed within the thirst centre of the hypothalamus, leading to antidiuretic hormone (ADH)-mediated increases in tubular water, sodium and chlorine reabsorption. This acts to increase BP (Figure 1.2). A fall in blood pressure is also sensed by the kidney macula densa cells, which signal to cause renin release (discussed further in Chapter 1.3). The aspartyl protease renin cleaves the N-terminus of substrate angiotensinogen (AGT) generating the decapeptide ANGI, which is subsequently converted to the octapeptide ANGII by the action of angiotensin converting enzyme (ACE) (Figure 1.2) (3, 4). ANGll contributes to the control of physiological homeostasis both directly, through vasoconstriction of blood vessels, or indirectly via the release of aldosterone from the adrenal gland, which in turn regulates sodium and water retention and increases blood pressure and volume. However the rate of renin synthesis and secretion is one of the main determinants of RAAS-mediated BP stabilisation, therefore it is vitally important that it is tightly regulated (5).

The vasoactive ANGII also provides negative feedback within the RAAS, inhibiting further renin release through an increase in intracellular Ca^{2+} (discussed further in Section 1.8,(6, 7, 8)). A widely used experimental tool for manipulating renin expression and secretion levels is the chronic administration of ACE inhibitors to decrease this ANGII generation, interrupting the inhibition of renin release and stimulating renin expression along the kidney afferent arterioles (AA) ((9), Section 1.5). Renin expression is also increased indirectly by reducing ANGII levels via the accompanying decrease in vascular resistance and blood pressure, sympathetic activity and sodium retention. In the present study, the widely-used ACE inhibitor captopril was used (9, 10, 11, 12).

Renin is released either acutely via secretion of active renin from dense core granules, or chronically via secretion of both inactive prorenin from small electron-lucent vesicles and active renin from electron-dense granules. Pathophysiological stimuli such as acute activation of sympathetic outflow to the kidney or drop in perfusion pressure are able to raise circulating levels of active renin from JG cells within minutes to initiate the RAAS cascade (13). The steady-state release of renin is reflected by the chronic change in plasma renin activity, mRNA levels and JG cell number (13), and is affected by factors such as salt status (14).

1.3 Physiological Control of Renin and the Juxtaglomerular Apparatus

1.3.1 Glomerular Filtration

Tubulo-vascular crosstalk between JG cells and the salt-sensing macula densa (MD) cells plays a significant role in the secretion of renin as part of the kidney tubuloglomerular feedback (TGF) regulation of tubular salt (15). The two major regulatory functions of TGF are the low distal tubular NaCl-induced release of renin, and the high distal tubular NaCl-induced vasoconstriction of the AA and subsequent decline in single nephron glomerular filtration rate (16).

MD cells are integral to regulating glomerular filtration, the process by which small molecules such as glucose, amino acids and water within the blood are filtered from the AA into the Bowman's capsule and subsequently the nephron. The tubular content is then refined by tubular reabsorption and secretion, where previously filtered substances are selectively reabsorbed back into the blood. Filtration is facilitated through

the maintenance of a delicately balanced pressure system within the Bowman's capsule. Outward pressure known as the glomerular hydrostatic pressure is provided by a mechanical pressure caused by the beating of the heart and the pressure difference between the afferent and efferent arterioles, acting towards filtration. Opposition to this force is provided by the Bowman's capsule pressure caused by the elastic recoil of the capsule itself, and the colloidal osmotic pressure. This is caused by the water concentration gradient between the blood plasma and the filtrate, since water is filtered but larger proteins are left in the capillaries. These forces act against filtration, and the balance between the filtering and opposing forces determines the net filtration rate within the kidney (17).

The net filtration rate in turn defines the glomerular filtration rate, which is a measurement of the volume of fluid filtered into the Bowman's capsule per unit time, and an indicator of kidney function (18). Therefore through alterations in the pressure balance within the Bowman's capsule, which is achieved through changes in the glomerular hydrostatic pressure, the kidney is able to fine tune glomerular filtration rate. Since the glomerular hydrostatic pressure is controlled by the BP entering the glomerulus, adjustments are made by altering the resistance of the AA through contraction and relaxation. To do this, tubuloglomerular feedback is employed.

1.3.2 Tubuloglomerular Feedback

Detection of tubular sodium concentrations by the MD cells enables fine tuning of kidney GFR via TGF signalling. The MD plaque is located on the ascending cortical thick ascending limb (cTAL) where it passes in close proximity to the glomerulus (Figure 1.1), and is highly specialised to sense NaCl concentration in the passing tubu-

lar filtrate. NKCC2 cotransporter on the apical surface of hyperpolarised MD cells facilitates re-absorption of filtered NaCl load (19). It is the primary NaCl entry mechanism, and even small changes in NKCC2 transport activity change the reabsorption of NaCl (20). When low tubular NaCl concentrations are detected, p38 and COX2 are activated, which further activate the transcription of prostaglandin E2 (PGE2) (21, 22, 23). PGE2 is then transported to the JG cells where it binds to the EP1 and EP2 receptors and initiates the cAMP-activated renin release pathway (24).

Conversely, high tubular NaCl is transported into the MD cells at the apical membrane through NKCC2 cotransporters, increasing Cl efflux through basolateral membrane channels, depolarising the basolateral membrane and triggering Ca^{2+} influx into the cell (Figure 1.3). Following this, ATP is released via a basolateral membrane channel, binding to the P2X receptors on the mesangial cells, allowing a Ca^{2+} influx into the cells (25). This Ca^{2+} then travels throughout the JGA via gap junctions, binding to P2X receptors on VSMCs, causing the activation of a non-selective, inwardly directed cation current, allowing the influx of extracellular Ca^{2+} (26), leading to the vasoconstriction of the AA and glomerular tuft. This is also brought about indirectly through the breakdown of ATP to adenosine (27). An additional mechanism which acts to increase intracellular Ca^{2+} in VSMCs is the direct flow-sensing of the primary cilia on the apical surface of the MD (28). Increases in intracellular Ca^{2+} are further reinforced by the action of the cation channel which is also thought to allow the simultaneous influx of Na^{+}, depolarising the membrane and stimulating additional Ca^{2+} influx through voltage-gated calcium channels (29, 30). The ATP released initiates a cascade of calcium, which travels via gap junctions from the MD to the VSMCs, mesangial cells and beyond into the intra-glomerular space. This participates in TGF

by contracting the glomerular tuft as well as the AA to reduce GFR by decreasing the glomerular filtration pressure. Adenosine also binds to inhibitory G-protein coupled receptors on the JG cell surface, inhibiting the cAMP-mediated renin production and release pathway (13, 31). Macula densa plaques contain very little baseline Ca^{2+} compared with neighbouring cell types, with little variation of Ca^{2+} seen during TGF due to its tight regulation within the cell (32).

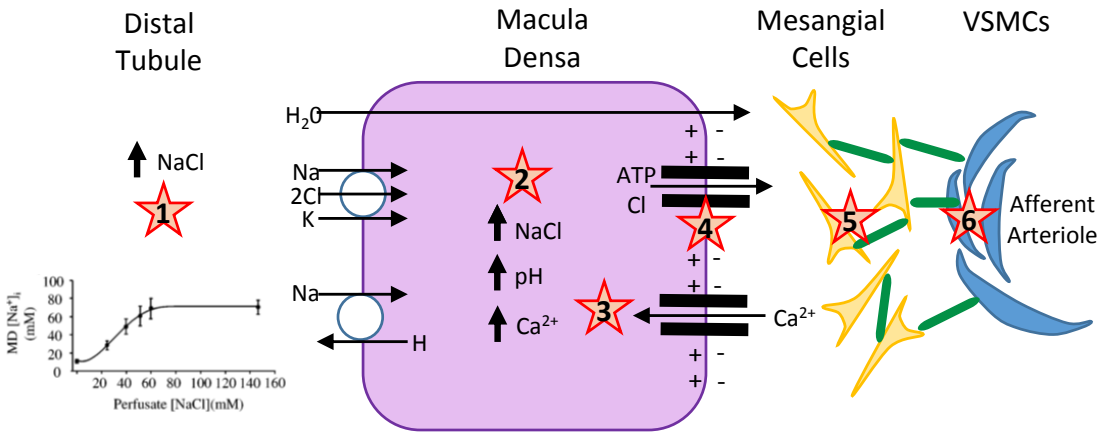

Figure 1.3: Macula densa cells initiate tubuloglomerular feedback by sensing tubular salt content - (1) Increased distal tubule NaCl concentration up to approximately 75mM is transported into macula densa cells via NKCC2 cotransporters on the apical membrane. (2) This NaCl increase causes an exit of chloide through basolateral channels, depolarising the basolateral membrane. (3) This allows an influx of Ca^{2+} and an increase in pH, leading to ATP release from the basolateral membrane (4). (5) This ATP binds with P2X receptors on mesangial cells, allowing an influx of Ca^{2+}, which is transported to the VSMCs and throughout the JGA via gap junctions (6). Figure adapted from Bell *et al* (25).

Imaging TGF Function

Due to the complexity of JGA architecture, the heterogeneity of cell type and the size of the tissue, study of tubulo-vascular crosstalk in living tissue is extremely difficult. The development of confocal and multiphoton microscopy has allowed rapid, high resolution, deep optical sectioning of living JGA, helping to elucidate the relationship between structure and function (33).

Multiphoton microscopy has been employed at the whole organ level to characterise and quantify not only basic physiological parameters, but also myogenic function (34). *In vivo* imaging is performed on anaesthetised mice or rats by cannulating the trachea to allow normal breathing, cannulating the left femoral vein and artery for dye infusion and BP measurements respectively, and making a dorsal incision to exteriorize the kidney, placing it on a coverslip-thickness microscope stage (34, 35). Using this experimental setup, single nephron GFR was quantified by analysing the changes in fluorescence intensity as the fluid marker lucifer yellow was filtered into the Bowman's space (34). Renal blood flow was measured in the peritubular and intra-glomerular capillaries using characteristic traces from autofluorescent red blood cells as they were transported through the vasculature, and the urinary concentration and dilution was measured using rhodamine-conjugated 70-kDa dextran dye (34). Finally, *in vivo* analysis of renin enzyme activity using FRET-based fluorogenic renin substrates have been used in conjunction with intravital stains such as quinacrine to image both granular content and release (34, 35, 36) (described fully in Section 1.9).

Disadvantages to performing *in vivo* multiphoton imaging include the inability image afferent arterioles due to insufficient penetration depth and confounding systemic effects. Therefore to investigate the mechanisms involved in TGF, the most successful and widely used technique is the isolated perfused JGA model, where the glomerular tuft is dissected from freshly cut kidney slices with the AA, the cTAL, MD plaque and, if possible, the efferent arteriole (EA) intact.

Using this technique, many important physiological mechanisms have been analysed in their native cellular environment under controlled flow conditions without compounding systemic factors. Peti Peterdi *et al.* showed for the first time that sphincter-like

constriction takes place in the terminal intra-glomerular segment of the AA, not the proximal segment. MD cell swelling in response to increased tubular [NaCl] was also shown to be larger than previously realised, which was subsequently linked to the generation of signals leading to renin release (33, 37). MD cells were also shown to have tubular flow-sensing cilia which contribute to MD cell function and TGF (28).

By analysing cell contraction and $[Ca^{2+}]_i$ elevations using the ratiometric calcium indicator dyes fluo-4 and fura red in conjunction with this technique, increased [NaCl] perfusion at the MD was shown to trigger a $[Ca^{2+}]_i$ wave which propagated through mesangial cells and VSMCs at approximately 12 μm/s (32). Indeed increased tubular flow rate at the MD is reported to induce a TGF response (32, 38, 39). A highly sensitive membrane-specific voltage-sensing dye was used to show even more rapidly propagating vascular TGF signals, which were linked to nephron synchronisation (40). Furthermore, $[Ca^{2+}]_i$ oscillations were visualised in cTAL cells surrounding the MD of isolated perfused JGA, indicating that this region also takes part in TGF (41).

1.4 Ontogeny of Renin Expression

Adult renin-producing cells are localised to the very distal end of the AA within the medial layer, constituting the vessel wall at the entrance to the glomerulus. However, during development renin expression is highly plastic (42).

The growth of the renal vascular tree is thought to occur both through the differentiation of blood vessels during vasculogenesis, and through angiogenesis, where new blood vessels grow from existing vessels. This commences during the metanephric phase with the induction of vascular endothelial growth factor (VEGF) and Flt-1 expression, leading to activation and maturation of endothelial cells (42, 43). These endothelial cells

produce platelet-derived growth factor-β (PDGF-β), enabling pericytes and smooth muscle cells to attach and stabilise the vessels (44).

In the mammalian metanephric kidney, the renal artery divides into a species-dependent number of interlobar branches, followed by branching of the arcuate arteries. The renin expression profile follows this sequential division, beginning on day 15 of development (Figure 1.4); as the renal artery divides into the interlobar arteries, expression begins to subside in the larger vessels, retracting in a retrograde direction. Simultaneously, expression is initiated in the newly formed vessels starting with the interlobular artery, which branches into the arcuate arteries, giving rise to the AAs where renin expression is finally retained (42).

Sauter *et al.* did not observe renin expression in the regions of greatest vascular growth and branching, hinting that an established functional vessel wall is necessary for the onset of renin expression. The factors triggering renin expression and the exact mechanisms governing the expression pattern and restriction to the JG location, remain unclear.

Renin-producing cells originate from a perivascular cell lineage (45). Renin and pericyte markers are coincidentally expressed during human kidney development, and primary cultures of pericytes isolated from the human fetal kidney can be induced to express renin after stimulation with IBMX and forskolin (45). Since pericytes share features with mesenchymal stem cells, they are strong candidates for potential renal progenitor cells. It is therefore hypothesized that JG cells are a type of specialized pericyte, however further work is needed to investigate this.

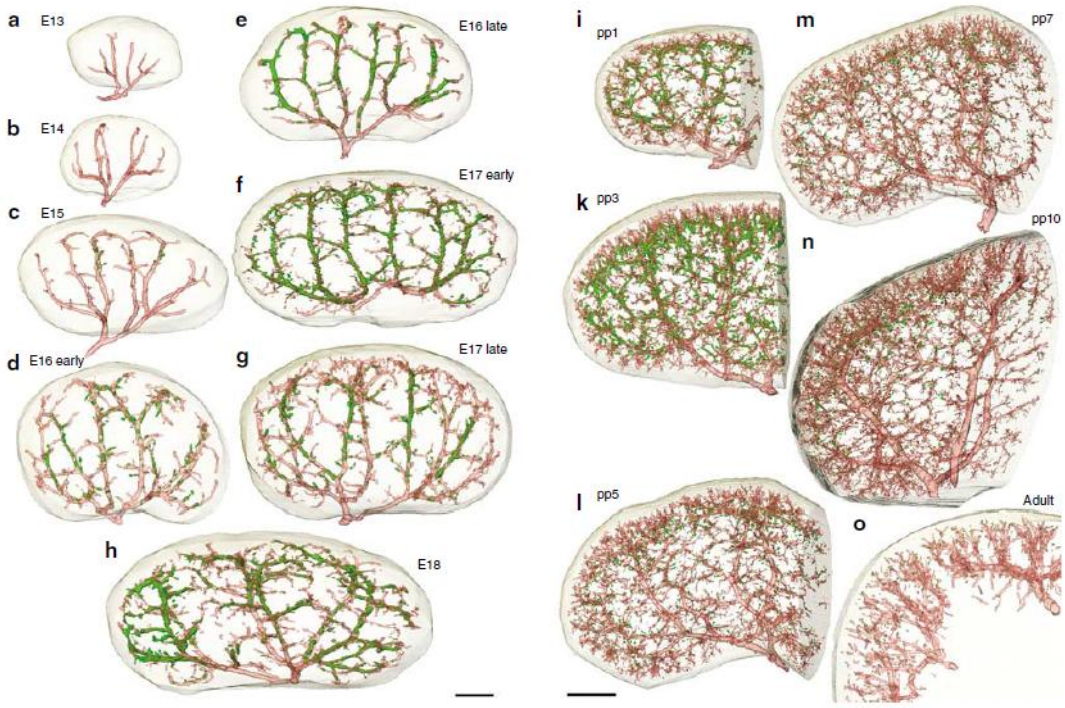

Figure 1.4: Reconstruction of vascular structure in the developing mouse kidney. - Kidneys were analysed at embryonic days e13, e14, e15, e16 early and late, e17 early and late, e18, post natal (pp) days 1, 3, 5, 7, 10, and at adulthood. Red represents α-SMA-positive staining, green represents renin-positive staining. Scale bars represent 300 μm for embryonic kidneys, 500 μm for post natal images. Image from Sauter *et al* (42).

1.4.1 Granulation During Ontogeny

There is a paucity of literature on granulation of JG cells during ontogeny. Wistar rat JG cells were shown to contain a small number of renin granules at e18.5 (46), granules were identified in the mesonephros and metanephros of the pig (47), and 0 - 1 granules per cell were observed in human fetal tissue (48). Furthermore, juvenile granules were shown to have lower fusion ability than adult granules (10). Unpublished work carried out by a former PhD student aimed to clarify the granulation status of JG cells in the developing kidney by performing EM on C57Bl/6 JG cells at different developmental time points and under maternal dietary and pharmacological manipulation (Nathalie L'Huillier, unpublished). No granules were present at el8.5, however granules were observed from PI onwards. When mothers were treated with ACE inhibitors, granules were evident from day 15 of pregnancy, with extensive granulation evident in the fetuses by e18.5.

1.5 Recruitment of Renin Producing Cells

When long term homeostasis is threatened, such as under chronic administration of the ACE inhibitor captopril or a low salt diet, the number of renin-producing cells along the AA increases (14). Adult renal VSMCs recruited from upstream of the AA, renal glomerular cells, mesangial cells and renal interstitial cells can revert to a renin-producing phenotype (49); this process is known as the 'metaplastic transformation'. The onset of this transformation is characterised by prorenin synthesis, granulopoiesis and the accumulation of mature secretory granules to process prorenin into active renin, accompanied by the atrophy of myofilaments and attachment sites (50).

The pattern of recruited cells strongly resembles the ontogeny of renin development within the cortical vasculature (49). Renin cells derive from progenitor cells in the mesenchyme of the fetal kidney, from which they become distributed throughout the intrarenal arterial tree and glomerulus prior to kidney vascularisation or renin secretion (49, 51).

Brunskill *et al.* investigated the differences in the genetic profiles of fully differentiated JG cells and VSMCs which had been induced to undergo the metaplastic transformation (52). They developed a single cell isolation and amplification procedure and performed microarray studies on P0 renin-expressing cells, adult JG cells, and recruited JG cells after captopril treatment (52). Of the genes enriched in renin cells compared to kidney cortex, a number were of particular interest. AKR1B7, an aldoketoreducase known to remove xenobiotics and aldehydes, localised with renin expression during development. It was similarly restricted to the distal AA location in adults, and also responded to captopril treatment by extending expression along the AA. However AKR1B7 expression was present in renin knockout mice, indicating that renin is not required for correct AKR1B7 expression.

CRIP1 (cysteine-rich protein 1), a protein which has previously been linked to muscle and myofibroblast differentiation, was highly expressed in JG cells and could be a potential regulator of the smooth muscle phenotype in JG cells (53, 54). Human VSMCs in the process of transitioning to a JG-like phenotype were identified ultrastructurally by an increased development of granules and frequent connections between the nuclear envelope and the rough endoplasmic reticulum (RER), both of which were noticeably dilated (55). Reduced prominence and compactness of myofibrils, additional mitochondria, secretory granules and junctions between cells to increase cell-to-cell

communication were also present in these transitioning cells (55).

In the Brunskill study the pericyte marker RGS5 (regulator of G protein signaling 5) was also enriched and showed an overlapping expression pattern with renin and platelet derived growth factor beta receptor (PDGFR-β) (52, 56). Further genetic links to pericytes were also found in JG cells, with enrichment of the transcription factor NFAT, which is integral to pericyte-VSMC wall attachment. These markers provide evidence linking renin-expressing cells to arterial and interstitial pericytes.

This study emphasised the dual endocrine and contractile role of renin-expressing cells for the maintenance of homeostasis, and highlighted the transcription network which drives the maintenance of both phenotypes within recruited JG cells. However it was concluded that interaction with surrounding JG, endothelial, VSMC and MD cells are required to maintain the JG cell phenotype (52). This intracellular communication within the JGA is predominantly achieved through gap junctions, which are found at a high density within the kidney (57). Gap junctions are defined by their composite connexin (Cx) proteins. A hemichannel is formed by six Cx proteins and sits within the plasma membrane, forming a larger intercellular channel between neighbouring cells through which charge- and size-controlled molecule permeation can take place (58).

Cx40 is highly expressed in the JGA and is localised to intra- and extra-glomerular mesangial cells, JG cells, AAs, and endothelial cells along the preglomerular vasculature. This allows formation of endothelial-endothelial, JG-JG, mesangial-mesangial and endothelial-JG cell gap junctions (59). Cx43, 37 and 45 are also expressed at lower levels, particularly in renin-producing cells (59).

Kurtz *et al.* (57) used Cx40 knockout mice to determine its role in angiogenesis, vasculogenesis, the localisation of JG cells and the recruitment of renin-producing cells.

$Cx40^{-/-}$ mice had increased numbers of JG cells compared to controls, however these renin-producing cells extended into the glomerulus and periglomerular interstitium surrounding the vessel wall. This indicated the importance of Cx40 to the maintenance of classic JGA architecture. Furthermore, renin-expressing cells were no longer epitheloid, displaying a mesenchyme-like, irregularly shaped phenotype, although the cytosol still stained positively for renin and exhibited a granular pattern. AA cells at the classic JG location did not stain positively for renin or granulation, and recruitment of renin-expressing cells via ACE inhibitor treatment increased the number of periglomerular JG cells, but not arteriolar JG cells (57). It was therefore hypothesised that under normal conditions renin-producing cells, endothelial cells and mesangial cells derive from the JG and periglomerular mesenchyme as a group of pericytes, connected via gap junctions (57). Since endothelial cells normally form Cx40 gap junctions with JG cells but not with VSMCs, the absence of Cx40 in $Cx40^{-/-}$ mice allowed renin-expressing pericytes to transform into VSMCs. This displaced the remaining renin-expressing pericytes to the edge of the AAs and outside the vessel wall. This hypothetical sequence of events would imply that Cx40 JG:endothelial gap junction contacts help constrain JG cells at the distal AA position, enabling signalling via the endothelium-coupled pericytes to suppress further proliferation and renin expression. This would leave the cells with the innate ability to secrete renin and hence undergo transformation in the extraglomerular mesangium and the larger vessels upon chronic stimulation of the RAAS.

JG cell localisation has an important physiological role, since a mutation in human Cx40 is associated with both hypertension and a complete absence of pressure sensitivity to renin secretion (60). This is seen in $Cx40^{-/-}$ mice which are hypertensive (61), along with a loss of inhibition of renin release by ANGII or perfusion pressure (58).

1.5.1 Pericytes

Pericytes are progenitor cells of mesenchymal origin that stain positively for mesenchymal stem cell markers (62). They are essential mural cells rooted within the vascular basement membrane of blood microvessels and regulate vascular development, stabilisation, maturation and remodeling (63, 64). Pericytes have extensive branching processes that surround the abluminal surface of endothelial cells by 10 - 50% (63). By being both enclosed within the basement membrane and exposed to the surrounding cellular environment, pericytes can develop peg socket contacts with surrounding cells, which form tight-, gap- and adherence-junctions (62). It is through these connections that one pericyte can link to multiple endothelial cells, facilitating intercellular communication and the regulation of proliferation and differentiation through secretion of active molecules (45, 62). For example pericytes have been shown to inhibit endothelial cell division via the activation of TGF-β (65).

Identifying these cells in vivo has proved challenging, since there is no single pericyte-specific surface marker and pericytes are morphologically distinct across organs (62, 66, 67, 68). However useful markers include PDGFRβ, which is crucial for pericyte function and stability, neuron glial antigen 2 (NG2), a transmembrane proteoglycan that is expressed by the mural cell component of mouse neovascular structures and α-smooth muscle action (α-SMA), which is expressed by all pericytes undergoing vascular remodeling and by VSMCs and myofibroblasts (62, 67). The perivascular location of pericytes is thought to be a stem cell niche (65) and they are able to differentiate into a number of cell types including chondrocytes, osteoblasts, fibroblasts, adipocytes and even VSMCs during vascular remodeling and vessel growth (69). Differentiation of

pericytes depends on chemical and environmental cues, allowing them to respond to homeostatic challenges by phenotypic changes (45). This is why JG and renal cortical arteriolar cells can be considered a subset of specialised pericytes.

Pericytes were first visualised in the kidney using EM (70) and were observed overlaying glomerular endothelial cells and residing on the peritubular capillaries of the tubulointerstitial space (62, 63). Furthermore, evidence suggests that both afferent and efferent arteriolar VSMCs and mesangial cells derive from common PDGFRβ^+ progenitor cells (71). Both podocytes and mesangial cells, which form a branched, multicellular core around which the glomerular capillaries wind, are thought to be specialised forms of perivascular cells (63). It is not known whether adult kidney pericytes can be induced to produce renin, or whether granulopoiesis occurs in these renin-expressing fetal or adult pericytes.

1.6 Models Of Juxtaglomerular Structure and Function

1.6.1 Primary Juxtaglomerular Cell Culture

Primary cultures of mouse and rat JG cells have been extensively used to study the intracellular signalling pathway leading to renin synthesis and release. For example primary cells have been used to clarify the roles phosphodiesterases play in cyclic guanosine monophosphate (cGMP)-stimulated renin release (72) and have been patch-clamped to provide evidence for cAMP-dependent renin exocytosis (24). JG cells can be extracted using a Percoll density gradient that separates cell types according to their densities. It is possible to isolate a heterogeneous, JG-enriched population of cells at a density of 1.07 g/ml (73), although identification of JG cells remains difficult and is often based

solely on cellular morphology and the presence of dense core granules in the cytoplasm (73, 74, 75).

However the culture of primary JG cells is extremely difficult and must be performed with care. JG cells only synthesise renin and respond to cAMP-mediated renin secretion for approximately 48-72 hours in culture (13). Poly-D-lysine (PDL) is used as the culture basement membrane protein, however cells often take on a 'balled up appearance' (73, 76, 77). Furthermore, they represent only 0.001 - 0.01% of the kidney cell population (52), therefore kidney digests must be pooled to obtain a sizeable population of JG cells, exposing the extremely sensitive JG cells to extended and relatively harsh environmental conditions. The development of a method whereby primary JG cells can be efficiently extracted, cultured and rapidly identified would therefore be greatly advantageous to the study of renin synthesis and secretion.

1.6.2 Cell Lines

To avoid lengthy and complex extraction and culture of primary cells, immortalized cell lines are often created. Immortalization of cells is performed to provide homogenous cell populations with genotypic and phenotypic similarities to their parent tissue, capable of extended periods of proliferation. Regulation of proliferation is maintained through balanced expression of two subsets of genes, proliferation-stimulating pro-oncogenes (eg. ras and myc), and proliferation-inhibiting tumour suppressor genes (eg. p53, p16, Rb) (78, 79). There are two main ways in which this delicately balanced system is induced to retain proliferation; through the introduction of the viral simian virus 40 T antigen gene (SV40Tag), or through expression of telomerase reverse transcriptase protein (TERT).

TERT immortalizes cells by maintaining telomere length. Telomeres create a cap at the ends of linear chromosomes, protecting them. The shortening of telomere length occurs every time a cell division occurs since DNA polymerase α is unable to fully replicate the ends of linear DNA molecules. Replicative senescence occurs when the short telomeres are so short they are unable to perform their function (80). The telomerase enzyme prevents this telomere degradation, but is only endogenously expressed in somatic cells during early embryonic development, and in the skin and digestive tract in the adult (80). However, exogenous overexpression of human TERT (hTERT), a catalytic subunit of human telomerase, is able to effectively prevent telomere shortening and immortalize human cells. A stable genotype is retained without the use of cancer-associated changes, and many cell types have been immortalized in this fashion (reviewed in (80)).

However the most commonly used immortalization method is the introduction of the SV40Tag. SV40Tag encodes a multifunctional nuclear phosphoprotein which has a number of biochemical functions. DNA replication is initiated by binding of the T-antigen to the SV40 origin, which is controlled by phosphorylation. Binding of the T-antigen inactivates the tumour suppressor proteins p53 and p105, allowing the cell to enter the S phase for DNA replication (78). This is important for the immortalization, since the SV40 genome is too small to perform DNA replication itself; when the host cell reaches S phase in the cell cycle, cellular DNA and the SV40 sequence are replicated simultaneously (81). It should be noted that in certain cell types, neither SV40T nor hTERT alone are enough to maintain immortalization.

Immortomouse tsA58$^{+/-}$ Mice

The Immortomouse is a transgenic mouse homozygous for a transgene which encodes

a temperature-sensitive mutant of the SV40Tag (tsA58) in every cell of the body. It is under the control of the mouse H-2Kb class 1 promoter which is induced using inteferon-γ (IFN-γ), allowing conditional immortalization of cell lines which retain their phenotype in long term culture (82, 83).

When cultured in the presence of IFN-γ and at the permissive temperature of 33 °C, cells from this mouse proliferate due to activation of functional expression of the large SV40Tag. However, when cultured at non-permissive temperatures such as $37 - 39$ °C, cells died within 7 days, even in the presence of IFN-γ (83). Similarly, removal of IFN-γ from the media of cells cultured at the permissive temperature leads to a decrease in the number of cells producing DNA, and cells senesce within 3 passages (83). This mouse has been effectively used to produce conditionally immortalised cell lines for a number of different cell types, including many different kidney cells, but has yet to be employed to create a renin-expressing cell line (reviewed in (84)).

Renin-Expressing Cell Lines

The most frequently used cell lines for the study of renin gene regulation are the AS4.1 and Calu-6 lines. Calu-6 is a human pulmonary carcinoma cell line which expresses human renin mRNA endogenously (85), and as such has been used to examine regulation of the human renin gene. For instance, the cAMP-mediated transcriptional control of the human renin gene was investigated, with the human renin promoter shown to be transcriptionally active in Calu-6 cells through the cAMP-PKA pathway, mediated through both a cAMP response element binding (CREB)-dependent and CREB-independent pathway (86).

AS4.1 cells are a renin-expressing cell line which was established by inducing neoplasia *in vivo* in renin-expressing cells of a transgenic mouse containing a renin-promoter

SV40Tag fusion transgene (87, 88). As4.1 cells highly express the Ren-1c gene and form granules (89). Despite the presence of prohormone convertases within these granules, prorenin release is 13-fold higher than that of active renin, both of which are released constitutively (89).

These cells have been widely used for investigation into mouse renin gene regulation and expression (90, 91, 92). However AS4.1 cells are not a good model in which to study granule dynamics and renin secretion (93) because they do not exhibit regulated release of active renin. Secondly, cAMP-mediated renin release is inappropriate in these cells, leading to complete degranulation when this pathway is stimulated, compared to 2-6% degranulation seen in primary cells (93). Therefore data from studies such as that by Lu *et al.* (94) where AS4.1 cells are used as a model in which to assess H_2S-mediated secretion must be analysed with care. The establishment of a cell line that faithfully recapitulated granule formation and regulated and constitutive secretion would therefore be of significant advantage to the field.

1.7 Renin Synthesis and Processing

Under standard physiological conditions the synthesis and secretion of active renin is confined to the JG cells of the JGA. Other tissues have been shown to produce inactive prorenin, however intracellular processing of prorenin to the active form does not take place. The exception is the submandibular gland (in mice only) in which active renin is secreted into the saliva (95, 96, 97).

Following cleavage of the signal peptide during transport through the rough endoplasmic reticulum (RER) (99), the majority of prorenin is packaged into small, clear vesicles during the subsequent transport through the Golgi apparatus. By measuring

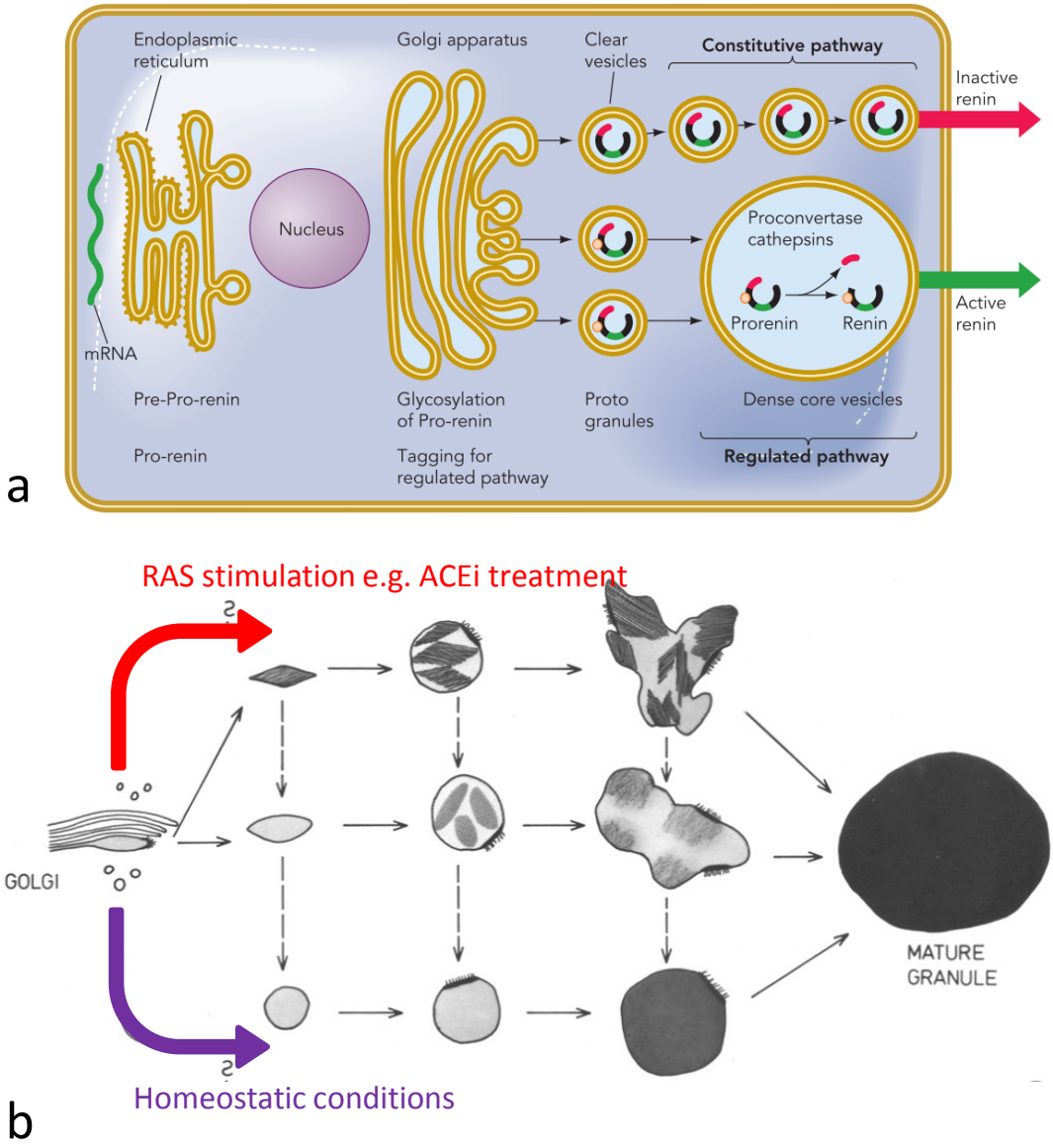

Figure 1.5: Renin synthesis and granulopoiesis within juxtaglomerular cells. - (a) A model of renin synthesis in JG cells. After cleavage of pre-pro-renin to pro-renin in the endoplasmic reticulum, passage through the Golgi apparatus introduces a glycosylation site to traffic a small proportion of prorenin onto the regulated release pathway. The non-glycosylated renin is thought to be packaged into small, clear vesicles which are released constitutively. Image taken from Schweda (98). (b) Granule formation is believed to follow the course along the bottom of the image under normal, homeostatic conditions, where fusiform protogranules round off and coalesce with other protogranules to form intermediate granules. However it is believed that under stimulation of the RAAS the granules take on a rhomboid aspect with paracrystalline interiors and follow the top branch, leading to polymorphous intermediate granules due to incomplete coalescence of the contents. The dashed lines represent the supposed transition from paracrystalliine rhomboid, fusiform and polymorphous granule interiors to the classically shaped spherical granules with homogenous material. This is thought to be possible at each stage of granulopoiesis. Purple arrows indicate the constitutive release of prorenin in vesicles. Image from Taugner *et al* (10).

the secretion kinetics of prorenin and active renin Pratt *et al.* (99) demonstrated that prorenin is released constitutively. However a small fraction of synthesised prorenin is glycosylated as it is transported through the Golgi and packaged into dense core storage granules for release on a regulated secretory pathway (100) (Figure 1.5a). It is within these granules that prorenin is processed into active renin via cleavage of the 43 amino acid NH_2 terminal propeptide at the Asp-43p-Leu-1 bond (99). The sorting of prorenin onto the regulated pathway is thought to depend on the co-operation of a number of mechanisms, not merely on glycosylation (99).

Formation of dense core renin-containing granules is believed to be initiated by budding of the Golgi apparatus, which is pinched off to form protogranules (Figure 1.5b). Under normal physiological conditions, granules take on a rounded appearance and evidence suggests that fusion with neighbouring protogranules leads to intermediate granule formation (lower track). When the RAAS is stimulated, the granules develop in a more paracrystalline formation within a membrane-bound electron-lucent region (101) (upper tracks). The coalescence of paracrystalline material within polymorphous granules is thought to be a longer process than the gradual increase of electron-dense material seen in spherical granules, making it less common. Despite this, the end products of the coalescing granular material are still homogeneous, electron-dense mature granules. Electron micrographs of JG cells from C57Bl/6 mice show these granules densely packed within the cytoplasm (Figure 1.6a), as well as examples of protogranules pinching off from the Golgi apparatus (Figure 1.6b). The presence of lysosomal trafficking regulator (Lyst) proteins, which targets proteins to lysosomes, is necessary for correct segmentation of granules (102). The JG cells of beige mice with heritable mutations of Lyst only contain 1 - 2 giant storage granules, indicating the essential role

Lyst plays in correct granule formation (Figure 1.6d).

The low pH within early renin granules (pH 4 - 6) is achieved through the action of intracellular H^+-ATPases which catalyse the transmembrane exchange of protons and aid aggregation of the granule core, giving primitive granules their paracrystalline structure (10, 103). It is low pH that allows identification of granules by acidotropic dyes such as quinacrine (104) and lysotracker (36).

Although a number of candidate prohormone convertases are able to cleave renin *in vitro*, mouse knockout models for these enzymes did not alter active renin secretion *in vivo* (105). Similarly, a number of lysosomal enzymes colocalised with JG dense core granules, but were not functionally relevent (106). The most likely candidate for intragranular cleavage of prorenin was cathepsin B since it colocalised with renin within dense core granules and showed site-specific cleavage of the human renin prosegment *in vitro* (107). However this was recently disproved in experiments using cathepsin B knockout mice: levels of circulating active renin were normal and administration of an ACE inhibitor lead to a similar rise in renin expression and active circulating renin levels in knockout and control C57Bl6/N mice (108). There is evidence to suggest that after inital cleavage at the dibasic site, the prosegment is 'nibbled' away until only the mature renin protein remains (109, 110).

JG cells in C57Bl/6 mice contain on average 100 granules of approximately 0.5 μm diameter (102) and the number of renin-expressing cells within the JGA differs considerably between species and pathophysiological conditions (111). Whilst 2D electron microscopy (EM) has historically been used to classify granule types, recent stereological reconstructions have revealed that these 2D snap-shots of granules are cross-sections of larger vesicular structures of varying levels of complexity (101, 112, 113). The role of

this vesicular network, its presence under different pathophysiological conditions and its interaction with granules are yet to be elucidated and many questions remain.

Many questions regarding the formation of renin-containing dense core granules remain unanswered. For instance, what causes the formation of the different protogranule types, and what is the significance of electron lucent granules? Fusion between immature granules has been imaged at the EM level, but is this a dynamic process that is continually occurring and, if so, what factors affect it? And what is the relationship between renin expression levels and granule type and number? It is hard to answer such questions due to the difficulty in imaging intracellular processes in live, cultured JG cells at sufficiently high resolution. The majority of the published work to date has been performed using EM, which allows exquisite resolution of intracellular structures and organelles. If these questions are to be answered in the future, a protocol whereby high resolution optical microscopy techniques coupled with optimised culture of primary JG cells or appropriate renin-expressing cell lines would be extremely advantageous.

1.7.1 Granulation in Human Juxtaglomerular Cells

Surprisingly few studies have been performed investigating the ultrastructure of human JG cells. One of the most comprehensive EM studies was carried out by Biava and West on renal biopsies from 7 normal patients (24-46 years old, normotensive, no detectable renal lesions) to determine normal, human JG structure (55, 115). On average, 4 - 8 JG cells were found at the distal end of the AA around the vascular pole, with varying JG cell morphology. Unlike the mouse, many isolated cytoplasmic vacuoles were seen in the majority of JG cells analysed (Figure 1.6a). Interestingly, branched myofibril-rich cytoplasmic processes were observed inter-digitating with processes of surrounding

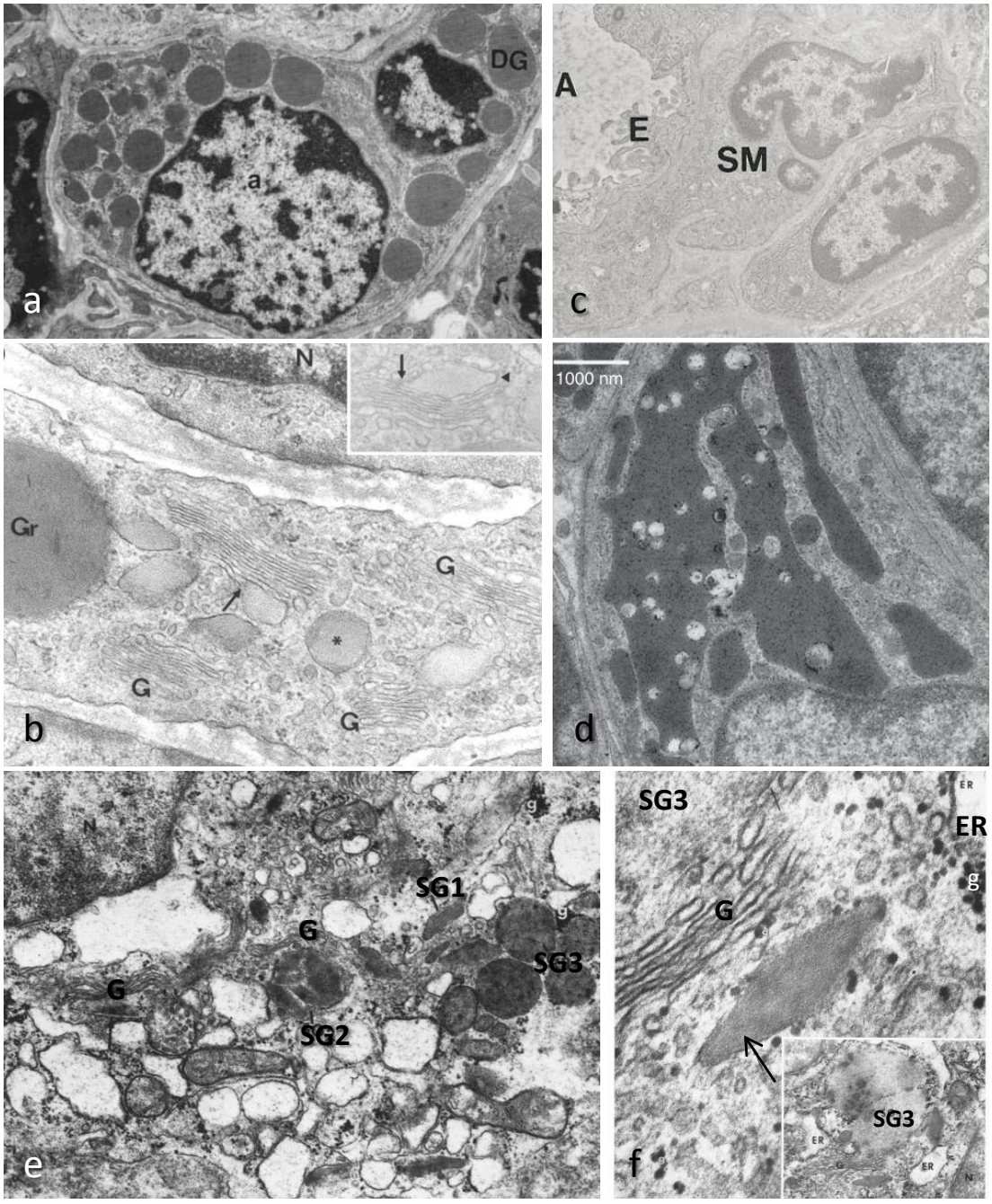

Figure 1.6: Ultrastructure of JG cells. - Mouse control C57Bl/6 JG cells (a) DG: dense core granule (9,000X). Image from (112). (b) G: Golgi, Gr: dense core granule, N: nucleus, arrow: fusiform protogranule pinching off from G, arrowhead: coated pit. (Main image 68,000X, inset 62,000X). Image from (10). (c) Non-granulated $Ren1d^{-/-}$ JG cell. A: afferent arteriole, E: endothelial cell, SM: modified smooth muscle (JG) cell (2,600X). Image from (114). (d) SCID-beige mouse JG cell with Lyst mutation. (3,800X). Image from (113). (e, f) JG cells from healthy human renal biopsies showing Golgi apparatus (G), and specific granules (SG) containing homogeneous material. SG1: elongated rhomboidal configuration, SG2: circular, containing rhomboidal material, SG3: circular, containing uniformly distributed material (26,000X magnification). (f) Rhomboid, crystalline granule in the vicinity of G (Main image 150,000X, inset 22,000X, lead hydroxide stain). ER: endoplasmic reticulum, g: glycogen particles, N: nucleus Ce: centriole. Images from Biava and West (55, 115).

cells, suggesting significant cell-to-cell communication, which decreased in density on cells further from the glomerulus.

Granules were routinely found in close proximity to the Golgi (Figure 1.6e). Although they showed different structural characteristics, three types of granules were identified. SG1-type granules were rhomboid, diamond-shaped paracrystalline granules, similar to those seen in mouse JG cells. These granules contained tightly packed filamentous material within a single outer membrane and were located close to the Golgi (Figure 1.6e, f). SG2-type granules were larger, with a circular granule membrane containing several rhomboidal SG1 granules (Figure 1.6e). Some of these SG1-type granules appeared to be disintegrating within SG2 granules, indicating that they were fusing and maturing to become the third type of granule, SG3. These granules were the most common and contained finely filamentous, electron-dense material (Figure 1.6e). These mature granules were more uniform in shape, distributed around the periphery of the cell cytoplasm and were between 800 - 1200 nm in diameter. Gradations between these granular types were seen, indicating that a similar granular accumulation process as that outlined for mice in Figure 1.5 is also present in human JG cells. No images of fusion between the membrane of granules and the cell membrane were observed.

1.7.2 The Renin Gene in Mice

The *Ren* loci in humans, rats and some strains of mouse (e.g. C57Bl/6) contain a single structural renin gene, *Ren*-1^c, which is highly conserved between species. However a sub set of mouse strains (e.g. DBA/2) carry two renin genes within the *Ren* locus: another Ren-1 allele, *Ren-1d*, and an additional *Ren2* gene (100, 116). *Ren2* is likely an ancestral duplication of the $Ren-1$ gene which was deleted in certain strains (117).

The three genes encode highly homologous proteins with Ren1c having 99% and 97% similarity in the coding region to Ren1d and Ren2 respectively (118). Although the encoded proteins are very similar, there are some key differences, notably the presence of three potential asparagine-linked glycosylation sites in Ren1d and Ren1c which are not present in Ren2 (118).

Work carried out by Sharp *et al.* on the inactivation of the *Ren-2* gene in mice revealed no histopathological variations in renin-expressing tissue or differences in BP regulation between $Ren2^{-/-}$ mice and wild-type littermates. However active plasma renin concentrations in $Ren2^{-/-}$ mice increased commensurate with a decrease of plasma prorenin concentration, indicating that $Ren1d$ and $Ren1c$ are functionally equivalent with respect to the regulation of BP (119).

Clark *et al.* (114) generated $Ren1d^{-/-}$ mice, which displayed sexually dimorphic hypotension in females. A rise in inactive plasma prorenin levels was seen, coupled with a decrease in active plasma renin concentration. Furthermore, there was a striking lack of granulation within the JG cells of the kidney (Figure 1.6c), suggesting that $Ren1d$ is necessary for the formation of dense core storage granules.

Interestingly, MD cells in the distal tubular epithelium of $Ren1d^{-/-}$ mice were hyper-cellular, with columnar epithelial cell morphology, and showed a 30% increase in basolateral to apical height compared to controls (114). As highlighted in Section 1.3.2, MD cells are integral to the regulation of tubular NaCl and perfusion pressure within the kidney, playing a major role in RAAS-mediated BP stabilisation. The altered morphology of MD cells in $Ren1d^{-/-}$ mice revealed that the renin protein is necessary for normal maintenance of JGA morphology, however it was not clear whether this altered morphology affected function.

To ensure that these phenotypes were not caused by a random mutation introduced during gene targeting, a transgene spanning the *Ren-ld* and *Ren2* genes was used to rescue the phenotype and demonstrated complete restoration of both JG cell granulation and MD morphology (120). Parallel studies using a β-Geo reporter introduced into the *Ren-ld* gene confirmed that ungranulated cells were indeed bona-fide JG cells (120).

These data confirmed that two distinct renin secretory pathways were functioning for *Ren*-1*d* and *Ren*2. The presence of the glycosylation sites on *Ren*-1*d* appears to be key for the correct trafficking of this enzyme onto the regulated secretory pathways. As it is transported through the Golgi, the initial glycosylation of prorenin appears to add directional specificity to the prorenin destined for storage granules. If the renin isoform remains unglycosylated it will follow the constitutive pathway, as evidenced by the lack of dense core storage granules when *Ren*1*d* is not present (100). Furthermore, these studies indicated that *Ren*2 contributes to the maintainance of normal arterial BP, at least in females, but was unable to fully maintain JGA structure.

Following these studies, it was unclear whether Ren-1d protein structure or enzyme activity was causing the granulation and altered MD phenotypes observed in *Ren*1*d*$^{-/-}$ mice. The renin protein is highly conserved between mouse and human, carrying two of the three glycosylation sites present in the mouse (121). Therefore it was hypothesised that appropriate factors were present in the mouse allowing accurately processing and trafficking of human renin through JG cells.

To address these questions, transgenic mice containing a 55kbp human renin transgene on a *Ren*1*d*$^{-/-}$ background were made within the Mullin's Labratory, the *huRen*-Ren1d$^{-/-}$ mice (Dr Robert Nelson, unpublished data). Assuming that the hypothesis

held true, if the renin protein was responsible for the altered granulation and MD morphology, both phenotypes would be restored in this mouse. However, if it was the enzymatic activity causing the morphology shifts, they would not be restored due to the species specificity of renin and angiotensinogen (122, 123). In fact, granulation was restored in huRen$^{+/-}$Ren1d$^{-/-}$ mice in an apparently transgene expression-dependent manner, indicating the importance of the renin protein structure and conservation of functional regions integral to dense core granule formation. However MD morphology remained atypical, suggesting an as-yet undefined role for renin enzyme activity in maintenance of MD structure. However, the role of this altered MD morphology on TGF function and salt handling ability remains to be elucidated.

1.8 Intracellular Signals Controlling Renin Synthesis and Release

Although many aspects of renin synthesis and secretion remain unclear, there is general agreement that cAMP signalling mediates the renin release pathway and calcium signalling mediates the inhibition of renin release within JG cells. The known signalling pathways are collated in Figure 1.7, which is arranged according to the modified Edinburgh Pathway Notation (mEPN) scheme. This notation scheme is particularly good for literature collation since reference management is facilitated through storage in each component, which can also be linked to external webpages or documents.

1.8.1 Cyclic AMP

Renin release is stimulated through receptor binding events complexed with a G-protein coupled receptor (Gnas). Mice with Cre recombinase-mediated deletion of G-protein

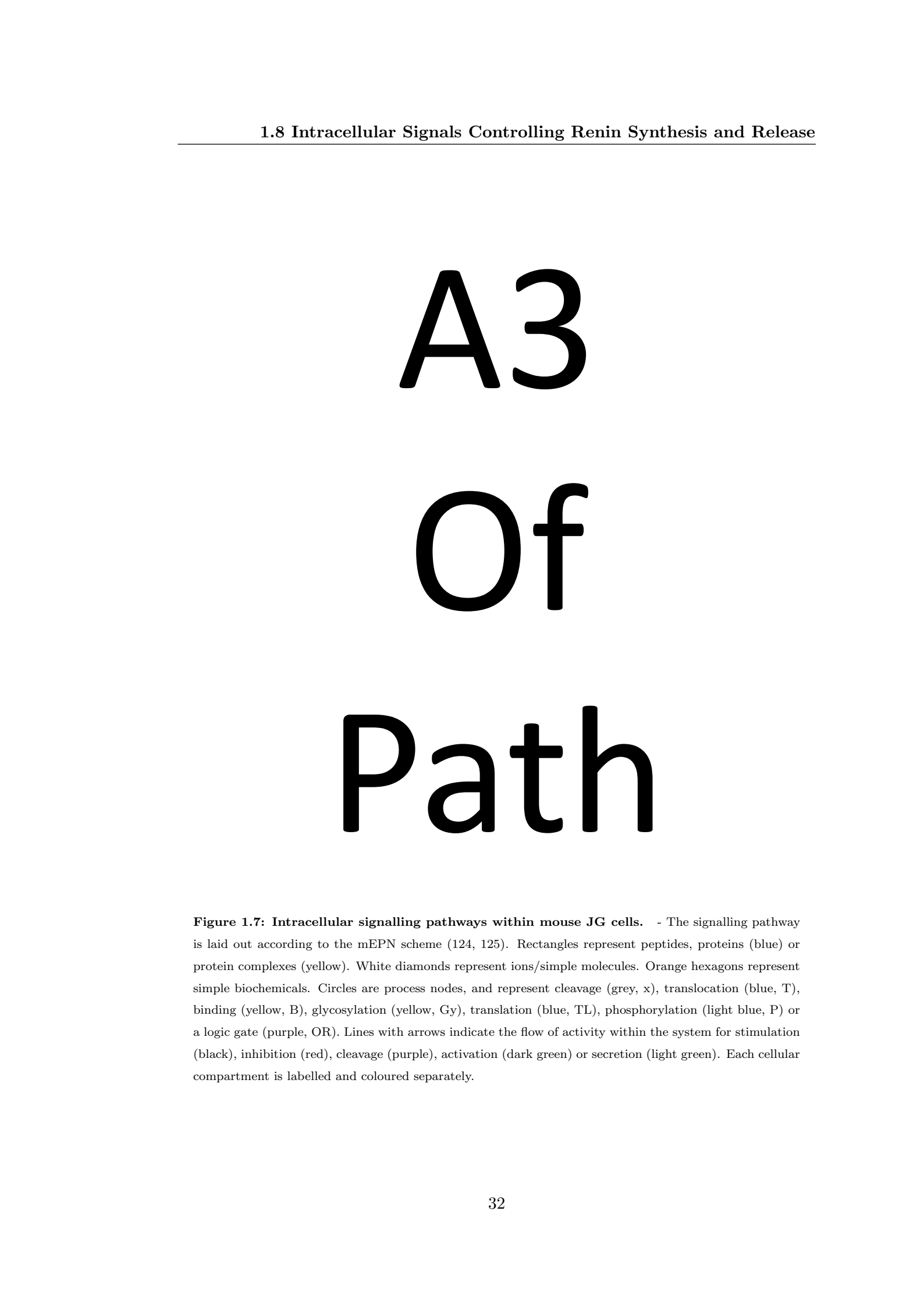

Figure 1.7: Intracellular signalling pathways within mouse JG cells. - The signalling pathway is laid out according to the mEPN scheme (124, 125). Rectangles represent peptides, proteins (blue) or protein complexes (yellow). White diamonds represent ions/simple molecules. Orange hexagons represent simple biochemicals. Circles are process nodes, and represent cleavage (grey, x), translocation (blue, T), binding (yellow, B), glycosylation (yellow, Gy), translation (blue, TL), phosphorylation (light blue, P) or a logic gate (purple, OR). Lines with arrows indicate the flow of activity within the system for stimulation (black), inhibition (red), cleavage (purple), activation (dark green) or secretion (light green). Each cellular compartment is labelled and coloured separately.

Gsα specifically within JG cells showed significantly reduced basal renin expression levels, low plasma renin concentration (PRC) and the abolition of acute responses to isoproterenol (74). Major ligands of Gnas, and hence stimulators of renin secretion through this pathway, are PGE2, which binds to the EP2 and EP4 receptors, and prostacyclin (PGI2), which binds to the prostaglandin IP receptor (24). Patch clamping individual rat JG cells and stimulating them with EP2, EP4 and IP agonists lead to an increase in intracellular cAMP and a decrease in the granule pool present (24). Adenylyl cyclase activating polypeptide 1 (Adcyap) binding to adenylyl cyclase activating polypeptide receptor 1 (Adcyap1r1) also stimulated renin release from isolated perfused kidneys in rat (126). This was confirmed using Adcyap1r1$^{-/-}$ mice, which did not show the increase in renin release seen in C57Bl/6 controls when perfused with Adcyap (126). β-adrenergic stimulation of renin release has also been shown to be particularly effective, with signalling molecules such as cathecholamines stimulating renin secretion *in vivo*, in isolated perfused kidneys and kidney slice models (127, 128, 129). The importance of adrenoreceptor B (Adrb1) was also confirmed using $\beta1/\beta2$ADR$^{-/-}$ mice (130).

These binding events create complexes with Gnas which activate adenylyl cyclases 5 and 6 (Adcy5/6) (131). Using isolated perfused kidneys from Adcy5$^{-/-}$ and Adcy6$^{-/-}$ mice, Aldehni *et al.* showed that isoproterenol-, PGE2- and PACAP-stimulated renin release was attenuated in these mice, proving the involvement of Adcy5/6 in renin stimulation (132). Two different subsets of dopamine receptors have been found in JG cells; Drd1a (133) and Drd5 (134) create complexes with the Gnas receptor and cause the activation of Adcy5/6. This stimulatory effect has been confirmed using isolated JG cells (135), kidney slices, isolated perfused kidneys and *in vivo* (101).

Activated Adcy5/6 leads to the generation of cAMP from ATP (131). cAMP was shown to activate protein kinase A (Pka), which is able to directly lead to the secretion of mature renin from storage granules (72) or is translocated to the nucleus where it phosphorylates the CREB protein, enabling it to bind to the cAMP response element (CRE) in the regulatory sequences of the renin promotor and activate transcription (136, 137).

Inhibitory G-protein coupled receptors act to prevent Adcy activation. Two further dopamine receptors have been found on JG cells, Drd3 and Drd4, which bind with the inhibitory G-protein coupled receptor (Gnai2) to inhibit Adcy5/6 activation (138). It should be noted that the main inhibitory role that dopamine plays in renin secretion is through its effects on the proximal tubule sodium reabsorption and increase in tubular sodium chloride concentration at the MD (101). Adenosine also inhibits renin secretion by binding to the adenosine receptor (AR-1) to complex with Gnai2. Isolated primary JG cell cultures stained positively for the AR1 subtype, and showed decreased renin release after incubation with increasing concentrations of adenosine (139). This adenosine is likely to originate from the MD in response to tubuloglomerular feedback (discussed in Section 1.3.2).

1.8.2 Calcium

In the majority of secretory cell types calcium is the major, if not the only, trigger for the secretion of granular cargo. Intracellular Ca^{2+} levels are regulated by entry of extracellular Ca^{2+} or from release of intracellular Ca^{2+} stores found in the RER (140). Whilst intracellular Ca^{2+} levels are similarly controlled in JG cells, increased levels of Ca^{2+} inhibit both the release and synthesis of renin, both directly and indirectly: this

is termed the 'calcium paradox' (141).

Within JG cells, one of the major regulators of intracellular Ca^{2+} content is receptor binding with natriuetic peptides. The binding of AngII to angiotensin II receptor type 2 (Agtr2), arginine vasopressin (AVP) to arginine vasopressin receptors and endothelin 1 (ET-1) to endothelin receptor type B are all able to active phospholipase C (Plc) (6, 7, 8). Plc then activates the IP3 pathway and ryanodine receptor by cleaving PIP2 into DAG and IP3 (142). IP3 translocates to the RER where it binds with the IP3 receptor, releasing calcium from stores into the cytosol (142). The DAG fragment also contributes to increases in intracellular Ca^{2+} by activating protein kinase C (Pkc), which transiently increases the Ca^{2+} permeability of the cellular plasma membrane, allowing an influx of extracellular Ca^{2+} into the JG cell to further inhibit renin secretion (143).

Free intracellular Ca^{2+} has multiple mechanisms of action. By clamping cAMP using membrane-permeable cAMP derivatives in primary JG cells, increased levels of Ca^{2+} did not suppress renin secretion, indicating that cAMP levels are modulated by Ca^{2+} (141). Furthermore, small interfering RNA (siRNA)-mediated knock down of Adcy5/6 prevented Ca^{2+}-dependent inhibition of cAMP levels, indicating that Ca^{2+} interferes with Adcy5/6 activation (141). Ca^{2+} also activates calmodulin (Calm1) which, along with the calcineurin (CN) that it activates, inhibits the secretion of renin (144, 145).

Very little is known about the mechanism by which Ca^{2+} and Pkc modulate renin synthesis. Since the inverse relationship between Ca^{2+} levels and renin secretion is similar to that of the parathyroid hormone (PTH) from the chief cells of the parathyroid gland, it was hypothesised that the same molecular transcriptional mechanisms

were involved (146). Fuchs *et al.* discovered that a negative calcium response element (nCaRE), identical to a PTH promoter region, was present in the human renin proximal promoter, the mutation of which suppressed the sensitivity of the renin promoter to increased intracellular Ca^{2+} (147). However very little else is known about the transcriptional mechanisms relating to Ca^{2+} inhibition of renin synthesis.

Ca^{2+} has also been shown to interfere with the cAMP release pathway via phosphodiesterases (Pdes). Pde1, 3 and 4 are present in JG cells and reduce renin release by contributing to the breakdown of cAMP to 5'-AMP (148). Whilst Pde4 inhibition has been shown to stimulate renin release (149), Pde3 is the dominant isoform (72). Pde1 is thought to inhibit renin release in a calcium-dependent manner, however Pde3 is the most important isoform in the renin secretory pathway. Pde3 activation is negatively controlled by the cGMP pathway, thereby preventing the breakdown of cAMP, allowing higher levels of renin secretion (149, 150, 151, 152).

1.9 Mechanisms of Renin Release

Whilst the factors affecting intracellular and extracellular control of renin secretion have been well studied, relatively little is known about the mechanisms of secretion and the proteins involved. Initially, classical endocrine exocytosis was thought to be responsible for renin release. Granules are transported to the membrane where fusion and subsequently exocytosis occur through bridging of the vesicle and the plasma membrane (140).

Evidence for exocytotic release of renin lies in observations of discontinuous, quantised release of renin *in vitro* (36). Observations of large, electron-dense granules at the cell membrane in fixed mouse EM sections indicate that granules move to the membrane

to release renin exocytotically (153). The episodic release of renin was confirmed using superfused rat AAs, with approximately 1 exocytosis event recorded every 5 minutes, sufficient to meet physiological demands (154). In mice, this release rate was calculated to be 20 - 500 per minute across both kidneys (153). Membrane capacitance studies of whole-cell patch-clamped primary JG cells were performed under basal and increased cAMP-/isoproterenol-stimulated conditions. 0.9% total renin content was shown to be released per hour under basal conditions (155). This release rate increased to 40% per hour after stimulation with 10 μmol/l isoproterenol, which equated to approximately 7% additional membrane area gained during exocytosis and corresponds to 10 - 20 storage granules released per cell (155). Even under this maximal stimulation, only a subset of storage granules released renin.

Peti-Peterdi *et al.* attempted to visually verify the exocytotic release of renin using isolated perfused rabbit glomeruli (36). A fluorescence resonance energy transfer (FRET) probe system was used to gauge renin secretion, where tissue preparations were bathed in EDANS- and DABCYL-conjugated fluorescence renin substrate. EDANS fluorescence is quenched by the DABCYL acceptor molecule due to FRET but fluoresces on cleavage by renin. Renin granules were stained with the acidotropic fluorophores quinacrine or Lysotracker red (36), which have high binding affinities with granules in JG cells (104). Granular and renin secretory responses to the perfusion of 100 μM isoproterenol through the JGA were imaged using time-lapse multiphoton microscopy. Although no granular trafficking was imaged, individual granule fluorescence was seen to dim and disappear. The renin FRET probe indicated that this quantal release of granular content occurred from both luminal and interstitial compartments of the JGA. It should be noted that images were acquired every 10s for 10 minutes; movement of

granules could potentially occur on a much faster time scale, since exocytosis takes place over tens of milliseconds in neuroendocrine cells (156).

Whilst granule tethering to the membrane and associated omega-shaped membrane configurations typically associated with exocytosis have been reported (153), deep invaginations into the interior of JG cells containing electron-dense material have also been interpreted as stages before or after exocytosis (157). It has been implied that instead of the direct movement of the vesicles, as is the case during exocytosis, these invaginations could provide a route through which renin is released (101). Renin release may therefore resemble lysosomal secretion, a hypothesis which is reinforced by the lysosomal nature of storage granules. As well as the positive staining for lysosomal enzymes within renin storage granules (106) and the acidic pH within granules, the lysosomal trafficking protein Lyst is necessary for correct granule formation (102).

Steppan *et al.* performed 3D EM analysis on JG cells from isolated perfused kidneys on SCID-beige mice with this Lyst mutation and showed that only 1 - 2 large storage granules were present (113). When this 3D reconstruction was applied to C57Bl/6 mice, granules appeared in different stages of formation, from isolated granules up to large interconnected granular networks, suggesting that granule development may be dynamic and interchangeable. No signs of exocytosis was visualised at baseline, or in cells in which renin secretion had been stimulated by isoproterenol alone. However simultaneous perfusion of isoproterenol and ethylene glycol tetraacetic acid (EGTA) resulted in a 20-fold increase in renin secretion and approximately five exocytotic events per cell (113). This evidence points towards compound exocytosis of renin from JG cells, where intracellular fusion of vesicles forms large storage networks which fuse focally with the plasma membrane, releasing the contents of the vesicle whilst retaining

granular structure.

The contradictory nature of the literature in this area is clear, with no instances of granule motion under any conditions published to date. Despite this, exocytosis appears the most likely mechanism by which renin is secreted. However there is a paucity of direct evidence for the mechanisms involved in renin release and the identity of the proteins involved in granule-membrane binding. In classic exocytosis, membrane-bound SNARE proteins on the surface of vesicles (*v-SNARES*) and the target membrane (*t-SNARES*) mediate fusion to the target membrane by creating trans-SNARE complexes (140). This is initiated when syntaxin is released from its complex with munc18, allowing complexing of the membrane SNAP and syntaxin proteins with the vesicle VAMP protein, causing the lipid bilayers to fuse (Figure 1.8). Vesicles which initially dock either immediately uncouple or are strongly tethered through the action of soluble NSF (*N*-ethylmaleimide-sensitive factor), moving into a fusion-competent state (158). These SNARES have been shown to be essential for exocytosis to occur through genetic ablation in *Drosophila*, *C. elegans* and *Mus Musculus*. There are many different isoforms of the main proteins involved, with exocytosis from distinct organelles within a single cell involving distinct SNARE combinations (159).

Studies by Mendez *et al.* showed that the SNARE proteins VAMP2 and SNAP23, but not SNAP25, are present both on the surface of dense core granules and the plasma membrane in primary JG cells, and that they mediate cAMP-stimulated renin release (76, 160). SNAP23 was only found on a small subset of granules and siRNA knockdown experiments suggest that this isoform may only mediate release from dense core granules on the regulated pathway (160).

Phosphorylation of SNAP25 by constitutive Pka activity has been shown to be

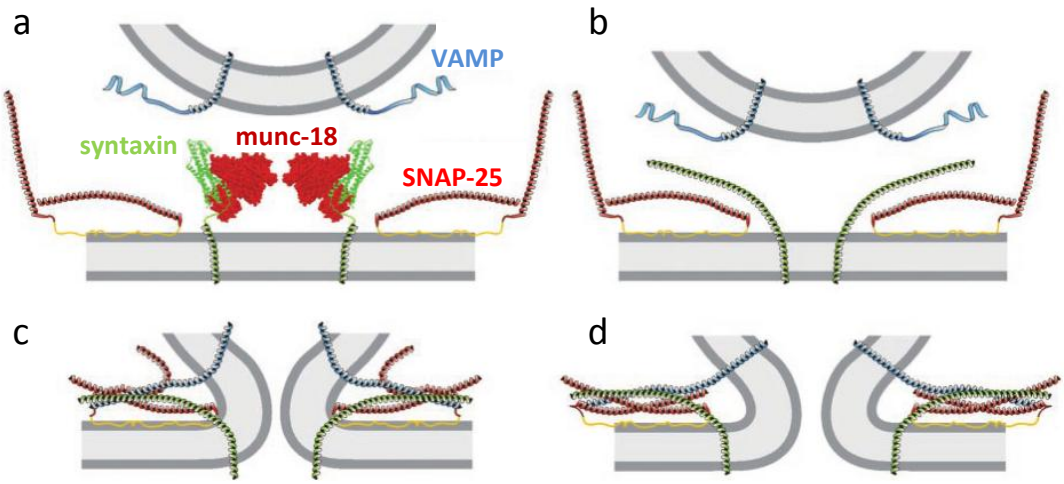

Figure 1.8: SNARE-driven membrane fusion model. - (a) Munc-18 is complexed with syntaxin at the membrane, leaving it unavailable. (b) When the granule approaches, syntaxin is released from munc-18, opening up the conformation for binding within the SNARE complex. (c) The SNARE complex is formed between syntaxin, SNAP and VAMP, and the four helix bundle assembled. (d) The close proximity of the plasma membrane and granule lipid bilayers allows bilayer fusion to occur. Image from Burgoyne, R and Morgan, A (140).

necessary to maintain large numbers of primed secretory vesicles, whilst calcineurin antagonised this effect (161). As previously outlined, Pka facilitates renin release whilst calcineurin, activated through the Ca^{2+} - Calm1 pathway (144), inhibits renin secretion (145). Phosphorylation of SNAP23 has also been shown to facilitate exocytosis in mast cells (162), however this phosphorylation was carried out by Pkc, which is known to inhibit renin release. Even more intriguingly, the practically ubiquitous interaction of Ca^{2+} with SNARE-complexing proteins is a trigger for exocytosis; synaptotagmin proteins are Ca^{2+} sensors which interact with SNARE complexes to mediate secretion, not as an inhibitor as is the case for JG cells (140).

1.10 Aims and Hypothesis

Although renin is a critical physiological enzyme, many fundamental questions remain unasnwered, particulary with regards to the generation of granules and secretion of renin from dense core granules within JG cells. I hypothesise that renin is released exocytotically, and that for this to occur granules respond dynamically to exocytotic stimulus. It is clear that appropriate *in vitro* models in which to answer many of these questions are required. I therefore aim to develop an appropriate *in vitro* JG cell model and to use it to image and analyse granule dynamics in juxtaglomerular cells for the first time.

Furthermore, I hypothesise that expression levels of renin dictates the extent of intracellular granule formation, and that altered macula densa morphology such as that seen in $\text{Ren1d}^{-/-}$ and $\text{huRen}^{+/-}\text{Ren1d}^{-/-}$ mice is indicative of altered tubuloglomerular feedback, suggesting that active renin is necessary for normal TGF function. I therefore aim to elucidate the relationship between renin expression levels, granulation of juxtaglomerular cells, macula densa morphology and macula densa function using an isolated perfused juxtaglomerular apparatus model and electron microscopy.

2

Materials & Methods

2.1 Standard Solutions

Recipes for the standard solutions used are found in Table 2.1.

2.2 Animal Husbandry

2.2.1 Maintenance of Colony

Experiments were conducted in accordance with the Animals (Scientific Procedures) Act 1986 and the Guiding Priciples for Research Involving Animals and Human Beings as well as approved by the Institutional Animal Care and Use Committee of the University of Southern California. The sources of the animals used are outlined in Table 2.2.

Mice were housed and bred in the Biological Resource Facilities at the University of Edinburgh or at the University of Southern California. To identify and genotype animals, ear clippings were taken. A 12 hour diurnal cycle was maintained (7AM - 7PM), with free access to water provided. Mice were maintained on a standard

Reagents and Buffers	Recipe	Supplier
1X PBS	10 tablets, 1 L ddH_20	OXOID (BR0014G)
4% PFA	4% w/v paraformaldehyde in PBS 1M NaOH used to adjust pH to 7.2	Sigma (D2650)
0.5 M EDTA	EDTA in dH_20, 1M NaOH to adjust pH to 8.0	VWR Chemicals (443885J)
TBE buffer (5X stock)	54 g Tris base, 20 ml 0.5 M EDTA (pH 8) 27.5 g boric acid, per 1 L	VWR Chemicals (192346H)
TAE buffer (50X stock)	121 g Tris base, 50 ml 0.5 M EDTA (pH 8) 28.6 ml glacial acetic acid per 500 ml	Promega (H5135) VWR Chemicals
0.2 M Phosphate Buffer A: $Na_2HPO_4.2H_2O$ B: $NaH_2PO_4.2H_2O$ Working solution	 35.6 g in 1 L dH_2O 13.8 g in 500 ml dH_2O 72 ml A, 28 ml B, 100 ml dH_2O pH adjusted to 7.2	Fisher Scientific (S/P525/53) (11462904)
Goat or Donkey Blocking buffer	5% Goat or donkey serum, PBS, 0.3% Triton X-100	Jackson Sigma (79284)

Table 2.1: Table detailing standard solutions used.

mouse chow containing 0.25% Na, 0.38% Cl, 0.67% K, Rat and Mouse Maintenance diet (RM1). Environmental conditions were maintained at $19 - 21\,^{\circ}C$ and 40 - 55% humidity. The genetic backgrounds of the mice used in the current study are detailed below.

RenGFP$^{+/-}$ Mice

Mice with a targeted knockin of GFP into exon 1 of the renin gene in animals on a single renin gene (Ren1c) background have previously been described (163). In sum-

Strain	Origin	Reference
RenGFP$^{+/-}$	Prof. Kenneth Gross Roswell Park Cancer Institute, Buffalo	(11)
tsA58$^{+/-}$	Prof. Parmjit Jat Ludwig Institute, London	(82, 83)
Ren1d$^{-/-}$	Prof. John Mullins	(114)
huRen$^{+/-}$Ren1d$^{-/-}$ 1446 and 1317 strains	Prof. John Mullins	Dr Robert Nelson (Paper in preparation)

Table 2.2: Source of experimental animal strains.

mary, GFP was introduced into exon 1 of Ren1c within a BAC clone (RP23-88k07) using homologous recombination, ensuring that GFP expression was under the control of the natural genomis sequence of renin (163). Restriction analysis and pulsed field gel electrophoresis confirmed correct insertion of GFP, and zygotic microinjection performed and implanted into female mice. PCR screening was used to identify animals positive for insertion of the construct, and the insertion of a single copy of the transgene confirmed using Southern Blot analysis and ImageQuant software.

GFP is therefore expressed in renin-expressing cells where it is localised cytoplasmically. It is under the control of the renin promoter but is not fused to the renin gene; having been inserted into a random section of the genome, it is not packaged into granules or secreted. RenGFP mice could therefore be bred as either heterozygotes or homozygotes, however the line was bred as heterozygotes to ensure that GFP was not overexpressed within JG cells.

Glenn *et al* (163) showed that GFP reporter mice faithfully recapitulate the developmental and physiological expression of kidney renin, which was detected at the classic

JG cell location at the distal end of the AA. Treatment with the ACE inhibitor captopril (10 mg/kg intraperitoneal injection; 3 days) induced the metaplastic transformation of VSMCs to GFP-expressing renin-expressing cells along along the afferent arterioles, interlobular and arcuate arteries, consistent with previous reports of endogenous mouse renin expression (9). GFP was also observed in the granular convoluted tubules of the submaxillary gland, another known site of renin expression in mice (164), along with expression at e13 in the cords of the adrenal gland, and at e14 in the renal and intrarenal arteries (11). GFP expression continued to follow known renin expression patterns at e15 and e16 (11, 42).

Ren1 Knockout Ren1d$^{-/-}$ Mice

The *Ren*1*d*$^{-/-}$ mouse was generated using a *Ren*1*d* targeting construct for the 129 mouse renin locus with appropriate 5' and 3' homology arms and a neomycin cassette replacing 92 bp of exon 3, intron 3 and 35 bp of exon 4 (114). Homologous recombination between the linearized targeting construct and the endogenous *Ren-1d* gene after electroporation into 129 mouse embryonic stem cells inactivated *Ren-1d*. Clones showing appropriate targeting were chosen, one of which was used to generate male chimaras via microinjection. These animals were crossed with 129 females to generate heterozygous offspring, with F2 breeding leading to lines with the desired homozygous *Ren*1*d* deletion (114). These animals were then crossed onto a C57Bl/6 background.

Human Renin Rescue huRen$^{+/-}$Ren1d$^{-/-}$ Mice

The human renin transgenic lines were made in our laboratory by Dr Robert Nelson (paper in preparation) and were bred in the Mullins laboratory. A 55kbp fragment of clone PAC111L11 which contained the 35kb flanking sequence around 10kb structural human renin gene introduced by pronuclear microinjection into fertilized C3H x

CBA/Ca F1 oocytes on a *Ren*1*c* background. Animals with correct insertion of the transgene were identified by PCR and digestion of tail DNA, which was analysed by Southern blot hybridisation. These animals were crossed onto a $Ren1d^{-/-}$ background over many generations.

Of 20 offspring, four showed correct targeting, of which two were fertile - the 1317 and 1446 lines. Line 1446 was used in the current study. Appropriate crosses were made to ensure animals of these lines were on a $Ren1d^{-/-}$ background, which were confirmed by Southern Blot analysis in F1 and F2 litters. Therefore these animals lack the *Ren-1d* gene necessary to granulate JG cells, but have the active human renin (*hRen*) gene randomly inserted into their genome, under the appropriate renin promoter sequences.

2.2.2 Pharmacological Manipulation *in vivo*

Stimulation of the Macula Densa

For low-salt-mediated stimulation of the macula densa, a low salt diet and increased salt wasting using chronic administration of an ACE inhibitor was performed. Mice were placed on a sodium-deficient diet (Harlan Teklad, TD.90228) containing 0.01-0.02% Na, 0.07% Cl, 0.8% K and 0.2 mg/ml captopril (Sigma, C4042) dissolved in the drinking water for five days.

Stimulation of Renin Expression

To increase renin expression levels through decreased ANGII-mediated renin inhibition, chronic administration of an ACE inhibitor was performed. Captopril (Sigma, C4042-5G) was administered dissolved in the drinking water at 1 mg/ml for 7 or 10 days.

2.2.3 Genotyping

2.2.3.1 Digestion of Ear Notches

Ear punches were digested with agitation overnight at 55 °C in 80 μl DirectPCR Lysis Reagent (Viagen Biotech, 102-T) with 80 μl dH_2O and 4.8 μl proteinase K (10 mg/μl working concentration, Ambion, Life Technologies, AM2548).

Heat inactivation of the proteinase K at 85 °C on a heat block (Stuart, SBH130D) for 1 hr was followed by centrifugation at 13,000 g for 1 min. Samples were stored at −20 °C.

2.2.3.2 PCR Genotyping Reaction

PCR reaction mixes were made up by adding 5 μl VWR 2 mM $MgCl_2$ Red Taq DNA Polymerase 2X Mastermix to 0.2 μl 10 mM forward and reverse primer each, 4.1 μl ddH_2O and 0.5 μl sample DNA. Primer pair sequences are detailed in Table 2.3. For each sample, a PCR reaction for nNOS was also performed as a positive control to ensure successful extraction of DNA. Example PCR products run out in gel electrophoresis are shown in Figure 2.1.

Samples were cycled in a ThermoCycler (Applied Biosciences, Veriti 96 well) at temperatures detailed in Table 2.4 in order to denature, anneal and extend DNA segments, amplifying them for visualisation. All genotyping reactions were performed using the same mastermix and primer concentrations, and amplified as outlined.

2.2.3.3 Agarose Gel Electrophoresis

PCR amplification products were separated on a 1X TAE-buffered 1.5% (w/v) agarose gel (SeaKem LE Agarose, Lonza, 50050). 1 μg/ml ethidium bromide (Sigma, 46066)

Gene to Amplify	Direction (5' - 3')	Sequence	Product Length (bp)
GFP Cassette	F	AGCAAGGGCGAGGAACTGTTCACTG	594
	R	GGTGGACAGGTAATGGTTGTCTGGG	
Human Renin	F	AACCTCAGTGGATCTCAGAGA	394
	R	CTCTGGGCAGGAAGCAAAAGT	
Mouse Renin	F	CCAAGCTGGAGACTCAGGAA	Ren2: 139
	R	TAGAAGGCTCAGAGGCAGGA	Ren1c: 111
Ren1d	F	GGCTGAACCAGATGGACAGA	500
	R	AACTCTCTCGCCAAAGCCAAAG	
Immortomouse	F	CCTCTGAGCTATTCCAGAAGTAGTG	590
	R	TTAGAGCTTTAAATCTCTGTAGGTAG	
nNOS	F	CGTCATTTCTGTCCGTCTCTT	657
	R	ATTCCTGTGTCTTTCATCTCTGC	

Table 2.3: Primer sets used to genotype RenGFP$^{+/-}$, HuRen$^{+/-}$Ren1d$^{+/-}$, Ren1d$^{-/-}$ and Immortomice tsA58$^{+/-}$.

was added to allow visualisation of DNA.

Samples were loaded alongside a 100 bp molecular weight ladder (Gene Ruler DNA Ladder or New England Biosicences 100 bp ladder) for fragment size analysis. After electrophoresis, the gel was visualised on a UV Transilluminator (UVP inc.) with an Olympus C-4000 digital camera attached.

2.3 Cell Isolation Techniques

All standard cell culture media and buffers are detailed in Table 2.5. All cell culture medium, PBS, fetal calf serum (FCS), penicillin/streptomycin (pen/strep), collagenase, trypsin EDTA (TE), ITS were purchased from Life Technologies. All media were filtered

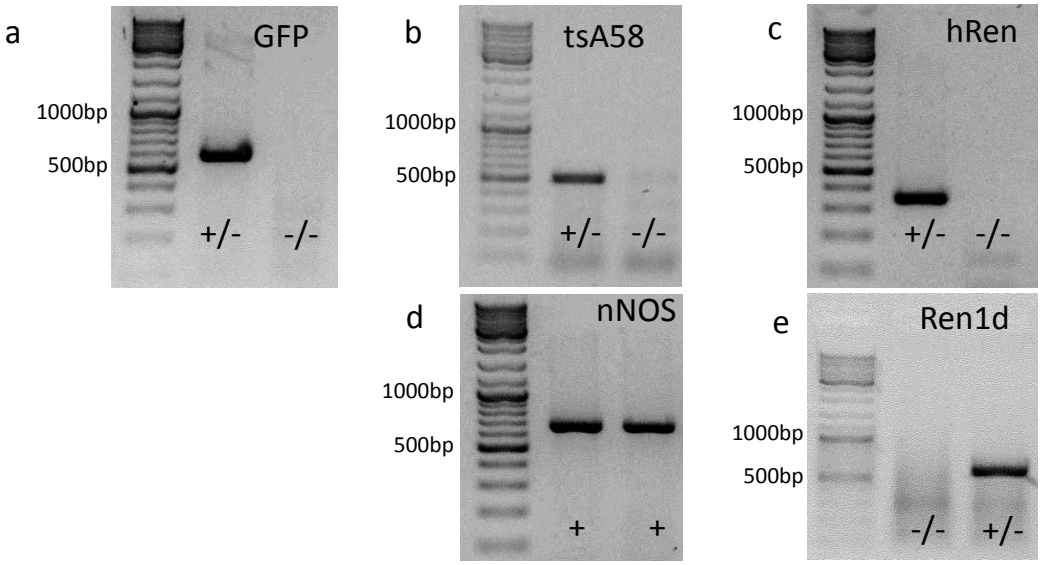

Figure 2.1: Representative gel electrophoresis images of genotyping PCR products. - The presence of (a) GFP to identify RenGFP$^{+/-}$ animals, (b) tsA58 to identify immortmouse tsA58$^{+/-}$ animals, (c) hRen to identify HuRen$^{+/-}$Ren1d$^{-/-}$ animals, (d) nNOS for the internal control and (e) Ren1d to differentiate between Ren1d$^{+/-}$ and Ren1d$^{-/-}$ animals was assessed by PCR. GeneRuler ladder was used to identify molecular weight of PCR products.

through a 0.22 μm filter (Millix, VWR, 20842.323) before use and stored at 4 °C.

2.3.1 Cell Isolation Procedure

2.3.1.1 Dissociation of Adult Kidneys

Animals were sacrificed by cervical dislocation, the kidneys dissected out and decapsulated, and placed in ice cold basic medium. Under a tissue culture hood, the kidneys were diced finely with sterile blades in a petri dish. The homogenate was transferred to 5 ml pre-warmed digestion buffer (Table 2.5) and incubated in a shaking waterbath (30-45 mins, 37 °C, 150 rpm), titurated by pipette every 15 mins until the digestion was complete.

The digestion was stopped using 15 ml basic medium. The homogenate was passed

Temperature (°C)	Duration	Number of Cycles
94	4 mins	1
94	10 mins	35
60	30 secs	
72	1 min	
72	7 mins	1
4	∞	-

Table 2.4: Temperature cycles used to amplify DNA extracted from ear notches for genotyping of animals.

through a 100 μm sieve (Fisher, 22363549) to remove any fibrous tissue and a 70 μm sieve (Fisher, 22363548) to remove contaminating tubular fragments. Cells were pelleted by centrifugation at 139 g for 8 mins and the supernatant discarded. Pelleted cells were resuspended in 1 ml red blood cell lysis buffer (Sigma Aldrich, R7757) and incubated at room temperature for 2 mins. 20 mls PBS was added and the mixture vortexed, before pelleting the cells by centrifugation for 5 mins at 139 g. The pellet was resuspended in 1 ml sorting medium, the cells counted then filtered through a 40 μm cell strainer to remove remaining tubules and glomeruli.

2.3.1.2 Dissection and Dissociation of Immortomouse$^{+/-}$ Embryonic Kidneys

Pregnant mothers were sacrificed by cervical dislocation and the uterus placed in ice cold PBS. Under a dissecting microscope, embryos were dissected from the uterus in a petri dish containing fresh DMEM. Using two 1ml syringes with 20 gauge needles attached, the embryos were decapitated using a scissor-like motion and the torsos transferred to a separate petri dish containing fresh DMEM. Manipulating the embryos with the syringe and needles, they were placed face down in the dish and the forelimbs

Medium Type	Recipe
Kidney digestion buffer	Prewarmed DMEM, supplemented with collagenase I, II, IV (1 mg/ml final conc.)
Basic culture medium	DMEM, 10% FCS
Sorting medium	PBS, 2% FCS
Primary culture medium	DMEM, 10% FCS, 1X Pen/Strep
Immortalisation medium	1:1 DMEM/F:12, 10% FCS, IFN-γ (Peprotech, 315-05) at 100 μg/ml 1% ITS, 1X glutamine, 1X pen/strep 1X antioxidants (Sigma, A1345)
ROCK inhibitor medium	Immortalisation medium, 10μM Y-27632 (Tocris, 1254)
Freezing medium	$^{8}/_{10}$ DMEM, $^{1}/_{10}$ DMSO (Sigma, D2650), $^{1}/_{10}$ FCS
Dissection medium	1:1 DMEM/F:12, 1.2 g/l sodium bicarbonate, 3% FCS (pH 7.4)

Table 2.5: Standard medium used in cell and tissue culture.

and tail removed. One needle was used to scour gently down the spine, cleanly halving the fetus. The kidneys were located by disturbing surrounding tissue and finding the end of the mesonephros, gently prying them out to be transferred to a fresh collection dish containing immortalisation media (Table 2.5).

Kidneys were cultured on transwell membranes as described in Section 2.3.1.3. To digest the kidneys, they were removed from the membranes and placed in a 0.5 ml eppendorf tube containing 200 μl 1X TE and incubated at 37 °C for 5 mins. 200 μl DMEM primary culture medium were then added and the kidneys titurated until the cells were fully dissociated. Cells were pelleted and resuspended in sorting medium.

2.3.1.3 Embryonic Kidney Culture

Embronic kidneys (dissected as described in Section 2.3.1.2) were cultured on 24 mm transwell membrane inserts of 0.4 μm pore size (Corning, 3450) in 6 well plates; 6 kidneys were evenly spaced around a single transwell containing basic culture medium below. After 48 hours in culture at 37 °C, the culture medium was changed to ROCK inhibitor medium (Table 2.5) for 24 hours, then immortalisation medium for 24 hours. The transwell membranes were then removed and the kidneys taken forward for dissociation and sorting.

2.3.2 Flow Cytometry

For flow cytometry, the cells isolated in Section 2.3.1.1 were placed in a suspended beam and analysed with lasers positioned both in line with the beam, giving forward scatter (FSC) information, and perpendicular to it giving side scatter (SSC) information. FSC correlates with cell volume and SSC with cell complexity. If cells are tagged with fluorophores or fluorescent proteins, these can be excited by the lasers and the resulting fluorescent signal collected to derive information about the physical and chemical properties of the cells.

2.3.3 Sorting of GFP Positive Juxtaglomerular Cells

To sort GFP-positive cells, negative control gates were first set up. A control $RenGFP^{-/-}$ kidney digest was performed and the cells run through the FACS ARIA II cytometer, with analysis performed on FACSDiva v6.0 software (Figure 2.2). Appropriate FCS gating was used to eliminate cell doublets (a) and small debris from the isolation procedure (b). The live-dead marker DAPI (Life technologies, P-36931) was added (d) and

cells evaluated for their GFP and DAPI expression; control kidneys were $RenGFP^{-/-}$, therefore this gate was created to encompass the GFP-positive, DAPI-negative area on the plot and hence contained no cells. The control $RenGFP^{-/-}$ digest was then removed, the sample of interest loaded into the machine and the cells sorted using the same gates, yielding GFP-positive, DAPI-negative cells.

2.4 Cell Digestion and Isolation using a Percoll Gradient

RenGFP$^{+/-}$ mice, which had been treated with captopril for 7 days, were sacrificed by cervical dislocation and the kidneys digested as outlined in Section 2.3.1.1.

A Percoll (Sigma, P4937) gradient was created by layering 5 mls each of 50% Percoll (DMEM + phenol), 40% Percoll (DMEM − phenol), 30% Percoll (DMEM + phenol), 20% Percoll (DMEM − phenol) and 10% Percoll (DMEM + phenol), all supplemented with 10% FCS, into a 30 ml glass test tube. The resuspended cell suspension was then applied to the top of the gradient and centrifuged (27,000 g, 4 °C, 30 mins) in an SS-34 rotor/ Sorvall RC 5CPlus centrifuge.

Appropriate bands were removed using a sterile pasteur pipette, discarding the layers containing low-density fragments and cells, pooling the cells at the expected JG cell density (1.07 g/ml^3, (73)). This pooled subset was diluted with 20 ml primary culture medium and the cells pelleted by centrifugation at 139 g for 8 mins. This pellet was resuspended in 2 mls primary culture medium, passed through a 40 μm cell strainer, counted using a standard haemocytometer and plated appropriately for the experiment (outlined below).

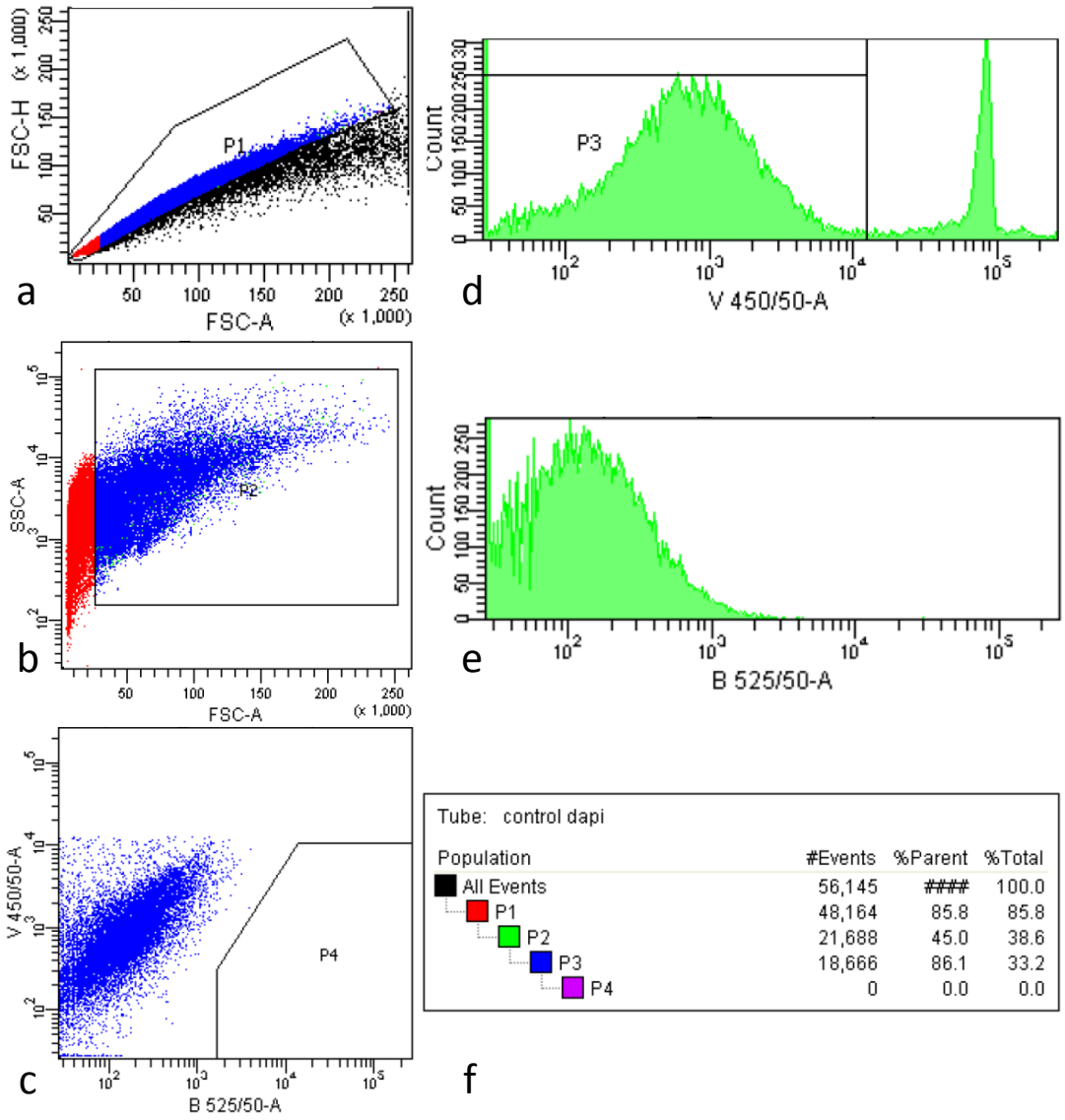

Figure 2.2: Gating used for FACS sorting of juxtaglomerular cells. - Using cells from control $RenGFP^{-/-}$ kidney digests, (a) singlet cells were gated on by plotting the forward scatter area (FSC-A) against forward scatter height (FSC-H). (b) The population of live, single cells were gated on by plotting the FSC-A of the singlet cells against the side scatter area (SSC-A), P2. (d) Gating on this population, cells negative for the live-dead marker DAPI were gated on. (c) The 525 nm laser was used to assess the GFP autofluorescence of these cells and the 450 nm laser to assess their DAPI fluorescence to create a GFP-positive, DAPI-negative gate (P4). This population is GFP-negative from the control $RenGFP^{-/-}$ cells (e), and the percentage of cells in each gating shown (f). All sorting was performed on a FACS ARIA II cytometer, with analysis performed on FACSDiva v6.0 software.

2.5 Cell Culture Techniques

2.5.1 Coverslip Preparation

Cleaning Process

25 mm diameter coverslips (SLS, MIC3350) for live cell imaging were cleaned prior to plating cells to remove dust and dirt. Coverslips were immersed in 0.1 M NaOH/0.1% Decon-90 solution for 30s followed by sequential immersion in three 1 litre beakers of dH_2O. They were then submerged in 250 ml fresh 100% ethanol, 100% acetone and then washed in a beaker of 1 litre dH_2O to remove any remaining solvent before being placed in dH_2O.

Coverslip Coating

Fibronectin (Sigma, F1141), laminin (Sigma, L2020), poly-D-lysine (PDL) (Sigma, P6407) and collagen IV (R& D, 3410-010-01) were used to coat coverslips (50 μg/ml).

For fibronectin, PDL and collagen IV coating, coverslips were placed in the appropriate diluted coating and incubated for 1 hr with gentle agitation. For laminin coating, coverslips were first incubated for 1 hr with poly-D-lysine (100 μg/ml) followed by a further 1 hour incubation in 50 μg/μl laminin.

Lab tissue soaked in 70% ethanol was allowed to dry in a laminar flow hood; coated coverslips were placed individually on the tissue and air dried in the flow hood under UV for 1 hr. The base of a 6 well culture dish was scoured and the clean, coated sterile coverslips were placed in the wells and stored at 4 °C for use.

Matrigel (BD, 354230) was prepared by thawing on ice and 25 μl added to 10 mL medium, applied to the well and left for 45 mins before being removed.

2.5.2 Maintenance of Cells

Cells were cultured at 37 °C (unless otherwise stated) in 5% CO_2, 95% air in an HeraCell (Heraeus) incubator in Thermo Biolite cell culture flasks (25 cm^2 or 75 cm^2) with a vent lid until > 90% confluency was reached. Media and reagents were warmed to 37 °C in a waterbath before use.

2.5.3 Culture of Immortomouse tsA58$^{+/-}$ Cells

Sorted cells were initially plated on matrigel for 24 hours at 37 °C in ROCK inhibitor medium (Table 2.5) before being transferred to an incubator at the permissive temperature of 33 °C. After 24 hours in this medium, cells were then placed in immortalisation medium and cultured in this medium thereafter.

Cells were initially plated in a 96- or 48-well plate (dependent on the number of cells sorted) and cultured until confluent. Cells for imaging were plated on glass coverslips coated with 5 $\mu g/cm^2$ fibronectin as described in Section 2.5.1. Cells were imaged in phenol-free primary culture medium (Table 2.5).

2.5.4 Culture of Primary Juxtaglomerular Cells

For widefield and TIRF microscopy live cell imaging, freshly isolated cells were transferred to parafilm-sealed cryotubes and placed in a flask containing pre-warmed autoclaved water at 37 °C. These were then taken to Heriot Watt University, Edinburgh within 1 hour and the cells plated there on fibronectin-coated coverslips.

Primary JG cells were cultured in pre-warmed phenol-free primary culture medium at 37 °C in 5% CO_2. Cells were cultured for less than 24 hrs for all live cell imaging experiments, and for a maximum of 72 hrs for staining experiments.

2.5.5 Passaging Cells

At confluency, medium was aspirated and cells were washed 3 times in room temperature PBS. The appropriate amount of TE (1 ml/25 cm^2 flask) was added to detatch cells, and the flask left at 37 °C for 5 mins or until a single cell suspension had been attained. 9 ml pre-warmed basic medium was added to the flask to inactivate the TE, and the cells pelleted at 139 g for 3 mins. Cells were then resuspended in the appropriate medium and a quarter transferred to a fresh flask for culture.

2.5.6 Cryopreservation of Cells

Cells were passaged as outlined in Section 2.5.5 but were resuspended in freshly-made, filtered freezing medium (Table 2.5).

The resulting cell suspension was placed in a freezing tube (CryoPure, Starstedt, 73.377) and transferred immediately to the −80 °C freezer where it was stored for no longer than a week before being transferred to storage in liquid nitrogen (−230 °C).

2.5.7 Cell Counting

1 μl single-cell suspension was diluted in 9 μl PBS, added to 10 μl Trypan Blue (0.4%, Sigma, T8154) and mixed well. 10 μl was applied to a Hemocytometer (Neubauer, Hawksley) and the number of non-trypan blue stained cells counted.

2.5.8 Renin Induction

To induce renin expression, cells were plated on 6 well plates at a seeding density of $0.3x10^6$ per well. After adhering overnight, FCS-free medium was applied to the well for 24 hrs prior to induction. The medium was then replaced with 2 ml FCS-free DMEM

containing 10 μM forskolin (Cell Signaling, 38285) and 100 μM IBMX (Sigma, I7018) for a further 24 hrs. Cells were then washed in PBS 3 times, 500 μl Trizol (Ambion, 15596018) added to each well, titurated and the resulting mixture removed and stored at $-80\,^{\circ}$C until needed.

2.5.9 Fixation and Mounting of Cells

Cells cultured on coverslips were washed twice with PBS, fixed in 4% PFA for 20 mins, and washed twice in PBS. Cells were then incubated in 50 mM NH_4Cl for 10 mins and washed 2 times with PBS.

To mount cells cultured on coverslips, coverslips were air dried and Prolong Gold antifade mountant with added DAPI to the centre of the coverslip. Coverslips were then placed on a glass slide and left overnight in the dark at room temperature. Nail varnish was applied to the edge of the coverslip to fix the coverslip in place and the slides stored at $4\,^{\circ}$C.

2.6 Microperfusion of Isolated JGA

2.6.1 Pipette Preparation

Pipette Type	Outer Diameter (inches)	Inner Diameter (inches)	Divisions at bottom	Length of pipette (mm)
Holding	0.084	0.064	2-3	45-50
Glomerular holding	0.084	0.064	2-3	45-50
Perfusion	0.047	0.04	< 1	120

Table 2.6: Parameters for perfusion pipettes used during microperfusion experiments.

All pipettes were from the Drummond Scientific Company, and manipulated in a

single stage glass microelectrode puller (Narishige Scientific Instrument Lab, Model PP-830). I assisted with creation and assembly of perfusion pipettes, which were performed by Professor Janos Peti-Peterdi. A fresh pipette of the appropriate dimensions (Table 2.6) was placed into the chuck and lowered into a platinum heating element loop, in close proximity with the glass sphere heating element. This was used to form a hook on the end of the pipette. Adding a weight to the hook, the pipette was further heated whilst rotating to elongate the pipette until it was the appropriate number of divisions in width (Table 2.6). This process is shown schematically in Figure 2.3 (a). The base of the pipette was then cut off cleanly at approximately the correct length using the heating element. The pipette end was then lowered to heat the bottom to ensure all debris from the cutting process was eliminated. For the glomerular holding pipette, the heating element was finally used to bend the pipette approximately 30 °.

2.6.2 Perfusion Pipette Assembly

The perfusion and holding pipette holders were thoroughly washed with Kreb's Ringer Solution, made up as outlined in Table 2.7. The setup of the assembly is shown in Figure 2.3 (b). The perfusion pipette was filled with Kreb's Ringer solution and advanced backwards into the apparatus through the holding pipette holder and sealed at the perfusion pipette holder. The perfusion pipette and holder were then pulled back such that the tip of the perfusion pipette was within the holding pipette holder. The holding pipette and its holder were then filled with Kreb's Ringer solution. The holding pipette was then advanced backwards into the holding pipette holder and tightened. The perfusion pipette and its holder were then gently moved towards the holding pipette until they were approximately 1 cm from the end of the holding pipette.

To construct the exchange pipette, the plastic mount was removed from a P20 precision glide needle and an exchange pipette of 0.02 inch outer diameter, 0.064 inch inner diameter with glue applied around the edge was inserted into the needle and fixed. The exchange was then inserted through the back of the perfusion pipette holder and pipettes were aligned. The apparatus was then secured onto the micromanipulator on the microscope, with the holding pipette connected to a syringe to create a vacuum whilst the perfusion pipette was connected to a glass reserve with a valve attached to create pressure. The exchange pipette was connected to the pressurised perfusate syringes.

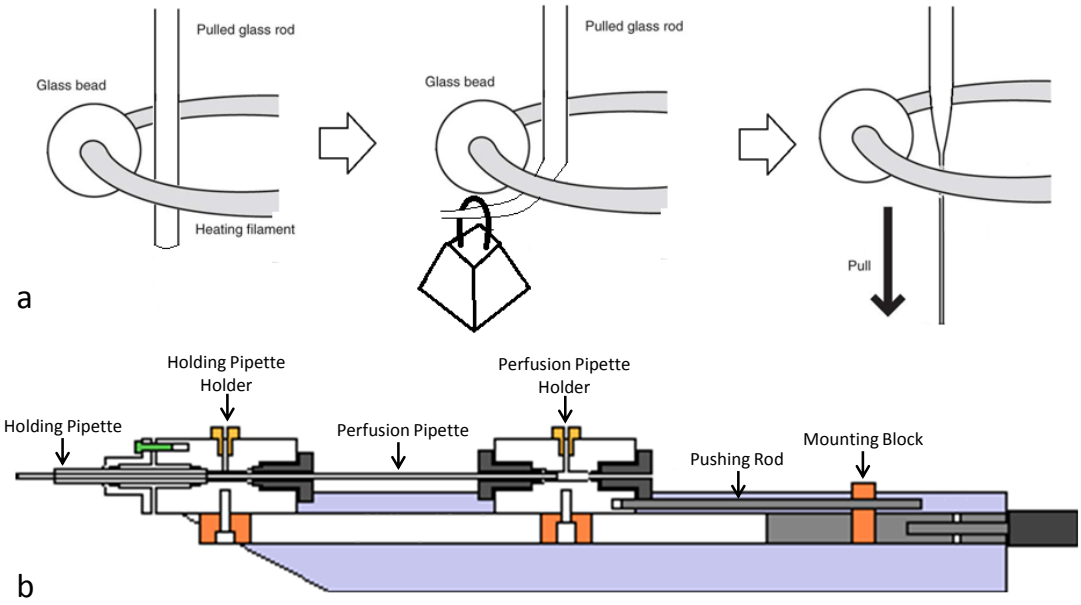

Figure 2.3: Schematic representation of pulling and assembly of perfusion pipettes. - (a) Perfusion pipettes were pulled by manipulating a glass rod with a heating element to create a hook. A weight was added to the hook and the pipette rotated to pull the glass rod to the appropriate thickness. (b) Schematic image of the apparatus with which the perfusion pipettes are assembled. Image modified from http://www.microperfusion.com/perfusion.htm (website accessed 06/09/2014).

2.6.3 Dissection and Perfusion of JGA Preparations

I assisted with dissections of JGA preparations and perfusions, which were performed by Professor Janos Peti-Peterdi since dissection and perfusion of JGA is technically challenging. Mice were anesthetised using 1:1 ketamine:xylazine (10 mg/100 g body weight) and the left ventricle perfused with ice cold PBS to flush red blood cells from the kidney. The kidneys were then removed, decapsulated and placed on a chilled plate. Thin sections of approximately 2 mm thickness were taken radially and placed in fresh, chilled dissection medium.

As previously described (28, 32), glomeruli with attached AA, MD and, where possible, cTAL attached were carefully hand-dissected under a microscope at 4 °C, ensuring that the vessels and tissue were touched as little as possible. An image of one such freshly dissected JGA preparations is shown in Figure 2.4 (a). Preparations where the MD plaque was attached to the JGA, but was not part of a complete cTAL, could also be used since TGF is triggered in both preparations when fluid flow is applied at the MD, regardless of the NaCl concentration of the perfusate (28).

Preparations were transferred to the centre of a thermo-regulated Lucite chamber (Vestavia Microperfusion System) mounted on the microscope (described in Section 2.9.2) and kept at 4 °C until the AA was cannulated, with the perfusion pipette extended into the lumen of the AA (Figure 2.4). The glomerular holding pipette, seen on the right hand side of Figure 2.4 was then gently rested on the top of the glomerulus to ensure the preparation remained stationary.

With the preparation mounted and cannulated, the temperature was raised to 37 °C and the bath continuously aerated with 95% O_2 and 5% CO_2. Both the VSMCs of the

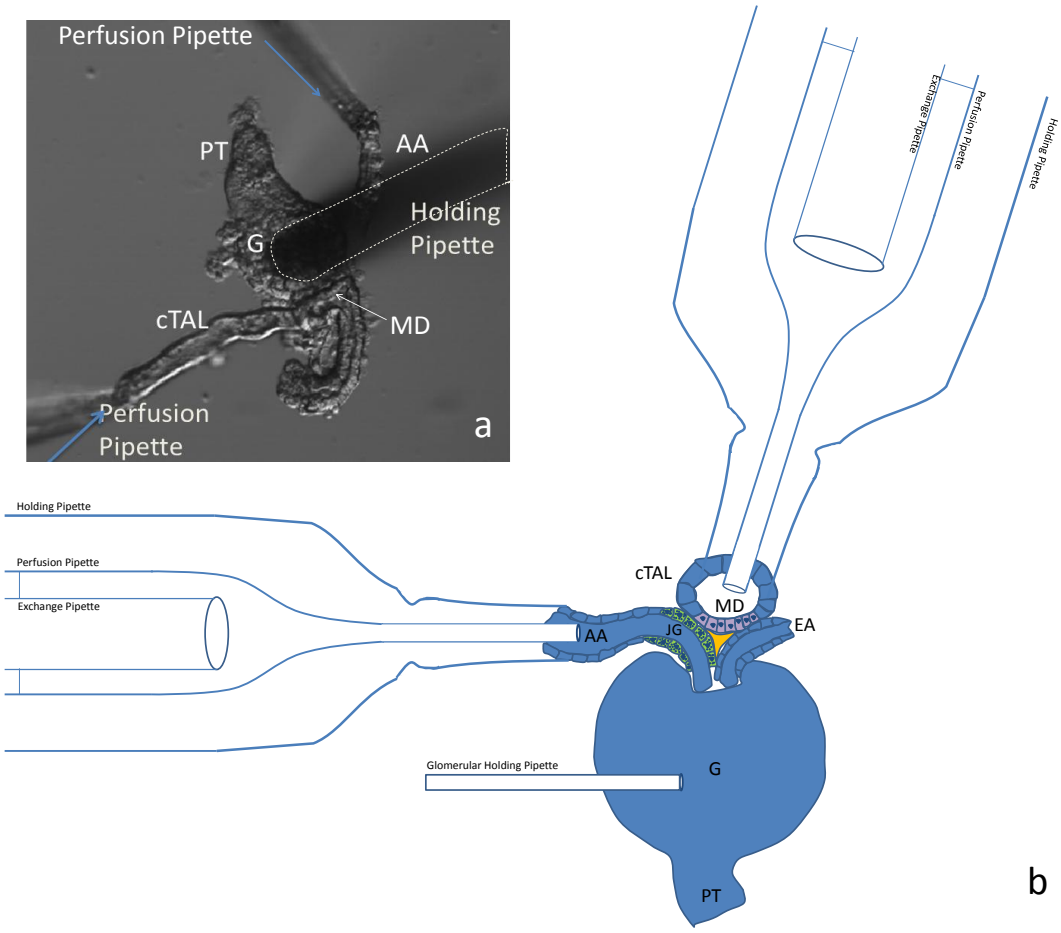

Figure 2.4: Isolated perfused juxtaglomerular apparatus set up. - (a) Brightfield image of freshly-dissected JGA and (b) schematic image of the glomerulus (G) with proximal tubule (PT), afferent arteriole (AA) with juxtaglomerular cells (JG) and efferent arteriole (EA) attached, as well as the cortical thick ascending limb (cTAL) with the macula densa (MD) attached. The AA and cTAL are being perfused using perfusion pipettes. The vessel is held securely using the holding pipette, whilst the exchange pipette feeds perfusate into the perfusion pipette. This pipette is extended into the AA, which is held securely by the holding pipette. The glomerular holding pipette ensures that the preparation doesn't move, whilst a constant pressure of 50 mmHg is applied to the AA (as previously published (32)). The perfusion of the cTAL and MD is experimentally varied through the perfusion pipette.

Reagent	Molecular Weight	Low Salt mM	Low Salt g/l	High Salt mM	High Salt g/l	Kreb's Ringer mM	Kreb's Ringer g/l
NaCl	58.44	10	0.58	80	4.68	115	6.72
KCl	74.55	5	0.37	5	0.37	5	0.37
$MgSO_4$	120.37	1	0.12	1	0.12	1.2	0.12
Na_2HPO_4	141.96	1.6	0.23	1.6	0.23	0.24	0.03
NaH_2PO_4	137.99	0.4	0.05	0.4	0.05	0.96	0.12
D-Glucose	180.16	5	0.90	5	0.90	5.5	0.99
$CaCl_2$	110.98	1.5	0.17	1.5	0.17	2	0.22
NMDG	195.2	135	26.49	65	12.69	0	0
HEPES	238.3	10	2.38	10	2.38	0	0
$NaHCO_3$	0	0	0	0	0	25	2.10

Table 2.7: Low (10 mM), high (80 mM) and Kreb's Ringer (115 mM) NaCl Solutions (pH 7.4)

AA and the tubular preparation were loaded with 10 μM of the ratiometric intracellular calcium indicators Fluo-4 AM (Life Technologies, Molecular Probes, F-14201) and Fura Red AM (Life Technologies, Molecular Probes, F-1201), made up in DMSO. Dyes were dissolved in the bathing solution (made up as shown in Table 2.7) until the cells were fully loaded (Figure 2.5). Preparations were flushed with Kreb's Ringer solution and left for a minimum of 20 mins to allow stabilisation of fluorescent signals. The AA was perfused with a constant pressure of 50 mmHg (1 psi) throughout the remainder of the experiment to maintain vascular tone (as previously reported (32)).

Cannulated MD-containing distal tubule segments or the apical surface of the MD were perfused at a baseline perfusion rate of 2 nl/min. The perfusate was identical to the AA perfusate, both kept at a constant 95% O_2, 5% CO_2 aeration. During the experiment, TGF was activated in one of two ways; flow-induced or NaCl-induced.

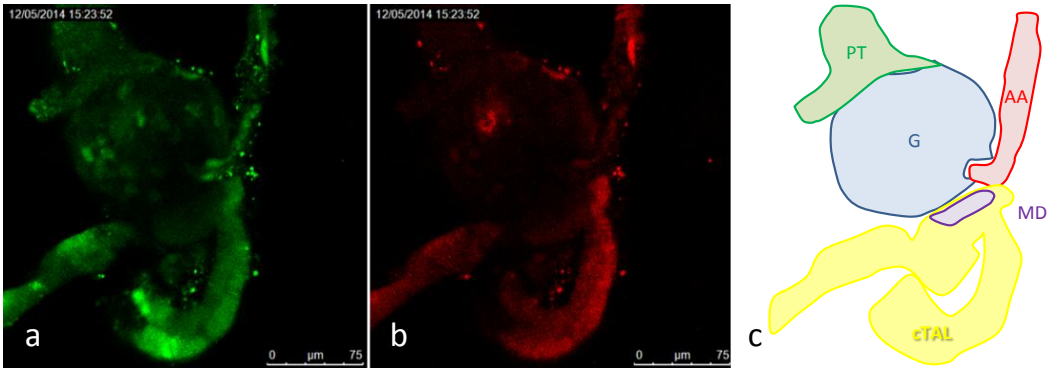

Figure 2.5: Fluo-4 and Fura Red staining of microdissected juxtaglomerular apparatus. - JGA were dissected from C57Bl/6, $Ren1d^{-/-}$ and $huRen^{+/-}Ren1d^{-/-}$ mice for microperfusion studies. Cells were loaded with 10 μM (a) Fluo-4 and (b) Fura Red AM calcium indicator dyes made up in DMSO for ratiometric calcium imaging. (c) Schematic showing the location of the glomerular tuft (G, blue), the afferent arteriole (AA, red), the proximal tubule (PT, green), the macula densa cells (MD, purple) and the cortical thick ascending limb (cTAL, yellow).

Flow-induced TGF was triggered using a constant 10 mM NaCl tubular perfusate applied at a baseline perfusion rate of 2 nl/min which was increased to 20 nl/min (5 psi). NaCl-induced TGF was triggered by keeping the perfusion rate constant at 2 nl/min whilst the NaCl concentration of the tubular perfusate was raised from 10 to 80 mM. The composition of these perfusates are shown in Table 2.7. NMDG Cyclamate was used to keep the solution isoosmotic. Calibration and optimal tubular perfusion rate has been determined in the Peti-Peterdi laboratory, using a range of perfusion rates within the physiological range of TGF sensitivity (32).

2.7 Histological Analysis

2.7.1 Tissue Preparation

Sectioning of kidneys for Fluorescent Reporter Visualisation

Dissected, decapsulated kidneys were fixed in freshly prepared 4% PFA, rotating overnight

at 4 °C in the dark. These were then washed for 5 mins in PBS three times and left in 10% sucrose for a minimum of 1 hour, after which they were cryopreserved in 30% sucrose overnight and subsequently embedded in OCT (VWR, 361603E). Samples were stored at −80 °C until mounting was required. Cryosections of 10 μm thickness were cut on a cryostat (Bright, Model OTF 5040) at −23 °C.

Sectioning of Kidneys for Immunohistochemistry

Mice were anaesthetised using 1:1 ketamine:xylazine (10 mg/100 g body weight) and the left ventricle cannulated. Mice were perfusion fixed with freshly made, ice cold 4% PFA. Kidneys were dissected, decapsulated and left overnight at 4 °C in 4% PFA before being transferred to 14 ml 30% sucrose made up freshly in ice cold PBS where they were left until they sank to the bottom of the falcon tube. The kidneys were then cut into three equally sized coronal slices before being dried thoroughly, embedded in OCT, frozen and stored at −80 °C. Coronal sections were taken at 30 μm thickness on a cryostat and left at room temperature overnight before being stored at 4 °C prior to staining.

2.7.2 Immunohistochemistry

Unless otherwise stated the staining protocol was performed at room temperature, and washes were performed three times in 1X PBS, each for 5 mins.

Staining of Kidney Sections

Slides were washed, and then immersed in 50 mM NH_4Cl for 10 mins. A further wash was performed and the sections permeabilized by incubation for 10 mins in 0.1% Triton X-100 in PBS. Post-fixation for 20 mins in freshly made 4% PFA was followed by a further wash.

Antigen retrieval was performed one of two ways (see Table 2.8 for the method used for specific antibodies). The sections were either immersed in 10 mM sodium citrite (0.05% tween-20, pH 6) in a pressure cooker for 8 mins before being cooled down to room temperature in 1X PBS for 10 mins, or incubated in 1% SDS made in PBS for 5 mins then washed.

Sections were then incubated for 30 mins in the appropriate blocking buffer, before being incubated with one of the primary antibodies in Table 2.8 overnight at 4 °C or for 2 hrs at room temperature. Slides were washed and incubated with the appropriate secondary antibody listed in Table 2.9 in the dark for 60 mins before being washed.

Slides were dried completely without disturbing the tissue, mounted using Vectashield Mounting Medium for Fluorescence with DAPI (Vector Laboritories, H-1200) and stored at 4 °C.

Control staining was performed in the same way as outlined above but instead of a primary antibody being applied, only blocking buffer was added to the sections.

Antigen Protein	Host	Blocking Buffer	Dilution	Antigen Retrieval	Incubation Type	Company	Catalogue Number
NG2	Rabbit	Goat	1:100	8', Pressure	O/N, 4 °C	Millipore	5320
Renin	Rabbit	Goat	1:100	5', SDS	2 hrs, 22 °C	Anaspec	54371
Ki-67	Rat	Goat	1:100	8', Pressure	O/N , 4 °C	Biolegend	652401
Cox-2	Goat	Donkey	1:300	8', Pressure	O/N, 4 °C	Santa Cruz	sc-1747
mRen	Rabbit	Goat	1:1000	N/A	O/N, 4 °C	Inagami	N/A
α SMA	Mouse	Goat	1:100	N/A	O/N 4 °C	Sigma	A2547

Table 2.8: Antibodies and the optimised staining conditions used. Inagami mRen antibody was a gift from Vanderbilt University.

Secondary Antibody	Conjugate	Dilution Used	Company	Catalogue No.
Donkey anti-Rabbit	Alexa Fluor 594	1:500	Life Technologies	A21207
Donkey anit-Goat	Alexa Fluor 594	1:500	Life Technologies	A11058
Goat anti-Rat	Alexa Fluor 488	1:500	Life Technologies	A11006
Goat anti-Rat	Alexa Fluor 594	1:500	Life Technologies	A11007
Goat anti-Rabbit	Alexa Fluor 555	1:500	Life Technologies	A-21428
Goat anti-Mouse	Alexa Fluor 555	1:500	Life Technologies	A-21422

Table 2.9: Secondary antibodies (IgG H+L) used in immunofluorescence staining.

2.7.3 Immunocytochemistry

Renin staining

Cells were fixed according to the method outlined in Section 2.5.9 and washed. Cells were blocked for 1 hr with 5% goat serum. The primary anti-mRen antibody (Table 2.8) was applied to cells, or a control performed by adding blocking buffer without primary antibody, and the cells incubated overnight at 4 °C. A wash was followed by a 1 hour incubation in a goat anti-rabbit AF-555 secondary, a further wash and the cells mounted according to Section 2.5.9.

Actin Staining

Primary JG cells fixed according to the method outlined in Section 2.5.9 were washed, permeablised in 0.1% Triton X-100 for 8 mins, and washed again. Blocking was performed with 10% goat serum for 1 hr, aspirated and the primary α-SMA antibody (Table 2.8) applied and incubated overnight at 4 °C. A wash was followed by a 1 hour incubation in goat anti-mouse Alexa Fluor-555 secondary antibody and a further wash performed. Coverslips were then mounted according to Section 2.5.9.

2.8 Electron Microscopy

Fixatives for electron microscopy were prepared fresh in the appropriate buffer as detailed in Table 2.10, and measurements are (w/v).

Fixative	Buffer	Perfusion Time	Use
2% Gluteraldehyde (50% EM Grade, Sigma)	0.1 M Cacodylate (pH 7.2) (Agar Scientific, R1104)	5 mins	3D Reconstructions
2.5% Gluteraldehyde	0.1 M Phosphate (pH 7.2)	5 mins	Ultrastructure analysis
3% Paraformaldehyde 0.05% Gluteraldehyde	0.1 M Phosphate (pH 7.2)	5 mins	Immunogold Labelling
0.2% Tannic Acid	0.2% tannic acid, PBS (Sigma, 403040)	10 mins	Exocytosis Identification

Table 2.10: Fixatives prepared for samples assessed using electron microscopy.

2.8.1 Perfusion Fixation

Mice were anaesthetised by an intraperitoneal injection of 1 mg/kg medetomidine with 75 mg/kg ketamine. The abdomen was opened and the right kidney clamped, removed, decapsulated and snap frozen on dry ice for RNA extraction. The descending abdominal aorta was clamped below the branch of the renal artery to stop blood flow and cannulated using a 24 gauge intravenous catheter (Surflo intravenous catheter (VWR, TERUSR-OX2419CF). The vena cava was cut, the clamp removed and organs perfused in a retrograde fashion with 5 ml heparinised PBS, followed by the appropriate fixative (Table 2.10) at a perfusion pressure of 120 mmHg - 180 mmHg, monitored using a manometer. When tannic acid analysis was being performed in conjunction with a fix-

ative, perfusion of heparinised PBS was followed by tannic acid perfusion then fixative perfusion.

A successful perfusion left the liver blanched, clear fluid was expelled from the vena cava and the kidney completely blanched. When incomplete perfusion occurred, the mottled kidney was diced into 1 mm^3 cubes and fixed in the appropriate fixative.

Perfused kidneys were placed in the buffer in perfusion fixative for approximately 4 hours at 4 °C then transferred to a 1:10 dilution of the fixative in the correct buffer and stored at 4 °C prior to embedding and EM analysis.

2.8.2 Embedding of Tissue

For ultrastructure and immunogold analysis, embedding of tissue and EM imaging was carried out by Dr. Helen Christian (Oxford), and for 3D reconstructions by Anita Zügner (Regensburg).

Embedding for 3D Reconstruction

In brief 1 mm^3 segments of renal cortex were cut and embedded as previously described (113). An automatic microwave (Leica EM AMV, Germany) was used to embed tissue segments in epoxyde resin (epoxy embedment kit, Fluka, Neu-Ulm, Germany), which were then cut into 70 nm ultrathin serial sections using an ultramicrotome (EM UC7, Leica, Germany). They were then transferred onto copper grids coated with pioloform and contrast stained using 4% uranyl acetate solution and 0.5% lead citrate solution.

Images were acquired using a transmission electron microscope (Phillips CM12 TEM, Fei & Co, Einhoven, Netherlands) with a LaB_5 cathode and an acceleration voltage of 120 keV (113). Digitalisation was performed using a TEM-1000 slow-scan CCD camera and EM-Menu 4.0 software (TVIPS-Tietz GmbH, Germany) (113).

Embedding for Ultrastructure Analysis

For ultrastructure analysis, 1 mm^3 segments of renal cortex were cut and embedded as previously described (165). Segments were post-fixed in 1% w/v osmium tetroxide in 0.1 M phosphate buffer, then stained with 2% uranyl acetate made up in distilled water. Dehydration with increasing concentrations of 70% to 100% ethanol was followed by embedding in spurr resin (Agar Scientific) and 70 nm ultrathin sections prepared using a Reichert ultracut S microtome.

Sections from mice (n = 3 per group) were mounted onto 200 mesh nickel grid and lightly counterstained with lead citrate and uranyl acetate before being imaged on a Jeol transmission electron microscope (JEM-1010, JEOL, Peabody MA).

Embedding for Tannic Acid and Immunogold Analysis

For immunogold analysis, 1 mm^3 segments of renal cortex were cut and embedded as previously described (166). Segments were stained with 2% uranyl acetate made up in distilled water, followed by dehydration with increasing concentrations of methanol from 70% to 100%. These segments were then embedded in LR Gold (London Resin Company) and ultrathin sections of 70 nm prepared as outlined above.

Samples were incubated at room temperature for 2 hrs with anti-human renin (R&D Systems, AF4090, dilution 1:1000) or anti-mouse renin (Table 2.8, 1:10,000) and for 1 hr with Protein A-15 nm gold complex (British Biocell). All antisera were diluted in 0.1 M phosphate buffer containing 0.1% egg albumin. As a control, the primary antibody was replaced by phosphate buffer/egg albumin.

Sections from mice (n = 3 per group) were mounted onto 200 mesh nickel grid and lightly counterstained with lead citrate and uranyl acetate before being imaged on a Jeol transmission electron microscope (JEM-1010, JEOL, Peabody MA).

2.9 Imaging Modalities

2.9.1 Epifluorescent Microscopy

A Nikon microscope (Eclipse Ti; Nikon Instruments) in fluorescence mode with the DAPI (Ex: 350/50 nm; Dichroic: 400 nm long pass; Em: 470/40 nm; Em: 525/50 nm), FITC (Ex: 470/40 nm; Dichroic: 495 long pass; Em: 525/50 nm) and TRITC (Ex: 540/25 nm; 565 long pass; Em:605/55 nm) filters applied for DAPI/Hoerscht 33342, Alexa Fluor 547 and GFP expression respectively was used, with an appropriate exposure time. A mercury arc lamp light source was used (X-cit 120 series, Lumen dynamics). Either a 60X 1.4 NA Plan Apo or a 40X 1.3 NA Plan Flur oil objective lens was used.

2.9.2 Confocal Light Scanning Microscopy

Image acquisition was performed on a DMI 6000 CS inverted miscroscope with a Leica SP5 confocal scan head at 0.5 μm per slice, using Leica LCS imaging software. Either a 63X 1.4 NA or 40X 1.25 NA Plan Apo oil objective lens was used. Laser lines at 488 nm and 596 nm as well as a blue 405 nm diode laser were used for excitation and signal collected between 494 - 537 nm (green) or 606 - 719 nm (red). Gain, offset and laser power was kept constant between experiments, with a line average of 5 and a frame average of 1 used with a sampling rate of 600 Hz.

Imaging of calcium transients in isolated perfused JGA preparations was performed on a Leica TSC SP2 AOBS MP confocal microscope system (Peti-Peterdi Laboratory) in a time series at 1 frame/ 2 s with Leica LCS imaging software. A Leica DM IRE2 inverted microscope was used in conjunction with a blue 488 nm, 20 mW laser. Calibration of tubular perfusion pressure to flow was previously performed by the Peti-Peterdi

laboratory (32), allowing absolute calcium values to be obtained from fluorescence intensity (12 bit) measurements using Fluo-4 AM (excitation at 488 nm, emission at 520 ± 20 nm) and Fura Red AM (excitation at 488 nm, emission at > 600 nm). Gain, offset and laser power were kept constant between experiments.

When immunohistochemical results were analysed using confocal microscopy, for each protein of interest a slide from each of 3 animals was stained. On each slide, 3 separate kidney sections were stained and 3 control sections used. 3 images of staining and 1 control image were acquired per slide.

2.9.3 Widefield Microscopy

Live cell imaging was performed on an Olympus Cell Excellence IX81 using a 1.45 NA, 150X oil immersion lens. Cells were initially located using epifluorescence from a Xenon mercury lamp with a quad filter containing DAPI, GFP and mCherry emission filters. 100 mW diode lasers providing excitation at 405 nm, 491 nm and 561 nm were used for data acquisition in both widefield and TIRF.

100 nM Lysotracker Red DND-99 (Molecular Probes, L-7528) was added to the culture medium 30 mins prior to acquisition. Once a GFP-positive cell of interest was identified, the light source was changed to laser excitation. Granules loaded with lysotracker were then imaged by acquiring 1000 frames at a frame rate of 14 Hz (70 ms/frame) using the 591 nm laser. Culture medium containing isoproterenol (Sigma, I-5627) was then added to culture dish (100 nM final concentration) and a further 1000 frames acquired using the 591 nm laser in the same cell to capture the granule response to isoproterenol.

A Hamamatsu EMCCD (electron multiplying charge coupled device) camera was

used for image acquision, operated through the Xcellence advanced live cell imaging software package at a constant gain level. A temperature controlled block stage with CO_2 integration ensured cells remained at 37 °C and 5% CO_2. All equipment was surrounded by a black insulation box to ensure no laser light escaped during image acquisition and to keep the temperature constant. During acquisition, the CO_2 air pump was switched off to ensure image stability was not affected by unwanted motion.

2.9.4 Total Internal Reflection Fluorescence Microscopy

Total internal reflection fluorescence (TIRF) microscopy was performed on the microscope system outlined in 2.9.3. Once a cell of interest had been identified, the angle of the laser was increased and the focus moved towards the coverslip. TIRF was reached when fluorescence from granules further than approximately 150 nm from the cell membrane was no longer visible, decreasing the number of granules visible in the field of view.

In order to image continuously whilst adding isoproterenol to the medium, a syringe with a metre of tubing and a needle attached at the end was constructed. This was filled with 500 μl 200 nM isoproterenol, ensuring that the volume was at the very end of the needle. The needle was attached to the edge of the perfusion chamber above the line of the medium and fed out of the insulation box. Image acquisition was started and the isoproterenol gently syringed into the 500 μl medium on the cells after 500 frames had been acquired.

2.10 Image Analysis

2.10.1 Deconvolution

Deconvolution was performed using Huygens Deconvolution software (Scientific Volume Imaging) on z-stacks of images acquired using widefield microscopy. For images acquired using the Olympus1X81 with the 1.45 NA, 150X objective lens, the following parameters were applied to the 'Operations Tab' of the deconvolution wizard: SNR = 30, x-y = 106 nm, z = 258 nm, quality = 0.01.

2.10.2 Reconstruction of Juxtaglomerular Cells From Widefield z-Stacks

Deconvolved images were loaded into Imaris 7.7; the signal from the diffuse GFP in JG cells from RenGFP$^{+/-}$ mice was excited using the 488 nm laser, whilst signal from the lysotracker accumulated in granules was excited using the 591 nm laser. The surface wizard was used to apply surfaces separately to signal from each of the channels. For each of the surfaces the volumes were extracted and the volume of lysotracker with respect to GFP signal determined.

2.10.3 Granule Tracking

Granule tracking was performed using Imaris 7.7 (Bitplane). For granule tracking in images acquired using widefield microscopy, stacks consisted of 1000 frames from baseline granule motion and 1000 frames from granule motion after isoproterenol treatment. For granule tracking in images acquired using TIRF microscopy, the 2000 frames were split into 500 frame segments using ImageJ; frames 1-500 comprised baseline granule movement, frames 501-1000 comprised isoproterenol administration, whilst frames

1001-1500 and 1501-2000 comprised post-treatment phases.

Time series image stacks in TIFF format were loaded into Imaris, ensuring the *'Swap time and z'* option had been chosen and the correct time and voxel size parameters loaded (70 ms/frame, pixel size of 106 nm). Spots were created by choosing the *'Create Spot'* option, and the instructions followed. In brief, spots were assigned to each granule, identified by fluorescence intensity from the lysotracker dye. A diameter of 700 nm was chosen to track large granules, 300 nm to track small granules. Tracking was performed assuming Brownian motion and a maximum distance and gap size of the granule diameter chosen. Examples of spots assigned to granules and the accompanying tracks can be seen in Figure 2.6.

Individual granule tracks were checked to ensure that the tracking process had worked correctly. If only 1-2 frames were lost the spots were connected manually, otherwise the tracks were dismissed.

From these tracks, key parameters such as instantaneous speed, average speed, track length and displacement were extracted for each granule. Furthermore, the diameter of each of the granules taken forward for analysis was measured in ImageJ by measuring the diameter manually three times and averaging. Granules were deemed to be dense core granules if their diameter exceeded 500 nm. Graphical representations of these parameters are shown in Figure 2.7.

2.10.4 Analysis of Tubuloglomerular Feedback Response

Leica LCS imaging software (LCS 2.61.1537) was used for image analysis. Regions of interest (ROIs) were chosen from within single cells of the cell type of interest by referring to DIC, Fluo-4 and Fura Red images (Figure 2.8c, d). The Quantification

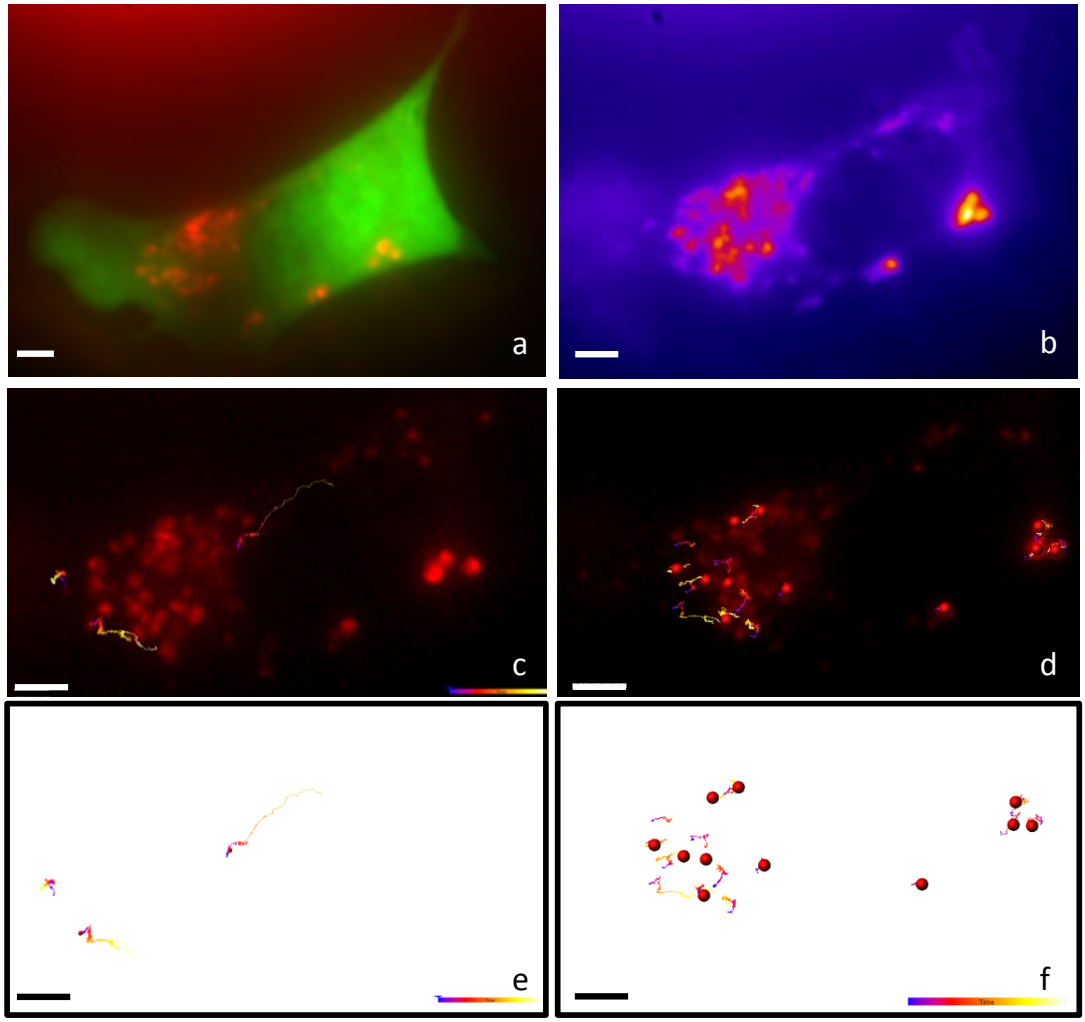

Figure 2.6: Representative process of image acquision for granule tracking analysis. - (a) JG cells were identified using their GFP expression and stained with lysotracker red to identify renin-containing granules. (b) 1000 or 2000 frames were acquired at 14 Hz using the 561 nm laser; the summed z-projection of all images acquired is shown using a heat map ('fire' LUT) for ease of visualisation. (c,e) Small vesicles and (d,f) large granules were tracked by assigning the red 'spots' visible in the images to granules and tracking their motion in Imaris 7.7. These tracks are shown either (c,d) with or (e,f) without the corresponding raw data from the lysotracker signal for ease of visualisation.

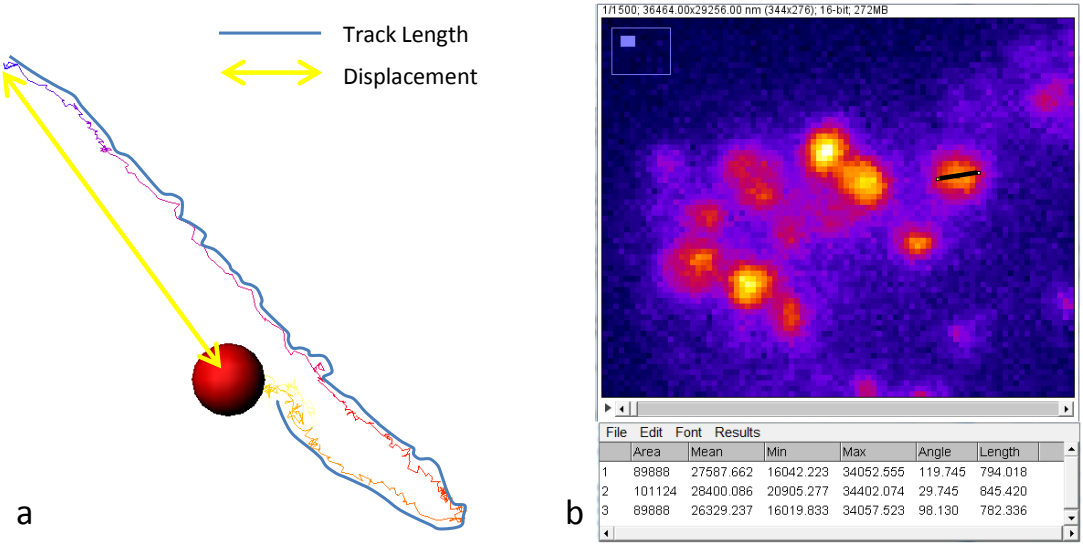

Figure 2.7: Parameters extracted from granules during the tracking process. - (a) Track length and displacement of the track were extracted from tracks which met the correct criteria. (b) The diameter of the corresponding granule was then measured manually in ImageJ three times (black line) and averaged to evaluate granule size.

Tools application allowed measurement of Fluo-4 and Fura Red fluorescent signal from within these ROIs, at baseline and at the peak TGF signal. *In situ* intracellular calibration of absolute calcium concentrations corresponding to the Fluo-4 to Fura Red signal has previously been performed according to Lipp *et. al* (167) in the Peti-Peterdi Laboratory (32, 168, 169). Using these calibration results, Equation (2.1) was used to convert the Fluo-4 to Fura Red fluorescence intensity signal ratio (R) into an absolute calcium concentration. The percentage change in intracellular calcium concentration during TGF was then calculated using Equation (2.2) and compared between groups.

Internal diameter of the AA, glomerular tuft diameter and area were measured at baseline and at maximal stimulation of TGF (Figure 2.8), and an average of 3 measurements taken. The percentage change was calculated using Equation (2.2) and compared between groups.

$$Ca = 1000(-0.0789 + 0.3R) \tag{2.1}$$

$$\Delta\% = 100(a_{after} - a_{before})/a_{before} \tag{2.2}$$

Here, a represents the measured quantity, whether that is diameter of the AA, diameter of the glomerular tuft, area of the glomerular tuft or calcium measured in a specific cell type. At least 6 preparations were analysed from 3 animals for each phenotype group, with at least 3 measurements made per analysis parameter.

2.10.5 3D Reconstruction of Juxtaglomerular Cells

Two adult male and female 1446 $huRen^{+/-}Ren1d^{-/-}$ animals were perfusion fixed for EM according to the protocol in Section 2.8. Serial sections were taken of at least two JG cells for each animal at 70 nm thickness, using data from at least 2 animals per group.

2.10.5.1 Labeling Cellular Structures

Images were loaded into ImageJ where they were stacked sequentially then saved and loaded into Amira 3D Software for Lifesciences (FEI). The voxel sizes were 5.2 nm in the x-y directions and 70 nm in the z direction. The slices were aligned using the inbuilt *'AlignSlices'* function, aligning as accurately as possible for the cell of interest. If more than one cell was present in the electron micrograph stack, the images were aligned separately for each cell (Figure 2.9a, b). Once the images were aligned the stack was resampled to create a new stack.

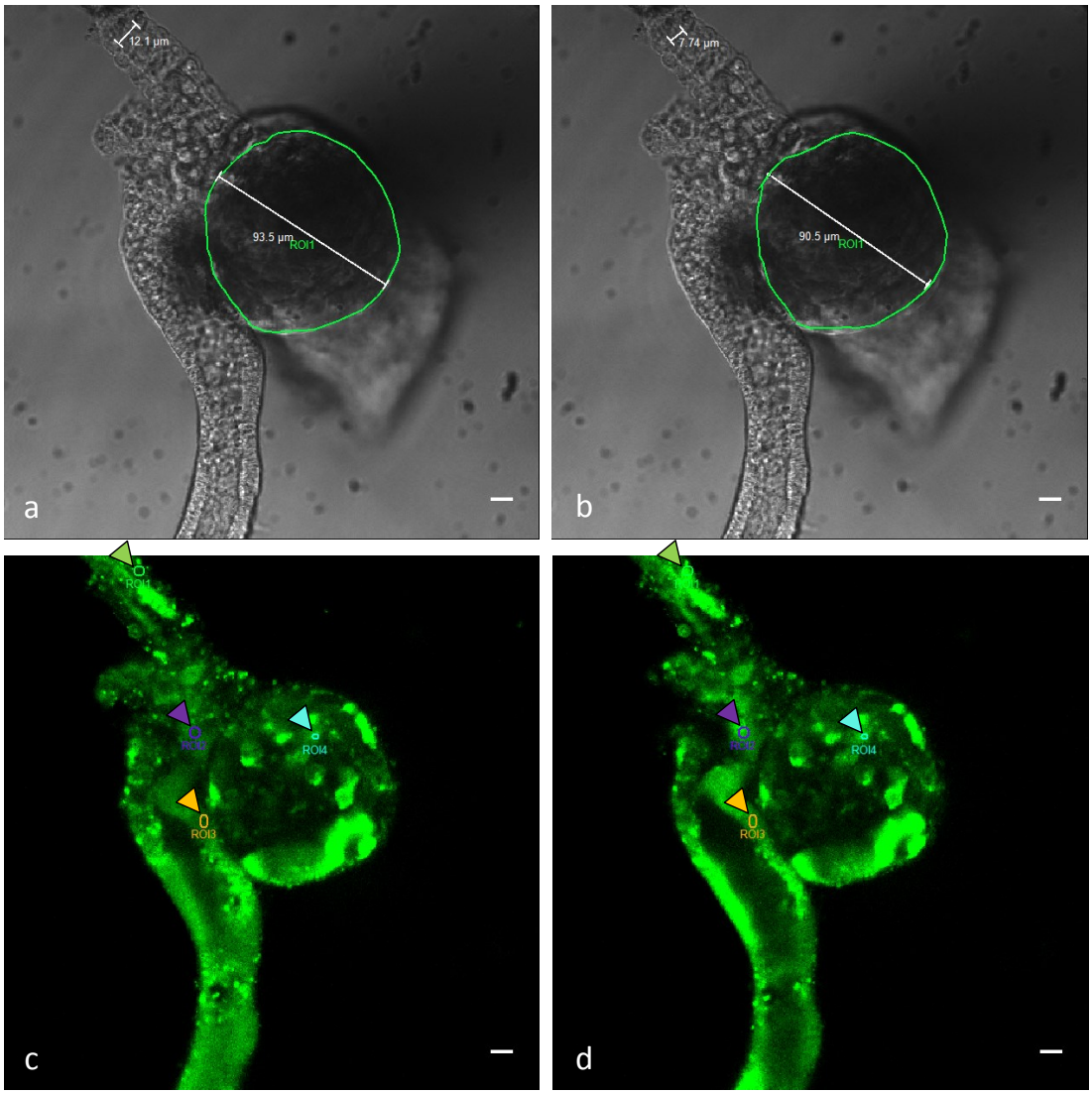

Figure 2.8: Analysis of tubuloglomerular feedback mechanism responses in microdissected juxtaglomerular apparatus. - DIC images were analysed (a) before and (b) after TGF stimulation and the afferent arteriole diameter, the glomerular tuft diameter and area measured. Regions of interest (ROI) within cells, indicated with arrows, were then drawn in different cell types and the Fluo 4 and Fura Red (not shown) signal measured (c) before and (d) after TGF stimulation. Calcium signalling responses are shown in a vascular smooth muscle cell (ROI 1, green), a MD cell (ROI 2, purple), a cTAL cell (ROI 3, orange) and a podocyte (ROI 4, blue). Scale bars represent 10 μm.

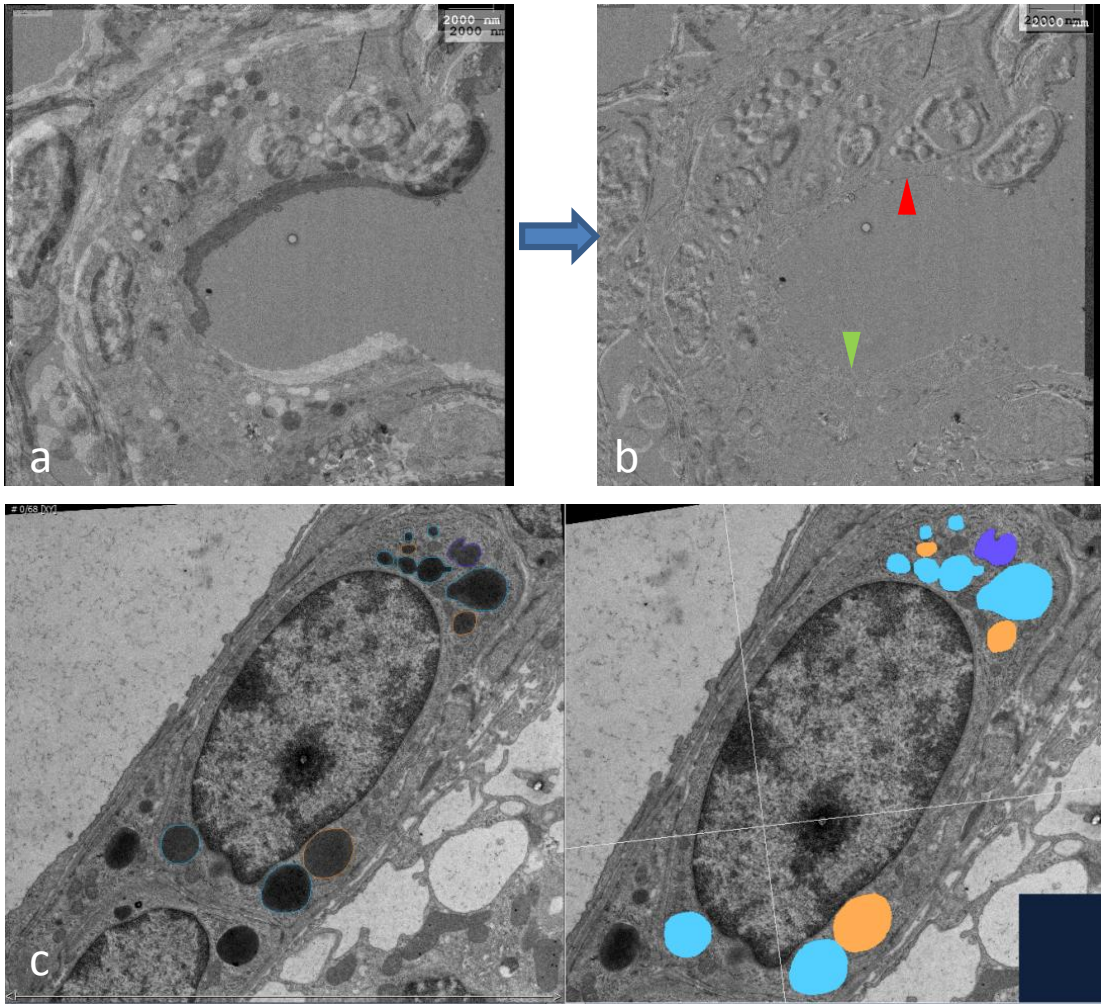

Figure 2.9: Alignment of electron micrograph image stacks for labelling granules. - (a) Electron micrograph image stacks of JG cells were saved in ImageJ and loaded into Amira 3D Software for Life Sciences (FEI). Two sequential micrographs can be seen (one light and one dark). By manipulating the location and angle of the new image, the two micrographs could be aligned (b), and repeated for the entire stack. This was performed for each cell within a set of micrographs, since it was not often possible to align both the top and bottom of the image. Within the image, the green arrow indicates good alignment and the red arrow indicates bad alignment. (c) Granules were labelled by creating a label field and manually defining each granule; when granules were close together but not joined a different colour was used.

A label field was created using the *'LabelField'* function. Labels were drawn onto each slice of the stack and interpolated between slices. To do this the brush or lasso tool was used to label the cell membrane, the nucleus and each renin granule network; each of these cellular structures was added to a specific material. If granules were too close together they were added to different materials to ensure that they did not fuse together, creating a false network. This is visually represented in Figure 2.9 (c).

2.10.5.2 Generating Surfaces

Each of the label fields corresponding to different cellular structures were saved individually. Each surface was interpolated using the *'Interpolate labels'* function. When complete, a surface was generated around the interpolated data using the *'SurfaceGen'* function. Once applied, the *'Unconstrained smoothing'* option was selected, ensuring that the *'Compactify'*, *'Add border'*, *'Adjust coords'* and *'Extra material'* options were also selected. This generated a new surface module which could be saved. To visualise the rendered surface, a *'SurfaceView'* module was added to it. Once these surfaces had been rendered for each of granule groups, the nucleus and the membrane separately, the .SURF files were loaded into the modules pool and a *'SurfaceView'* module added to each to acquire images.

2.10.5.3 Volume Calculation

To calculate the volume associated with each of the structures, the surfaces were remade as outlined above by using the *'SurfaceGen'* option but this time with no smoothing; the *'Unconstrained smoothing* option was not selected, nor were the *'Compactify'*, *'Add border'*, *'Adjust coords'* and *'Extra material'* options selected. This was done for all

of the surfaces. The newly-generated surfaces were analysed using the *'Measure'* function, creating a spreadsheet containing the data on the volume and surface area of the generated surfaces. The percentage of extranuclear space occupied by granules in each JG cell could then be calculated.

2.10.5.4 Statistical Analysis

Data are presented as the mean ± S.E.M, calculated by taking the standard deviation and dividing it by the square root of the number of data points. Statistical significance was tested with Student's *t*-test for paired samples (significance reached when $p < 0.05$).

2.11 RNA Extraction

2.11.1 Tissue RNA Extraction

Tissue RNA extraction was performed using an RNeasy Mini Kit (Qiagen, 74106). Half a frozen kidney sample thawed on ice was placed in a 2 ml Eppendorf tube with 600 μl RLT buffer with a magnetic bead (OpsDiagnostics, Grinding Balls, 5/32" Stainless Steel (5000)). Samples were placed in a magnetic mixer mill (Retsch MM301) and samples shaken for 90 s at 30/s to homogenise tissue. The bead was then removed and the lysed tissue centrifuged for 3 mins to pellet any unhomogenised material. 450 μl homogenate was then snap frozen on dry ice for storage at -80 °C. 150 μl homogenate was mixed via inversion with 150 μl RLT buffer and 300 μl 70% ethanol (VWR Cheimcals, 20821.330). Both the 70% ethanol and the RLT buffer encouraged selective binding of the RNA with the RNeasy spin column. Samples were loaded onto the spin column and the

manufacturers instructions followed. Using this method 5 - 25 μg RNA was routinely extracted in 50 μl RNase-free water.

2.11.2 Cell RNA Extraction

1 ml TRIzol (Ambion, 15596018) was added to each 35 mm diameter dish (one well of a six well plate) to lyse cells. This was left for 1 min and cell lysate titurated with the pipette before being transferred to a 1.5 ml eppendorf. This was incubated for 5 mins at room temperature; at this point TRIzol-lysed cells were either stored at -80 °C for future extraction after thawing or used immediately.

200 μl chloroform (Fisher Chemicals, 0/4960/17) was added to each tube, shaken vigorously by hand for 15 s and incubated at room temperature for 3 mins. The resulting mixture was centrifuged at 10 x 10^3 g at 4 °C for 15 mins to separate out the aqueous phase from the interphase and organic phase. The upper, aqueous phase was transferred to a fresh tube containing 500 μl isopropanol (VWR Chemicals, 20842.323) and mixed thoroughly, ensuring no contamination from the other phases was carried over. After 10 mins incubation at 4 °C, the mixture was centrifuged at 8.4 x 10^3 g for 5 mins at 4 °C. The supernatant was removed and the pellet air dried for 10 mins at room temperature before being resuspended in 50 μl RNAse-free H_20. RNA yield was expected to be between 8 - 15 μg RNA per million cultured cells.

Removal of Genomic DNA

Contaminating genomic DNA, DNase and divalent cations such as calcium and magnesium which can catalyse RNA degradation, were removed from the RNA samples using a DNAFree Kit (Ambion, AM1906) immediately after extraction either by spin column or Trizol. Using this kit, DNA was digested until it was below the level of detection

by PCR. 1 μl rDNase1, the recombinant DNase1, and 5 μl DNAse1 buffer was added to the sample, the mixture votexed briefly and incubated at 37 °C for 25 mins. 5.5 μl resuspended DNase inactivation reagent was then added to the mixture, vortexed and incubated at room temperature for 2 mins. Samples were then vortexed and centrigued at 10,000 g for 2 mins and the supernatant transferred to a fresh tube, ensuring no inactivation reagent was carried over.

The amount of RNA present and its integrity was then quantified using a Nanodrop (ND-1000 Spectrophotometer). RNA routinely showed a A_{260}/A_{280} ratio of between 1.8 - 2.0. Samples were stored at -80 °C.

2.12 Quantitative Polymerase Chain Reaction

2.12.1 RNA Agarose Gel Elecrophoresis

To check RNA integrity, a 0.8% agarose gel was made in 0.5X TBE buffer following the same protocol as outlined in Section 2.2.3.3, and 500 ng RNA was separated using electrophoresis. A representative gel image is shown in Figure 2.10 (a).

2.12.2 Reverse Transcription

cDNA synthesis was performed using a High Capacity cDNA Reverse Transcription kit (Applied Biosciences, 4368814) according to the manufacturers instructions. 500 ng cDNA was transcribed by creating a mastermix containing 10X reverse transcription (RT) buffer, 25X dNTP mix (100mM), 10X RT random primers, Multiscribe reverse transcriptase and nuclease-free H_2O. 10 μl volume of mastermix and 500ng RNA made up to 10 μl with nuclease-free water were mixed gently, the tubes sealed, centrifuged briefly and placed in a ThermoCycler (Applied Biosciences, Veriti 96-well). The mixture

was cycled through a 10 mins incubation at 25 °C, a 120 mins incubation at 37 °C and a 5 mins incubation at 85 °C. The resulting cDNA was then stored at -20 °C.

2.12.3 qPCR

A 1:32 dilution of sample cDNA (25 ng/μl) was performed, ensuring enough cDNA was diluted to allow amplification of all genes of interest, and aliquoted. cDNA was also used to create an 8-point standard curve series of 1:8, 1:16, 1:32, 1:64, 1:128, 1:256, 1:512 and a no template control. Triplicates were performed. A mastermix containing 5 μl Lightcycler 480 Probes Master 2X mastermix (Roche, 04 887 301 001), 0.1 μl primer pairs (20 μM, Eurofins Genomic EU the sequences of which can be found in Table 2.11 and designed using the Roche Applied Science Universal Probe Library Assay Design Centre), 0.1 μl relevent probe from the Roche Universal Probe Library (final concentration 100 nM) and 2.8 μl Lightcycler 480 Probes Master PCR Grade H_2O per rection was created. 2 μl of cDNA was added to each well with 8 μl mastermix, and a no-template control run. The reactions were run on a Roche Lightcycler 480 at 95 °C for 15 mins, followed by 95 °C for 10 s, 60 °C for 30 s, 72 °C for 1 s, repeated for 50 cycles, ending with 40 °C for 30 s. Automated identification of the C_P value by finding the maxima of the second derivative of a plot showing fluorescence against time was performed using Roche Light Cycler Software. The triplicate values of both the samples and the standard curve were evaluated to ensure that the standard deviation on the C_P value did not exceed 0.45; any points exceeding this threshold were excluded. A representative amplification and standard curve can be seen in Figure 2.10.

18S and HPRT were the most effective endogenous housekeeping control genes to quantify the genes of interest to correct for sample variation and in qPCR efficiency.

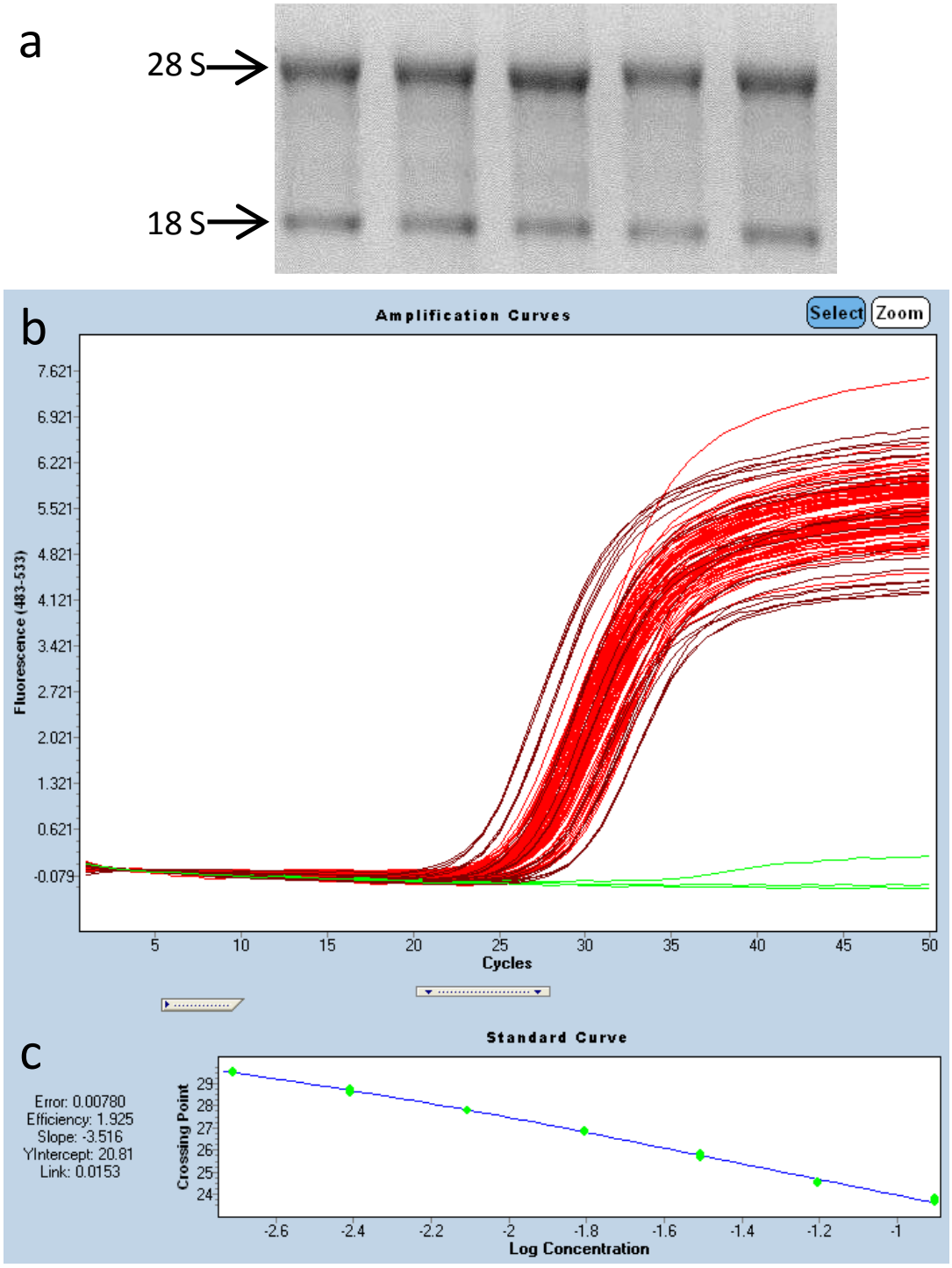

Figure 2.10: Representative quality checks used when performing qPCR - (a) RNA integrity was assessed by checking the discrete 28S and 18S rRNA bands. An approximate intensity ratio of 2:1 indicate good quality RNA. (b) Sample amplification curves (red) were checked to ensure that they lay between the standard deviation curves (brown), and no template control was negative (green). (c) An acceptable standard curve had an error < 0.05 and an efficiency of 1.9 to 2.1.

Protein Name Gene Name	Accession Number	Product Length (bp)	Forward Sequence Reverse Sequence	Probe Number
Hypoxanthine guanine phosphoribosyl transferase *HPRT*	NM_013556.2	91	cctcctcagaccgcttttt aacctggttcatcatcgctaa	95
18S rRNA *Rn18s*	NR_003278.1	110	ctcaacacgggaaacctcac cgctccaccaactaagaacg	77
tata Box Binding Protein *tbp*	NM_013684	90	gggagaatcatggaccagaa gatgggaattccaggagtca	97
β Actin *ACTB*	NM_007393.3	104	ctaaggccaaccgtgaaaag accagaggcatacagggaca	64
Renin (*homo sapiens*) *hRen*	NM_000537.3	65	tacctttggtctcccgacag ttgagggcattctcttgagg	77
Renin (*mus musculus*) *mRen2*	NM_031192.3	96	cccgacatttcctttgacc tgtgcacagcttgtctctcc	16

Table 2.11: Primer sequences and Universal Probe Library probes used to measure mRNA levels in qPCR reactions.

2.12.4 Statistical Analysis

Data are presented as the mean ± S.E.M, calculated by taking the standard deviation and dividing it by the square root of the number of data points. Statistical significance was tested with Student's *t*-test for paired samples (significance reached when $p < 0.05$). For *hRen* and *mRen2* analysis in Section 6.2.1, 2-way anovas were performed in conjunction with appropriate post hoc analysis.

3

Isolation of Renin Expressing Cells

3.1 Introduction

Though many of the mechanisms and signalling events leading to the synthesis and packaging of renin within JG cells have been uncovered, key aspects remain unclear - particularly factors leading to the onset of granulation and the subsequent secretion of renin from JG cells.

Live imaging in appropriate cell lines or primary cells is commonly performed to understand the processes involved in granule dynamics and secretion. However cultured primary JG cells only synthesise renin and respond to cAMP-mediated renin secretion for approximately 48-72 hours (13). Since they represent only 0.001 - 0.01% of the kidney cell population (52), a large number of kidney digests must be pooled and FACS-sorted to obtain a homogeneous population of JG cells, exposing the sensitive JG cells to extended and relatively harsh environmental conditions (room temperature and atmospheric CO_2).

An alternative is to separate the whole kidney digest on a Percoll gradient. This has been used effectively for JG cells (73, 170). Although the population of cells extracted is heterogenous, the JG cell population is enriched and the extraction process shortened. However identification of JG cells within the heterogeneous population is difficult.

The establishment of an immortalised JG cell line, which faithfully replicates renin granule synthesis and extrusion, would be an attractive alternative to primary cell culture. The AS4.1 cell line (89) is the most frequently used renin-producing cell line of JG origin (discussed in Section 1.6.2). Although they are a good model for use in the investigation of mouse renin gene regulation (90, 91, 92), renin is not transported onto the regulated pathway or packaged into dense core granules; instead, renin is released constitutively. Therefore these cells are unsuitable for *in vitro* granulation or secretion studies.

A cell line that packaged renin in dense core granules would enable manipulation of renin transcription and granulation levels through the transfection of appropriate renin constructs. In principle, imaging of granule dynamics could also be facilitated through transfection of a fusion construct where the renin gene has been fused to a fluorescent protein, allowing accurate identification of renin-containing granules.

Establishing a novel JG cell line using the Immortomouse would allow us to control the immortalization of renin-producing cells (83). Under the permissive culture conditions (33 °C in the presence of IFN-γ) cells from this mouse are able to proliferate, however under non-permissive conditions (37 °C in the absence of IFN-γ) cells differentiate and senesce (83). By isolating JG cells from mice of defined genotypes and culturing them under permissive conditions, it was anticipated that the immortalised cell lines would retain the ability to package renin into dense core granules and release

active renin on a regulated pathway.

3.1.1 Aims

To establish a model in which *in vitro* characterisation of granule dynamics could be performed, the following experimental aims were addressed:

1. Evaluate, in parallel:

    a) Percoll gradient isolation of primary renin-expressing cells, and

    b) the derivation of immortalised, GFP-positive JG cell lines.

2. Assess the culture conditions, renin expression profiles and the response to cAMP-stimulation of isolated JG cells.

3.2 Results

3.2.1 Verification of RenGFP$^{+/-}$ Reporter Expression in JG Cells

Visualisation of GFP-tagged renin in JG cells from cryosections of RenGFP$^{+/-}$ mouse kidneys allowed their identification at the classic juxtaglomerular location (Figure 3.1) despite autofluorescence within the cortical kidney tubules. GFP expression within the JG cells was predominantly distributed throughout the cytoplasm. Two different orientations are shown in Figure 3.1; the very distal end of the AA (transverse) where the JG cells reside (top panel) and JG cells along the distal length of the AA (bottom panel).

3.2.2 Isolation and Culture of Primary JG Cells using a Percoll Gradient

3.2.2.1 Culture of Primary JG Cells

Primary JG cells were isolated from RenGFP$^{+/-}$ mice using a Percoll gradient, as described in Section 2.4. To determine which coating would be more appropriate for the culture of primary JG cells, different basement membrane proteins were tested. Isolated cells were plated on culture dishes coated with matrigel, poly-d-lysine (PDL), fibronectin, collagen IV or PDL-laminin and the renin-expressing cells identified by their GFP expression (Figure 3.2). JG cells remained 'balled-up' on matrigel or PDL-coated dishes, but adhered more effectively on collagen-IV and PDL-laminin-coated culture dishes. Further improvement was seen in cells plated on fibronectin-coated dishes, where the majority of JG cells showed rapid, full adhesion. This was therefore deemed the most appropriate for culture of primary JG cells.

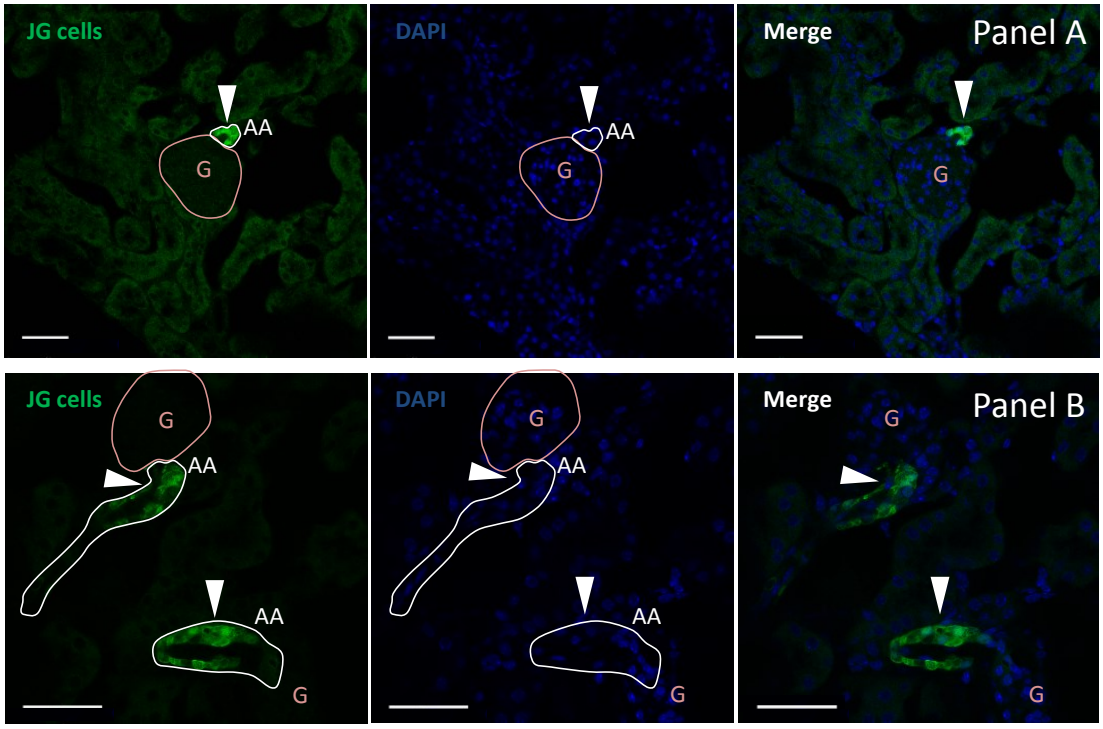

Figure 3.1: Confocal images of JG cells at the glomerular end of RenGFP $^{+/-}$ AAs. - Kidneys from a male RenGFP$^{+/-}$ mouse were fixed as described in Section 2.7.1 and sectioned at 10 μm thickness. These were mounted with DAPI and visualised on the Leica SP5 Confocal microscope. Samples were visualised at 40X magnification. The argon 405 nm blue diode laser was used to visualise DAPI (b,e), and the 488 nm Argon laser to visualise GFP (a,d). Merged images are provided (c,f). White arrows indicate GFP-positive JG cells, G: glomerular tuft. Scale bars: 50 μm.

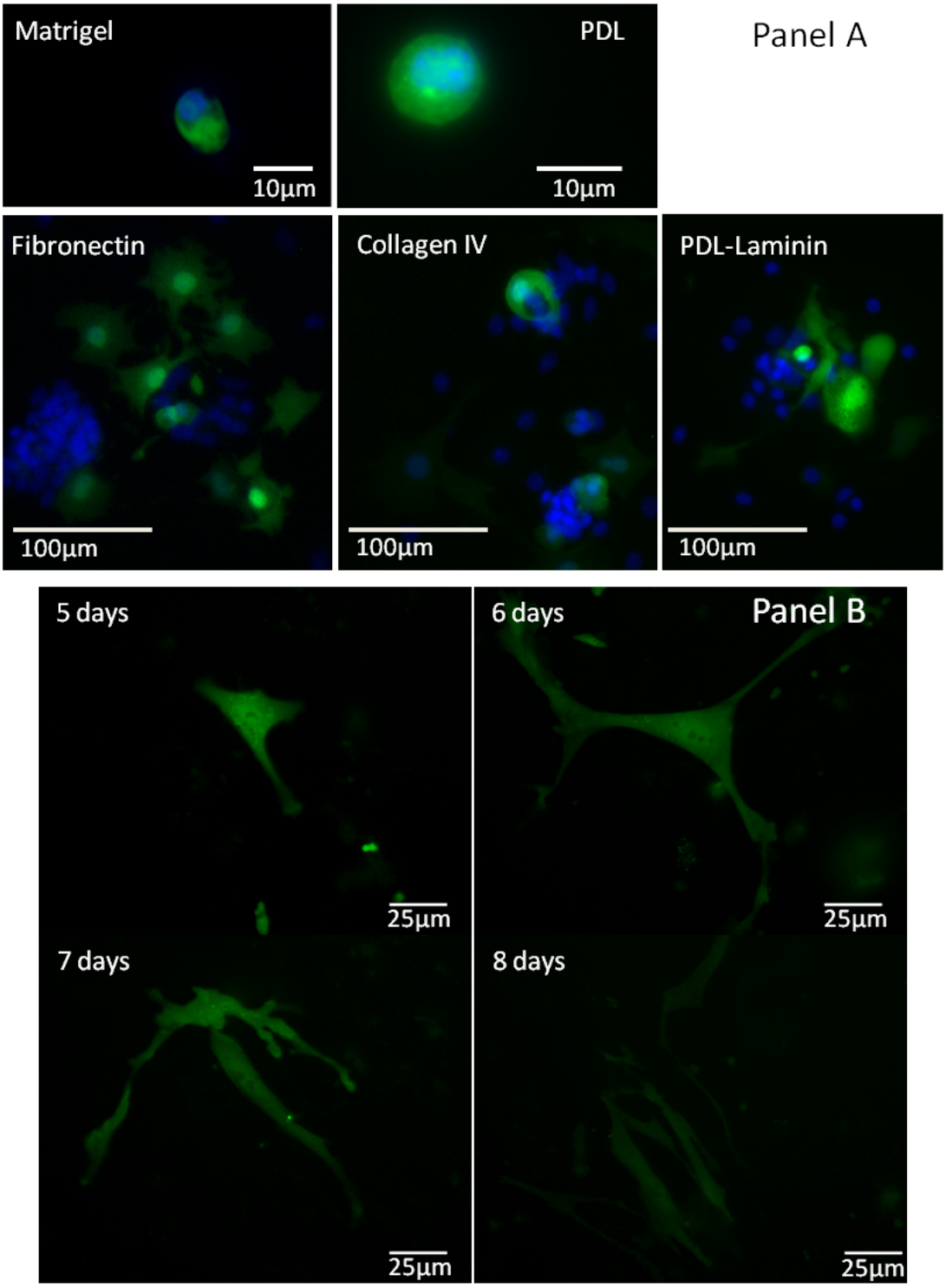

Figure 3.2: Adherence of primary JG cells to different basement membrane protein coatings. - Cells from $RenGFP^{+/-}$ mice were isolated using a Percoll gradient and plated on coverslips coated with: Panel A - 2% matrigel, 50 μg/ml poly-D-Lysine (PDL), fibronectin, Collagen IV or PDL-Laminin, and images acquired at 2 days in culture; Panel B - 50 μg/ml fibronectin, and images acquired at 5, 6, 7, 8 days in culture. Images were acquired on an epifluorescence microscope. Green: GFP expression in JG cells; blue: Hoescht 33342 live nuclear stain.

To determine the ability of JG cells plated on fibronectin to maintain renin expression, $RenGFP^{+/-}$ JG cells were freshly isolated using a Percoll gradient, plated in culture dishes and imaged daily. Cells readily adhered to the dishes and maintained expression of GFP, and hence renin, for up to 8 days (Figure 3.2). By day 8, GFP-positive cells were difficult to locate in the dish, however expression was still evident. On day 9, no GFP-positive cells were visible.

3.2.2.2 Protocol Optimisation for Live Imaging Experiments

The ability to culture fully-adhered primary JG cells for up to 8 days opened up the possibility of investigating granule dynamics using high resolution microscopy. To perform live imaging experiments using a 150X lens, cells needed to be plated on 25 cm^2 coverslips for placement in a coverslip chamber. Cells isolated from untreated $RenGFP^{+/-}$ kidneys still contained too few GFP-positive cells for practical studies at this magnification.

To increase the number of renin-expressing cells in the JGA, $RenGFP^{+/-}$ mice were given captopril (1 mg/ml; 7 days) in their drinking water. Flow cytometry was performed on cells isolated from untreated and treated kidneys and a substantial increase in the number of GFP-positive cells was achieved following treatment (Figure 3.3). On average, captopril treatment increased the GFP-positive cell number from $0.02 \pm 0.01\%$ (untreated) to $0.22 \pm 0.02\%$ ($p=0.0002$). This 10-fold increase was sufficient to allow rapid location of GFP-positive cells using a 150X magnification lens.

To ensure that primary JG cells isolated from captopril-treated mice using a Percoll gradient responded to cAMP stimulation, cells were either cultured under baseline conditions or underwent the renin induction protocol (described in Section 2.5.8). Upon

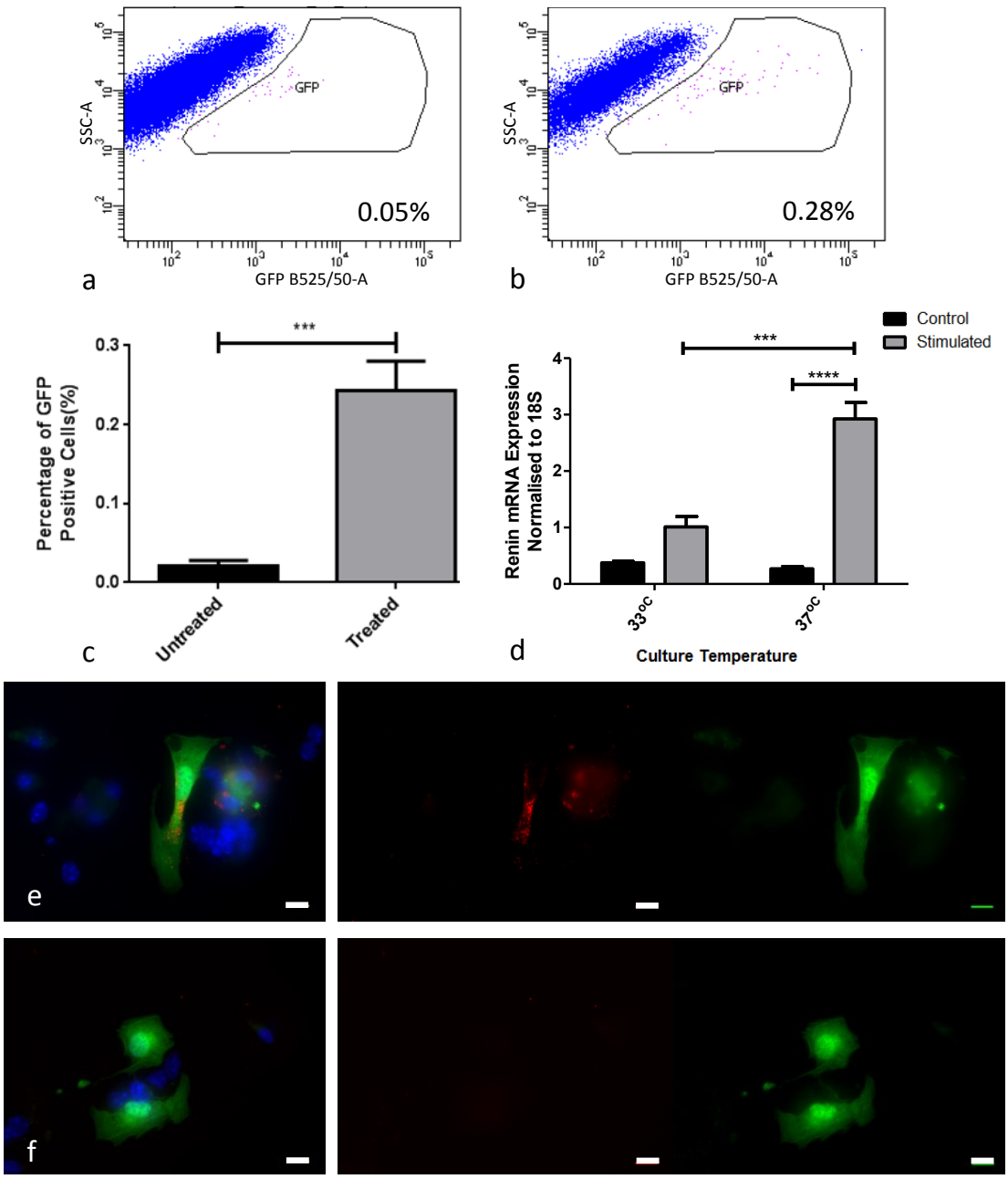

Figure 3.3: Analysis of GFP-positive cells from RenGFP$^{+/-}$ mice after treatment with captopril. - Representative plots from flow cytometry using isolated RenGFP$^{+/-}$ cells (a) at baseline and (b) after captopril treatment (1 mg/ml, 7 days). GFP-positive cells increased from 33 in 69,778 (0.05%) to 70 in 24989 (0.28%). (c) The average increase in GFP-positive cell number measured using flow cytometry (n=3-5). (d) Renin gene expression in primary JG cells isolated using a Percoll gradient, cultured at 33 °C or 37 °C under baseline conditions or after renin induction (passage 0, n=3). Two way anova and Sidak post hoc tests performed. All error bars represent S.E.M. *** indicates $p < 0.001$, **** indicates $p < 0.0001$. (e) Isolated JG cells were cultured, fixed, stained for renin and imaged using an epifluorescence microscope with a 60X oil immersion lens, with a no-primary control shown in (f). Scale bar represents 10 μm. Green: renin-producing cells, red: renin expression, blue: DAPI.

stimulation, renin expression tended towards an increase (2.7- fold, Figure 3.3) when cultured at 33 °C. Expression levels increased significantly by ∼11-fold following stimulation when the cells were cultured at 37 °C (p=0.0008, Figure 3.3). Renin staining was also performed in JG cells isolated from captopril treated mice. Staining was punctate, consistent with the presence of renin within the granules of the GFP-positive JG cells and not in a diffuse pattern such as that exhibited by the GFP expression (Figure 3.3).

To determine the effect of captopril on the location of GFP, and hence renin expression in RenGFP$^{+/-}$ mouse kidneys, tissue from treated mice was processed and a confocal tile scan performed across the medulla and cortex. Expression was seen within the cortex of the kidney exclusively along the AAs (Figure 3.4), verifying that GFP-positive cells were found at the expected JGA location. The glomeruli associated with the GFP-positive AAs are clearly visible, with no expression seen within the medullary segment. This indicated that the GFP-positive renin-expressing cells isolated from captopril-treated kidneys were of JG origin.

3.2.3 Isolation and Culture of Immortalised JG Cells

3.2.3.1 Breeding Scheme for Derivation of Immortalised, Fluorescently Labelled Renin-Expressing Cells

RenGFP mice heterozygous for the GFP transgene were crossed with Ren1d$^{-/-}$ mice to produce progeny which were GFP$^{+/-}$Ren$^{+/-}$ (Figure 3.5). Further crosses with Immortomice were performed such that half the progeny displayed granulated, GFP-positive JG cells and were tsA58$^{+/-}$. Genotyping was performed as described in Section 2.2.3.

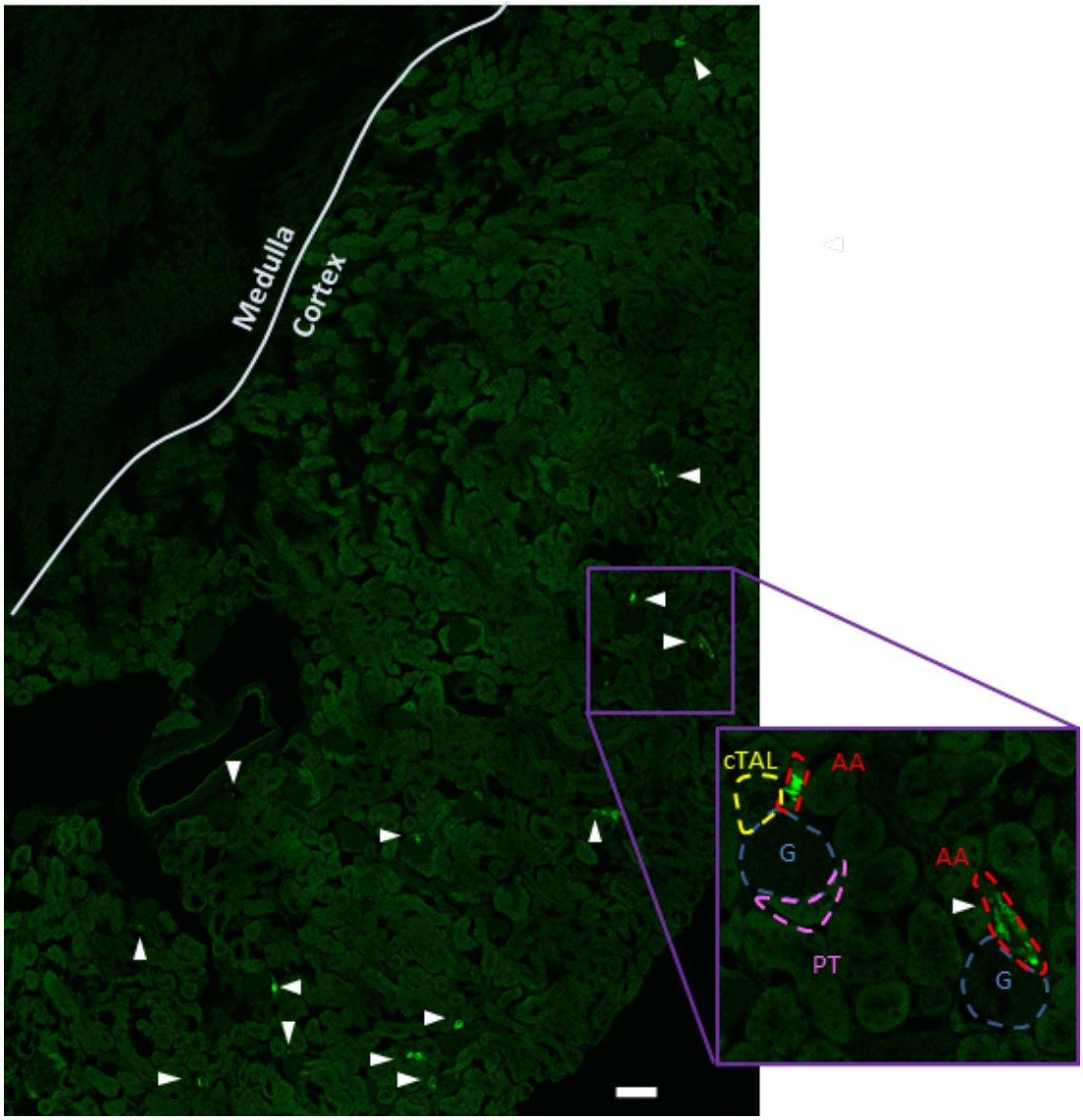

Figure 3.4: RenGFP$^{+/-}$ kidney cross section after treatment with captopril. - Mice were administered captopril (1 mg/ml, 7 days) and the kidneys prepared as outlined in Section 2.7.1. Medullary and cortical regions are identified, with white arrows identifying GFP-positive structures. The purple boxed area was enlarged to label example JGA structures; G = glomeruli (blue), PT = proximal tubule (pink), cTAL = cortical thick ascending limb (yellow), AA = afferent arterioles (red). Sections of 10 μm were taken and a tile scan acquired on the Leica SP5 Confocal microscopy using a 40X oil immersion lens with the 488 nm excitation laser, collecting emission between 495 - 530 nm. Scale bar represents 100 μm.

Figure 3.5: Breeding scheme performed to establish GFP-positive granulated and non-granulated JG cell lines - Mice heterozygous for RenGFP were first crossed with non-granulated Ren1d$^{-/-}$ mice to produce progeny heterozygous for Ren1d, which were then crossed with an Immorto-mouse to produce green granulated cell lines. A further cross of GFP$^{+/-}$Ren$^{+/-}$IM$^{+/-}$ with Ren1d$^{-/-}$ mice yielded cells appropriate for establishing cell lines of green, non-granulated JG cells. Octagonal boxes indicate the genotypes used for cell line derivation.

3.2.3.2 Sorting Homogeneous Populations of GFP-Positive JG Cells

Adult kidneys were dissected from mice with the appropriate genotype and digests of whole kidneys performed. GFP-positive JG cells were then sorted (representative plots are shown in Figure 3.6 (a); derived cell lines, genotypes and sorting statistics - Table 3.1). Low seeding number made routine expansion of the cultures from sorted cell populations difficult. Despite this, two putative granulated cell lines, RGI19 and RGI, were derived. To increase the seeding number, fetal renin-expressing cells were used (Figure 3.6 and Table 3.1) and the percentage of GFP-positive renin-expressing cells increased from 0.02 ± 0.01% in adult kidneys to 0.32 ± 0.08% in fetal kidneys (P<0.01, Figure 3.6c). Two cell lines were established - the $Ren1d^{+/-}$ 524 cells from e18.5 fetal kidneys and $Ren1d^{-/-}$ P7 cells from P7 pups.

Age	Number of mice	GFP Positive cells (%)	Number of cells isolated	Cell Line derived?	*Ren*1*d*
Adult	1	0.07	973	*RGI*19	+/-
Adult	3	0.004	460	No	-/-
Adult	3	0.02	4196	No	+/-
Adult	4	0.001	250	No	+/-
Adult	5	0.01	4304	*RGI*	+/-
e17.5	9	0.18	2804	No	+/-
e17.5	11	0.18	5556	No	+/-
e18.5	9	0.54	8613	524	+/-
P7	3	0.21	35815	*P*7	-/-

Table 3.1: Statistics for example GFP-positive renin-expressing cell sorts.

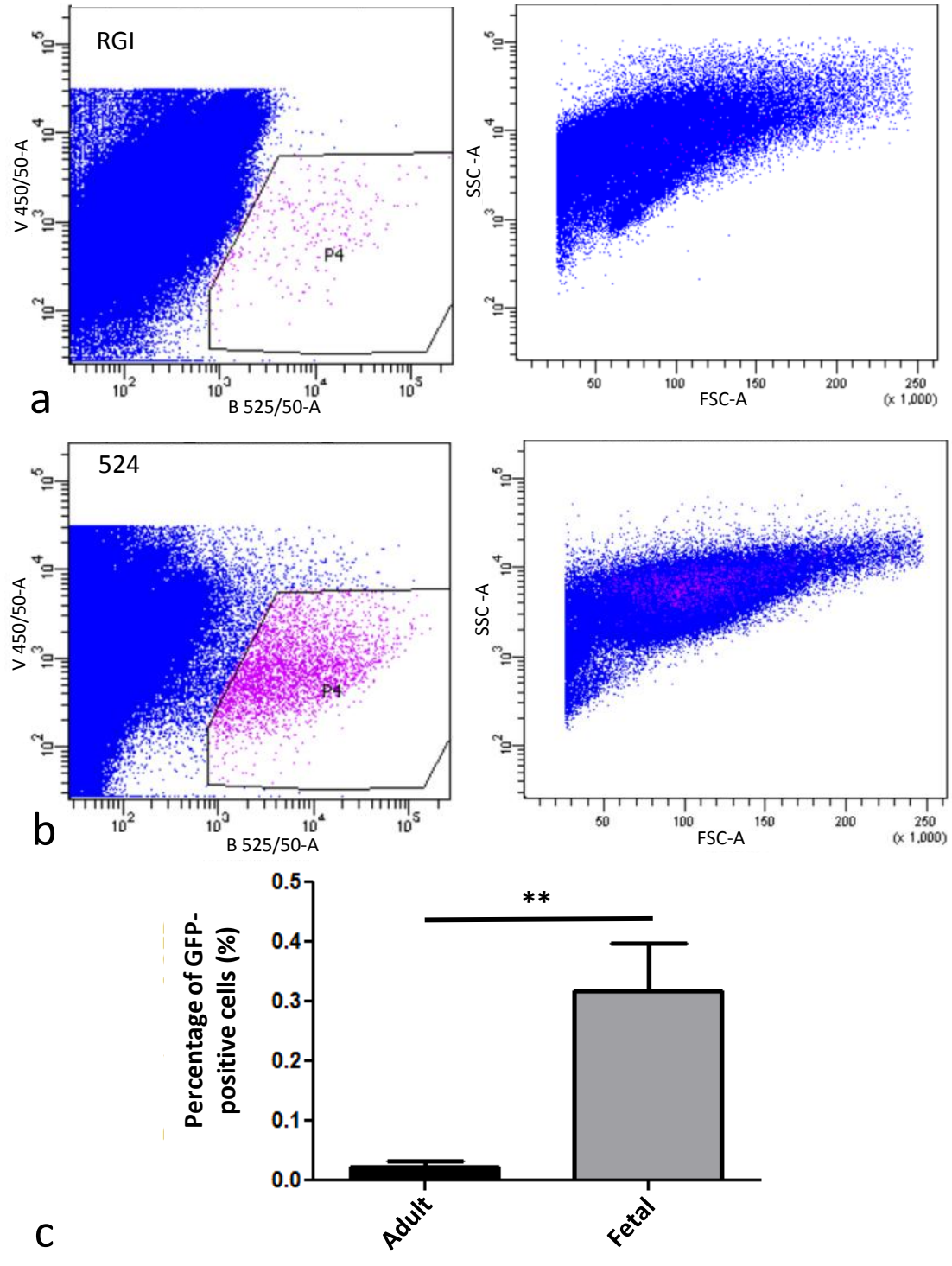

Figure 3.6: FAC Sorting of immortalised, GFP-positive JG cells. - Example plots from sorting (a) five $RenGFP^{+/-}Ren1d^{+/-}IM^{+/-}$ adult kidneys (RGI cell line) and (b) nine e18.5 $RenGFP^{+/-}Ren1d^{-/-}IM^{+/-}$ embryonic kidneys (524 cell line). DAPI-negative (y-axis, 450 nm laser) and GFP-positive (x-axis, 525 nm laser) cells were sorted (shown in pink) from the population of live cells (shown in blue). The forward scatter (FSC) vs. side scatter (SSC) plot indicates where GFP-positive cells lay in relation to other kidney cells. (c) The percentage of GFP-positive cells isolated (n=5,6). **: $p < 0.01$.

3.2.3.3 Verification of GFP Expression in Freshly Sorted JG Cells

Sorted GFP-positive renin-expressing cells from $tsA58^{+/-}$ mice were plated on matrigel- or fibronectin-coated culture dishes, and epifluorescence microscopy was used to determine GFP expression. JG cells did not initially adhere fully to matrigel-coated culture dishes, taking on a 'balled-up' appearance, but adhered fully to fibronectin-coated culture dishes in the same manner as JG cells from RenGFP$^{+/-}$ mice (Figure 3.7). Cells were checked daily and by three days post-plating the GFP expression was no longer present. Although cells did not adhere to matrigel-coated dishes within the 3 days over which renin was expressed, they did eventually settle and proliferate.

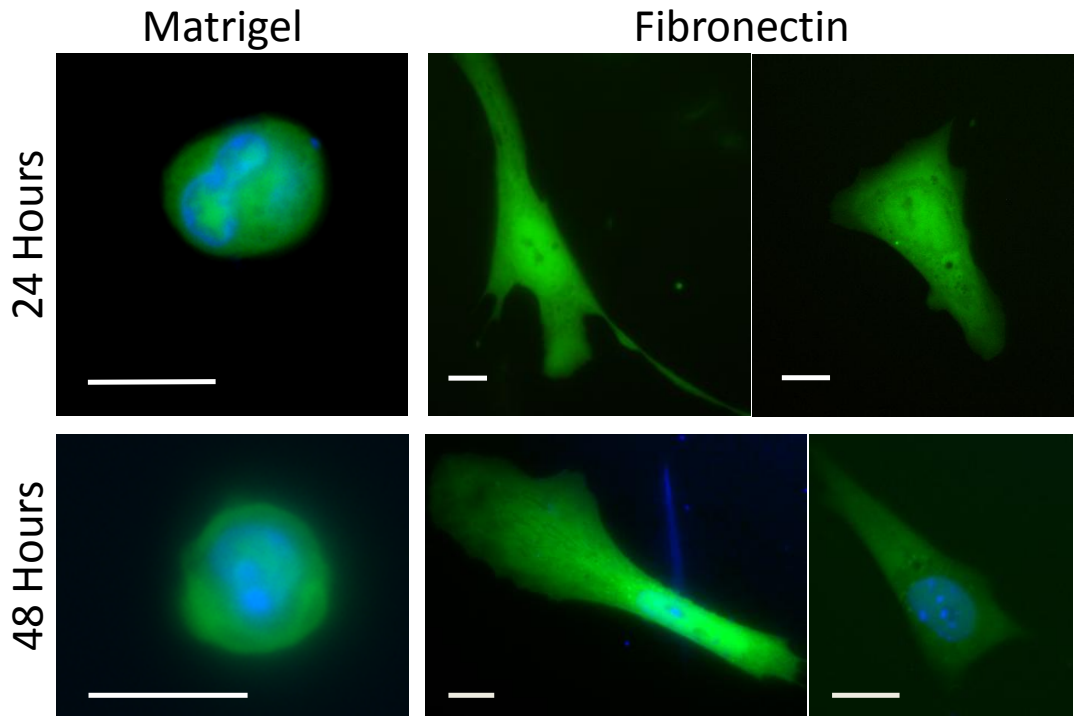

Figure 3.7: GFP expression in JG cells freshly sorted for cell line derivation. - Cells from $RenGFP^{+/-}tsA58^{+/-}Ren1d^{+/-}$ mice were isolated and plated on coverslips coated with matrigel (2%) or fibronectin (50 μg/ml), cultured for 24 hours (top panel) or 48 hours (bottom panel) and imaged using an epifluorescence microscope with a 40X (matrigel) or 60X (fibronectin) oil immersion objective lens. Green: GFP expression in renin-expressing cells, blue: Hoescht 33342 live nuclear stain.

3.2.3.4 Renin Expression In Sorted, Immortalised JG Cell Lines

To determine whether the established cell lines retained the ability to express renin in culture, gene expression was analysed using qPCR. This was performed in RGI and RGI19 granulated cell lines since active renin should be produced. Cells were either cultured under baseline conditions, or following the renin induction protocol (described in Section 2.5.8). Since tsA58$^{+/-}$ cells are known to differentiate when transferred to non-permissive culture conditions (37 °C) or in the absence of IFN-γ (due to the disappearance of the large T antigen), cells were also cultured either with, or without, IFN-γ, at 33 °C or 37 °C.

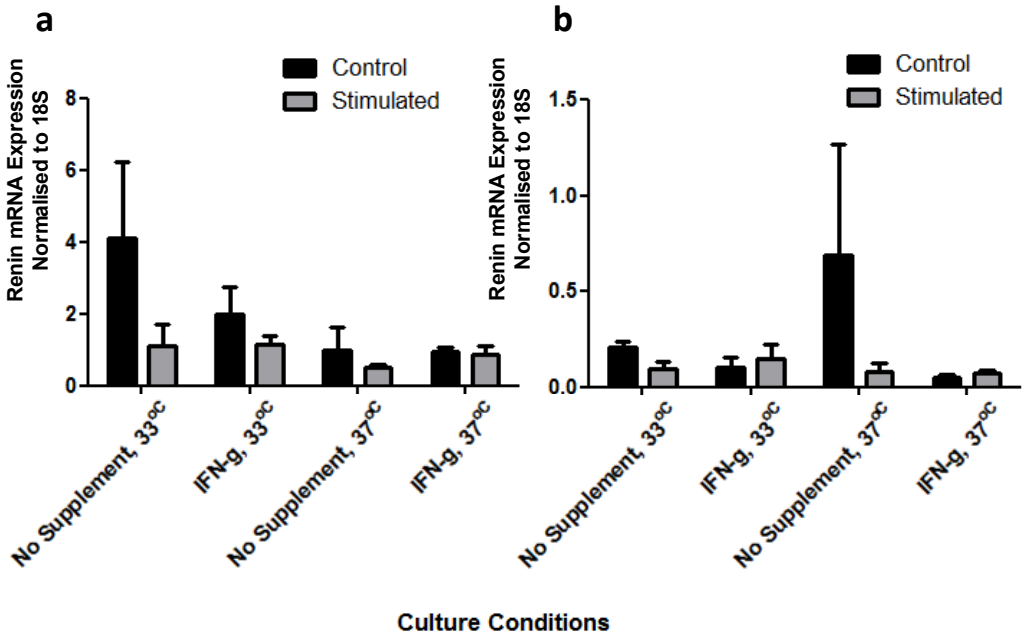

Figure 3.8: Renin gene expression analysis in derived cell lines at early passages. - qRT-PCR analysis of renin expression in granulated (a) RGI (passage 7) and (b) RGI19 (passage 9) cell lines. Cells were cultured at 33 °C or 37 °C, with or without IFN-γ (100 μg/ml) on matrigel-coated (2%) 6-well dishes and renin induction performed (serum starved for 24 hours then treated with fresh media or forskolin (10 μM) and IBMX (100 μM) for 24 hours). n=3 for each group. Two-way anova and Bonferroni post-hoc analysis was performed. Data are mean ± S.E.M.

The renin induction protocol was previously shown to work effectively in primary JG cells (Figure 3.3) and induction of renin expression was therefore performed on RGI and RGI19 cell lines at the earliest possible passage. No significant increase in renin expression in either RGI or RGI19 cells was seen upon stimulation (Figure 3.8); in fact, there was a trend towards a decrease in renin expression upon stimulation in RGI cells. These data also indicate that the presence of IFN-γ and the culture temperature did not affect the expression of renin. Despite not expressing renin after long-term culture, established cells lines survived to over 30 passages, indicating that the immortalisation of the cells was successful.

No staining for renin or GFP was observed by immunofluorescence analysis in either RGI19 (passage 9) or RGI (passage 10) cells, either at baseline or after stimulation, nor was any GFP expression observed.

A radioimmunoassay was performed on the supernatant from 524 (passage 10) and RGI (passage 14) cells, cultured at 33 °C or 37 °C, under control conditions and after stimulation using the renin induction protocol, to determine whether any functional renin enzyme was translated. Counts were below the limit of detection.

3.2.3.5 Embryonic Kidney Culture and JG Cell Isolation

To try and harness the immortalisation potential of the cells as early as possible, a technique reported by the Davies Laboratory (171) to derive cells lines from embryonic Immortomouse kidney cells was used.

To establish the technique as described by the authors, $RenGFP^{+/-}tsA58^{+/-}Ren1d^{-/-}$ mouse kidneys were dissected at e12.5 and cultured for 4 days (Figure 3.9). This time-point was chosen as the Davies Laboratory have established cell lines from Immor-

tomouse kidneys isolated at this time point (171). The kidneys grew well in culture however, as expected, there was no visible development of the vasculature, or GFP expression, indicating that renin was not being expressed. Therefore given the success of the technique, kidneys were dissected at e15.5, the timepoint at which vascular development is known to commence (42). The kidneys grew well in culture, increasing in size and starting to show signs of the medullary and cortical regional development after 2 days in culture (Figure 3.9). Cultured e15.5 kidneys showed strong vascular expression of renin, which appeared to follow the main interlobar arteries. This expression increased along the arteries after 1 day in culture but rapidly declined along the major arteries by 2 days in culture, concurrent with the expression starting to localise to the minor arterioles.

After 3 days in culture, kidneys were disaggregated. From 5 kidneys, 344 GFP-positive cells were FACS-sorted from a total of 350,000 cells (0.1% of the total cell population). These cells were plated on specialised culture dishes with a coverslip glass bottom coated with fibronectin and cultured at 37 °C for 24 hours before being transferred to 33 °C. Images of sorted cells acquired 24 hours and 48 hours post-plating indicated that sorted cells were expressing GFP, and hence were capable of renin exression (Figure 3.10). Hoescht nuclear dye was used to confirm that the cells were alive. After 3 days in culture these cells lost their GFP expression, similar to observations in primary adult JG cells.

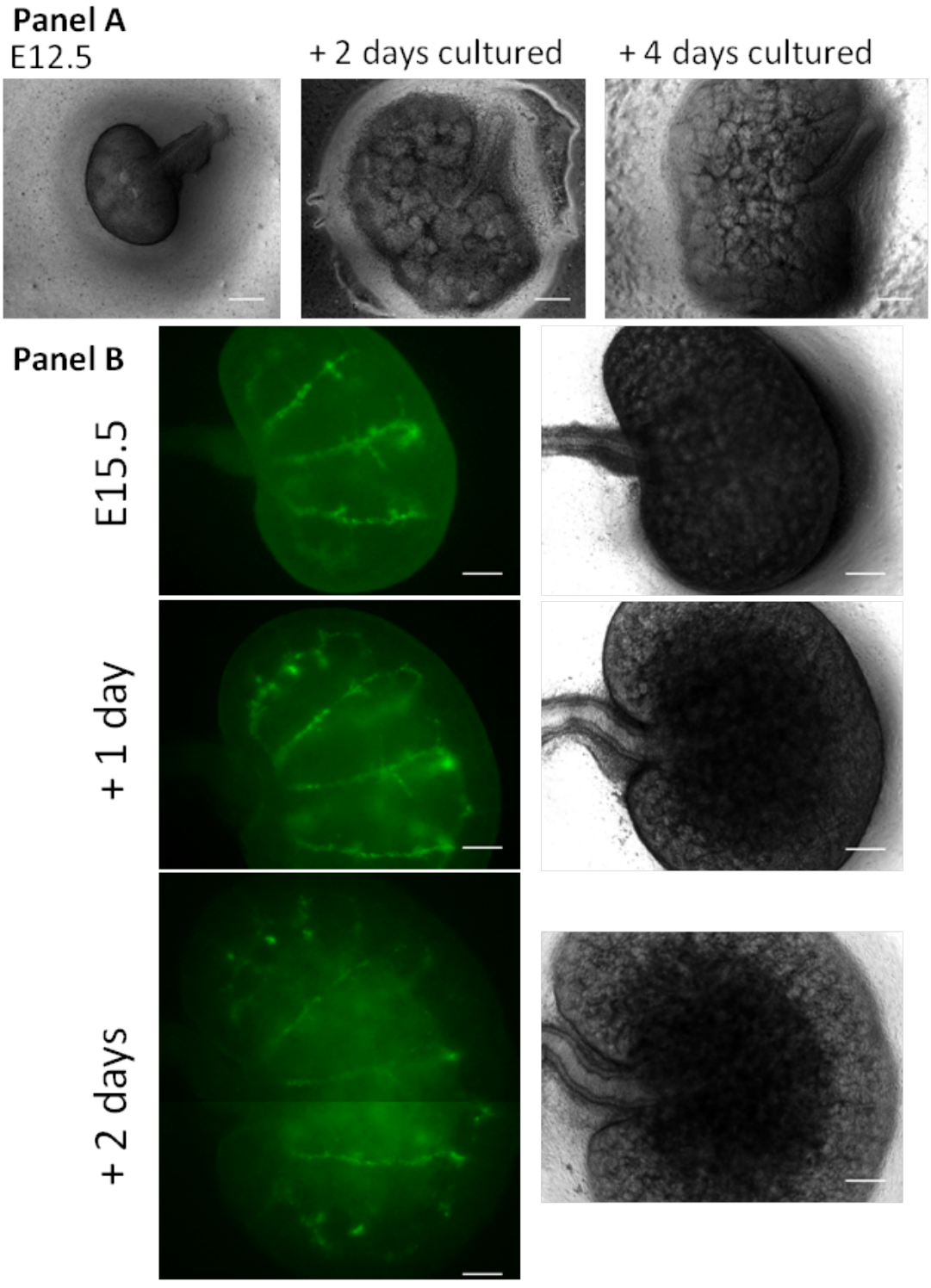

Figure 3.9: Localisation of renin expression in cultured embryonic kidneys. - $RenGFP^{+/-}tsA58^{+/-}Ren1d^{-/-}$ kidneys were dissected and cultured in immortalisation media at 37 °C. Panel A: e12.5 kidneys were cultured for 4 days. Brightfield images were taken daily. Panel B: e15.5 kidneys were cultured for 2 days. Epifluorescence (LHS) and brightfield (RHS) images were taken daily. Green: GFP expression in renin-expressing cells. Scale bars represent 250 μm.

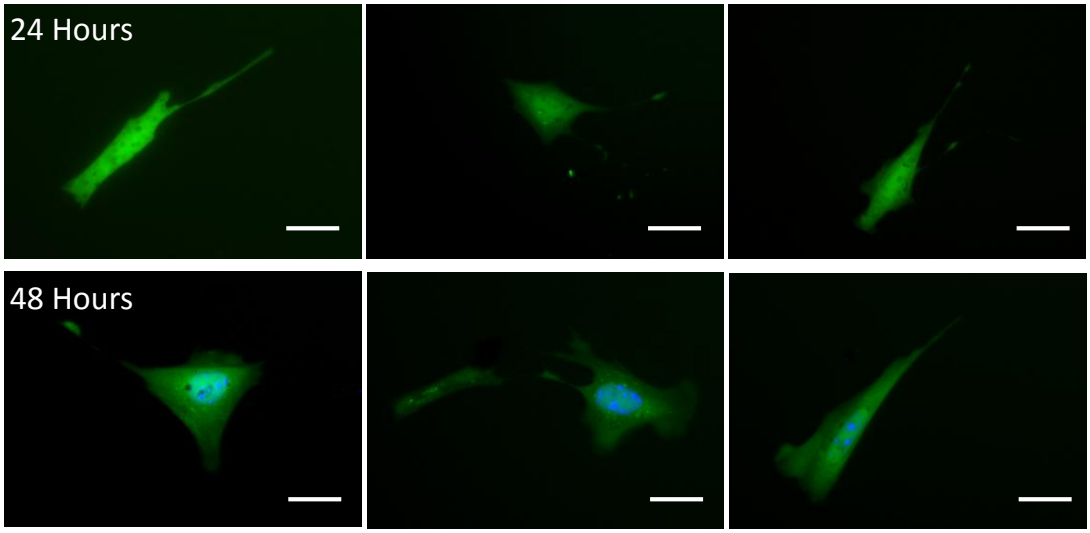

Figure 3.10: Confirmation of GFP expression in renin-expressing cells isolated from cultured e15.5 embryonic kidneys. - Renin-expressing cells from cultured e15.5 $RenGFP^{+/-}tsA58^{+/-}Ren1d^{-/-}$ kidneys were FAC sorted on their GFP-expression and plated on fibronectin-coated (50 μg/ml) dishes. Images were acquired after 24 (top panel) and 48 hours (bottom panel) on an epifluorescent microscope using a 40X objective lens. Green: GFP expression in renin-expressing cells, blue: Hoescht 33342 live nuclear stain used at 48 hours. Scale bars: 25 μm.

3.3 Discussion

3.3.1 Isolation Methodology and Culture of Primary JG Cells

Significant effort was put into developing a method by which JG cells could be isolated and successfully cultured on glass coverslips. Percoll gradients are widely used for isolation of primary JG cells, particularly by Kurtz (144, 172), and Beierwaltes (73, 76, 173, 174), to investigate fundamental signalling mechanisms associated with renin transcription and secretion. The basic methodology between these published protocols and that carried out in the present study are similar, though subtle changes were made to improve both the isolation and culture process.

The Percoll gradients used in the literature were 30% (172), 35% (73, 173, 174) or 40% (76). By using a discontinuous gradient containing 10%, 20%, 30%, 40% and

50% Percoll steps (distinguished by incorporation of phenol red in alternate layers), reproducibility of the extraction was improved.

The inability of primary JG cells to adhere fully to matrigel- or PDL-coated culture dishes within the 72 hours period when renin was expressed was unexpected. PDL is a positively charged amino acid polymer, which acts as an adherence factor, and is historically the coating of choice for culture of primary JG cells. Interestingly, the 'balled-up' appearance described here was also observed in studies describing intracellular signalling and renin secretion from JG cells (73, 75, 76, 160).

Collagen IV, PDL-laminin and, most significantly, fibronectin were significantly more effective at allowing rapid adhesion of primary JG cells to the culture dish, and are known to contribute to the extracellular matrix (ECM) *in vivo* in the JGA: type IV collagen and the glycoprotein laminin are localized to the JGA basement membrane whilst the glycoprotein fibronectin is localised to the distal end of the AA within the ECM (175). This suggests that factors provided by the ECM are necessary for efficient adherence of primary JG cells, and perhaps contribute to the increased longevity of GFP expression seen in primary JG cells when plated on fibronectin.

The renin induction protocol was used to determine whether cells were responding to cAMP-stimulation through administration of IBMX (iso-butyl-methyl-xan-thine) and forskolin. IBMX non-selectively inhibits cAMP phophodiesterases whilst forskolin directly activates Adcy5/6, stimulating renin transcription and secretion (76, 141, 176, 177). Freshly isolated JG cells from RenGFP$^{+/-}$ mice responded effectively to this stimulus, with an increased expression seen in cells cultured at 33 °C, and an augmented increase in expression seen at 37 °C. This is in the same range as the 3-fold increase reported by Klar *et al.* (137) upon addition of 5 μM forskolin and 100 μM IBMX.

Although secretion was not measured in the current study, administration of 10 μM forskolin and 500 μM IBMX for 1 hour to primary JG cells isolated using a Percoll gradient has previously been shown to induce an approximately 3-fold increase in renin release (76).

3.3.2 Derivation of Immortalised Juxtaglomerular Cell Lines

In an attempt to retain JG cell traits such as regulated release of active renin in long term culture, the Immortomouse was used. This approach seemed particularly promising since kidney cell lines have previously been established using this method (171). Importantly, cells are only conditionally immortalized when cultured at the permissive temperature of 33 °C and in the presence of IFN-γ, otherwise the cells senesce (82, 83).

GFP expression in JG cells from $RenGFP^{+/-}tsA58^{+/-}Ren1d^{+/-}$ mice was used as a reporter for renin expression in culture. Plating on matrigel and fibronectin confirmed that expression of GFP, and hence renin, was limited to 72 hours in culture as previously reported (178), even in the presence of the $tsA58$ immortalising gene. GFP localisation was homogeneous in the majority of these cells as expected (11).

In order to derive immortalised cells of JG origin from tsA58$^{+/-}$ mice, a number of technical issues needed to be addressed, a major one being the low number of JG cells sorted per kidney. Because of very stringent gating, FACS sorting of adult kidney digests produced extremely low numbers of GFP-positive JG cells (0.02 $\pm$ 0.01%), in keeping with the previously reported range of 0.001 - 0.01%, from a Ren-YFP mouse model (52). Scaling up the protocol was detrimental to JG cell survival even when using a rapid-yield sort for a highly JG-enriched population, followed by a slower high-purity

sort (dramatically decreasing the sort time and exposure to room temperature).

Whilst two cell lines were successfully established from adult kidney digests (RGI19 and RGI) there were generally too few cells isolated by FACS to establish lines effectively, however seeding density was increased by using fetal tissue as a source of cells.

During development, renin expression extends along the trunk of the arcuate artery, branching off into the juxtamedullary AAs. By e17.5 renin expression in the arcuate trunk begins to regress, firstly to the majority of AAs, and then further to the classic AA location (42). By using e17.5 and e18.5 kidneys of the correct genotype, advantage was taken of this increased number of renin expressing cells in the developing kidney and the percentage of GFP-positive renin-expressing cells was enriched 10-fold, despite the small amount of tissue. Postpartum, kidney and vascular volume continue to increase but by P7 renin expression has fully localised to its terminal AA location (42). Since the kidney is not fully mature at P7, the relative percentage of GFP-positive JG cells is increased, yielding the more efficient sorting percentages seen in the present study. I was able to establish two cell lines using fetal (524) and P7 kidneys (P7). Although cells from these time points are renin-expressing, their renin expression remains plastic and they are not fully differentiated JG cells (13).

It is important to note that JG cells are not granulated at e17.5 or e18.5 - granules start to appear immediately following birth (LHuillier, unpublished, discussed in Section 1.4.1). However, if the mother is placed on a low salt diet or is administered an ACE inhibitor during fetal development, renin-expressing cells in e18.5 kidneys have been shown to granulate (d'Huillier, unpublished). Cell lines of JG origin from such mice might therefore provide an interesting model in which to study the onset of gran-

ulation through pharmacological manipulation, provided that the cells subsequently retain the granular phenotype.

3.3.3 Characterisation of Established Immortalised Cell Lines of JG Origin

Because of low seeding density, it was not possible to assess renin gene expression at the earliest passages; gene expression was assessed at passage 7-9. Since renin expression is particularly sensitive to environmental conditions (178), it was unclear how long-term culture at 33 °C or the addition of IFN-γ would affect the transcription or expression of renin in JG cells. In decidual cells, renin mRNA levels, renin expression and renin release decreased in response to prolonged culture with IFN-γ (179), whereas the presence of IFN-γ in the culture media for human erythroid cell lines had no effect on prorenin mRNA and increased the levels of prorenin significantly (180). To establish whether either of these factors affected renin expression, a radioimmunoassay for renin activity and qPCR were performed on cells cultured at 33 °C and 37 °C, with and without IFN-γ in the culture media, under baseline conditions or after renin induction.

The anticipated increase in renin expression in response to the addition of IBMX and forskolin was not seen. This raises questions about the signals and stimuli required to maintain renin expression and granulation ability in both primary and immortalised JG cells. It is well established that arteriolar SMCs upstream of the glomerulus remain capable of expressing renin when physiologically challenged, and these cells show similarities in their gene expression profile with pericytes, suggesting that JG cells may be a subset of specialised arteriolar pericytes (52). Interestingly, cultured fetal pericytes showed renin expression and synthesis under the same induction protocol (45). Since

induction was unsuccessful in the derived immortalised cell lines (both fetal and adult), this suggests that there may be a difference at the gene expression level between arteriolar pericytes and pericytes which have commited to a JG cell lineage and been immortalised.

The data presented in this study suggests that the local JGA architecture is important for maintenance of renin expression. Although the immortalised JG cells were able to survive over 30 passages, they had lost their capacity to express renin and respond to cAMP-stimulated renin release. The altered localisation of renin expression in $Cx40^{-/-}$ mice to the periglomerular interstitium did not result in a reduction of regulated release, indicating that it is not the flow at the apical surface of JG cells which is necessary for renin expression (57). Therefore it is likely that paracrine signaling is integral to maintaining renin expression in JG cells, in particular the interaction with the underlying endothelium, as well as the appropriate gene expression profile. This suggests that perhaps a monoculture is not optimal for long-term culture of renin-expressing cells. To address this, initial co-culture experiments were performed for $RenGFP^{+/-}tsA58^{+/-}Ren1d^{-/-}$ cells on a layer of immortalised endothelial cells. No significant improvement was seen in cell adhesion or longevity of expression was seen, however further experiments would be needed to verify this. It is also possible that a non-adherent culture method such as a hanging drop culture would allow faithful maintenance of renin expression (181). This was not addressed within this project but could be pursued in future studies.

To try and harness the immortalisation potential of the cells as early as possible whilst maintained in native kidney architecture, kidneys from pups of the correct genotype were isolated and cultured *in vivo* in the presence of immortalisation medium

(171). As previously stated, renin expression develops in the metanephric tissue of blood vessels early in day e15, and is clearly evident by e15.5 (42), as seen in the cultured kidneys, which grew well despite lack of environmental signal found *in vivo*. After 4 days in culture, approximately 0.1% total kidney cell population were GFP-positive, which is not significantly different to the 0.17% GFP-positive cells sorted from freshly isolated e18.5 kidney cells. Whilst JG cells sorted from cultured kidneys were shown to express renin for up to 3 days in culture on fibronectin-coated coverslips, they lost expression in longer term culture. This approach may, in future studies, prove more successful at allowing retention of a renin-expressing ability under cAMP stimulation.

3.4 Conclusions

In conclusion, cell lines of JG origin were derived from $RenGFP^{+/-}Ren1d^{+/-}tsA58^{+/-}$ and $RenGFP^{+/-}Ren1d^{-/-}tsA58^{+/-}$ kidneys. They were unable to respond to cAMP stimulation and did not show evidence of renin expression. However JG cells isolated using a Percoll gradient from captopril-treated $RenGFP^{+/-}$ mice adhered fully to fibronectin-coated coverslips, were easily identifiable on 25cm^2 coverslips and responded to cAMP stimulation. This protocol is therefore optimised for use in studies to investigate granule dynamics in JG cells.

4

Granular Dynamics in Juxtaglomerular Cells

4.1 Introduction

Granule behaviour in JG cells and the role granules play in the secretion of renin remain controversial, as discussed in Section 1.9. Despite apparent exocytosis, no evidence has been published to date showing granule motion in JG cells under any conditions.

The development of high-speed image acquisition has enabled highly accurate granule tracking in real time under controlled conditions. One such technique is TIRF microscopy (182); by increasing the angle the laser beam makes with the coverslip on which cells are plated, the critical angle at which light is totally internally reflected within the coverslip can be reached. At this angle no light from the laser beam is probing the cell, however an evanescent electromagnetic wave is generated at the surface of the coverslip. This field rapidly decays, and only propagates approximately 100 - 150 nm into the sample. Therefore only fluorophores within this thin optical section are excited, eliminating out of focus light from the majority of the cell and improving axial

resolution and signal to noise ratio (SNR) (183) (detailed in Figure 4.1).

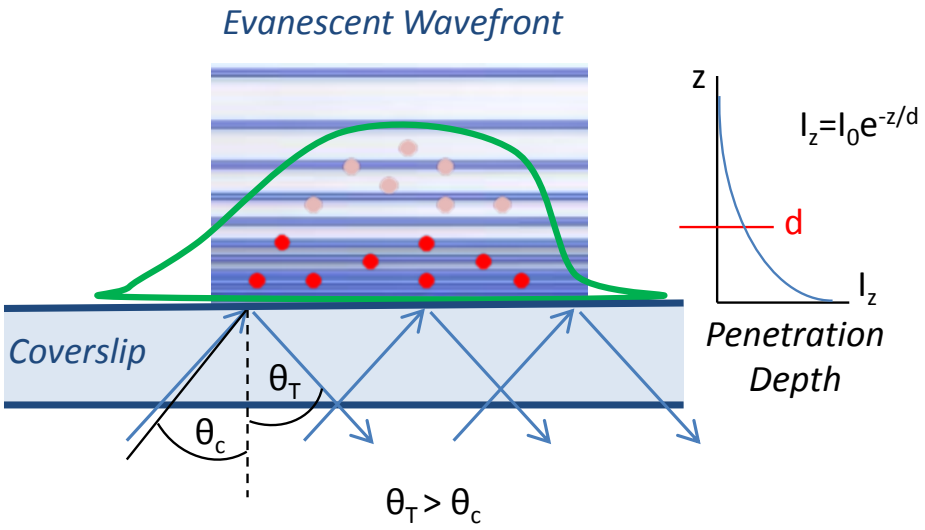

Figure 4.1: Schematic diagram representing TIRF microscopy. - The angle of incidence (θ_T is increased to greater than the critical angle for total internal reflection (θ_c), creating an evanescent wave which propagates into the cell. This wavefront is rapidly decaying, meaning that the majority of fluorophores excited are found below the penetration depth (d). Here, z is the distance from the coverslip and I_z is the intensity of the evanescent wave.

4.1.1 Aims

It is hypothesised that large, dense core granules respond dynamically to renin secretory stimulation. The following experimental aims were therefore addressed:

1. Identify both vesicles and large dense core granules optically in live, primary cultured JG cells.

2. Determine whether granules are stationary or dynamic under basal and stimulated conditions in primary JG cells.

4.2 Results

4.2.1 Imaging Granule Dynamics in Widefield Microscopy

4.2.1.1 Image Acquisition of Renin Containing Granule Motion

Cells were isolated from captopril-treated RenGFP$^{+/-}$ kidneys, plated and cultured for 24 hours on fibronectin-coated coverslips. The acidotropic fluorophore lysotracker red (100 nM) was allowed to accumulate in granules 30 mins prior to the experiment, and the coverslips mounted onto an Olympus Cell Excellence IX81 with a 150X oil immersion lens with TIRF capabilities. Renin-expressing cells were identified on the basis of their GFP expression. Two-channel imaging was performed in each cell to ensure that the lysotracker signal being collected was from granules within renin-expressing cells (Figure 4.2, upper panel).

Granules were catagorised as 'large' (d $>$ 500 nm) or 'small' (d $<$ 500 nm). Movement of both large and small granules was captured for the first time. Interestingly, a number of the large granules moved appreciably in response to isoproterenol treatment (Figure 4.2, white arrows, top panel), however since images were not acquired during addition of isoproterenol the movement itself was not captured. Whilst these larger granules exhibited motion around a fixed location (caged), small granules (d $<$ 500 nm) appeared to move much greater distances around the cell in a directed motion at a more rapid speed. To visually demonstrate the movement of granules, a maximum intensity projection was performed on the time series at baseline and after treatment (Figure 4.2, top panel, bottom row). A maximum intensity projection displays the maximum signal intensity recorded in each pixel over the 1000 frames, rendering a representation of the tracks followed by granules over the image acquisition period. Movement of the

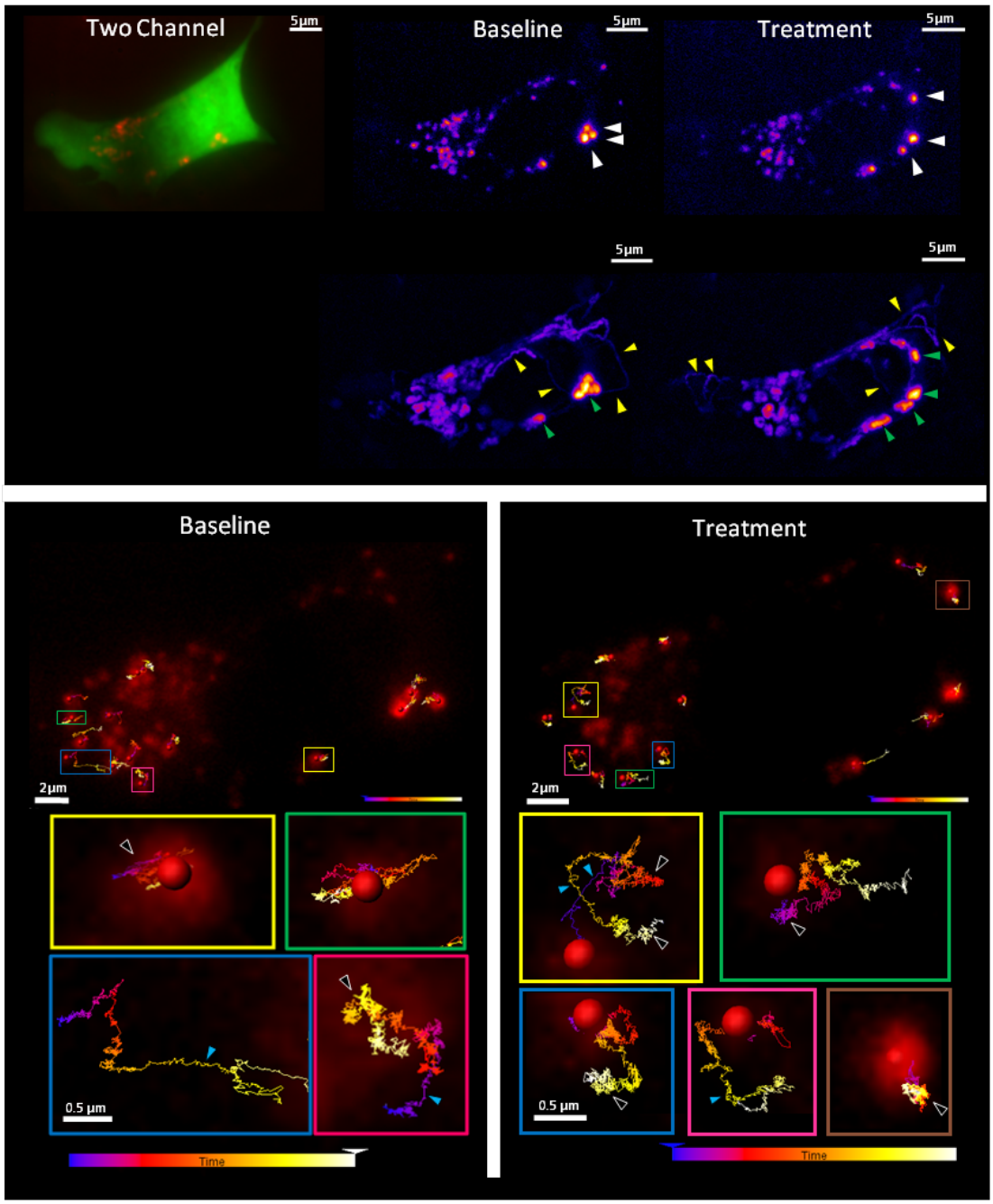

Figure 4.2: Cells imaged using widefield microscopy from which renin-containing granule dynamics were analysed. - Top panel: Cells were stained with lysotracker (100 nM) and identified on the basis of GFP signal. Merged GFP and lysotracker images verified correct lysotracker localisation within the cell. Signal from lysotracker-filled granules at baseline and after addition of isoproterenol are shown for a single cell and displayed using the ImageJ heat map LUT 'Fire' for ease of visualisation, presented as a single frame (top line) or a maximum intensity projection over the 1000 frames (bottom line). White arrow: examples of large granules which moved appreciably in response to isoproterenol; yellow arrows: tracks taken by small granules. Bottom panels: Large granule (d > 500 nm) tracking was performed using Imaris 7.7. Tracks are superimposed onto raw lysotracker signal intensity data, zooming in on example tracks. Track colour correlates with time (from blue at the start to yellow at the end, as indicated in the legend).

larger granules is clearly restrained (green arrows), whilst the smaller granules tracked out much longer tracks around the cell (yellow arrows).

4.2.1.2 Tracking of Renin Containing Granule Motion

To quantify this motion, granule tracking was performed using Imaris 7.7. Due to low SNR, small granules were not able to be tracked using widefield microscopy despite the large amount of movement seen, therefore only large granules were included in the analysis.

Examples of individual large granule tracks are displayed in the lower panels of Figure 4.2, sections of which are shown magnified in corresponding coloured boxes under baseline and treated conditions. The majority of granules displayed caged behaviour (black arrows) with elements of directed behaviour interspersed (blue arrows, paricularly in the blue box under baseline conditions), with a small number of granules showing purely caged behaviour. Examples of caged granule behaviour can be seen under baseline conditions (yellow box: track length 19.5 μm, average speed 0.28 μm/s), and after treatment (brown box: track length 20.2 μm, average speed 0.29 μm/s). In the granules showing directed behaviour the average speed and track length increased, both under baseline conditions (pink box: track length 31 μm, average speed 0.47 μm/s) and after treatment (green box: track length 39 μm, average speed 0.56 μm/s).

This analysis was performed on large granules in three cells. The average speed of the dense core granules increased significantly from 340 $\pm$ 10 nm/s to 590 $\pm$ 30 nm/s ($p<0.0001$) upon administration of isoproterenol, an increase of 76% (Figure 4.3a), however the average track length did not change significantly from 20100 $\pm$ 800 nm to 21000 $\pm$ 2000 nm (Figure 4.3b).

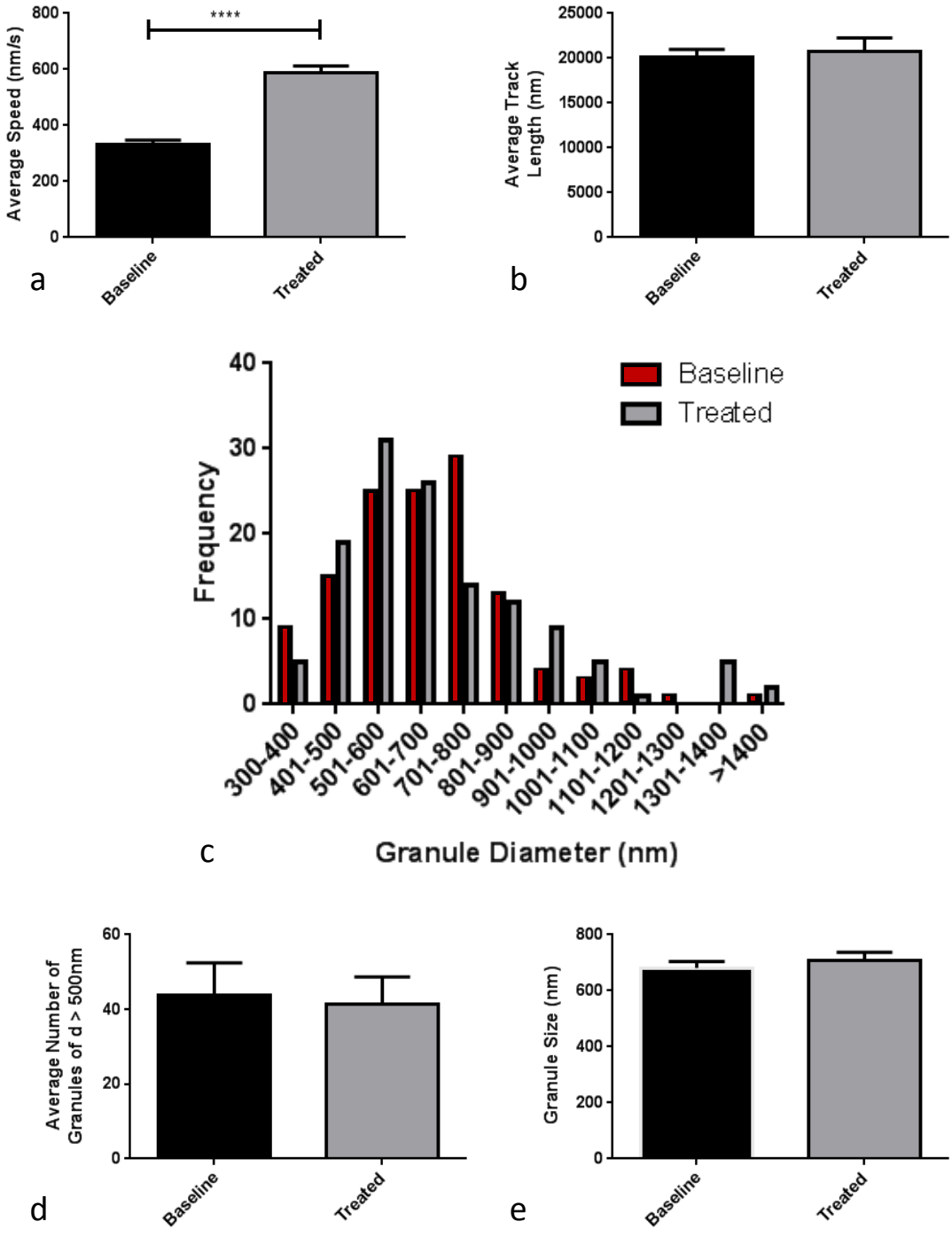

Figure 4.3: Analysis of large granule dynamics, imaged using widefield microscopy. - Measurement of (a) number and (b) diameter of granules from 8 data sets was performed in ImageJ and granules with d > 500 nm included in analysis. (c) A histogram of granule diameters in the 3 datasets taken forward for tracking analysis, which was performed in Imaris 7.7 on granules of d > 500 nm. Average granule (d) speed and (e) track length was extracted. Data are mean ± S.E.M. **** indicates $p < 0.0001$

The diameter of granules was measured manually in ImageJ in eight cells, before and after treatment, and the number of large granules calculated. The average number of large granules in the cell did not significantly change with the addition of isoproterenol (43 ± 8 before and 41 ± 7 granules following treatment, Figure 4.3d). The average size of the granules also remained unchanged (680 ± 20 nm before and 710 ± 30 nm after treatment, Figure 4.3e). This can be further seen in the histogram of granule diameter sizes from within the three cells taken forward for tracking analysis (Figure 4.3c), where the addition of isoproterenol did not change the distribution of granule sizes. This was verified visually, with no granule exocytosis events seen in the raw data.

Although no exocytosis events were observed, the addition of isoproterenol caused a displacement of large granules and a significant increase in their speed of movement. To image this displacement during the addition of isoproterenol, the experiment was repeated using TIRF microscopy.

4.2.2 Imaging Granule Dynamics in TIRFM

4.2.2.1 Image Acquisition of Renin Containing Granule Motion in TIRFM

JG cells were located in widefield mode by their GFP expression and loaded with lysotracker red. The angle of incidence of the laser was then increased until total internal reflection of the laser beam within the coverslip had been achieved (Figure 4.4). This was clear since only the membrane in contact with the coverslip was visualised and the number of visible granules was greatly reduced. An example of this is presented in Figure 4.4.

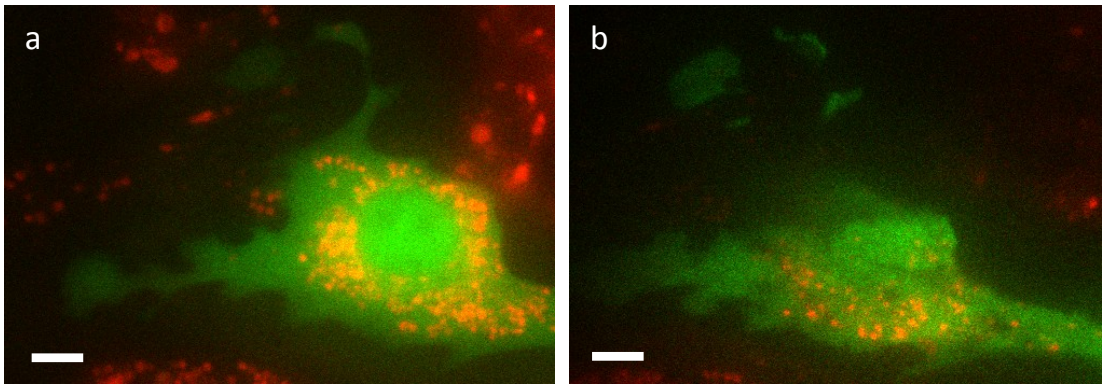

Figure 4.4: Example of a JG cell imaged in widefield and TIRF mode. - A GFP-positive JG cell is shown loaded with 100 nM lysotracker red. Images were acquired using a 150X TIRF lens in (a) widefield and (b) TIRF mode. Scale bar represents 5μm.

Eight cells were imaged, of which the three showing the clearest granule motion were taken forward for tracking analysis; Figure 4.5 shows one of these cells. Lysotracker-filled granules residing within GFP-positive JG cells were tracked and again, large (d $>$ 500nm) and small (d $>$ 500nm) granules were tracked separately. Qualitative assessment of granule tracking fidelity was performed by comparing images of tracked granules (c-d) to the maximum intensity projection across frames 501-1000 (e-f). As expected, tethered motion of large granules was observed in both Imaris-tracked and

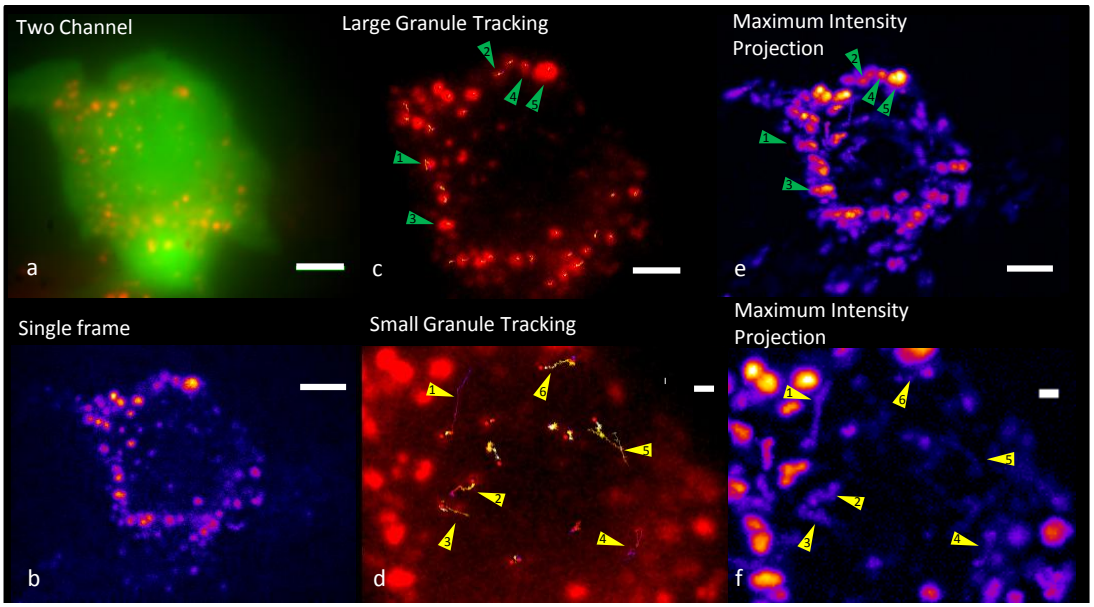

Figure 4.5: TIRFM analysis of granule dynamics in juxtaglomerular cells. - (a) JG cells were identified by their GFP expression and loaded with 100 nM lysotracker. (b) An example of a single frame of the 500 taken during addition of isoproterenol as an example, using the ImageJ heat map LUT 'Fire' for ease of lysotracker signal visualisation. (c) Large (d > 500nm) and (d) small (d > 500nm) granules were tracked separately. These images are re-represented as maximum intensity projections in (e) and (f) respectively. Scale bar represents 5 μm.

maximum intensity projection images. Small granule tracks again showed more directed motion (d) which is also clearly visible at the same location in the maximum intensity plots (f).

Specific examples of granule movement are more clearly visualised in Figure 4.6, where a time course of granule motion from a sub-cellular region is demonstrated by showing every 500th frame, the maximum intensity projection of the lysotracker signal and the corresponding Imaris tracks. Examples of granule motion in response to isoproterenol treatment have been chosen (arrows), either for motion to the membrane (a), away from the membrane (green arrow b) or laterally at the membrane (b-e) for large granules (a-d) and small granules (e). It is again evident from these images that granule motion is taking place; this is particularly striking in the directed path taken by the large granules in (d), which moved in a particular direction for most of the time course, before turning and travelling at 180^o to its original motion. Similarly, the directed motion of small granules are prominent in (e), where a granule tracks out a large horseshoe shape and another moves directly up through the middle. In this case though the motion is much more rapid, taking place within the 1001-1500th frames such that it is not visibile on the single frames.

The number of large granules present did not differ significantly after treatment, and no bursts of fluorescence associated with exocytosis were observed. Movement away from the membrane was distinguished from exocytosis by examining the fluorescence intensity profile of these granules (Figure 4.7). If these granules were undergoing exocytosis the fluorescence intensity would rapidly increase followed by a rapid decrease in tens of milliseconds, which would occur within a few frames, instead of the gradual decrease in fluorescence of the granules observed.

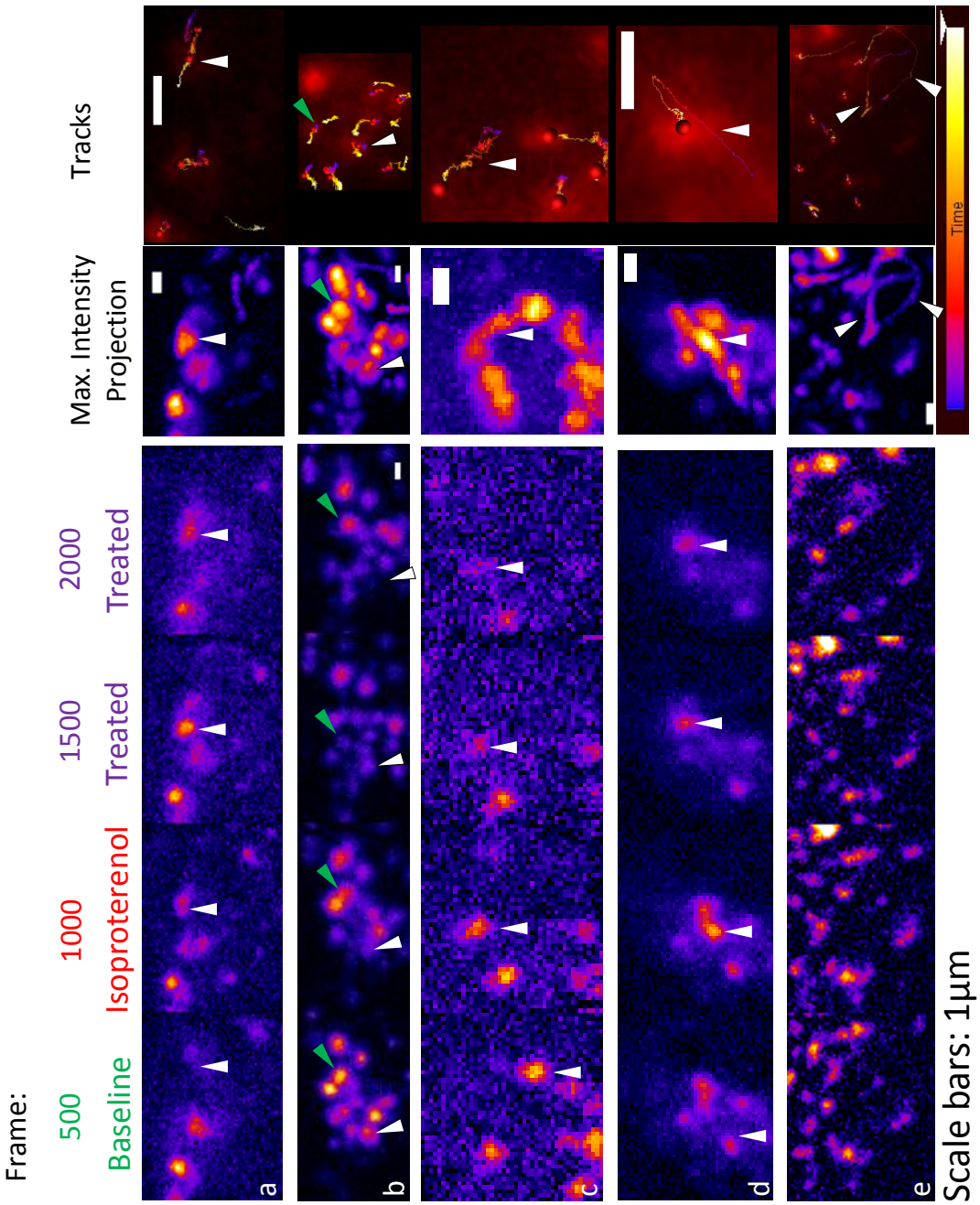

Figure 4.6: Time course illustrating granule movement during and after stimulus, imaged using TIRFM. - Images are shown at baseline (frame 500), during addition of 100 nM isoproterenol (frame 1000), and after treatment (frames 1500, 2000) for five different cell regions (a-e). The maximum intensity projection is also shown for the region of interest, and the corresponding Imaris tracks provided. Lysotracker signal is displayed using the ImageJ LUT 'Fire'. White arrows indicate granule motion towards the membrane; green arrows represent motion away from the membrane. Track colour correlates with time (from blue at the start to yellow at the end, as indicated in the legend).

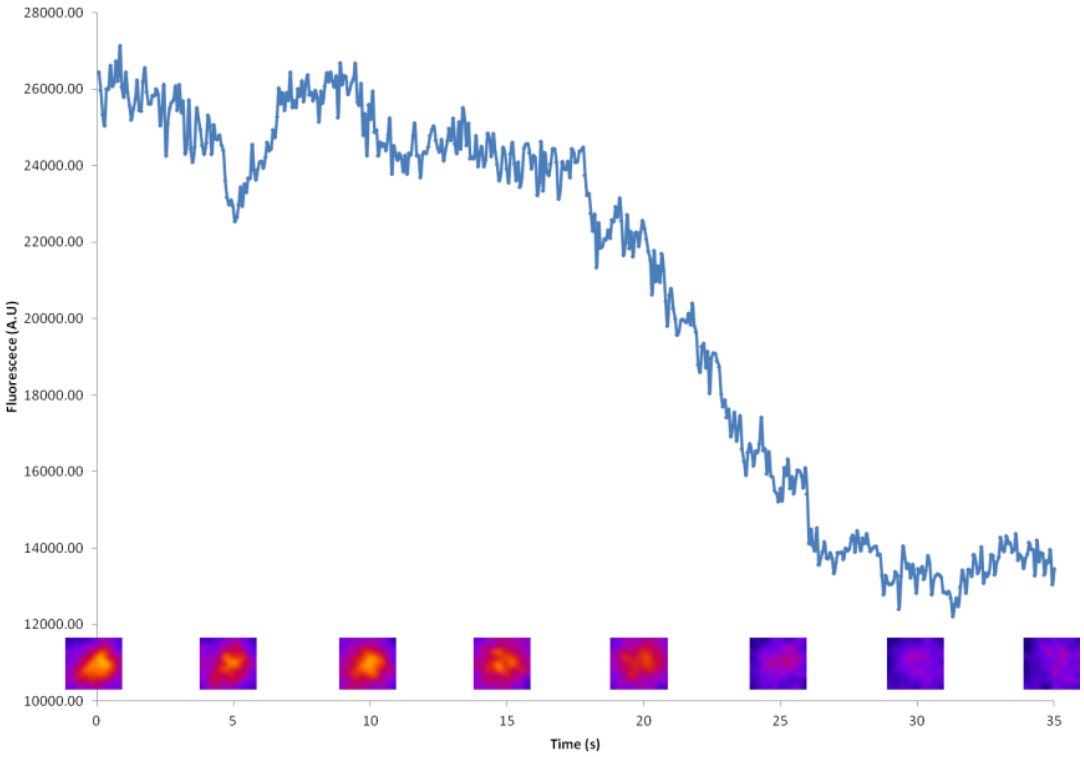

Figure 4.7: Representative single-granule fluorescence intensity plot during addition of isoproterenol. - The fluorescence intensity over the 35s period (0.07s frrame rate) from frame 501 to 1000, during which 100 nM isoproterenol was added, are illustrated for a single granule of diameter 615 nm as it moves away from the membrane. The accompanying fluorescence image is shown along the x axis every 5s.

4.2.2.2 Tracking of Renin Containing Granule Motion in TIRFM

Granules were tracked as above, however by imaging granule motion in TIRF mode it was possible to track both large and small granules. The diameter of every granule tracked was also measured in ImageJ. When diameter was plotted against the mean speed of the granule two clear populations of granules were present: large granules showed a constrained range of speeds which remained below 1000 nm/s for the vast majority of granules analysed (Figure 4.8a) and small granules which exhibited a more diverse range of speeds from 250 nm/s to 2370 nm/s.

To determine whether there was a noticable overall change in the diameter of granules in response to isoproterenol, a histogram of tracked granule diameters was plotted (Figure 4.8b). A change in granule diameter could suggest that granule swelling may be involved in the process of renin secretion, however this did not appear to be the case. No shift in granule diameter was seen between conditions compared to the baseline measurements taken between frames 1-500 (Figure 4.8b).

Results of granule tracking are shown in Figure 4.9 with mean granule speed, track length and displacement calculated before, during and after isoproterenol addition. It should be noted that granules were only included for mean speed analysis if they were tracked for the entire duration they remained within the field of view. Only granules tracked over the full 35 seconds (500 frames) were included in analysis of track length travelled and displacement.

To illustrate how these speeds, track lengths and displacements compare to individual granule tracks, dynamic parameters for the tracks outlined in Figure 4.6 were determined. The large granule indicated by the white arrow in (a) measured an average

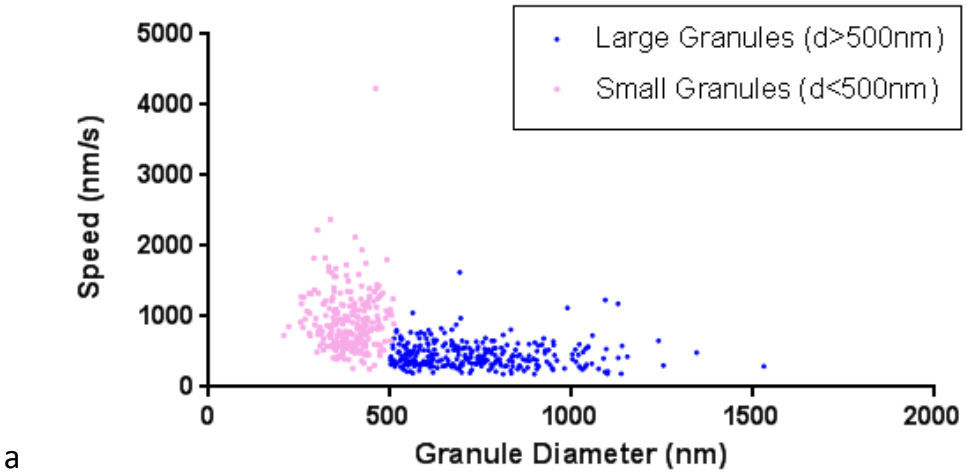

a

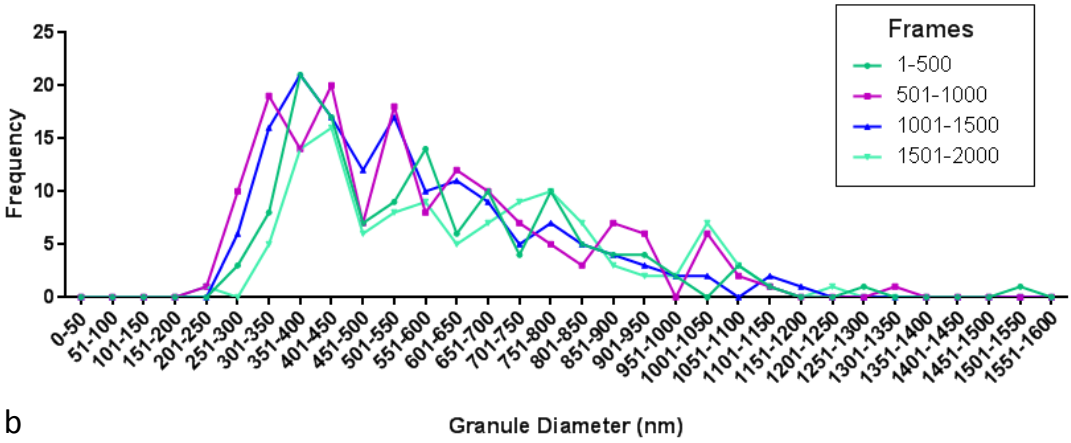

b

Figure 4.8: Distribution of granule sizes and speeds in primary JG cells, imaged using TIRFM. - The diameter of each granule tracked was measured in imageJ prior to being tracked using Imaris 7.7. (a) Diameter was plotted against speed for each granule analysed, using 500 nm to distinguish between large (blue) and small (pink) granules. (b) A histogram of granule diameter is shown prior to (1-500), during (501-1000) and after (1001-1500) addition of 100 nM isoproterenol.

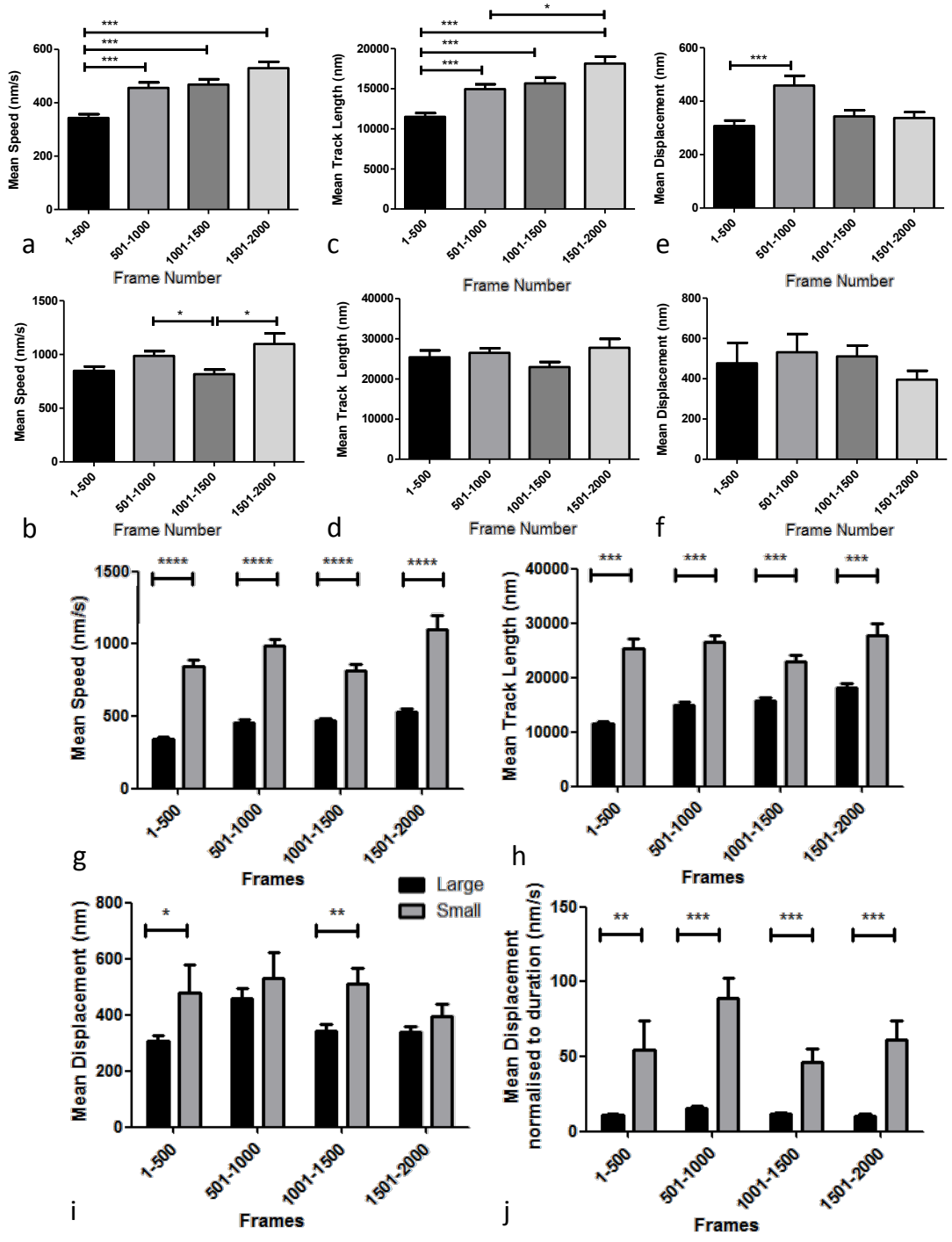

Figure 4.9: Dynamic parameters of large and small granules imaged using TIRF microscopy. - Granules were tracked at baseline, during addition of 100 nM isoproterenol, and after (frames 1-500, 501-1000 and 1001-2000 respectively; 70 ms/frame) using Imaris 7.7. (a,b) Mean speed, (c,d) track length and (e,f) displacement were extracted for large (d > 500 nm) (a,c,e) and small (d < 500 nm) (b,d,f) granules . The same data for (g) speed, (h) track length and (i,j) displacement were rerepresented to visualise differences in small and large granule dynamics. 3 cells were analysed with on average 77 large and 60 small granules tracked per condition. A one way anova using the non-parametric Kruskal-Wallis test with Dunn post hoc analysis was performed. Data are mean ± S.E.M. *: $p < 0.05$, **: $p < 0.01$, ***: $p < 0.001$, ****: $p < 0.0001$.

speed of 281 nm/s, a track length of 9825 nm and a displacement of 539 nm. The large granule indicated by the white arrow in (b) measured an average speed of 682 nm/s, a much longer track length of 23835 nm and a displacement of 291 nm, whilst the granule indicated by the green arrow moved on average slower at 310 nm/s over a track length of 8515 nm, with a displacement of 302 nm. The large granule in (d) moved on average at 247 nm/s over a track length of 8617 nm, though had a much larger displacement of 1099 nm. Finally, the small granules in (e) moved at speeds of 1038 nm/s (horseshoe path) and 787 nm/s, with track lengths of 27684 nm and 27494 nm and displacements of 2579 nm and 1943 nm respectively.

Large granules responded dynamically to the addition of isoproterenol, showing a significant increase in mean speed from 343.2 nm/s at baseline to 455.5 nm/s during addition of isoproterenol (frames 501-1000, Figure 4.9a). This average speed was maintained at 468.0 nm/s over the next 500 frames. From frames 1501-2000, the average granule speed significantly increased to 529.6 nm/s, a 54% increase from baseline. This shows a regulated dynamic response to addition of the renin secretory stimulus. These speeds, averaged over the 50-80 granules measured, are in keeping with the speeds measured for the individual tracks.

The mean track length travelled by large granules mirrored this response to addition of isoproterenol (Figure 4.9c, 70 ms/frame). At baseline, large granules travelled on average 11488 nm, which increased to 14941 nm following the addition of isoproterenol. Track length was maintained at 15666 nm between frames 1001-1500, but increased to 18131 nm during frames 1501-2000, a 58% overall increase in track length from baseline. Although the average response in the mean displacement of the granules showed a significant, acute increase from a baseline distance of 307 nm to 459 nm during the

addition of isoproterenol, it then decreased back to the baseline distance of 343 nm during frames 1001-1500, where it remained (Figure 4.9e). Although the individual granules presented in Figure 4.6 are either slightly below or above the averages given here, they still remain within the same order of magnitude.

The mean speed of small granules showed an acute, significant increase in speed from a baseline speed of 847.6 nm/s to 987.3 nm/s during the addition of isoproterenol (Figure 4.9b). However the speed decreased back to 817.3 nm/s from frames 1001-1500, which was not significantly different to baseline. The speed significantly increased to 1098.4 nm/s during frames 1501-2000. These speeds are in keeping with the example tracks displayed in Figure 4.6 (e), where an average speed of 1038 nm/s was measured for the granule tracking out a horseshoe shape, along with an average track length of 27683 nm. It was particularly striking that addition of isoproterenol had no significant effect on either the track length or displacement travelled by small granules (Figure 4.9d-f).

A comparison of the data for large and small granules is plotted in Figure 4.9 (g-j). Small granules showed signficantly higher dynamic parameter values than those of large granules. This was particularly true for the mean speed of granules (Figure 4.9g), which travelled on average 110% faster than large granules. Similarly, the track length of small granules travelled was, on average, 75% longer than that of large granules (Figure 4.9h). The difference in displacement between large and small granules was not as pronounced (Figure 4.9i). Whilst only granules tracked over the entire 500 frames captured were included in analysis for displacement in (i), all granules tracked were included in analysis for (j), normalised to the duration of time over which they were present in the field of view. Here, small granules were shown to have a significantly

larger displacement per unit time whilst within the field of view compared to large granules.

4.2.2.3 Actin Staining of Primary Juxtaglomerular Cells

Since evidence for the presence of actin fibers within JG cells is sparse, an intial attempt was made to identify possible mechanisms of intraceullular granule transport by staining for α-smooth muscle actin. Primary JG cells were plated, cultured for 48 hours, fixed and stained. Staining confirmed that JG cells contained actin filaments, with suggestions of filopodia (yellow arrows) and stress bundles (purple arrows) evident throughout the cells (Figure 4.10a-b). Actin bundles were seen to run along the edge of the cells and across the intracellular space (Figure 4.10, orange arrows), however further experiments will be required to determine whether they are involved in granule transport.

4.2.2.4 Reconstruction of JG cells and Lysotracker Stained Granules

Primary cultured GFP-positive JG cells were identified and the granules stained in the same manner as for tracking experiments. A z-stack over the depth of the cell was then rapidly taken at the Nyquist sampling limit for each wavelength, first with the 488 nm laser then with the 591 nm laser. These images were deconvolved and surfaces applied to the signal in Imaris 7.7. Using this methodolgy the volume of the surfaces corresponding to the lysotracker signal could be compared to that of the volume from the homogeneous diffuse GFP signal within the cell, giving an estimate of cell and granular volume (Figure 4.11).

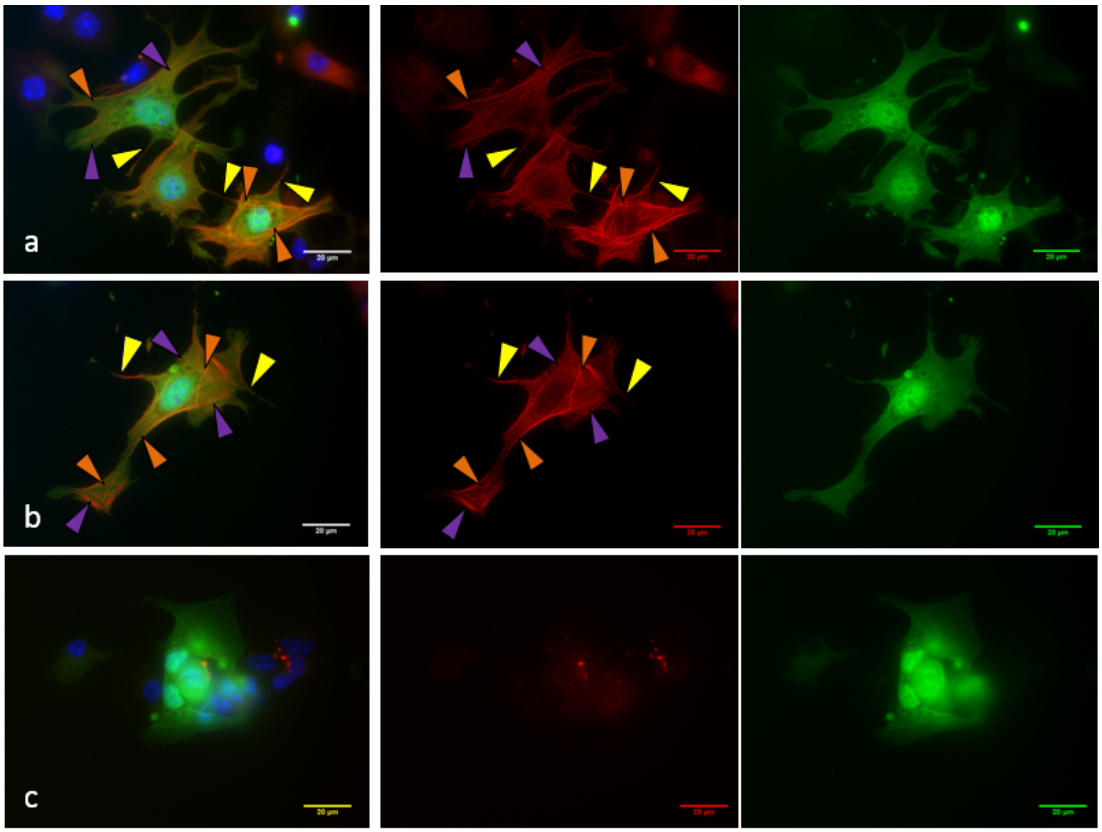

Figure 4.10: Actin staining of primary juxtaglomerular cells. - Primary isolated JG cells from RenGFP$^{+/-}$ mice placed on captopril (1 mg/ml, 7 days) were cultured on fibronectin-coated coverslips (50 μg/ml) for 48 hours. They were fixed and either (a, b) stained for α-smooth muscle actin according to the protocol in Section 2.7.3 or (c) a no-primary antibody control stain performed. Cells were imaged using an epifluorescence microscope with a 60X oil objective lens. Scale bars represents 20 μm. Yellow arrows: filopodia-like structures. Purple arrows: stress-fiber-like structures. Orange arrows: actin bundle-like structures. Green: renin expressing, GFP positive JG cells, blue: DAPI, red: α-smooth muscle actin.

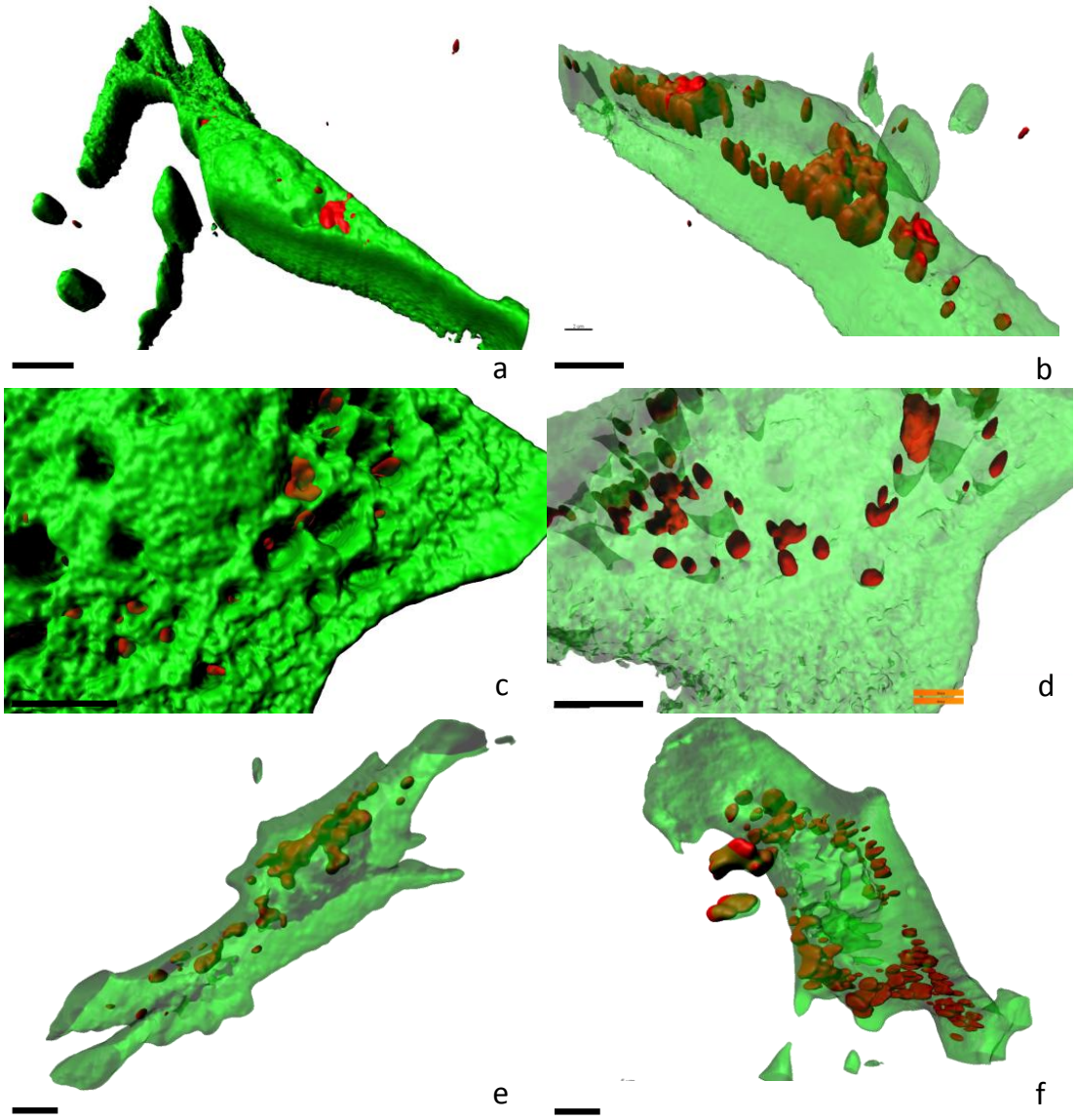

Figure 4.11: 3D Reconstruction of GFP-positive JG cells with lysotracker-stained granules. - GFP-positive JG cells were stained with 100 nM lysotracker red and z-stacks taken at the Nyquist sampling limit using the 150X TIRF lens in widefield mode. Images were deconvolved using Huygen's deconvolution software. Surfaces were rendered and volumes measured using Imaris 7.7. Scale bars represent 5 μm.

The shape of the cell is clearly represented by the chosen surface for the GFP signal, although small areas near the membrane did not contain diffuse GFP signal, allowing glimpses of the lysotracker-filled granules below (Figure 4.11a). When this outer surface was made transparent using Imaris, the underlying granules became clearly visible (Figure 4.11b). It was possible to resolve large granules using this method, unless the granules were in an area of high granule density when the surfaces merged together. Due to the low axial resolution associated with any widefield microscopy technique, both the granules and the depth of the cell appear more elongated than they really are. These problems are further illustrated in Figure 4.11 (e, f): granules appeared as a large vesicular network, which was not present in the instantaneous images collected in both widefield and TIRF, suggesting that the elongated axial aspect of both the granules and the cell depth are artefacts of deconvolution. Interestingly, in Figure 4.11 (c) the rendered GFP-positive cytoplasm reveals pitted areas where no GFP is present. These were also evident in a number of cultured primary JG cells, such as those in Figure 3.3 and Figure 4.5 (c). In Figure 4.11 (c), the reconstruction clearly shows that although the granules did not fill the entire pit, they were present at the bottom of some of these pits. The granules are shown without the pits in Figure 4.11 (d).

4.3 Discussion

4.3.1 Labelling of Dense Core Granules

The ease and rapidity of accumulation of acidotropic dyes within the granules and their strong fluorescent signals make them particularly well suited to identification of granules and high speed acquisition live imaging. Classically, quinacrine ($C_{23}H_{30}CIN_3.2HCL.2H_2O$) has been the acidic dye of choice since it was shown to bind with high affinity to granules within JG cells, even though it doesn't specifically bind to renin. It has been used as a fluorescence intravital stain of renin granules both in fixed samples (104, 184), in microperfused JGA preparations (36, 185) and in multiphoton imaging in live mice (34, 186). Since quinacrine and GFP have very similar excitation and emission spectra, a similar acidotropic dye, lysotracker red (excited at 591 nm), was more appropriate for the present study. This dye has previously been used to label large dense core vesicles in live cultured secretory cells (187) and in live JG cells as part of an isolated perfused JGA preparation (36). Therefore although lysotracker, like quinacrine, does not specifically localise to renin, it is a well-recognised method of identifying renin-containing dense core granules within JG cells.

4.3.2 Stimulation of Renin Secretion

A renin secretory stimulus of 100 nM isoproterenol was used on the primary JG cells. Isoproterenol is a non-specific β-adrenergic agonist which, through its binding to the ADRB1 receptors (132) and subsequent action of the second messanger cAMP (176), activates the most significant renin release pathway in JG cells. The concentration of isoproterenol required to stimulate secretion varies with respect to the experimental model used. In isolated perfused kidney models a concentration of 10 nM was reported

to stimulate renin secretion (132, 188, 189), whilst in isolated perfused JGA preparations 100 μM stimulated the quantal release of renin with concomitant decrease in fluorescence signal (36). However addition of 100 nM isoproterenol was reported to stimulate renin release from primary isolated JG cells (141); due to time constraints I was not able to optimise the concentration of isoproterenol used, therefore this concentration was chosen for my studies.

Initial experiments using widefield microscopy enabled the successful visualisation of large, dense core granule motion as well as rapid motion of smaller granules in primary JG cells. Since no pervious studies have been able to capture renin granule motion, a high frame rate was used to ensure that no rapid motion or exocytosis event was missed. This is the first direct evidence for movement of large renin-containing granules in response to a secretory stimulus, however this motion was not captured while the drug was being added. Peti-Peterdi *et al.* (36) reported dimming and disappearance of fluorescence from individual quinicrine-loaded granules in response to 100 μM isoproterenol perfused in JGA preparations, but no associated granule trafficking. However images were acquired at 0.1 Hz over 10 minutes using CLSM, compared to the 14 Hz frame rate used in the present study. Granule movement and disappearance would be visually identical when imaged at 0.1 Hz, and indeed a significant amount of granule motion was seen in the primary JG cells imaged using widefield and TIRF microscopy over this time scale.

No differences were seen in the average size of large granules, using widefield or TIRF microscopy. This supports the findings of Friis *et al* (155), who did not see evidence of granule-swelling during renin secretion as proposed by Skott and Taugner (190).

The use of TIRF microscopy allowed the experimental design to be refined, and by eliminating much of the axial out of focus light it was possible, for the first time, to track the smaller granules as well. Granule motion could be imaged continuously from baseline, throughout isoproterenol administration to 1000 frames beyond the stimulus. There was a tendency for the image to go slightly out of focus on addition of the isoproterenol, however this did not hinder analysis of granule motion and allowed me to verify the accurate addition of isoproterenol.

TIRF allowed motion at, to, and from the cell membrane to be captured and distinguished from exocytosis (191) however, unlike using widefield microscopy, it is not possible to collect data from the entire cell volume. Some groups have attempted to extract information on the z-axis motion of granules imaged in TIRF(192), however this type of data difficult to analyse and interpret.

Visual analysis of the datasets collected in widefield and TIRF confirmed that no flashes of fluorescence intensity associated with exocytotic events occurred, even after addition of isoproterenol. Furthermore no significant difference in the average number of large granules was observed in widefield, suggesting that exocyosis of entire renin-containing granules was not taking place. Evidence for the disappearance of storage granules has previously been reported in ultrastructure studies of JG cells at the EM level (193). Exocytosis was stimulated by an acute decrease in perfusion pressure to 40 mmHg for 5 minutes in rats which had been administered ACE inhibitor and a low salt diet for 14 days. This led to a 45% reduction of granules per AA, however without the 14 day stimulation prior to the secretory stimulus no difference in granule number was recorded. Similarly, Steppan *et al.* (113) only observed compound exocytosis and granular interactions with the cell membrane at the EM level after kidneys were

perfused with both isoproterenol and EGTA to lower intracellular Ca^{2+}. Even under these conditions, no reduction in granule number was measured, and no exocytotic events were observed under baseline conditions. The lack of flashes or disappearance of granules in the present study could therefore be explained by the fact that JG cells are known very rarely to show evidence of exocytosis events (178).

It is also possible that no exocytosis was visualised due to much longer secretion timescales. For instance mast cell secretory granules take up to 72 hrs to release their cargo (194). Indeed patch clamp studies of single JG cells in primary culture showed that under basal conditions only 0.9 ± 0.1% total renin content was released per hour (then 16 ± 2% over 20 hrs) (155). After stimulation with 10 μM isoproterenol the exocytosis rate increased to 40 ± 5% per hour (155). This is 100 times more concentrated than the isoproterenol used in the present study. It has also been suggested that only severe secretory stimulation leads to observable occurances of exocytosis (112), suggesting that treatment with 100 nM isoproterenol for around two minutes may be insufficient to elicit a pronounced, easily recordable exocytotic response. All these studies provide evidence for exocytotic release of renin, however the contradictory nature of the means by which this occurs demonstrates the need for a system such as the primary JG cell-TIRF experimental design optimised in the current study for further in-depth study.

An attempt was also made to perform 3D reconstructions of the entire JG cell volume based on signal from cytoplasmic GFP and granular lysotracker accumulation. It was hoped that this could be performed before and after treatment with isoproterenol to estimate the change in granular volume without the need for patch clamping. Widefield microscopy was chosen over confocal microscopy for a number of reasons: since the

granule tracking experiments were performed using the widefield/TIRF system with the 150X objective lens under temperature and CO_2 controlled conditions, removal to the confocal microscope before and after tracking would have been experimentally disruptive and time consuming. Furthermore, acquiring z-stacks using widefield microscopy is extremely rapid, reducing exposure to intense light and ensuring that granule motion over the acquisition time was limited. However gain in acquisition speed reflects loss in axial resolution when using widefield techniques, requiring deconvolution to resolve objects. The elongated shape of the granules and of the cell itself were artefacts of this process, creating elongated 3D point spread functions. The use of the cytoplasmic GPF expression to estimate cell volume may also have introduced error; a membrane marker in the far red would give a more appropriate estimate of cell volume. Therefore, although deconvolution of the images and their reconstructions were successful, the resulting volumes were not accurate enough to give confident estimates of changes in granule volume. Although a spinning disk confocal would have been a good method to use due to the rapid acquisition time and good axial resoltion, no spinning disk confocal was available at Heriot Watt where these experiments were performed.

4.3.3 Granule Dynamics Under Baseline and Stimulated Conditions

By tracking the average speed of each granule and manually measuring its diameter, my data revealed the existence of different populations of granules with dynamic parameters that correlate with their size. Large granules of d $>$ 500 nm showed much more constrained ranges of speeds than granules of d $<$ 500 nm. Historically the differentiation of granule pools within JG cells has been performed via visual analysis of the electron density in EM sections; large dense cargo granules, small electron-dense vesi-

cles and small clear vesicles were identified in this manner (101). Prior to my studies it has not been possible to optically differentiate between the different pools of granules in live JG cells.

Whilst granule tracking using Imaris software is a well-established technique (e.g. (195), (196)), there was the worry that the results from the software may have yielded false-positive results, such as an apparent long track length for tethered granules which moved with a random motion around a fixed point. Qualitative verification of the accuracy of data yielded from Imaris granule tracking was performed by comparing the maximum intensity projection over the 1000 (widefield) or 500 (TIRF) frames of analysis with the tracks yielded using Imaris. Furthermore, data from individual tracks of granules exhibiting caged or directed motion were compared with respect to each other and the averages calculated over all granules measured.

Future experiments will include more stringent controls, such as performing the same image analysis protocol on fixed samples, where the only motion should be brownian. A further control to test whether image noise contributes to apparent velocity could also be performed on fixed cells by moving the image out of focus and again performing the same image analysis protocol. The high frame rate used in this experiment could also contribute to caged granules measuing a higher apparent velocity than they have; their random motion would be more averaged out using a lower frame rate. To test this in the future, images could be binned to simulate a lower acquisition rate and the tracking re-performed.

Very little research on granule transport has been performed in JG cells. Granules and vesicles are transported around cells by motor proteins on either microtubules or actin filaments; although it is known that motors on microtubules drive long-range

transport and actin-based motors tether cargo, how the two interact remains to be fully understood (197).

There is very little published evidence for the presence of actin filaments within JG cells. In one of the only studies on actin filament function in JG cells, Ogawa *et al* (112) used a cortical slice model followed by EM analysis to show that actin filaments were present on electron-dense granules. It was shown that when the slice was incubated in the actin filament-disrupting drug Cytochalasin B, these granules moved closer to the cell membrane. This indicated that the disassembly of the actin filament network, a process which occurs when intracellular Ca^{2+} increases, allowed the mature secretory vesicles to move closer to the cell membrane. Tracking renin granules using widefield microscopy revealed that whilst the average speed of large granules significantly increased after treatment with isoproterenol, the average track lengh did not. This suggests that the period of time over which large granules move is shorter after isoproterenol treatment, which could be indicative of a short burst of rapid motion towards the membrane, followed by tethering such as that described by Ogawa. In his study, it was further suggested that it was the mature granules already attached to this network which underwent exocytosis, in some cases through fusion with nearby granules (112).

The presence of the actin cytoskeleton was confirmed in the present study through the use of α-SMA smooth muscle actin staining. The 3D actin filament network is assembled to facilitate different functions: filopodia are finger-like structures which protrude out of the lamellipodial actin network, which are filled with filamentous actin and are involved in cell migration (198). Stress fibers are composed of actin and myosin bundles and mediate contraction (198). Myosin is an actin-mediated motor protein

which responds to ATPase activity, driving motion along actin filaments during muscle contraction (199). The α-smooth muscle actin antibody does not differentiate different actin types, therefore staining with an antibody such as phalloidin to specifically stains the f-actin along which granules are transported would be beneficial. Interestingly, both precursor and mature versions of renin have been shown to bind to microtubules (200). Along with the experiments performed in the present study, these studies suggest that active transport is important for the renin secretory process.

There is a particularly marked difference in the dynamic parameters of the two pools of granules identified; the small granules are significantly faster and, presumably as a consequence, travel a much longer track length and displacement than large granules. These pools of granules also respond independently to the addition of isoproterenol. It is known that under an acute stimulus, increased secretion of active renin ensues, whereas under chronic stimulation a concomitant increase in both prorenin and active renin is seen in the circulation (201). Since the large granules respond in a regulated fashion to the acute stimulus whilst the smaller granules do not, it is tempting to speculate that measurement of dynamic parameters allows different pools of renin-containing granules on different regulatory pathways to be distinguished.

The fast speeds of the granule transport measured are also noteworthy; at their fastest, large granules travelled at approximately 500 nm/s whilst small granules were transported on average at 1200 nm/s. Although it is possible that granular diffusion is taking place, it is unlikely that this is the only mechanism responsible for transport. Instantaneous diffusion has been shown to transport vesicles at approximately 10-15 nm/s (202), a speed too low to account for many of the tracks identified. What's more, the actin mesh near the plasma membrane is known to be highly restrictive, holding

larger granules of > 1 μm diameter in place, unable to diffuse (192, 203).

These granule speeds measured in the current experiments give an indication of the motors transporting them. The two most common motor proteins are kinesin and dynein. The dynein molecular motor moves vesicle along microtubules towards the 'minus' end of microtubules, where tubulin subunits are commonly removed, using 16 nm steps via an overlapping hand-over-hand mechanism and has been shown to transport granular cargo at velocities of $\sim$ 800 - 1000 nm/s, or forces of up to 7 - 8 pN (204). On the other hand, kinesin travels towards the 'plus' microtubule end, where tubulin subunits are added, only allows movement of up to 600 nm/s, or forces of 2 - 5 pN (205). It is therefore possible that kinesin motors are responsible for motion of larger granules whilst dynein motors are responsible for transport of smaller granules. However, further studies would need to be performed to verify this. Actin motors may also be invovled in short-range granule transport, particularly in the tethering of cargo. Myosin-V can be recruited to cargo transported via kinesin motors to slow down their transport to be driven slow ly over a 1 - 5 μm range (197).

Whist many of the smaller granules revealed motion which appeared to be directed by tubular transport, exemplified by the tracks shown in Figure 4.6, many of the larger granules moved in a much more constrained, caged manner. This raises the possibility that granular diffusion may be taking place.

Granules may therefore be transported rapidly and directionally on microtubules but tethered to the actin mesh near the cell membrane, where caged motion occurs, to briefly await exocytosis. Given that increased mobility of granules has been related to an increase in fusion in neuropeptide secreting cells (206), the increase in granule speed observed in JG cells could suggest an increased motion of granules to the membrane

to allow fusion to occur. Indeed examples of both caged and directed behaviour as described in Huet *et al* (207) were readily seen in both pools of granules. TIRF studies tracking granules in chromaffin cells before and after an exocytotic stimulus similarly showed an increase in mobility is associated with secretion. Short bursts of movement over hundreds of nanometres immediately prior to secretion were also shown to occur close to the plasma membrane, causing the granules to be in motion until they bound with the plasma membrane (192).

4.3.4 Conclusion

Granule dynamics have been captured and dynamic parameters analysed under baseline and stimulated conditions for the first time in primary cultured JG cells. Using the acidotropic dye lysotracker to identify granules, TIRF microscopy was used to optically identify and image granule motion at a high spatial and temporal resolution. Two pools of granules were identified by their size and behaviour: granules of d $>$ 500 nm and d $<$ 500 nm. Both pools of granules behaved dynamically under basal conditions, and addition of the β-adrenergic stimulus isoproterenol led to an increase in speed, track length and displacement in large granules corresponding to that seen in regulated secretion. Conversely, small granules did not respond in this regulated way to the addition of the secretory stimulus, indicating that optical identification of granules on different secretory pathways within JG cells may be possible for the first time, although more work needs to be performed to verify this.

5

Macula Densa Structure and Function in Ren1d$^{-/-}$ Mice

5.1 Introduction

The importance of normal renin synthesis and secretion to the maintenance of JGA architecture was highlighted in studies by Clark *et al*. (114). When the active renin gene *Ren*1*d* was knocked out, there was a striking lack of dense core renin storage granules in JG cells. Furthermore, MD plaques were hyper-cellular with columnar epithelial cell morphology (shown by a 30% increase in basolateral to apical height) in contrast to the normal cuboidal appearance in wild type mice (Figure 5.1) (114). What was not clear was how this altered MD morphology affected JGA function.

The JGA-mediated regulation of tubular salt operates via two main mechanisms: low distal tubular NaCl-induced release of renin (16), and high distal tubular NaCl-induced vasoconstriction of the AA and glomerular tuft, and subsequent reduction in single nephron GFR. Although the mechanisms behind these responses differ, the initial step is the salt-sensing ability of the MD cells (discussed in Section 1.3.2).

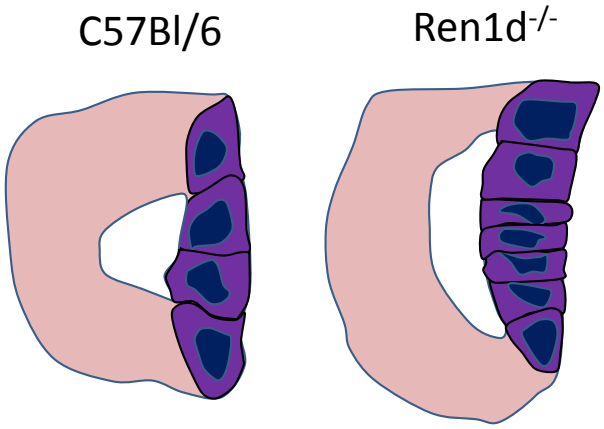

Figure 5.1: Schematic diagram of altered macula densa phenotype. - Schematic diagram of cTAL (pink) and MD cells (purple) illustratiing MD morphology in C57Bl/6 and *Ren1d*$^{-/-}$ mice.

In brief, low tubular salt is sensed by the NKCC2 cotransporter, activating COX2, which in turn initiates the transcription of the signalling protein PGE2 (21, 22, 23, 208, 209). PGE2 is then transported to the JG cells where it stimulates cAMP-mediated renin transcription and secretion (24). To assess this experimentally, a combination of a chronic low salt diet and ACE inhibitor is routinely used (210). This stimulates the MD by ensuring extremely low levels of NaCl in the tubular perfusate pass the MD, since there is very little salt in the diet and the ACE inhibitors increase salt and water excretion due to a decrease in ANGII generation (211).

Conversely, high tubular NaCl is sensed at the apical membrane of MD cells, initiating a cascade of ATP-dependent Ca^{2+} travelling via gap junctions from the MD to the VSMCs, mesangial cells and beyond into the intra-glomerular space (28). This participates in TGF by contracting the glomerular tuft and AA to reduce glomerular filtration. Experimentally, TGF is initiated by altering tubular NaCl concentration or flow speed at the MD of isolated perfused JGA (discussed in Section 1.3).

Due to the critical role MD cells play in the TGF response, the altered MD morphology coupled with the lack of dense core granules in JG cells observed in $Ren1d^{-/-}$ mice may have important potential physiological consequences for tubulo-vascular crosstalk.

5.1.1 Specific Chapter Aims

It is hypothesised that altered MD morphology impairs the TGF response of $Ren1d^{-/-}$ mice compared to C57B1/6 controls. The following experimental questions were addressed to test this hypothesis:

1. Do isolated perfused JGA from $Ren1d^{-/-}$ mice with altered MD morphology show impaired TGF function compared to C57Bl/6 controls

    a) under increased flow at the MD?

    b) under increased NaCl at the MD?

2. Do $Ren1d^{-/-}$ mice display altered MD signalling in response to a chronic low salt diet and ACE inhibitor administration compared to C57Bl6 controls?

5.2 Results

5.2.1 Flow-Induced Tubuloglomerular Feedback Response

To experimentally induce the TGF response via increased flow at the MD plaque, freshly dissected glomerular tufts with attached AA, cTAL and MD plaque were microperfused. TGF activity was measured by calculating elevations in intracellular calcium concentration or percentage of constriction of the glomerular tuft and AA.

Responses to TGF in preparations from C57Bl/6 and $Ren1d^{-/-}$ mice are shown in Figure 5.2 (blue arrows). An elevation in calcium dye signal after TGF stimulation is clearly visible in AA, cTAL and glomerular tuft cells. The AA vasoconstriction response to TGF can also be seen. Responses were quantified as percentage change in AA diameter, glomerular tuft diameter and glomerular tuft area, and change in the calcium signal in VSMC, cTAL, MD and podocyte cells in response to TGF stimulation.

During TGF, contraction of the glomerular tuft in $Ren1d^{-/-}$ mice (area 4.6 ± 0.6%; diameter 3.4 ± 0.3%) was less than that observed in C57B1/6 mice (n=3, area 10 ± 2% ($p = 0.011$); diameter 8 ± 3% (ns), Figure 5.3a, b). The AA vasoconstriction response to altered flow at the MD did not differ significantly between groups (65 ± 15% contraction in $Ren1d^{-/-}$; 58 ± 11% contraction in C57Bl/6, n=3, Figure 5.3c).

Whilst MD cells in $Ren1d^{-/-}$ mice demonstrated a calcium signalling response to TGF, albeit with large error bars, the C57B1/6 MD cells did not (n=3, Figure 5.3d). C57Bl/6 mice showed an average change of -11 ± 45 nM $[Ca^{2+}]_i$, whilst $Ren1d^{-/-}$ mice showed a 98 ± 80 nM increase. Due to the large error bars, this difference was not statistically significant.

$Ren1d^{-/-}$ mice showed a significant increase of $[Ca^{2+}]_i$ in cTAL cells in response to

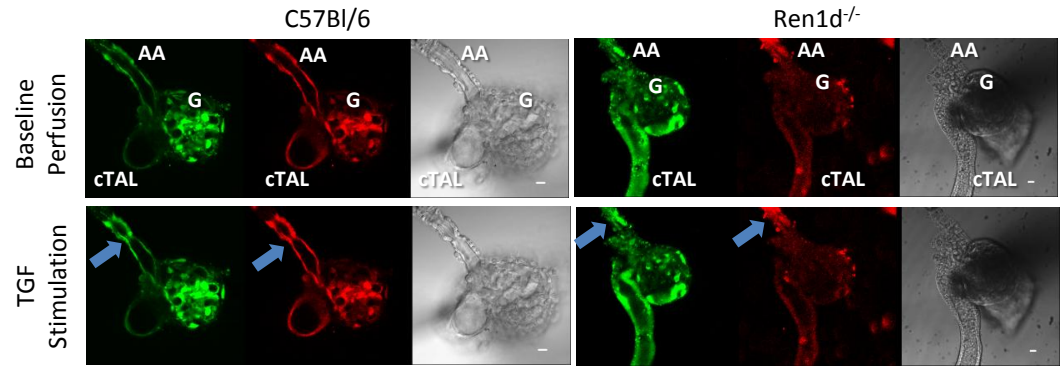

Figure 5.2: Flow-induced TGF in isolated JGA with attached MD plaque. - JGA from C57Bl/6 and *Ren*1$d^{-/-}$ mice are shown loaded with Fluo-4 AM calcium indicator dye (green), Fura Red AM calcium indicator dye (red) or in DIC (grey) at baseline and after flow-induced TGF was triggered by increasing the rate of constant 10mM NaCl-containing tubular perfusion from 2 to 20 nl/min. G: glomerulus, AA: afferent arteriole, cTAL: cortical thick ascending limb. Scale bars represent 10 μm.

TGF compared to C57Bl/6 preparations (593 ± 80 nM in Ren1$d^{-/-}$ mice; 201 ± 27 nM in C57Bl/6 mice (p=0.013), n=3, Figure 5.3e). No significant difference in intracellular $[Ca^{2+}]_i$ concentration was seen between groups in VSMCs (314 ± 54 nM in *Ren*1$d^{-/-}$ mice; 289 ± 100 nM in C57Bl/6 mice; n=3, Figure 5.3f) or in podocytes (222 ± 42 nM in *Ren*1$d^{-/-}$ mice; 155 ± 44 nM in C57Bl/6 mice; n=3, Figure 5.3g).

5.2.2 NaCl-Induced Tubuloglomerular Feedback Response

Though differences were seen in the magnitude of the flow-induced TGF response between C57Bl/6 and *Ren*1$d^{-/-}$ mice, it is evident that TGF still functions effectively in mice with altered MD morphology. To determine the effect of increased NaCl concentration at the MD, the same parameters were measured after the NaCl concentration in the perfusate was raised from 10 mM to 80 mM. No significant difference between the reductions of glomerular tuft area (4 ± 2% in *Ren*1$d^{-/-}$ mice; 6.9 ± 0.2% change in C57Bl/6 mice; n=3, Figure 5.4a) or glomerular tuft diameter (2.3 ± 0.3% in *Ren*1$d^{-/-}$

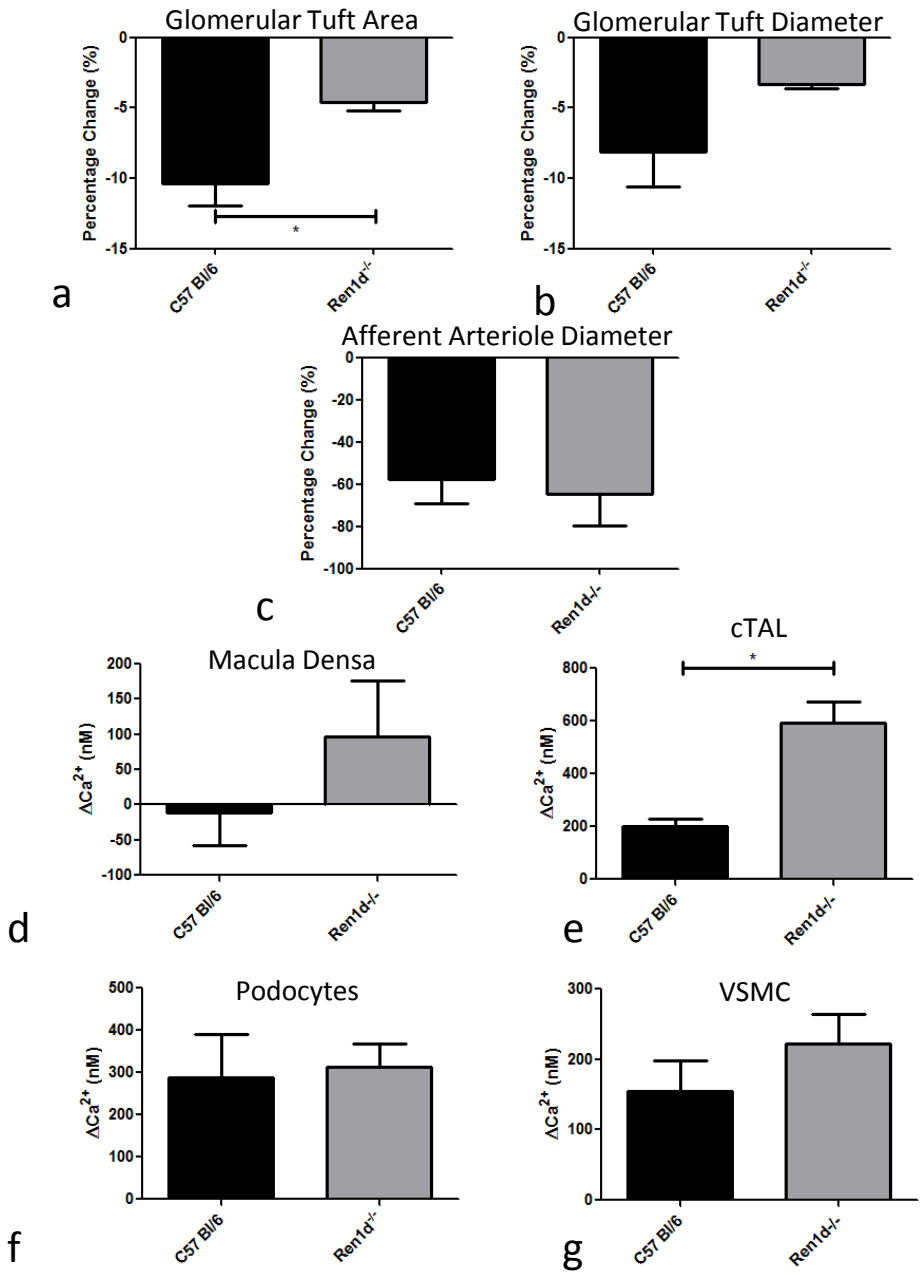

Figure 5.3: Flow-induced contraction and elevations in intracellular calcium in isolated JGA with attached MD plaque. - Percentage change in (a) glomerular tuft area, (b) glomerular tuft diameter and (c) AA vasoconstriction and changes in intracellular calcium in (d) MD, (e) cTAL, (f) podocyte and (g) VSMCs cells were analysed in preparations from male C57Bl/6 and $Ren1d^{-/-}$ mice. Flow-induced TGF was triggered by increasing the rate of constant 10 mM NaCl-containing tubular perfusion from 2 to 20 nl/min and the corresponding change in calcium measured. Data are mean ± S.E.M., n=3, * = $p<0.05$.

mice; 3.2 ± 0.7% in C57Bl/6 mice; n=3, Figure 5.4b) was seen in response to NaCl-induced TGF. No difference in afferent arteriolar vasoconstriction was observed between groups (36 ± 28% reduction in *Ren1d*$^{-/-}$ mice; 40 ± 7% reduction in C57B1/6; n=3 Figure 5.4c). These parameters show a trend towards a blunted TGF response under increased NaCl compared to increased flow stimulation.

There was no significant difference between intracellular $[Ca^{2+}]_i$ propagation within MD cells between groups, though *Ren1d*$^{-/-}$ mice showed a trend towards an increase (25 ± 44 nM in *Ren1d*$^{-/-}$ mice; 4 ± 16 nM in C57Bl/6 mice; n=3, Figure 5.5a). Plotting the data points individually revealed a range of responses between MD cells within the plaque in *Ren1d*$^{-/-}$ mice, with propagation of calcium signal seen only through a subset of MD cells within the plaque (Figure 5.5c, d). Intracellular $[Ca^{2+}]_i$ within C57B1/6 MD did not increase under either NaCl- or flow-induced TGF (Figure 5.5c, d). A similar trend in $[Ca^{2+}]_i$ signalling was also seen in *Ren1d*$^{-/-}$ MD cells under flow-induced and NaCl-induced TGF, though there was large inter-individual variation (Figure 5.5c, d). Representative images of calcium signalling in MD cells in response to NaCl-induced TGF are shown in Figure 5.6. Visual assessment also suggested that calcium did not appear to propagate through C57B1/6 MD cells (Figure 5.6a, b) whilst slight increases in signal were observed in MD cells from *Ren1d*$^{-/-}$ preparations (c, d).

The change of $[Ca^{2+}]_i$ in cTAL cells was significantly greater in *Ren1d*$^{-/-}$ compared to C57B1/6 preparations (422 ± 72 nM in *Ren1d*$^{-/-}$ mice; 84 ± 50 nM in C57Bl/6 (p=0.004), n=3, Figure 5.5b) but the responses of podocytes (336 ± 104 nM in *Ren1d*$^{-/-}$ mice; 182 ± 32 nM in C57Bl/6 mice (ns), n=3, Figure 5.5e) and VSMCs (190 ± 71 nM in *Ren1d*$^{-/-}$ mice; 104 ± 34 nM in C57Bl/6 mice (ns), n=3, Figure 5.5f) were broadly similar for the two genotypes. The magnitude of the intracellular $[Ca^{2+}]_i$

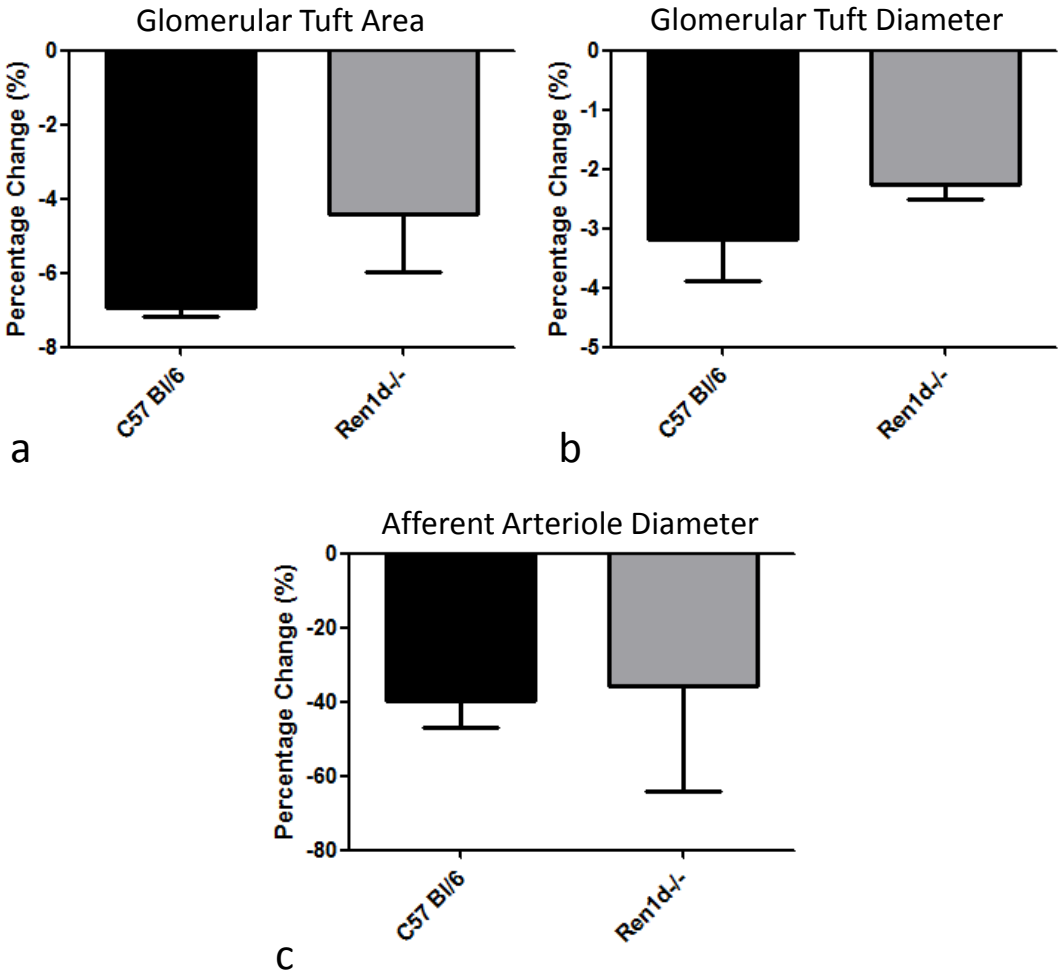

Figure 5.4: Tubular salt-induced constriction of the glomerular tuft and AA in isolated JGA with attached MD plaque. - Percentage change in (a) glomerular tuft area, (b) glomerular tuft diameter and (c) AA vasoconstriction in response to NaCl-induced TGF was analysed in preparations from male C57Bl/6 and *Ren*1$d^{-/-}$ mice. NaCl-induced TGF was initiated by increasing NaCl at the MD from 10 to 80mM. Data are mean ± S.E.M., n=3.

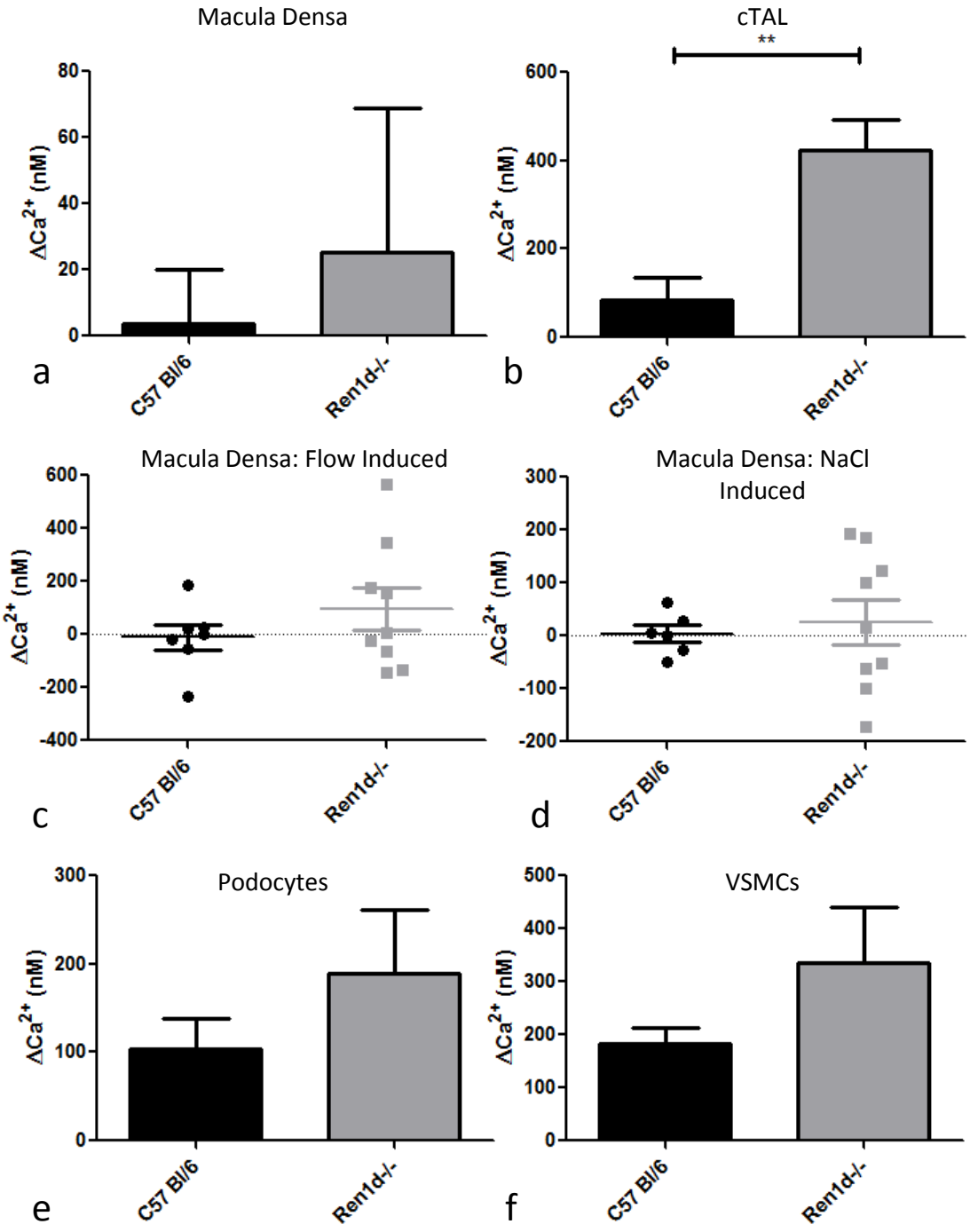

Figure 5.5: Tubular NaCl-induced elevations in intracellular calcium in isolated JGA with attached MD cells. - The change in intracellular calcium in (a) MD cells, (b) cTAL cells, (e) podocytes and (f) VSMCs in preparations from male C57Bl/6 and $Ren1d^{-/-}$ mice. Individual data points from intracellular calcium changes in MD cells under (c) flow- and (d) NaCl-induced TGF are presented. NaCl-induced TGF was initiated by increasing NaCl at the MD from 10 to 80mM. Data are mean ± S.E.M, n=3, ** = p<0.01

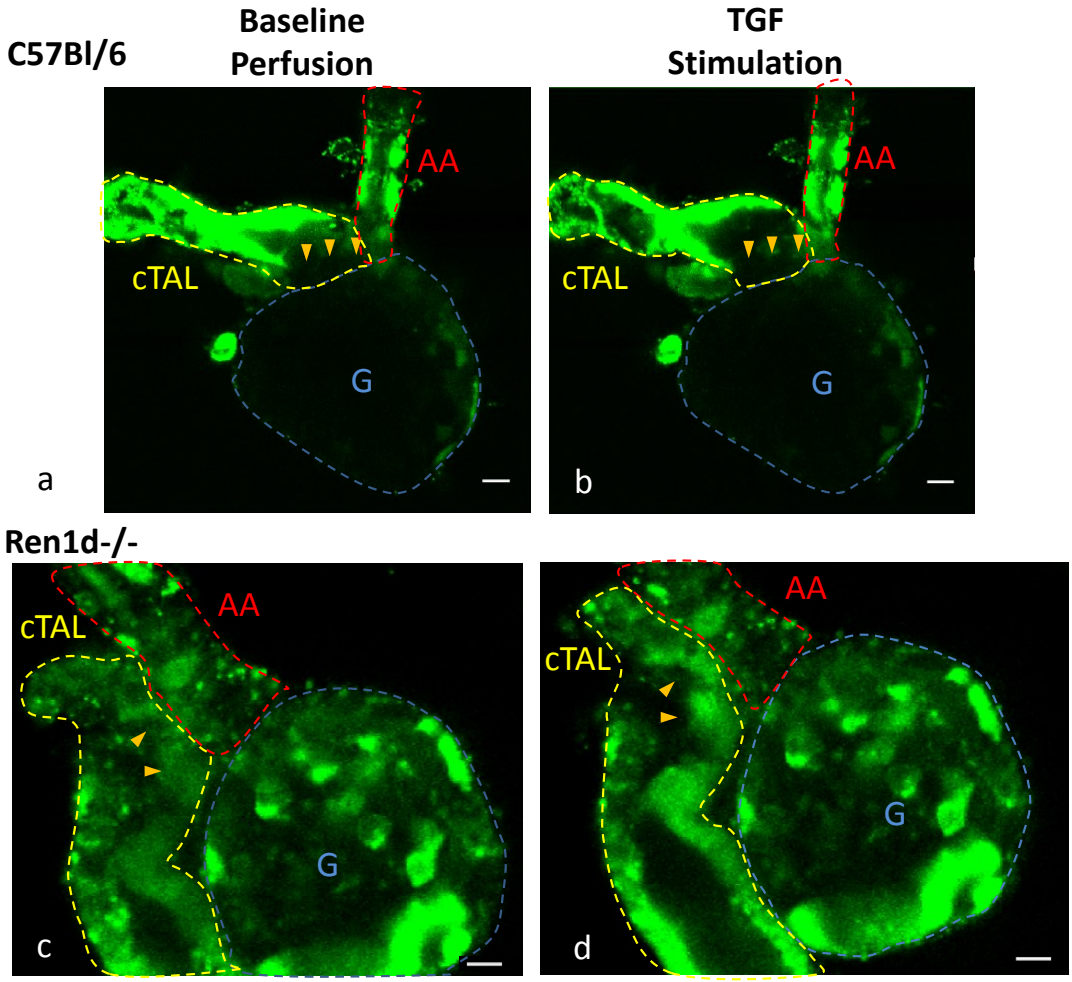

Figure 5.6: Images of flow-induced elevations in calcium in MD cells in isolated perfused JGA with attached MD cells. - Flow-induced TGF was triggered by increasing the rate of 10 mM NaCl-containing tubular perfusate from 2 to 20 nl/min in preparations from C57Bl/6, and $Ren1d^{-/-}$ mice. Orange arrows indicate MD cells, yellow dashed lines identify the cortical thick ascending limb (cTAL), red dashed lines identify the afferent arteriole (AA), blue dashed lines identify the glomerular tuft (G). Scale bar represents 10 μm.

response was not significantly different whichever method was used to stimulate TGF, though the NaCl-induced TGF response was slightly blunted.

5.2.3 Immunohistochemical Analysis of Low Salt- and ACE inhibitor-Stimulated Macula Densa

To assess whether low tubular salt-mediated MD stimulation also functioned effectively in $Ren1d^{-/-}$ mice with altered MD morphology and non-granulated JG cells, male $Ren1d^{-/-}$ and C57Bl/6 mice were given low salt and captopril (200 mg/l, 5 days) and compared to age matched, non-treated controls. All mice were then anaesthetised, flushed with ice-cold PBS, perfusion-fixed with 4% PFA and the kidneys OCT embedded for immunofluorescence analysis.

5.2.3.1 Effects of Low Salt and ACE inhibitor on Renin Expression

Under sodium depleted conditions, renin expression is induced in the VSMCs of the AA of wild type mice. To determine whether this classic metaplastic transformation was similarly induced in $Ren1d^{-/-}$ mice under low NaCl MD stimulation, renin staining was performed. As expected, renin staining localised to the classic JG location at the distal end of the AA under non-treated conditions in both C57Bl/6 and $Ren1d^{-/-}$ mice (Figure 5.7). Both treatment groups showed an extended expression pattern of renin along the AA, which is characteristic of the metaplastic transformation (Figure 5.7b, e).

5.2.3.2 Effects of Low Salt and ACE inhibitor on COX2 Expression

COX2 is expressed in MD cells when low tubular salt is sensed through NKCC2 co-transporters on the MD cell surface. To determine whether this response to low salt

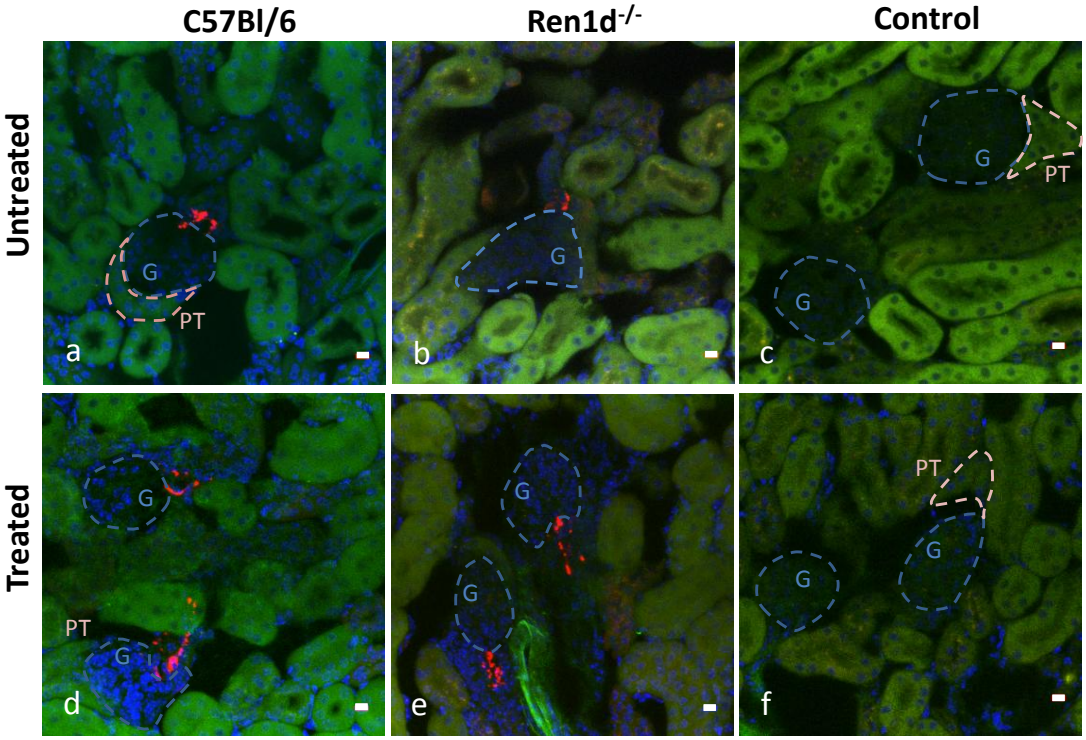

Figure 5.7: Renin expression pattern in mice after chronic low salt and ACE inhibitor stimulation of the MD. - Sections from (a, d) C57Bl/6 and (b, e) *Ren*1$d^{-/-}$ mice under (a-c) non-treated and (d-f) low salt diet and captopril (200 mg/ml, 5 days) treated conditions. Red: renin, blue: DAPI, green: autofluorescence of the tubules, shown for structural information. (c, f) Control, no-primary staining. 25-30 μm confocal stacks were taken and the maximum intensity z-projection shown. DAPI was excited with a multiphoton 706 nm laser, green signal from a 488 nm laser and red with the 594 nm laser using confocal microscopy and a 63X oil objective lens. Blue dashed lined: glomerular tuft (G); pink dashed lines: proximal tubule (PT). Scale bars represent 10 μm.

was functional in $Ren1d^{-/-}$ mice, COX2 staining was performed. No COX2 staining of the MD under non-treated conditions was found in either $Ren1d^{-/-}$ or C57Bl/6 mice (Figure 5.8a, b, orange arrows). However some non-MD specific staining was seen in cells surrounding the JGA (Figure 5.8, white arrows); this was particularly pronounced in the $Ren1d^{-/-}$ model where an increased amount of intra-glomerular staining was seen in comparison to the C57Bl/6 controls. Interestingly, a population of COX2 positive cells were identified between the MD plaque of the cTAL and the glomerular tuft in $Ren1d^{-/-}$ mice (white arrows). Although these were present in C57Bl/6 mice, the expression was less pronounced.

After low salt and ACE inhibitor were administered, the MD cells in both C57Bl/6 and $Ren1d^{-/-}$ mice stained positive for COX2 (Figures 5.8c, d, orange arrows). The COX2 positive staining revealed hyper-cellularity of the MD plaque and showed increased intra-glomerular COX2 expression in the treated $Ren1d^{-/-}$ mice compared to the C57Bl/6 controls. The population of COX2 positive cells between the MD and the glomerular tuft was again strikingly visible in the treated $Ren1d^{-/-}$ group (white arrows), versus the treated C57Bl/6 mice.

5.2.3.3 Effects of Low Salt and ACE inhibitor on NG2 Expression

To determine whether progenitor cell recruitment was occurring in response to low tubular salt MD cell stimulation, the pericyte marker NG2 was stained for in all groups. Untreated $Ren1d^{-/-}$ mice showed significantly increased staining within the glomerular tuft as well as along the AA when compared to untreated C57Bl/6 controls (Figure 5.9a, b). After low salt and ACE inhibitor treatments, the $Ren1d^{-/-}$ glomerular tuft showed increased NG2 staining when compared to the glomerular tufts in treated C57Bl/6 mice,

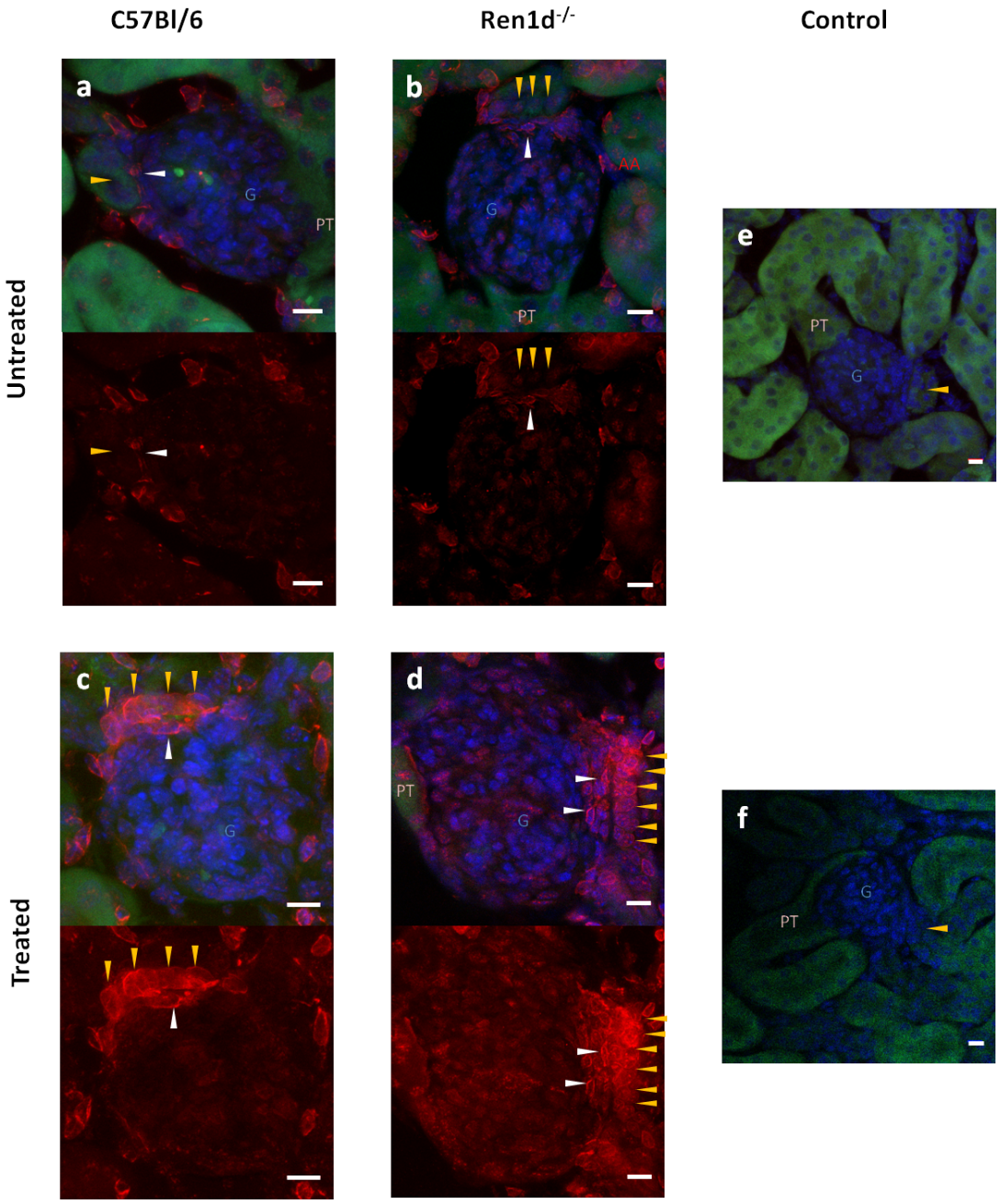

Figure 5.8: COX2 expression pattern in mice after chronic low salt and ACE inhibitor stimulation of the MD. - Sections from (a, d) C57Bl/6 and (b, e) *Ren1d*$^{-/-}$ mice under (a-c) non-treated and (d-f) low salt diet and captopril (200 mg/ml, 5 days) treatment. Red: COX2, blue: DAPI, green: autofluorescence of the tubules, shown for structural information. (e, f) Control, no-primary staining. 25-30 μm confocal stacks were taken and the maximum intensity z-projection shown. DAPI was excited with a multiphoton 706 nm laser, green signal with a 488 nm laser and red with the 594 nm laser using confocal microscopy and a 63X oil objective lens. White arrows: location of population of COX2 positive cells located between the glomerular tuft and the cTAL. Orange arrows: macula densa cells. G: glomerular tuft (blue); PT: proximal tubule (pink). Scale bars represent 10 μm.

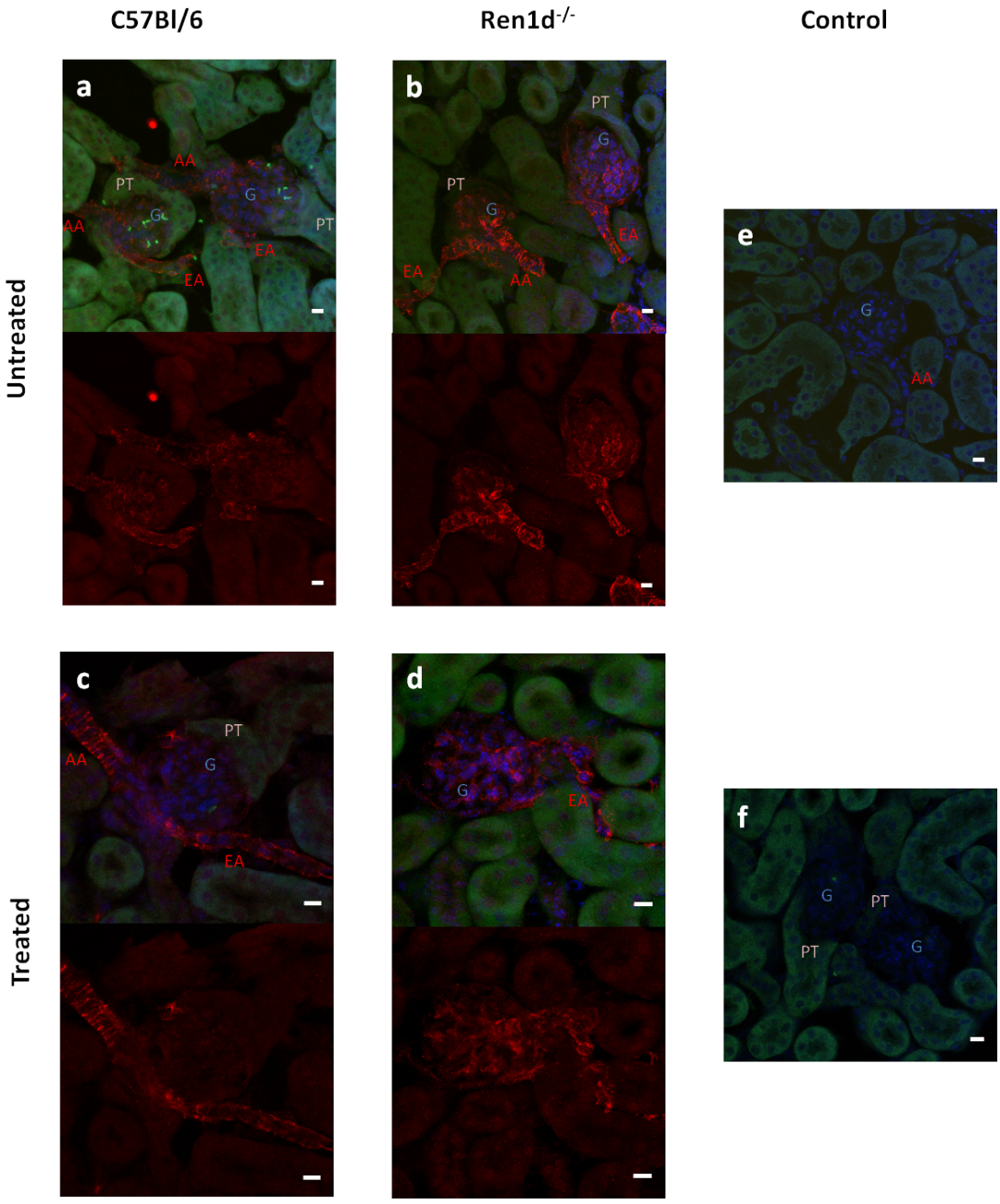

Figure 5.9: NG2 expression pattern in mice after chronic low salt and ACE inhibitor stimulation of the MD. - Sections from (a,c) C57Bl/6 and (b,d) *Ren1d*$^{-/-}$ mice under (a, b) non-treated and (c, d) low salt diet and captopril (200mg/ml, 5 days) treatment. Red: NG2, blue: DAPI, green: autofluorescence of the tubules, shown for structural information. (e,f) Control, no-primary staining. 25-30 μm confocal stacks were taken and the maximum intensity z-projection shown, with Dapi excited with a multiphoton 706 nm laser, GFP with a 488 nm laser and red with the 594nm laser using confocal microscopy and a 63X oil objective lens. G: glomerular tuft (blue); PT: proximal tubule (pink); EA: efferent arteriole (red); AA: afferent arteriole (red). Scale bars represent 10 μm.

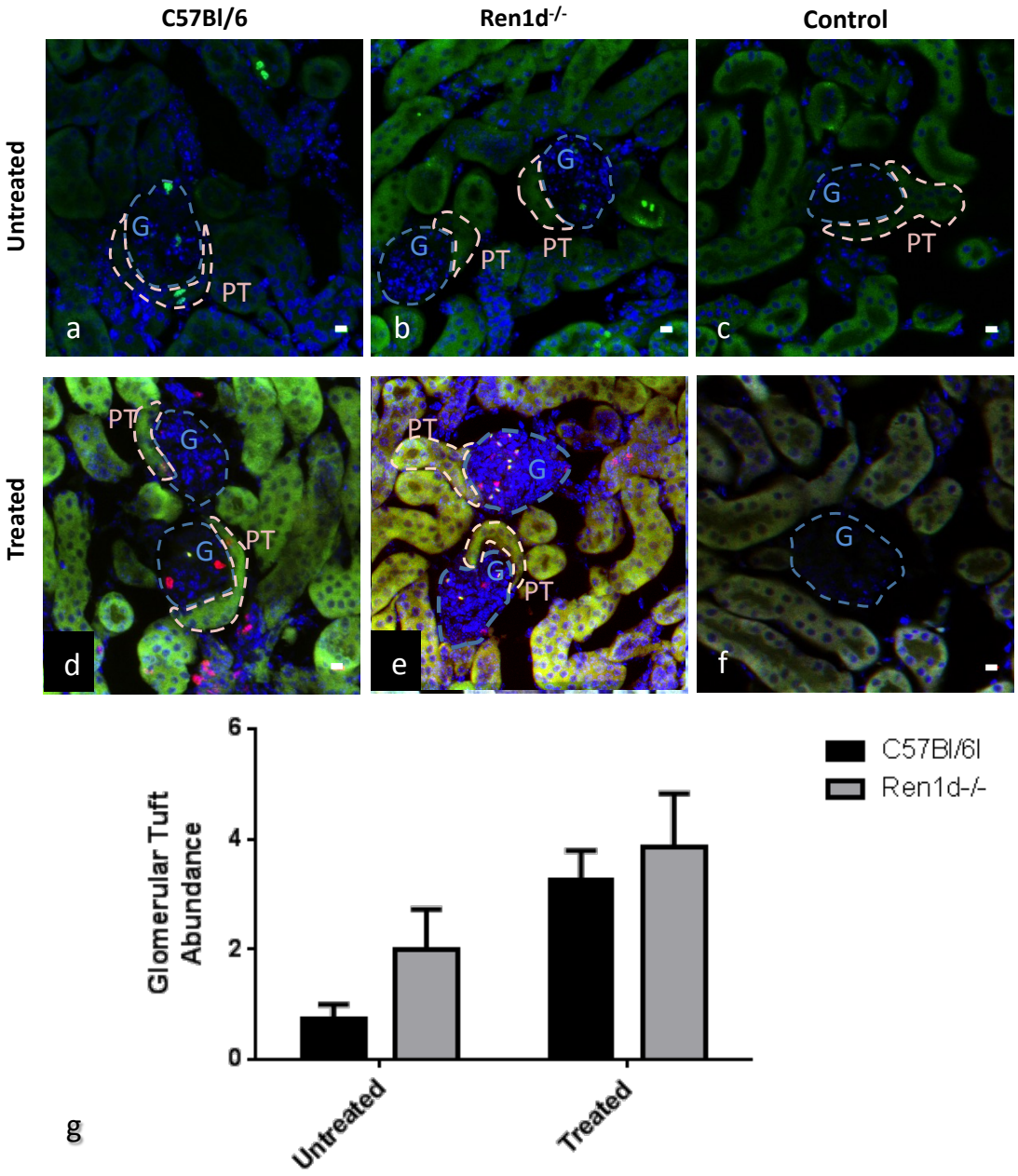

Figure 5.10: Ki67 expression in mice after chronic low salt and ACE inhibitor stimulation of the MD. - Ki67 staining of (a, d) C57Bl/6 and (b, e) *Ren*1$d^{-/-}$ mouse kidneys under (a-c) baseline or low salt and captopril (200 mg/ml, 5 days) treatment. (a-c) GFP: Ki67 positive nuclei, blue: DAPI, green: autofluorescence of the tubules, shown for structural information. (d-f) Red: Ki67 positive nuclei, blue: DAPI nuclear staining, green: autofluorescence of the tubules, shown for structural information. (c, f) Control, no-primary staining. 25-30 μm confocal stacks were taken and the maximum intensity z-projection shown, with Dapi excited with a 706 nm laser, GFP with a 488 nm laser and red with the 594nm laser using confocal microscopy and a 63X oil objective lens. Blue dashed lined: glomerular tuft (G); pink dashed lines: proximal tubule (PT). Scale bars represent 10μm. (g) The number of Ki67-positive nuclei within the glomerular tuft for each experimental group. Data are mean ± S.E.M., n = 3, two way anova with Tukey post hoc analysis performed (ns).

which showed very little NG2-positive staining (Figure 5.9c, d).

5.2.3.4 Effects of Low Salt and ACE inhibitor on Ki67 Expression

Ki67 staining was performed to identify whether increased proliferation was present in $Ren1d^{-/-}$ JGA compared to C57Bl/6 controls, under both baseline and treated conditions. Slightly increased staining was observed in treated compared to untreated samples from both groups (Figure 5.10). The main proliferating cell types were intraglomerular cells and proximal tubule cells, particularly in the glomerular cap. However there was very little evidence of MD cell proliferation in any group or treatment.

Since changes in COX2 and NG2 staining in the glomerular tuft of $Ren1d^{-/-}$ mice were seen after low salt MD stimulation, the number of Ki67 positive cells within individual glomerular tufts were counted. No significant difference in the number of Ki67 positive cells was seen, between C57B1/6 mice (0.7 cells) and $Ren1d^{-/-}$ mice (2 cells), either with, or without, the low salt and ACE inhibitor treatment (Figure 5.10). Glomerular tuft cell division was increased after low salt and captopril MD stimulation did not reach significance.

5.3 Discussion

5.3.1 Tubuloglomerular Feedback Response

Technical Considerations

By using isolated perfused JGA preparations, acute changes in TGF response were visualised under controlled conditions, independent of external signalling factors and BP changes. Both mechanical responses and cell-to-cell $[Ca^{2+}]_i$ propagation were quantified. The consequences of removing the JGA from its natural pressure and endocrine signalling environment were limited by ensuring the AA and cTAL were perfused at physiological pressures with the physiologically balanced Ringer solutions.

Alternative techniques, such as the kidney slice (129) or isolated perfused kidney (128) could be used, but carry confounding factors including endocrine signals from different cell types and reduced control over the perfusion rate and pressure at the single glomerulus level. *In vivo* multi-photon imaging is another technique that has previously been employed to investigate the link between tubular transport and glomerular structure and function (35). However, superficial AAs are very difficult to locate in adult mouse kidneys due to the depth of structures within the tissue. To visualise structures such as the afferent arteriole intravitally, unilateral ureteral obstructions (UUO) have been performed (212). This method involves the occlusion of the ureter using sutures, leading to increased intratubular hydrostatic pressure and ischemia, causing the kidney to swell in size and bring cortical glomeruli closer to the renal capsule (213). Whilst this facilitates *in vivo* imaging, it is a severe disease model and therefore not practical for studies of normal function. Furthermore, perfusion pressure at the cTAL and AA cannot be as easily controlled *in vivo*. Therefore although the JGA are removed from

their natural biological environment, the isolated perfused JGA preparation is the most tractable technique for faithfully measuring acute TGF responses experimentally.

The use of ratiometric calcium indicator dye pairs is a well-established method for quantifying calcium transits, both within the Peti-Peterdi Laboratory and other research groups, and has a number of advantages over using a single dye (28, 32, 33, 214, 215). Importantly, it minimises errors in concentration calculations from factors such as photobleaching, poor distribution of dye loading within the cell (particularly within VSMCs of the AA), dye leakage from the cell and differences in cell swelling or cell depth (214).

5.3.1.1 Calcium and Mechanical Response

It is evident that both flow- and NaCl-induced TGF are still able to function effectively in $Ren1d^{-/-}$ mice, which are known to have an altered MD morphology (114). Mechanical responses to TGF were seen in both C57Bl/6 and $Ren1d^{-/-}$ mice, with vasoconstriction acting at the very distal end of the AA in the same manner as previously characterised (33, 216). In agreement with previous reports, the TGF response to increased salt tended to be weaker than to increased flow in both groups (32). It has previously been shown that cilia on the apical membrane of MD cells are integral to flow sensing during TGF (28). The data currently presented would therefore seem to indicate that functionality of the cilia is not affected by the altered MD morphology in $Ren1d^{-/-}$ mice.

Contraction of the glomerular tuft confirmed previous observations that many cell types within the glomerulus participate in TGF to reduce glomerular filtration (32, 217). By measuring both diameter and area of the glomerular tuft before and after TGF

activation, the contraction response was monitored more reliably. $Ren1d^{-/-}$ glomerular tuft diameter and area showed significantly reduced contraction responses compared to those of C57Bl/6 mice. This suggests that a reduced GFR reduction exists in response to high NaCl or flow at the MD, indicating a slight impairment of BP regulation in $Ren1d^{-/-}$ mice.

Contraction of the glomerular tuft depends on the contraction of glomerular mesangial cells via calcium wave propagation. This would seem to indicate that calcium propagation is not as effective in $Ren1d^{-/-}$ mice, however calcium levels in podocytes was similar in both groups, suggesting that propagation functioned effectively. Interestingly, increased baseline expression levels of NG2 staining within the glomerular tuft were observed in $Ren1d^{-/-}$ mice compared to C57Bl/6 controls. It has been speculated that NG2-positive pericytes play a key role in renal fibrosis, particularly during diabetes. In STZ-induced diabetic rats NG2 expression was significantly increased in the mesangium of the kidney, where mesangial cells were seen to migrate and accumulate ECM such as type IV collagen and laminin (218). Therefore these intra-glomerular NG2-positive mesangial cells could contribute to increased deposition of ECM factors, which may result in the decreased contraction seen in $Ren1d^{-/-}$ JGA preparations undergoing TGF.

Interestingly, there was also a trend towards increased proliferation within the glomerular tuft of $Ren1d^{-/-}$ mice at baseline, indicated by an increase in Ki67-positive staining. The recruitment of proliferating NG2-positive pericytes to the glomerular tuft, even under baseline conditions, may indicate that the MD in these mice are under a more 'activated' state than the C57B1/6 controls.

$[Ca^{2+}]_i$ propagation throughout the JGA acts in parallel with these morphological characteristics of TGF. Whilst MD cells in preparations from C57Bl/6 mice did not show any Ca^{2+} signalling under either flow- or NaCl-induced stimulation, MD intracellular Ca^{2+} tended to increase after NaCl-induced TGF in $Ren1d^{-/-}$ preparations (though this did not reach significance). Importantly, analysis of calcium loading within the MD indicated that the plaque was heterogeneous, with only certain MD cells loading with the calcium indicator dye and subsequently responding to flow- or NaCl-induced TGF. MD cells are known to have an unusual relationship with cytosolic calcium regulation (168, 219), with a significantly lower cytosolic calcium concentration found in MD cells than other cells of the TAL. This is in part due to the tight regulation of calcium in MD cells through the action of different proteins such as ANX1 (220), which bind free calcium to maintain a low level of global calcium. Indeed it has previously been shown that MD calcium is not involved in TGF (32), (221). The increased calcium signalling in the MD plaque of $Ren1d^{-/-}$ mice could therefore indicate a slight imbalance in one or a number of these submembrane proteins. MD cells have a high concentration of mitochondria within the cytoplasm necessary for ATP production, which requires the uptake of cytosolic calcium (219, 222). Therefore the increased calcium observed in MD cells of mice lacking *Ren*1*d* may indicate a reduced density of mitochondria in the cytoplasm, leading to decreased uptake of calcium into mitochondria. Comparison of MD from C57Bl/6 and *Ren*1*d* mice either using electron micrographs or staining sections with mitotracker would show whether this was indeed the case. Increasing the number of biological replicates would further tease out whether this difference is indeed and to what extent MD Ca^{2+} plays a role in $Ren1d^{-/-}$ TGF.

5.3.2 Low Salt and ACE inhibitor Stimulation of the Macula Densa

A chronic decrease in tubular NaCl has previously been shown to increase renin expression and stimulate release in isolated perfused JGA preparations (16, 193, 223). It is important to note that although the *Ren*1*d* gene is knocked out in these mice, the highly homologous *Ren*2 gene is still present and able to produce 'inactive' prorenin. The renin antibody used in these studies binds to the C-terminal of the renin gene, indicating that it recognises both the inactive prorenin and active forms of renin and hence should stain the *Ren*2 present in the JG cells of Ren1d$^{-/-}$ mice.

Renin staining was seen clearly at both baseline and after treatment in both C57Bl/6 and *Ren*1*d*$^{-/-}$ mice. The pattern of staining was not punctate, nor was it solely cytoplasmic; it is possible that renin generation was localised to certain areas of the cell and signal is being collected from these areas of high renin density. This was in keeping with renin immunohistochemistry reported by Clark *et al* (114) who staining in *Ren*1*d*$^{-/-}$ mice compared to C57Bl/6 controls, though at a lower level.

*Ren*1*d*$^{-/-}$ mice are able to respond to the administration of an ACE inhibitor and a low salt diet in the same way as C57Bl/6 mice, showing recruitment of renin producing cells along the AA. Therefore, although these JG cells are not able to produce dense core granules and secrete active renin they are still in essence renin-producing cells which are producing *Ren*2, in agreement with previous studies (114, 120).

To determine whether the initial stages of the signalling cascade leading to the release of renin were functioning effectively in *Ren*1*d*$^{-/-}$ mice, staining for COX2 was performed. COX2 is highly inducible, and has been shown to localise to the MD in all species tested to date (224, 225, 226). A number of studies have shown that reduced salt

concentration at the cTAL significantly increases MD COX2 expression (102, 210, 227). This was similarly observed in the present study in both C57B1/6 and $Ren1d^{-/-}$ mice after treatment with low salt and an ACE inhibitor. However it was extremely difficult to identify COX2-expressing cells in the untreated mice, although slightly more were found in the $Ren1d^{-/-}$ group, particularly in a group of cells found between the MD plaque and the glomerulus.

One interpretation of these results is that these cells between the MD and the glomerulus are a line of interstitial progenitor cells which are destined to become mesangial cells. To establish the abundance and location of progenitor cells in both models under basal and treated conditions, staining for the progenitor cell marker NG2 was performed.

From the present study it is evident that a large population of NG2-positive cells reside in the JGA under baseline conditions in both C57Bl/6 and $Ren1d^{-/-}$ mice, particularly along the vasculature of the afferent and efferent arterioles. What is striking is that $Ren1d^{-/-}$ mice have a lot more NG2-positive cells residing within the intra-glomerular mesangium as well as along the vasculature, which is not present in C57Bl/6 mice. This was not quantified due to the fact that confocal stacks were not taken through entire glomeruli, however future work could address this. Work carried out in the Peti-Peterdi Laboratory has suggested that upon strong stimulation at the MD using a low salt diet to increase reabsorption, an ACE inhibitor to increase salt wasting and UUO, an increase in NG2-positive cell density is seen in the interstitium, and that these cells migrate to the MD (ASN2013 Abstract, (228)). Furthermore, inhibition of COX2 decreased NG2 cell proliferation, and the migratory NG2 positive cells showed partial co-localisation with renin after stimulation (228). All these factors

suggest that MD-derived paracrine signalling plays a significant role in glomerular maintenance. The increase in NG2 expression within the JGA of $Ren1d^{-/-}$ mice coupled with hyper-cellularity of the MD plaque suggest that a population of progenitor-like cells may be stimulated and participating in glomerular remodelling. Interestingly, there is not complete concordance between the COX2-positive putative progenitor cells and NG2-stained cells; whether this is because the staining patterns are temporally or spatially different remains to be seen. A double staining experiment would be needed to investigate this.

Razga and Nyengaard (229) also suggested that the MD plaque possessed a degree of plasticity. In their study on the relationship between RAAS activity and MD cell number, it was shown that MD cells in control mice had a significantly lower number of AT1 receptors than other tubular cells, and that MD cell volume was significantly smaller than cTAL cell volume. However after treatment with candesartan, an AT1 receptor blocker, an increase in the number of MD cells and consequently in the volume of the MD plaque was seen. ANGII binds to ATI receptors of the cTAL cells and inhibits COX2 expression, but after treatment with the ANGII receptor antagonist candesartan the number of cells expressing COX2 increased in the MD region, suggesting that tubular cells may transdifferentiate into MD cells (229, 230, 231). $Ren1d^{-/-}$ mice with altered MD cell morphology and number (114) could therefore have a reduced activation of AT1 receptors at the cTAL cells, leading to the same hypothesised transdifferentiation. This would make sense as the lack of circulating active renin at baseline would act in the same way as an ACE inhibitor, halting the generation of the ANGII involved in AT1 activation.

Ki67 was used to identify where proliferation was occurring in the two models under

baseline and stimulated conditions. Ki67 is a nuclear protein complex whose expression is maximal in the metaphase of the cell cycle (232). Although a trend towards more proliferation was seen in $Ren1d^{-/-}$ mice both at baseline and after low salt treatment, no MD-specific Ki67 staining was found in either groups under either condition. This is in agreement with the Ragza and Nyengaard study which showed that MD cells themselves were not proliferating as they did not show any Ki67 positive staining, with the majority of staining seen in tubular cells, particularly in the distal segment of the tubules (229). This suggests that the hyper-cellularity seen in the treated $Ren1d^{-/-}$ mice and previously reported in the baseline $Ren1d^{-/-}$ mice MD plaques (114) would be due to either migrating progenitor cells or a transformation of tubular cells to take on the specialised salt-sensing MD phenotype. It is tempting to speculate that these transforming cells render the MD plaque heterogeneous, leading to the heterogeneous calcium wave propagation observed.

5.3.3 Conclusions

Stimulation of the MD in $Ren1d^{-/-}$ and C57Bl/6 mice was successfully achieved acutely, through increased NaCl concentration or flow using isolated perfused JGA, or chronically through low salt and ACE inhibitor treatment for five days. TGF was effectively induced in all mice, indicating that altered MD morphology did not affect this acute feedback response. Subtle differences were seen in the magnitude of the response between groups; in particular, significantly reduced glomerular tuft contraction was seen in response to increased flow-induced TGF in mice on a $Ren1d^{-/-}$ background. Increased baseline NG2, Ki67 and COX2 staining within the glomerular tuft indicate that glomerular remodelling may be responsible for this altered contraction.

Ren1d$^{-/-}$ mice responded to chronic low salt and ACE inhibitor stimulation at the MD in the same way as C57Bl/6 controls, though the glomerular tuft stained more strongly for NG2 and COX2. MD COX2 expression was seen in a progenitor-like cell population in untreated *Ren1d*$^{-/-}$ mice, but was induced strongly in the MD of both models after treatment, which may indicate that transdifferentiation of other cell types into MD cells is taking place.

6

Renin Expression and Granulation in Human Renin Mice

6.1 Introduction

As previously discussed in Section 2.2.1, $Ren1d^{-/-}$ mice lack dense core granules within their JG cells and are therefore unable to process active renin (114). They also exhibit an altered MD morphology. It was proven that these phenotypes were not caused by a random mutation during gene targeting (120), however it remained unclear whether enzyme structure or activity was responsible for the phenotypes.

To address this, the human renin mouse strain were developed within the Mullin's laboratory (Dr Robert Nelson, manuscript in preparation). These mice were made by building a transgene containing a 55 kbp human renin gene fragment. This included the complete *hRen* gene, 35 kbp 5'-flanking sequence containing the renal enhancer, chorionic enhancer and proximal promoter to drive *hRen* expression, and 10 kbp 3'-

flanking sequence. This was introduced into fertilised oocytes via pronuclear injection to facilitate random insertion of the transgene into the genome. These mice were then backcrossed onto a $Ren1d^{-/-}$ background. Therefore only the $mRen2$ gene is present at the renin locus, meaning that no endogenous mouse renin should be packaged into dense core granules, although this was not confirmed.

Since mouse and human renin genes and proteins, both of which are both found on chromosome 1, are highly conserved, it was hypothesised that the structural features responsible for trafficking renin protein through the regulated secretory pathway would also be conserved. Therefore if normal JG and MD cell morphology were restored in human renin mice, enzyme structure was responsible; if MD morphology remained altered, enzyme activity was responsible since human renin is unable to cleave mouse angiotensinogen (122, 123).

Of the twenty offspring, four correctly targeted transgenic founders were established, three of which were fertile (lines 1317, 1446, 1448). Surprisingly the hyper-cellularity and altered morphology of MD cells displayed in $Ren1d^{-/-}$ mice was not rescued by introduction of the human renin gene (233). This suggested that the activity of active mouse $Ren-1d$ was necessary for maintaining normal MD structure, although the functional relevance of this altered morphology remained to be elucidated (233).

However restoration of granulation was observed in JG cells, indicating that functional regions in the human and mouse *Ren1d* protein are conserved, and that the onset of granulation is dependent on the renin gene structure. Whilst JG cells from the 1448 line remained ungranulated and 1317 mice displayed full restoration of JG cell granulation, 1446 mice displayed sexually dimorphic restoration of granulation, with males displaying significantly lower levels than females. Interestingly, after chronic treatment

with the ACE inhibitor captopril to increase renin expression levels, granulation was restored to a greater extent in males. Indeed the levels of granulation appeared to be renin expression level-dependent, suggesting that granulation levels within JG cells are expression level-dependent.

6.1.1 Aims

To investigate the hypothesis that JG cell granulation is renin expression level-dependent, 1446-huRen$^{+/-}$Ren1d$^{-/-}$ mice were used. JG cell ultrastructure, renin RNA expression and cytoplasmic granulation were assessed under basal conditions or after an increase in renin expression levels via ACE inhibition. This was achieved using qPCR to quantify renin gene expression and both 2D and 3D EM to assess JG cell granulation.

The test the hypothesis that the altered MD morphology retained in 1446-huRen$^{+/-}$Ren1d$^{-/-}$ mice is indicative of imparied MD function, TGF was stimulated in isolated perfused JGA from 1446-huRen$^{+/-}$Ren1d$^{-/-}$ mice by increasing flow and NaCl concentration at the MD.

6.2 Results

6.2.1 Characterisation of Renin Expression in HuRen Mice

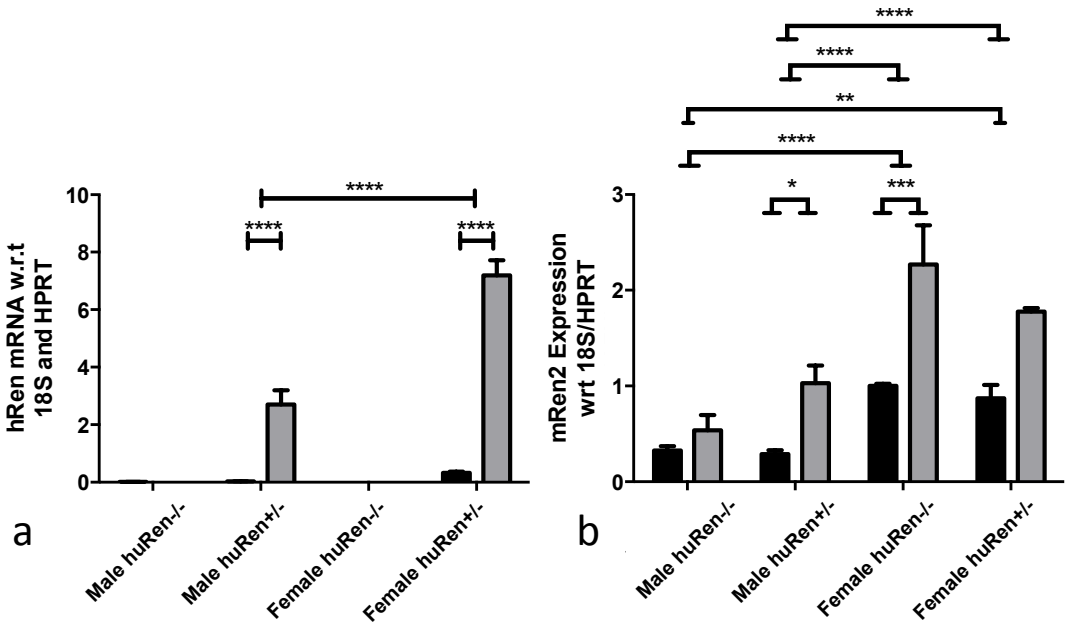

Figure 6.1: Quantification of renin expression in huRen mice. - Quantitative PCR analysis of (a) human renin (*hRen*) and (b) mouse renin (*mRen2*) expression in 1446 male and female $huRen^{+/-}Ren1d^{-/-}$ and $Ren1d^{-/-}$ mice was performed under baseline conditions and after treatment with captopril (1 mg/ml, 10 days, n=4-7). 2-way Anovas were performed in conjunction with Tukey's post hoc analysis. Data are mean ± S.E.M. * indicates $p < 0.05$, ** indicates $p < 0.01$, *** indicates $p < 0.001$, **** indicates $p < 0.0001$.

To quantify *hRen* transgene and native *mRen*2 expression levels, quantitative PCR was performed in male and female $huRen^{+/-}Ren1d^{-/-}$ and $Ren1d^{-/-}$ controls, at baseline or with captopril treatment. Human renin was not expressed in $Ren1d^{-/-}$ mice, either at baseline or after treatment with the ACE inhibitor captopril.

In 1446 $huRen^{+/-}Ren1d^{-/-}$ mice, captopril treatment led to a significant, 93.3-fold increase in *hRen* expression in males and 21.8-fold increase in females (Figure 6.1a). In untreated mice, females expressed 11.4-fold more *hRen* than males. There was a

significant overall increase in the amount of human renin mRNA expressed in 1446 females compared to males.

At baseline, $huRen^{+/-}Ren1d^{-/-}$ and $Ren1d^{-/-}$ mice of both genders showed no significant difference in mouse renin expression levels within gender but differed significantly between gender, with 3-fold higher expression levels in females (Figure 6.1b). Captopril treatment increased mouse renin expression levels in all groups, reaching significance in male $huRen^{+/-}$ (3.6-fold) and female $Ren1d^{-/-}$ mice (2.3-fold).

6.2.2 Immunogold Labelling of Juxtaglomerular Cells

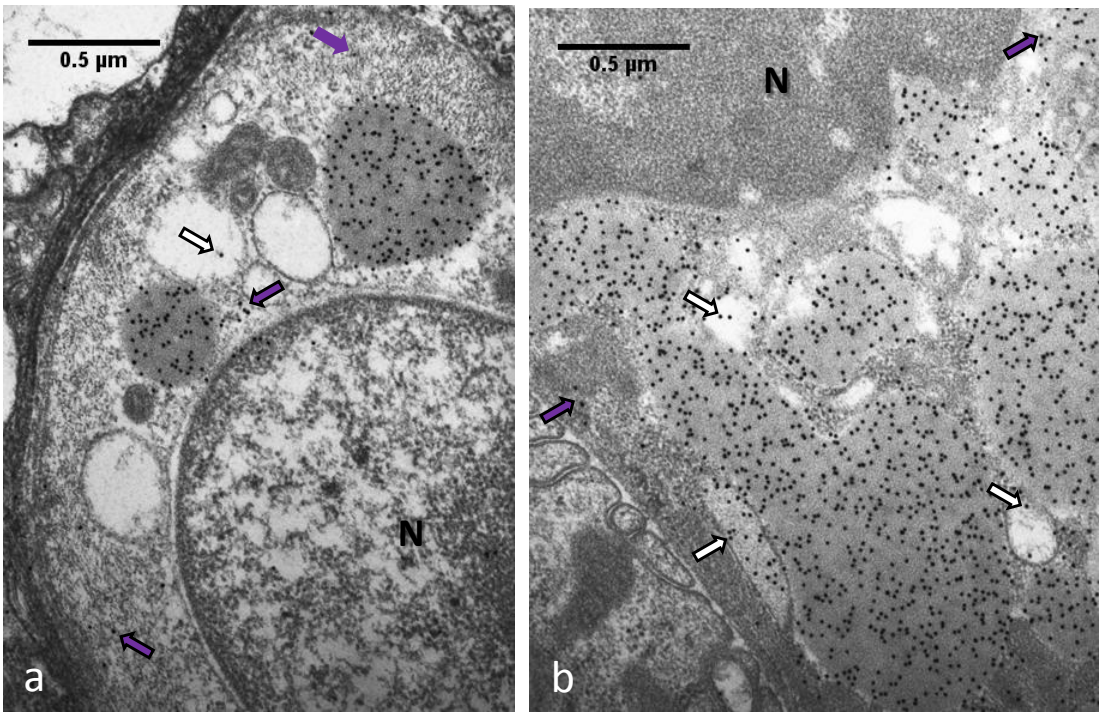

Figure 6.2: Immunogold labelling of granular content in $huRen^{+/-}Ren1d^{-/-}$ and C57Bl/6 JG cells. - Electron micrographs of JG cells from (a) 1446 $huRen^{+/-}Ren1d^{-/-}$ mice stained for human renin and (b) C57Bl/6 mice immunogold stained for mouse renin. N: nucleus, white arrow: electron-lucent granule staining, purple arrow: cytoplasmic staining.

To confirm the human renin content of dense core granules in JG cells from $huRen^{+/-}Ren1d^{-/-}$

mice, immunogold labelling against *hRen* and *mRen*2 (Figure 6.2a, b) was performed on ultrathin sections prepared for EM. It is evident that the vast majority of human renin signal was localised to the dense core granules, with no staining of the mitochondria. Approximately 88% of the immunogold particles were localised to dense core granules, with the remaining 12% found in the cytoplasm (purple arrows) and a single instance of staining within an electron-lucent granule (white arrow; Figure 6.2a). The majority of *mRen*2 staining in C57Bl/6 mice was localised to the dense core granules though more non-specific staining of the electron-lucent granules (white arrows) and the cytoplasm (purple arrows) was observed than with *hRen* staining (Figure 6.2b).

6.2.3 Ultrastructure of Juxtaglomerular Cells

Having assessed *hRen* transgene expression levels, intracellular JG cell ultrastructure was further studied at the EM level. Analysis of electron micrographs from JG cells of $Ren1d^{-/-}$ mice confirmed a lack of large dense-core granules (Figure 6.3a, b). Small cytoplasmic granules and mitochondria (white arrows) were visible in these micrographs, however no other distinctive features were present.

Presence of the human renin transgene in female $huRen^{+/-}Ren1d^{-/-}$ mice initiated the formation of large dense core granules throughout a large portion of the cytoplasm, each with a fairly uniform electron density (Figure 6.3c, d). JG cells from male $huRen^{+/-}Ren1d^{-/-}$ mice appeared to have a much more variable number of granules - some cells were devoid of dense core granules whilst others were akin to those seen in female mice of the same genotype (Figure 6.3e, f). Granules took on a more irregular shape, and a number of the granules demonstrated an electron-lucent appearance (shown in the 3D reconstructions, Figure 6.6e), which was not seen in female

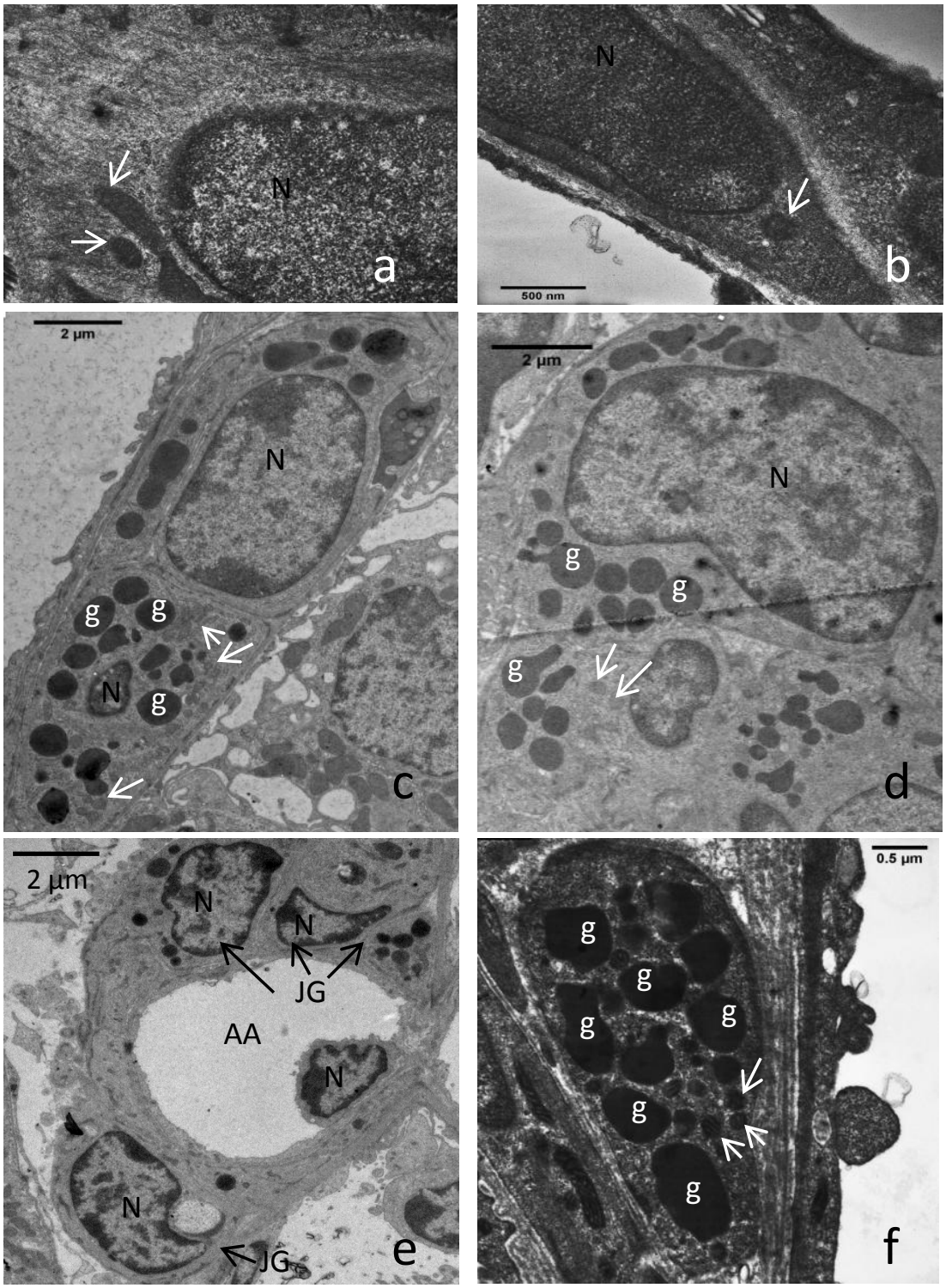

Figure 6.3: Ultrastructure analysis of JG cells from $huRen^{+/-}Ren1d^{-/-}$ mice. - Electron micrographs of JG cells from untreated 1446 (a, b) male $Ren1d^{-/-}$ mice, (c, d) male $huRen^{+/-}Ren1d^{-/-}$ mice and (e, f) female $huRen^{+/-}Ren1d^{-/-}$ mice. Kidneys were perfusion fixed (a-d) for ultrastructure analysis and (e, f) for 3D reconstruction (see Section 2.8). JG: juxtaglomerular cell, AA: afferent arteriole, N: nucleus, white arrows: mitochondria, g: granule.

$huRen^{+/-}Ren1d^{-/-}$ JG cells.

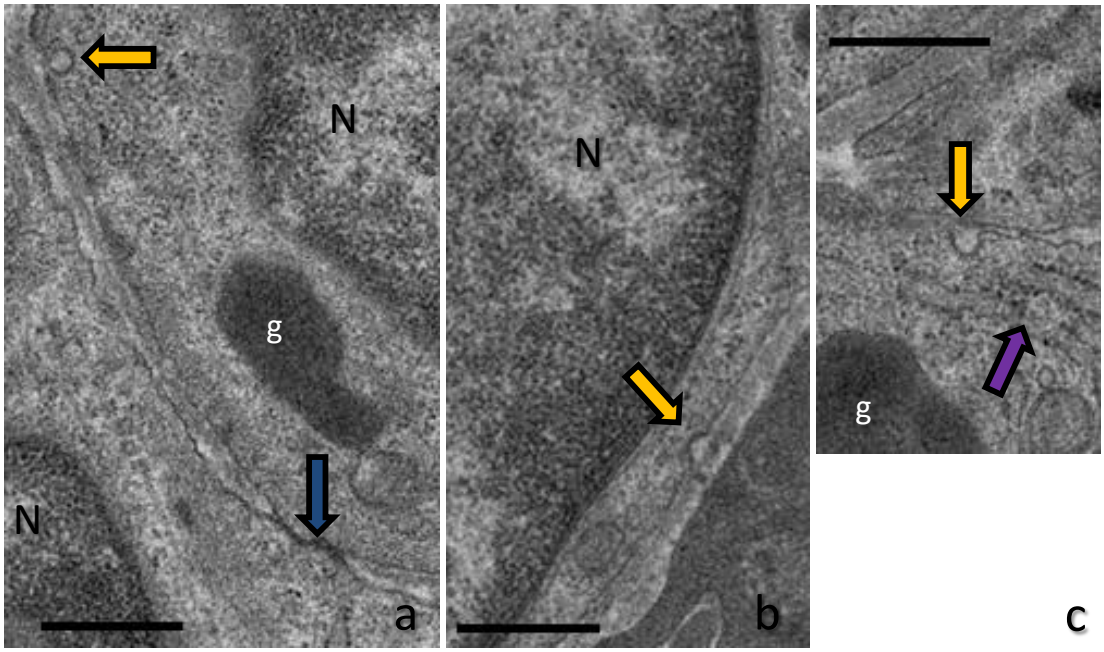

Figure 6.4: Small vesicle membrane-binding events imaged using EM. - JG cells from male and female 1446 $huRen^{+/-}Ren1d^{-/-}$ mice were imaged at the EM level. Kidneys were fixed for 3D reconstruction. Yellow arrows: small vesicle binding with the membrane, blue arrows: gap junctions between JG cells, purple arrows: rough endoplasmic reticulum, N: nucleus, g: electron-dense renin-containing granule. Scale bars represent 500 nm.

A number of membrane-associated vesicle-like structures were visualised in electron micrographs from both male and female $huRen^{+/-}Ren1d^{-/-}$ JG cells (yellow arrows, Figure 6.4). Measurement of 10 of these events revealed an average diameter of 68 $\pm$ 5 nm for these electron-lucent vesicles. A number of gap junction-like structures were also observed at JG-JG cell interfaces as well as JG-endothelial cell interfaces (blue arrow, Figure 6.4a). These were approximately 234 $\pm$ 3 nm in length. Despite the fact that a large number of images were taken for both genotypes (4 animals, 10 cells each), no interaction between dense core granules and the membrane was captured. Tannic acid was perfused through kidneys prior to gluteraldehyde fixative to highlight any granules

whose membrane were disrupted due to renin secretion. No instances of secretion were visualised in any of the JG cells analysed from either untreated $huRen^{+/-}Ren1d^{-/-}$ animals (male or female), or those treated with captopril for 10 days.

6.2.4 3D Reconstruction of Juxtaglomerular Cells

To attempt to quantify the granulation capacity of JG cells from 1446-$huRen^{+/-}Ren1d^{-/-}$ mice, kidneys were prepared for EM and ultrathin, 70 nm serial sections taken. The images were stacked and aligned such that the granules, membrane and nuclei could be rendered into 3D reconstructions.

The granules in JG cells from female 1446 $huRen^{+/-}Ren1d^{-/-}$ mice were densely packed within the cytoplasm (Figure 6.5). Certain linkages between granules were present, however the predominant granule shape was regular (Figure 6.5a,c). These granules had an approximate diameter of 0.5-3 μm at their widest, however quantifying this was complicated by the fact that often granules were irregularly shaped with linkages and non-uniform protrusions.

Conversely, granules found in JG cells from male 1446 $huRen^{+/-}Ren1d^{-/-}$ mice were more irregular in shape and size, and were less densely packed than those seen in JG cells from female 1446 mice (Figure 6.6) and were more variable in number. More granules showed non-uniform electron density; some appeared to be less electron-dense, whilst others were electron-lucent with areas of electron-dense material within them (Figure 6.6d,e).

To quantify how densely packed granules were, granule volume was calculated as a percentage of the extranuclear space for each of the reconstructions performed, and was significantly larger in C57Bl/6 male mice (40.1%; data from Dominik Steppan,

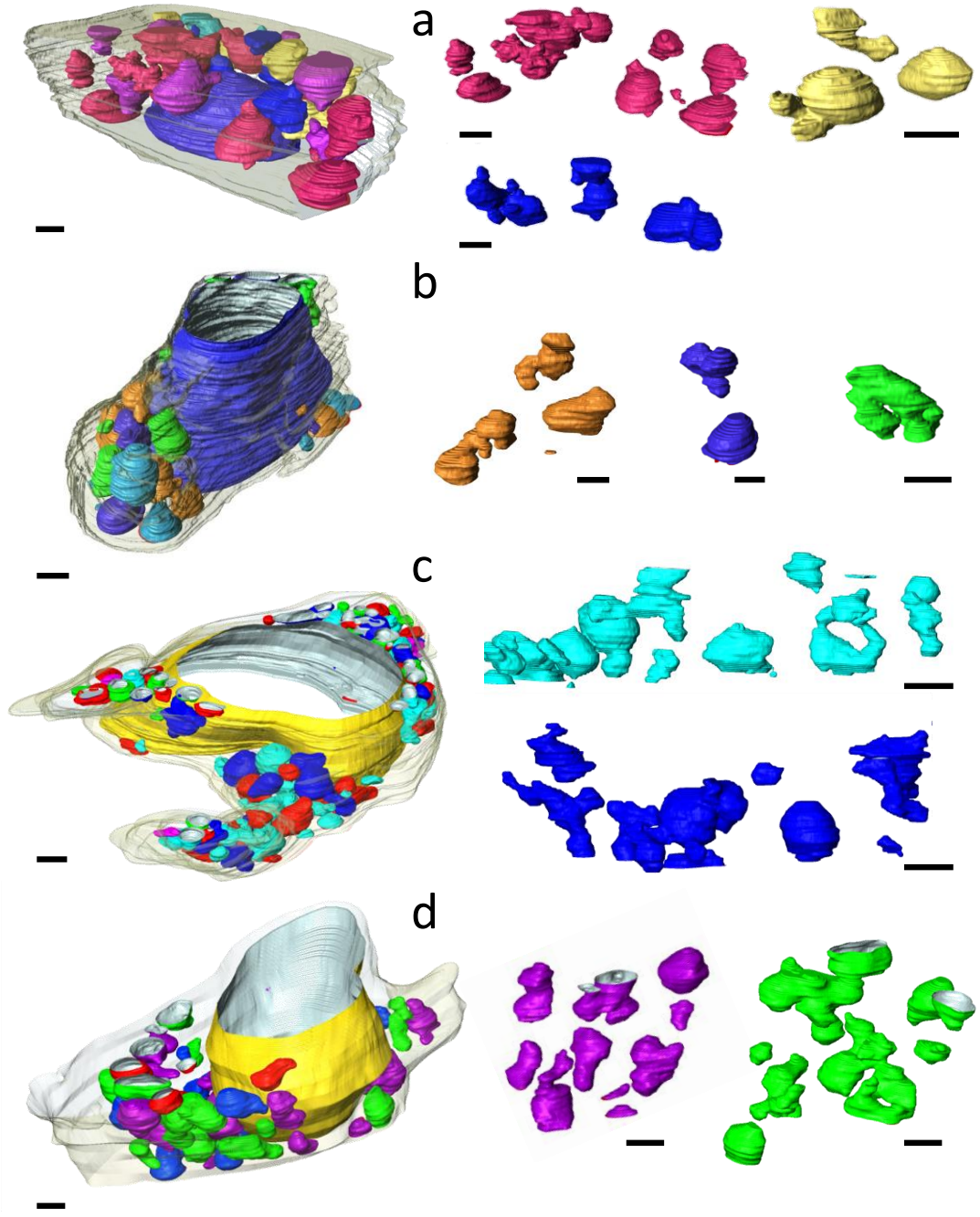

Figure 6.5: Representative 3D reconstructions of female 1446 $huRen^{+/-}Ren1d^{-/-}$ JG cells. - Reconstructions of JG cells were performed using Amira 5.5 FEI software from 40 electron micrographs taken at 70nm thickness. Whole cell reconstructions (LHS) are represented with the nucleus in dark blue (a,b) or yellow (c,d), the membrane transparent and the granules in multiple colours for ease of distinguishing between different structures. Examples of different granule structures within each reconstructed cell are also given (RHS). Scale bars represent 1 μm.

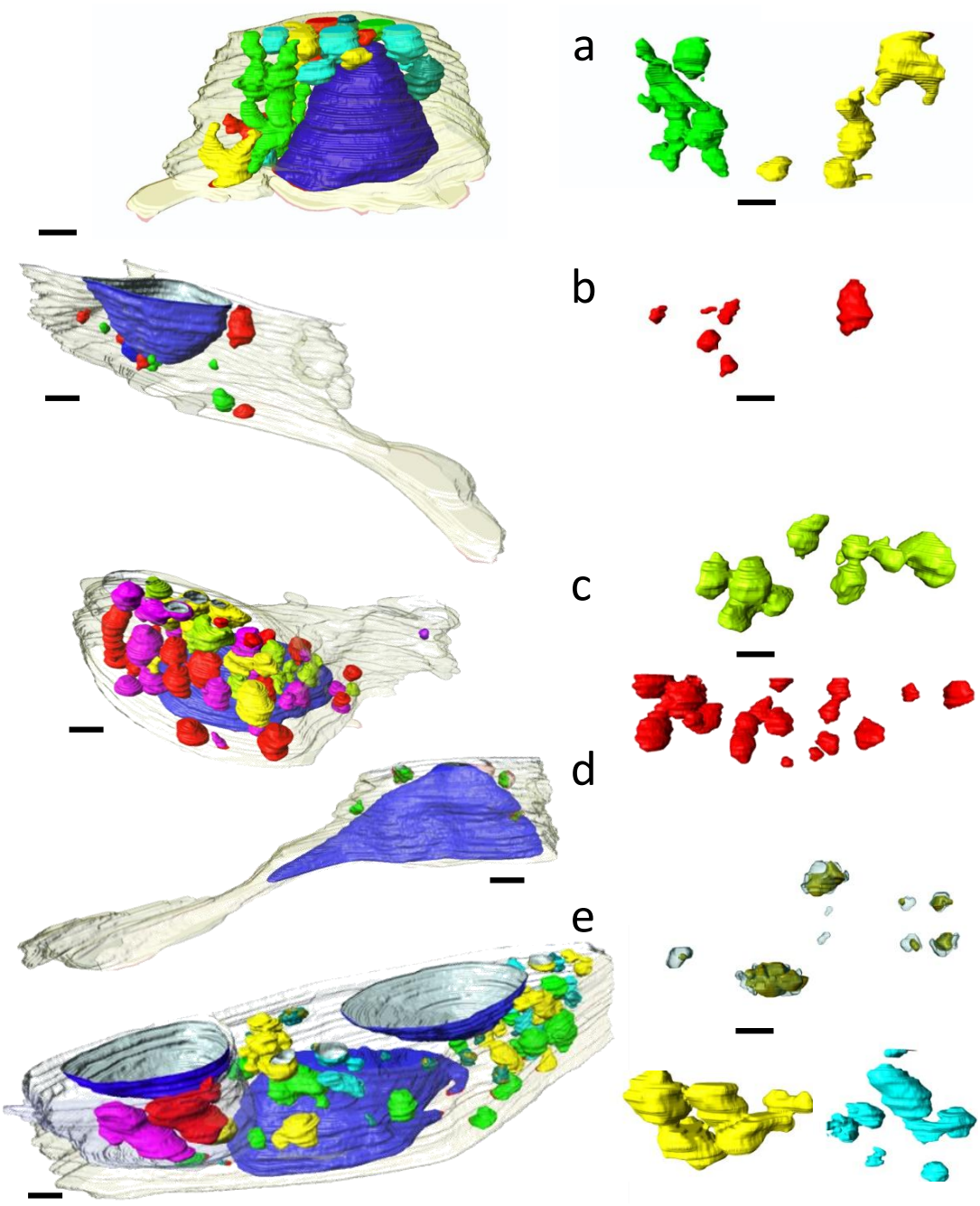

Figure 6.6: Representative 3D reconstructions of male 1446 $huRen^{+/-}Ren1d^{-/-}$ JG cells. - Reconstructions of JG cells were performed using Amira 5.5 FEI software from 40 electron micrographs taken at 70nm thickness. Whole cell reconstructions (LHS) are represented with the nucleus in dark blue, the membrane transparent and the granules in multiple colours for ease of distinguishing between different structures. Examples of different granule structures within each reconstructed cell are also given (RHS). Scale bars represent 1 μm.

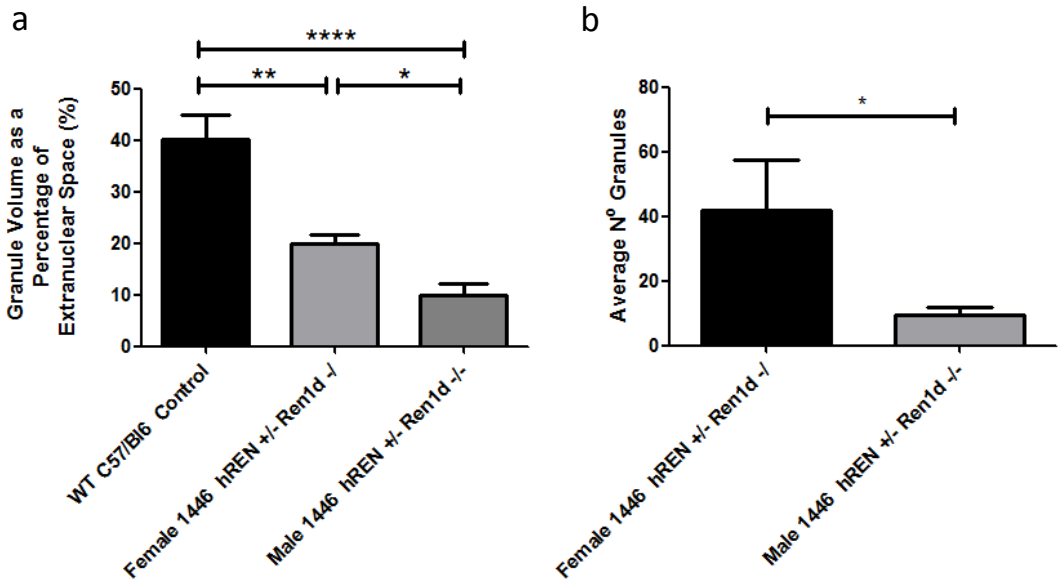

Figure 6.7: Quantification of granulation in reconstructed JG cells. - 3D Reconstructions of 1446 female and male $huRen^{+/-}Ren1d^{-/-}Ren2^{+/+}$ JG cells (n=4) were performed. Data from control C57Bl/6 mice are also represented (n=3), which was kindly donated by Dominik Steppan, University of Regensburg. (a) Granule volume as a percentage of the extanuclear cytoplasm. (b) The number of granules present in each cell. Data are mean ± S.E.M. * = $p < 0.05$, ** = $p < 0.01$, **** = $p < 0.0001$.

University of Regensburg) than in female 1446 $huRen^{+/-}Ren1d^{-/-}$ (20.0%, p=0.007) or male $huRen^{+/-}Ren1d^{-/-}$ mice (10.0%, p<0.0001, Figure 6.7a). The granulation number in female $huRen^{+/-}Ren1d^{-/-}$ JG cells was also significantly elevated compared to male $huRen^{+/-}Ren1d^{-/-}$ (p=0.010). Female $huRen^{+/-}$ mice had, on average, 42 ± 15 granules per JG cell, which was more than the 10 ± 2 granules present in male $huRen^{+/-}Ren1d^{-/-}$ (p=0.05, Figure 6.7b).

6.2.5 Ultrastructure of Juxtaglomerular Cells After Captopril Treatment

In order increase renin expression levels through stimulation of the RAAS, 1446 mice were administered captopril for 10 days and electron microscopy performed on ultrathin kidney sections to assess the resulting change in granulation within JG cells.

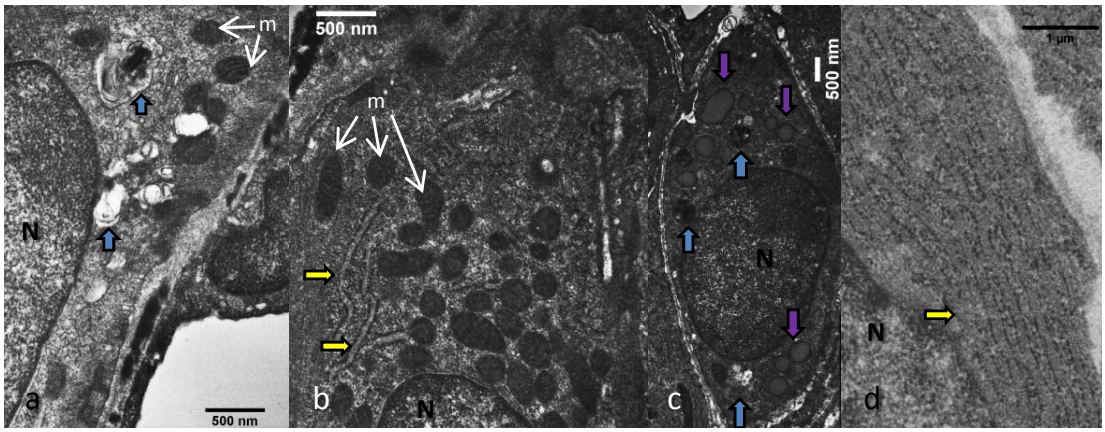

Figure 6.8: Ultrastructure analysis of JG cells from $Ren1d^{-/-}$ mice after captopril treatment. - Electron micrographs of JG cells from captopril treated (1 mg/ml, 10 days) 1446 male $Ren1d^{-/-}$ mice. Kidneys were fixed for ultrastructure analysis. White m and arrows: mitochondria; yellow arrow: rough endoplasmic reticulum; blue arrow: lysososomal structures; purple arrow: electron-lucent granules, N: nucleus.

In $Ren1d^{-/-}$ mice where prorenin is unable to be packaged into dense core granules, large, electron-lucent granules were produced (purple arrows, Figure 6.8). Numerous

mitochondria (white arrows) were present, as were some lysosomal-type structures (blue arrows). Furthermore, many small vesicles were identifiable in the cytosol (Figure 6.8), with the RER appearing much more prominent (yellow arrows).

Captopril also appeared to increase the number of large electron-dense granules seen within the cytoplasm of JG cells in 1446 male $huRen^{+/-}Ren1d^{-/-}$ mice, although 3D reconstructions were not able to be performed to confirm this due to time constraints. The 2D sections suggested that granules took on a largely regular shape. The RER also appeared dilated (yellow arrows, Figure 6.9) compared to untreated JG cell electron micrographs (Figure 6.3), suggesting an increase in the amount of renin being synthesized. A large number of mitochondria were visible throughout the cytoplasm (white arrows), and there was also an increase in the number of electron-lucent vacuoles seen in cells (purple arrows, Figure 6.9c, d). Although not linked to the captopril treatment, interactions between granulated JG cells and the underlying endothelium are visible via a gap junction and a peg and socket joint (Figure 6.9c, dark green arrow)

Captopril treatment produced both electron-dense and electron-lucent granules (Figure 6.9b-f). These granules ranged from almost entirely electron-lucent to the classic dense core appearance, with very clear membranes. The granules ranged in size, from small granules, surrounded by dilated RER, to larger, merged granules (Figure 6.9c). Coalescence of paracrystalline materials was visible within granules (Figure 6.9e, f). Granules of different electron densities are clearly delineated by a single layer of membrane, and immature granules, accumulating electron-dense material, are also visible.

The electron densities of granules within JG cells from baseline and captopril treated animals were assessed by manually marking out the granule border and measuring the

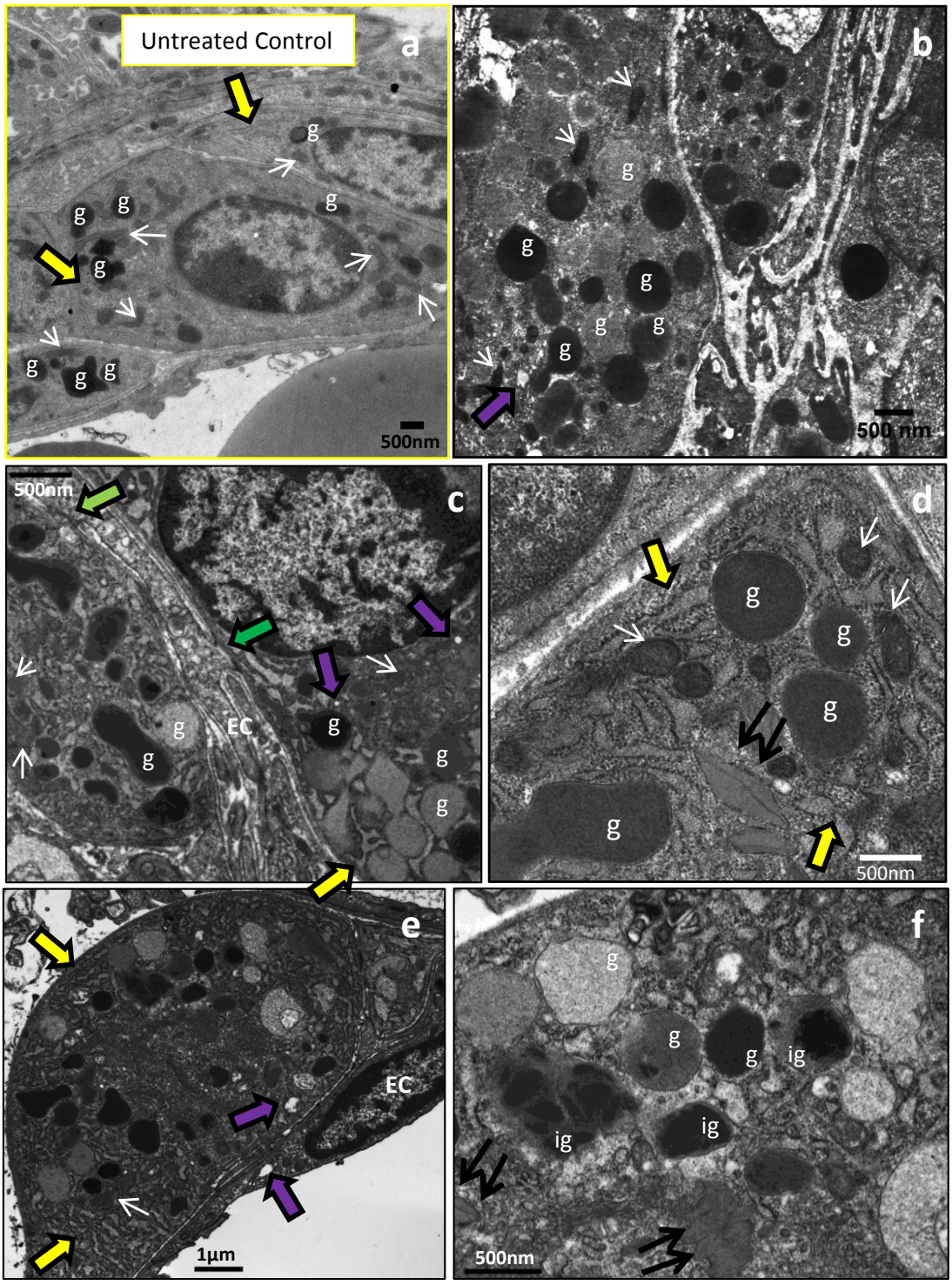

Figure 6.9: Ultrastructure analysis of JG cells from $huRen^{+/-}Ren1d^{-/-}$ mice after captopril treatment. - Electron micrographs of JG cells from captopril treated (1 mg/ml, 10 days) 1446 male $huRen^{+/-}Ren1d^{-/-}$ mice. (f) is a magnified image of (e). (a) Untreated JG cell from male 1446 $huRen^{+/-}Ren1d^{-/-}$ mouse for comparison. Kidneys were perfusion fixed for ultrastructure analysis (b-f) or 3D reconstruction (a). White arrows: mitochondria; doubleblack arrow: paracrystalline material; yellow arrow: rough endoplasmic reticulum; dark green arrow: peg and socket joint; light green arrows: gap junction; purple arrow: electron-lucent granules; g: granules; ig: immature granules; EC: endothelial cell.

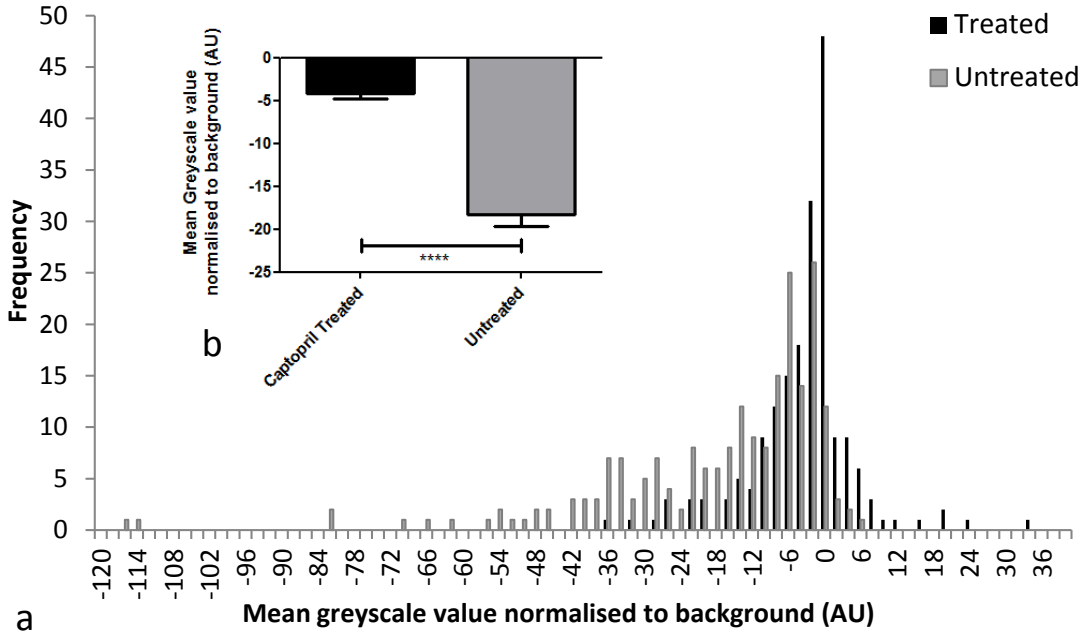

Figure 6.10: Quantification of granule electron density in JG cells. - Relative granule electron density in baseline and captopril treated (1 mg/ml, 7 days) $huRen^{+/-}Ren1d^{-/-}Ren2^{+/+}$ mice (n=8). (a) Data is represented as a histogram of average granule intensity in JG cells under basal and captopril treated conditions. (b) These values were averaged to produce a single bar chart comparison. Data are mean ± S.E.M. *** = $p < 0.0001$.

integrated signal density for each granule. The collected total cell signal intensity (CCSI) was then found by subtracting the product of the cell area and the mean signal intensity of the background (previously calculated for each cell). Therefore, the more positive the CCSI, the lighter the granule electron intensity was. Untreated 1446 $huRen^{+/-}$ mice showed a more electron-dense distribution of granules than captopril treated mice, as shown by the shifted histogram distribution towards the negative end of the scale (Figure 6.10a). Therefore administration of captopril to increase the level of renin expression within JG cells caused an increase in the number of electron-lucent renin-containing granules within JG cells (Figure 6.10b).

6.2.6 Macula Densa Function in $huRen^{+/-}Ren1d^{-/-}$ *Mice*

Flow-induced TGF response

Whilst insertion of the human renin gene was able to rescue the granulation phenotype observed in Ren1d$^{-/-}$ mice, normal MD morphology was not restored. In order to test whether the MD function was affected by this altered morphology, isolated perfused JGA with attached cTAL, AA and MD plaque from 1446 huRen$^{+/-}$Ren1d$^{-/-}$ mice were compared to C57Bl/6 mice under the same experimental conditions outlined in Chapter 5. Constriction of the AA and the glomerular tuft, as well as propagation of $[Ca^{2+}]_i$, in response to flow- and NaCl-induced TGF was seen in $huRen^{+/-}Ren1d^{-/-}$ JGA preparations (Figure 6.11a, blue arrows). There was no significant difference in VSMC contraction between groups under flow-initiated conditions (Figure 6.11d), but the glomerular tuft contraction was significantly reduced in $huRen^{+/-}Ren1d^{-/-}$ mice (glomerular tuft area: 5.1 ± 0.9% in 1446 mice, 10 ± 2% in C57Bl/6 mice, p=0.019, n=3; glomerular tuft diameter: 2.5 ± 0.5% in 1446 mice, 8 ± 2% in C57Bl/6

mice, p=0.04, n=3, Figure 6.11b, c). TGF did not cause significantly different increases in calcium propagation in MD, cTAL, podocyte or VSMCs between groups (Figure 6.11e-h), though a trend towards an increased calcium response was observed in $huRen^{+/-}Ren1d^{-/-}$ mice.

NaCl-induced TGF response

In both C57Bl/6 and $Ren1d^{-/-}$ mice, stimulation of TGF with increased NaCl concentration at the MD resulted in dampened glomerular tuft contraction and calcium propagation, therefore a similar trend would be expected in $huRen^{+/-}Ren1d^{-/-}$ mice. Indeed, when preparations were exposed to NaCl-induced TGF stimulation, a decreased responsiveness was observed in glomerular contraction compared to flow-induced responses. No significant differences were observed between groups (glomerular tuft area: 3 ± 1% in 1446 mice, 6.9 ± 0.2% in C57Bl/6 mice; glomerular tuft diameter: 2.8 ± 0.8% in 1446 mice 3.2 ± 0.7% in C57Bl/6 mice, n=3, Figure 6.12a,b). However, the AA vasoconstriction response was significantly reduced (8 ± 4% in 1446 mice, 40 ± 7% in C57Bl/6 mice, p=0.018, n=3, Figure 6.12c).

Whilst intracellular $[Ca^{2+}]_i$ didn't change within MD cells from C57Bl/6 mice during NaCl-induced TGF (Figure 6.12d), a significantly larger $[Ca^{2+}]_i$ response of 226 ± 60 nM was measured in $huRen^{+/-}Ren1d^{-/-}$ MD cells. There were large inter-individual differences within groups (Figure 6.13a, b). Propagation of the calcium signal through the MD plaque of $huRen^{+/-}Ren1d^{-/-}$ mice was only seen within certain cells, indicating that a heterogeneous population of MD cells may exist within the plaque. These changes in calcium signal measured can be seen in representative images before and after TGF stimulation (Figure 6.13c, d).

Preparations from $huRen^{+/-}Ren1d^{-/-}$ mice did not show significantly different

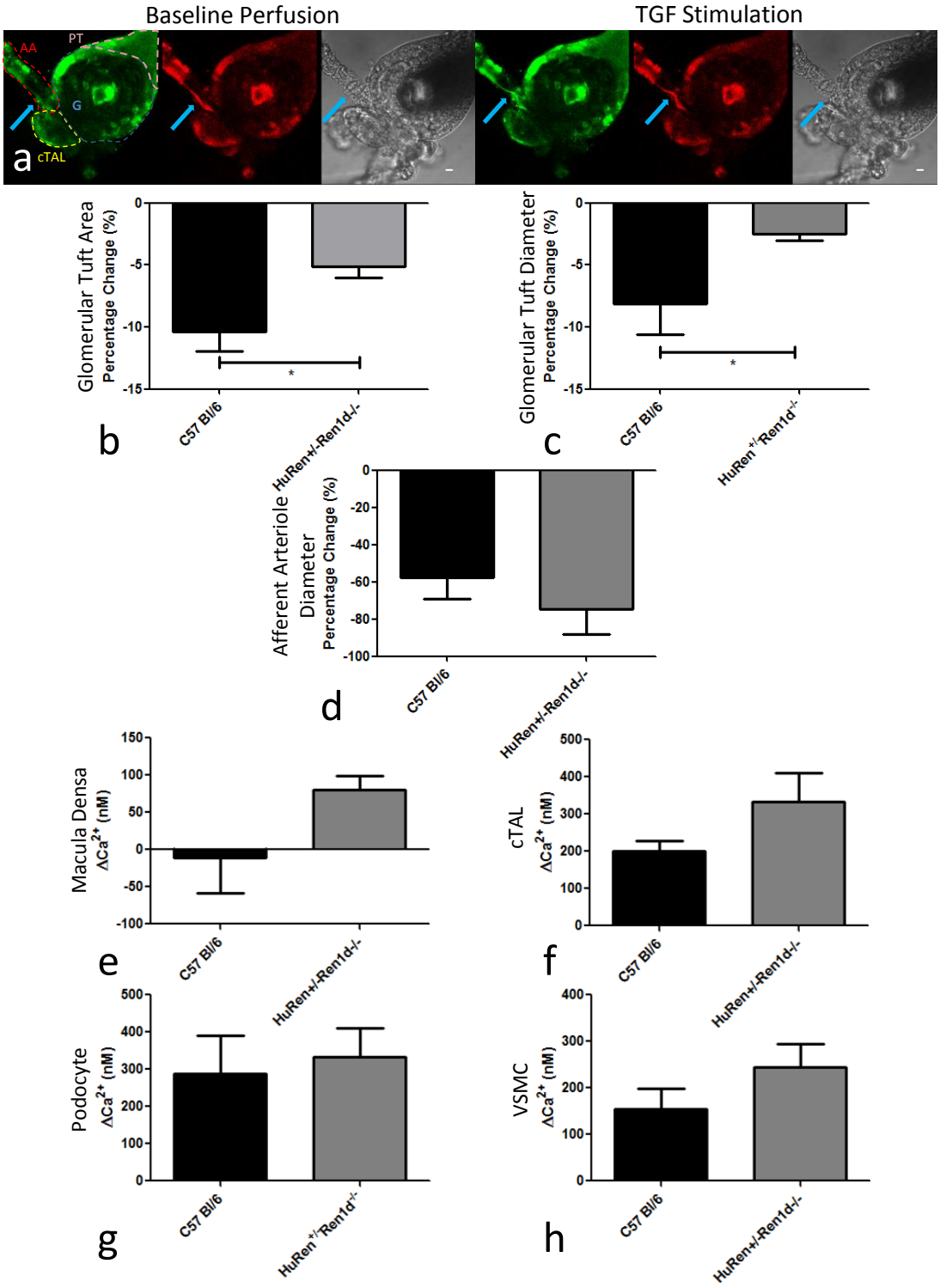

Figure 6.11: Flow-induced TGF in isolated JGA with attached MD plaque. - (a) JGA from a $huRen^{+/-}Ren1d^{-/-}$ mouse loaded with Fluo-4 AM (green) and Fura Red AM calcium indicator dye or in DIC. Scale bars: 10 μm. Percentage change in (b) glomerular tuft area and (c) diameter, (d) AA vasoconstriction response, and changes in calcium in (e) MD, (f) cTAL, (g) podocytes and (h) VSMCs in response to TGF, which was by triggered by increasing the rate of tubular perfusion from 2 to 20 nl/min. Data are mean ± S.E.M., n=3, * = p<0.05.

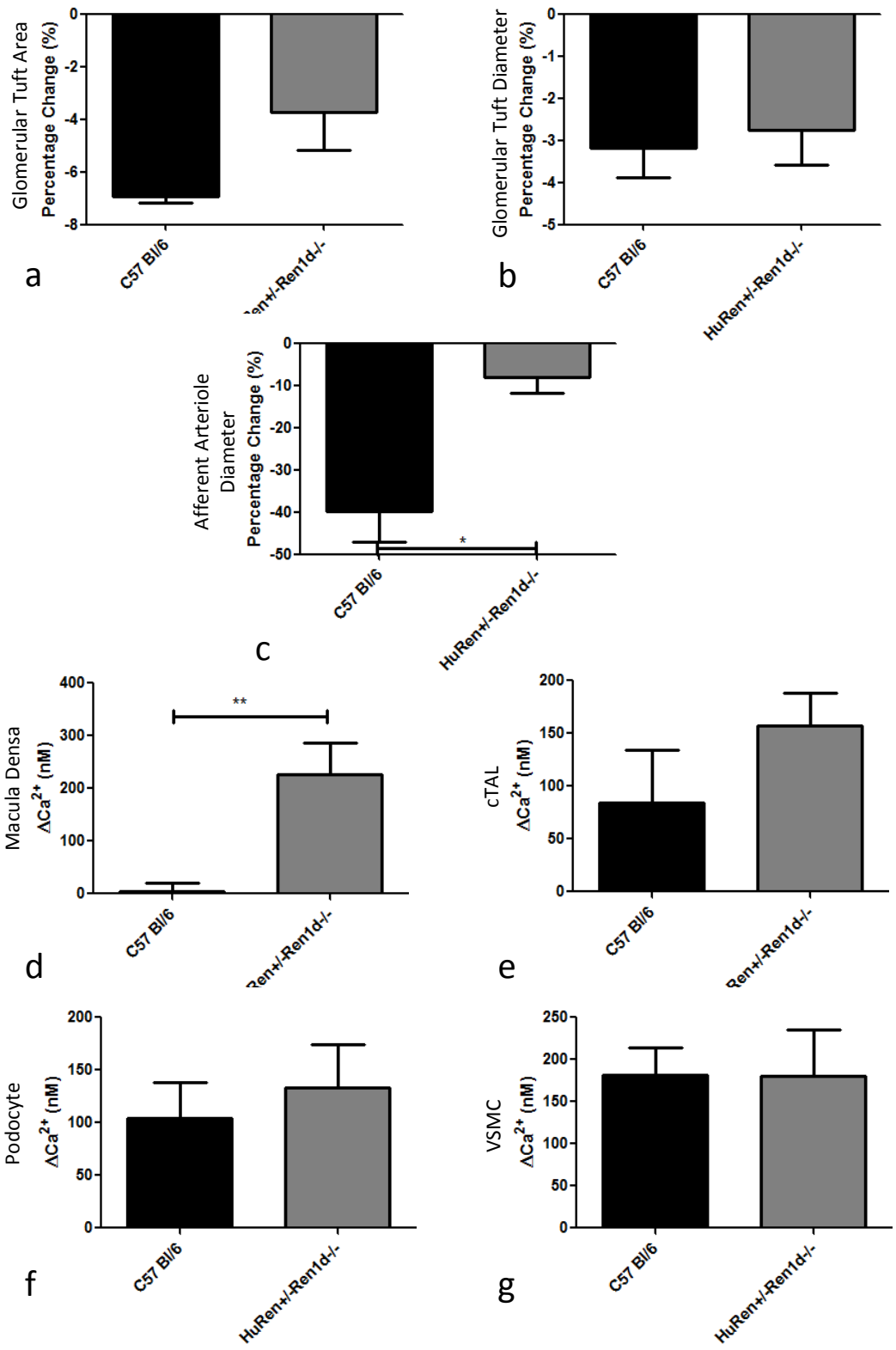

Figure 6.12: NaCl-induced TGF in isolated JGA with attached MD plaque. - Percentage change in glomerular tuft (a) area and (b) diameter, (c) AA vasoconstriction response, and changes in calcium in (d) MD, (e) cTAL, (f) podocytes and (d) VSMCs in response to TGF (triggered by increasing NaCl at the MD from 10 to 80mM) in $huRen^{+/-}Ren1d^{-/-}$ and C57Bl/6 mice. Data are mean ± S.E.M., n=3, * = p<0.05, ** = p<0.01.

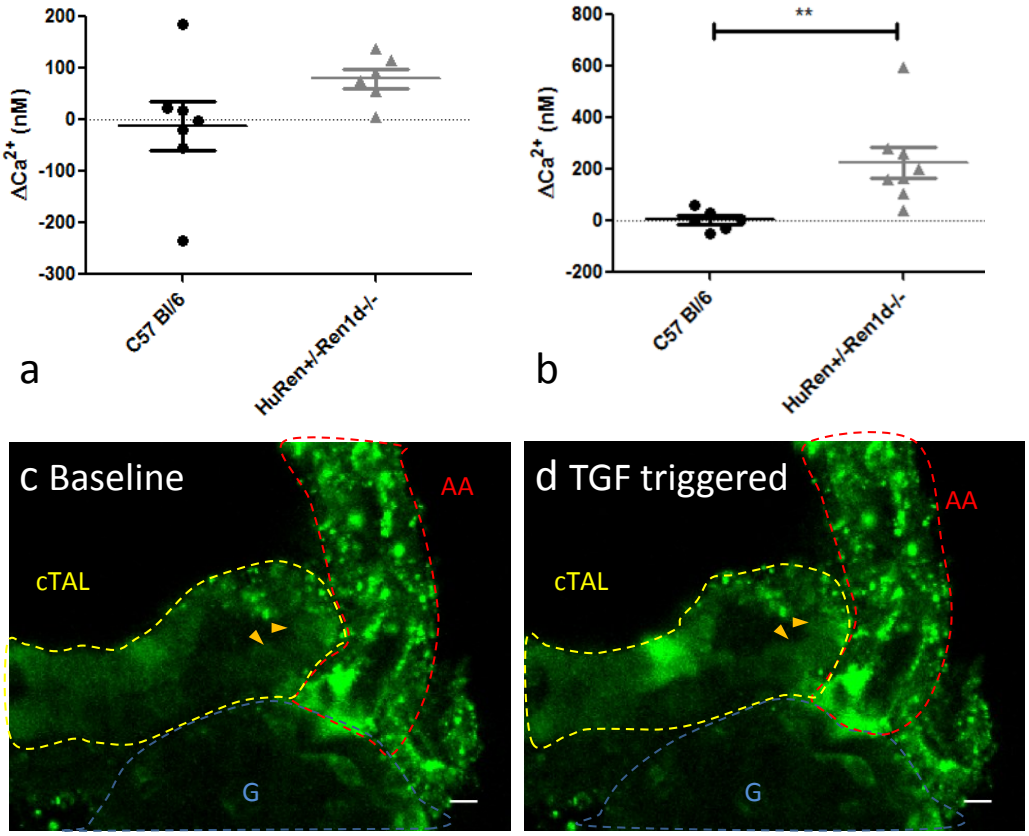

Figure 6.13: Images of calcium elevations in MD cells from isolated perfused JGA with attached MD cells. - Flow-induced TGF was triggered by increasing the rate of 10 mM NaCl-containing tubuar perfusate from 2 to 20 nl/min in preparations from $huRen^{+/-}Ren1d^{-/-}$ mice, whilst NaCl-induced TGF was initiated by increasing NaCl at the MD from 10 to 80mM. Individual data points from intracellular calcium changes in MD cells under (a) flow- and (b) NaCl-induced TGF are presented. (c, d) Increases in intracellular calcium in MD cells due to flow-induced TGF are shown. Orange arrows: macula densa (MD) cells, yellow dashed lines: cortical thick ascending limb (cTAL), red dashed lines: afferent arteriole (AA), blue dashed lines: glomerular tuft (G). Data are mean ± S.E.M., ** = p<0.01. Scale bar represents 10 μm.

$[Ca^{2+}]_i$ propagation through cTAL, podocytes or VSMCs compared to C57Bl/6 controls under NaCl-induced TGF (Figure 6.12e-g). NaCl-induced TGF responses tended to be blunted in magnitude compared to flow-induced responses.

6.3 Discussion

6.3.1 Renin Expression in 1317 and 1446 Human Renin Mice

Transgenic mice are ideal models for experimentally investigating and manipulating expression patterns of the human renin gene in a native cellular environment without the need for human tissues (234). The heterologous expression of human renin faithfully conserves tissue and cell expression patterns (123). Renin activity is species-specific allowing independent determination of plasma and tissue levels of mouse and human renin, and preventing interaction of human renin with the murine RAAS (122, 123). The important advantage to using the current mouse model over previously reported human renin mouse models (235) is that huRen$^{+/-}$Ren1d$^{-/-}$ mice are on a Ren1d$^{-/-}$ background. Therefore the dense core granules within JG cells from these mice process only active human renin, not active mouse renin. Using immunogold labelling, I was therefore able to verify that human renin was synthesised and processed into dense core granules in the absence of *Ren*1*d* in huRen$^{+/-}$Ren1d$^{-/-}$ JG cells. This implies that human and mouse *Ren*1*d* proteins have conserved structural features necessary for trafficking of renin proteins to the regulated secretory pathway. The increased renin immunogold staining present in C57Bl/6 JG cells is due to the increased granulopoiesis compared to *huRen*$^{+/-}$ mice; this is supported by the volume of extranuclear space occupied by granules in 3D reconstructions and by previous reports of increased expression of mouse compared to human renin (235).

HuRen$^{+/-}$Ren1d$^{-/-}$ mice responded appropriately to pharmacological manipulation of the RAAS via chronic ACE inhibition. *mRen*2 is still expressed in *huRen*$^{+/-}$*Ren*1*d*$^{-/-}$ mice and qPCR analysis suggested that, though levels of *hRen* and *mRen*2 expression

were very similar at baseline, captopril caused a considerably increased expression of *hRen* compared to *mRen*2. The relative insensitivity of *mRen*2 to the administration of captopril is likely to be due to the fact that expression and secretion of *mRen*2 is not controlled by the regulated release pathway of active renin, since *mRen*2 is constitutively released. This is supported by the observation that, in humans, acute administration of ACE inhibitors causes either a fall in prorenin secretion or no change at all, whist active renin is significantly elevated (201, 236).

On the whole the *hRen* and *mRen*2 expression levels in 1446 mice were very similar at baseline, though in male $huRen^{+/-}$ mice *hRen* was a tenth of the *mRen*2 expression level. This led to a particularly large fold change upon treatment with captopril, and male mice displayed a much larger increase in *hRen* expression after the addition of captopril. A significant elevation was measured in both *hRen* and *mRen*2 expression in the 1446 female mice compared to males. These observations could be attributed to the slight hypotension characterised in female $Ren1d^{-/-}$ mice (114), requiring increased expression of renin to stimulate the RAAS and increase BP (114). The male submandibular gland has been shown to express *mRen*2 at higher levels than females (237), which may play a role in blood pressure control and the sexually dimorphic hypotension present in $Ren1d^{-/-}$ mice. Alternatively, hypotension and hence increased renin expression levels in females could be due to the inappropriate integration of the *hRen* transgene into female-specific gene involved in blood pressure regulation. However in other human renin mouse models which process both human and mouse active renin, no significant differences were seen between gender (235), suggesting that the sexual dimorphism displayed in renin expression in $huRen^{+/-}Ren1d^{-/-}$ mice is indeed due to the $Ren1d^{-/-}$ background.

It should be noted that although the change in *mRen*2 expression seen in these mice was significant, it was only an approximately 2-fold increase compared to the almost 100-fold increase measured in *hRen* transgene expression. The increased *hRen* expression observed in female *hRen* mice suggests that required regulatory elements are present in the *hRen* transgene (233).

6.3.2 Ultrastructure Analysis of Juxtaglomerular Cells in Human Renin Mice

3D reconstructions were performed on kidney sections from adult, untreated 1446 mice and gender differences were seen. The extranuclear volume occupied by granules was reduced in male $huRen^{+/-}Ren1d^{-/-}$ JG cells, as were the size, shape, number and electron densities of the granules. These data are in keeping with the 2D electron micrographs of JG cells from animals of the same genotype; certain JG cells around the AA had very few granules whilst others were densely packed. JG cells from female mice showed a more uniform distribution of granules. This is consistent with the hypothesis that the level of granulopoiesis in the cell is dependent on the expression level of renin; in male 1446 $huRen^{+/-}$ mice where *hRen* expression levels are lower, granule volume as a percentage of extranuclear volume were significantly lower than that in female $huRen^{+/-}$ mice. The percentage of extranuclear volume occupied by granules in JG cells from C57Bl/6 mice (provided by Dominik Steppan, University of Regensburg) was significantly higher than that of either male or female 1446-$huRen^{+/-}Ren1d^{-/-}$ mice, reflecting the higher level of mouse renin expression compared to human renin (235). This supports the hypothesis that the expression level of renin dictates the amount of granulation in JG cells.

No instances of electron-dense granulation were seen in any sections of JG cells from $Ren1d^{-/-}$ mice, nor were any features visible in the cell apart from mitochondria, which is in keeping with previous reports (114, 120). A number of granules from male $huRen^{+/-}$ JG cells were electron-lucent, containing patches of electron-dense material. This could be evidence of incomplete granule formation, with partially electron-dense granules in the process of coalescing, visualised in three dimensions (101).

No secretion of renin from dense core granules was seen in $huRen^{+/-}$ mice, even when kidneys were perfusion fixed with tannic acid, an agent which allows visualisation of exocytosing granule cores by EM (238). The rarity of capturing such events is well documented (101, 113), and has been discussed in Section 4.3.2. However many vesicles and coated pits where vesicles were interacting with the membrane were seen. Coated pits and sub-plasmalemmal coated vesicles have previously been seen in EM images of fully differentiated JG cells (153). There were also a number of instances where JG:JG and JG:endothelial gap junctions were visible, as previously reported in JG cells (101, 112).

As hypothesised, treatment with captopril induced increased renin expression and granulation within JG cells of 1446-huRen$^{+/-}$ mice. This supports the findings of Rasch *et al.* who measured a 20-fold increase in the number of granules per arteriole from rats treated with a low-salt diet and ACE-inhibition for 14 days (193). Treated $Ren1d^{-/-}$ mice showed dilated RER as well as the appearance of electron-lucent granules and vacuoles in JG cells. This is particularly interesting since neither the human nor mouse renin gene required for active renin expression is present in these animals, and no electron-lucent graunles were observed at baseline. This could suggest that when the RAAS is stimulated to a certain level, granulopoeisis initiates irrespective of active

renin expression. Lysosomal enzymes such as acid phosphotase, β-glucorinidase, aryl sulphatase and N-acetyl-β-glucosaminidase have been shown to colocalise with granules (106), therefore these may be packaged prior to the trafficking of prorenin into the granules during aggregation. This may acutely facilitate the demand for renin when perfusion pressure drops (13).

Similar features were also present in captopril-treated $huRen^{+/-}Ren1d^{-/-}$ mice, where the increased number of granules exhibited a wider range of electron-lucency compared to untreated $huRen^{+/-}Ren1d^{-/-}$ JG cells. This diversity of granule electron densities has also been documented in C57Bl/6 mice after perfusion with isoproterenol and EGTA to stimulate secretion (112, 113). Granule electron densities were catagorised into normal, vesicles in transition from normal to lower density, low density and emptied, all of which are visible in captopril treated 1446-$huRen^{+/-}Ren1d^{-/-}$ cells. The appearance of electron-lucent granules were attributed to emptying of existing granules rather than production of new granules, due to their location at the cell periphery and the short incubation time used in the study, insufficient for the production of new granules (112). Furthermore, short term administration of the ACE inhibitor enalapril was reported to induce rapid secretion of renin from JG cells, degranulating mature granules (239).

The alterations in granule morphology seen after captopril treatment in JG cells of $huRen^{+/-}Ren1d^{-/-}$ and $Ren1d^{-/-}$ mice are also consistent with those documented in C57Bl/6 animals after enalapril treatment for 7 days (12, 239). JG cells from enalapril-treated mice showed an increased number and range of granule morphologies from small and round to large, irregular shaped granules. Well-developed Golgi cisternae had protogranules associated with them, dilated RER were observed and fusing granules were

present, all of which were also observed in $huRen^{+/-}Ren1d^{-/-}$ mice. After 14 days treatment, a further increase in granule number and granular fusion was observed, as was further development of the Golgi cisternae and the RER. Similar vacuoles containing membrane-like material akin to those seen in $Ren1d^{-/-}$ JG cells were also present, and vacuoles were seen in JG cells at all stages of enalapril treatment, though at no point was fusion of granules with the membrane observed. This would suggest that the electron-lucent granules seen in chronically captopril treated 1446-$huRen^{+/-}Ren1d^{-/-}$ mice were a combination of emptied renin granules at the JG cell periphery and *de novo* granule formation within the central cytoplasmic region, suggested by the presence of coalescing dense core material within granules.

6.3.3 Macula Densa Function

Although differences in the magnitude of the TGF response on certain parameters are statistically significant, it is evident that both flow- and NaCl-induced TGF function effectively in $huRen^{+/-}Ren1d^{-/-}$ mice which retain the same altered MD morphology seen in Ren1d-knockout mice (233). Due to the animal breeding at USC, female 1446 mice were used, however similar trends would be expected in male animals since they both show the same altered MD morphology as Ren1d$^{-/-}$ mice.

As was seen in Ren1d$^{-/-}$ and C57Bl/6 mice, a decreased sensitivity to NaCl-induced TGF compared to flow-induced TGF was observed in $huRen^{+/-}Ren1d^{-/-}$ mice. There was very little difference in the mechanical and $[Ca^{2+}]_i$ propagation responses, which is in keeping with the literature (32) although the mechanisms behind this observation are unknown. However it is unlikely to be due to sub-optimal stimulation, since the MD is known respond maximally to perfusate levels of just over 70mM NaCl and above (Figure

1.3). The one exception to this dampened sensitivity to NaCl-induced stimulation was the $[Ca^{2+}]_i$ propagation within MD cells. Changes in luminal NaCl have been shown to cause concomitant increases in MD calcium, therefore the factors regulating global intracellular calcium in these models could be more sensitive to the NaCl-induced TGF than flow-induced TGF (240, 241). The calcium propagation was even more prominent in $huRen^{+/-}Ren1d^{-/-}$ mice, which could indicate an even greater imbalance in one or a number of submembrane proteins, or a further reduced density of mitochondria in the cytoplasm, as discussed in Chapter 5.3.1.1. Again, comparison of electron micrographs from C57Bl/6, *Ren1d* and *huRen* mice would show whether this was indeed the case.

MD morphology was altered in both $Ren1d^{-/-}$ and $huRen^{+/-}Ren1d^{-/-}$ mice (233), however the granulation status of JG cells differed; $huRen^{+/-}Ren1d^{-/-}$ JG cells generate granules containing human renin, whilst $Ren1d^{-/-}$ JG cells are unable to perform granulopoiesis. Human renin is unable to interact with the murine RAAS as it is only able to cleave human angiotensinogen (122, 234, 242), however the generation of ANGII would not affect the acute TGF response. This indicates that the reduced glomerular tuft constriction and altered MD $[Ca^{2+}]_i$ observed in response to increased flow at the MD in both models on a $Ren1d^{-/-}$ background may be related to the altered MD morphology.

6.3.4 Conclusion

In conclusion, granule number and volume within the cytoplasm was significantly increased in $huRen^{+/-}Ren1d^{-/-}$ mice with higher expression levels of *hRen*, supporting the hypothesis that renin expression within JG cells dictates granulation status. Similarly, treatment with the ACE inhibitor captopril to increase renin expression levels

appeared to increase granule density, though due to time constraints 3D reconstructions were not performed to quantify this. Increased granule electron lucency coupled with dilation of the RER and development of the Golgi apparatus were consistent with the increased synthesis and secretion of renin from dense core granules. Despite the altered macula densa morphology of $huRen^{+/-}Ren1d^{-/-}$ mice, tubuloglomerular feedback functioned effectively and did not differ signficantly from $Ren1d^{-/-}$ responses, supporting the findings in Chapter 5 that the altered macula densa morphology does not affect macula densa function.

7

Discussion

7.1 Summary

In this thesis I aimed to develop an appropriate *in vitro* model in which to image and analyse granular dynamics in JG cells, to investigate the relationship between renin expression and granulation within JG cells and the functional link between JG granulation and MD structure and function. I have demonstrated for the first time that renin-containing granules respond dynamically to β-adrenergic stimulation and that the level of granulopoiesis is linked to renin expression levels. I have shown that in mice with altered MD morphology caused by the lack of active mouse Ren1 (114), the functionality of the MD cell was not affected, allowing TGF to take place acutely. A chronic exposure to a low salt diet stimulated expression of key functional and proliferative markers more strongly in $Ren1d^{-/-}$ mice compared to C57Bl/6 controls, particularly within the glomerular tuft.

7.2 Juxtaglomerular Apparatus Structure and Function

To date, the only evidence for movement of granules to the membrane has been from EM images of granules located adjacent to the membrane (153), and from granule disappearance in response to isoproterenol in isolated perfused rabbit glomeruli (36). Granule motion was observed and anlaysed in primary JG cells for the first time in the present study. Two pools of granules (d > 500 nm and d < 500 nm) were identified on the basis of their size and dynamic parameters. Granule activity was detected in both pools under basal conditions. The addition of isoproterenol, a β-adrenergic stimulus for regulated secretion, caused a significant, prolonged increase in the speed, track length and displacement of large granules. My work therefore supports the hypothesis that for renin release to occur, granules must be transported to the membrane where they dock, release their cargo, and move away from the membrane. Since this response was not observed in small granules in response to isoproterenol, I propose that dynamic parameters can be used to differentiate between granule pools on different secretory pathways when optically imaging JG cells.

Granules were often transported in close proximity of one another and an increase in fluorescent signal intensity was observed, which could suggest that the connected granular structures observed in EM 3D reconstructions of JG cells are snap-shots of rapid, dynamic coupling and uncoupling events. No large vesicular networks were established in response to isoproterenol to facilitate the compound exocytosis reported by Steppan *et al.* (113). The sparseness of renin exocytotic events calculated by Taugner *et al.* (20-500 per minute across both kidneys (153)) led Ogawa *et al.* to suggest that only marked increases in exocytosis events would allow observation of secretory processes

(112). Therefore this response is perhaps dose-dependent and could be replicated in primary JG cells upon addition of higher doses of isoproterenol. Furthermore, the compound exocytosis Steppan reported was seen in response to pharmacologically-lowered intracellular calcium levels, which was similarly reported in a number of other studies (112, 243). This extreme granule-binding effect could therefore be linked to the action of Ca^{2+}-independent SNARE-complexing proteins (140).

The increased prevalence of electron-lucent granules in JG cells from ACE inhibitor-treated huRen$^{+/-}$Ren1d$^{-/-}$ and Ren1d$^{-/-}$ mice, which may indicate increased emptying of the granules via exocytosis. This is in keeping with results reported by Ogawa *et al.*, who suggested that electron-lucent granules are mature granules that have exocytosed their contents, leading to a loss of electron density. However given the large number of electron-lucent granules observed, the observation of exocytosis events would be expected, as would a higher prevalence of electron-lucent granules by the membrane. Taugner *et al.* and Steppan *et al.* suggested that exocytosis events weren't often seen since only small, mature granules fuse to form a larger network which may not be visible in 2D sections, and that focal adhesions between this network and the membrane occur most commonly after chronic stimulation (113, 153).

A hypothesised mechanism for granule approach to the plasma membrane and renin release has previously been proposed by Ogawa *et al.* (112). They reported that the removal of the actin myofilaments present on the cell periphery led to increased instances of mature granule binding with the membrane. Indeed, actin filament disassembly is required for exocytosis in most secretory cell types, although this is normally Ca^{2+}-dependent (244). Their hypothesised model for renin exocytosis stated that: (1) inhibitory signals raise intracellular Ca^{2+} levels causing breakdown of the actin filament

network adjacent to the membrane, allowing transport of nearby granules to the plasma membrane and (2) these granules become primed for stimulatory signals, thereby allowing binding events to occur despite the actin filaments which had reassembled by this point. Results from the current study appear to contradict this: a stimulatory signal led to the increased movement of granules to and in the vicinity of the membrane. Preliminary experiments have been performed investigating whole-JG cell calcium signalling using the calcium indicator dye Rhod-2 which, in response to intracellular calcium, generated a decaying oscillatory calcium wave which propagated throughout the cell. Therefore, I propose that a different model of action may be functioning: (1) localised, low levels of free intracellular Ca^{2+} facilitate disaggregation of the membrane-adjacent actin, allowing movement of granules to the surface and (2) localised Ca^{2+} activates Ca^{2+}-dependent proteins involved in SNARE complexing.

It is evident that further studies are required to determine the role of Ca^{2+} on granular exocytosis in JG cells. It appears that small, localised increases in Ca^{2+} may facilitate exocytosis, however any significant increase which would cause too much renin to be secreted actually helps to restrict renin release. This could have evolved due to TGF, which functions such that increased salt or flow at the MD causes the propagation of a Ca^{2+} wave throughout the JGA. Consequently, significant increases in intracellular Ca^{2+} occur in all cell types, even JG cells. If JG cells were like normal secretory cells, this Ca^{2+} would stimulate renin secretion and lead to ANGII generation, further increasing arterial resistance and leading to an unsustainable positive feedback mechanism. Therefore it is possible that the negative correlation between high levels of Ca^{2+} and secretion has developed because of the location of JG cells within the JGA, such that runaway renin secretion does not occur.

The clinical importance of appropriate renin synthesis, packaging and secretion is highlighted by the fact that all major antihypertensive drug classes either directly or indirectly manipulate plasma renin levels: ACE inhibitors, ARBs, calcium channel blockers and diuretics increase renin activity, whilst β-blockers decrease plasma renin levels (245, 246). Control of arterial BP is managed through ACE inhibitor- or ARB-mediated inhibition of ANGII-binding at the JG AT1 receptors, increasing plasma renin levels several fold in patients (247). Diuretics increase plasma renin levels via a reduction in Na^+ at the MD and work particularly efficiently on patients with resistent hypertension (248). Conversely, β blockers work through the blockade of β-adrenergic cAMP-stimulation of renin secretion (249). These drug classes have repeatedly been proven effective at reducing heart failure mortalities and BP, particularly when drugs which lower Na^+ are administered in conjunction with drugs which block the RAAS (245). However BP can not be lowered to normal levels in many patients, particularly in cases of resistant hypertension. This is, in part, due to incomplete understanding of how the renin blockade works (245). In particular, deeper understanding of renin-salt interactions is extremely important to determine the optimal use of these antihypertensive drugs for treatment of hypertension (245).

Some of the most important signals dictating the onset and inhibition of renin synthesis and secretion originate from stimulation of the MD. When the Ren1d gene required for granulopoiesis is not present, MD morphology is altered (114). Although the presence of active human renin was sufficient to initiate granulopoiesis, MD morphology remained altered (233). There are very few other reported instances of altered MD morphology; significant enlargement of basal MD cell area and the surrounding JGA architecture is present in patients with Bartter's syndrome (250), which is char-

acterised by hypokalemia, increased blood pH and normal to low BP. Although female Ren1d$^{-/-}$ mice were hypotensive, males were normotensive (114), similarly indicating that homeostatic BP regulation was not markedly affected by this altered morphology. An increase in MD cell volume and number was also observed in rats treated with an AT1 receptor blocker, suggesting that the MD plaque has a certain degree of plasticity (229). The similarities in MD alteration suggest that Ren1d$^{-/-}$ may have altered AT1 receptor distribution on MD cells. However complete deletion of AT1a receptor has been shown to abolish the TGF response in mice (251). Since acute TGF stimulation of the MD in both huRen$^{+/-}$ and Ren1d$^{-/-}$ mice elicited calcium propagation, AA and glomerular tuft contraction responses comparable to C57Bl/6 controls, this suggests that Ren1d$^{-/-}$ mice still retain some AT1a receptors.

The surrounding milieu is incredibly important for correct JGA function. This was emphasized during initial attempts to immortalised JG cells, when granulopoiesis was not retained in an inappropriate environment. The coordinated TGF response seen in all mouse models was likely facilitated through intact gap junctions, such as those seen between JG cells and the underlying endothelium at the EM level in huRen$^{+/-}$Ren1d$^{-/-}$ and Ren1d$^{-/-}$ mice. These are likely to be composed of Cx37, Cx40 and Cx45 (252). Further connections between JG cells via membrane processes were also obseved in 3D reconstructions, similar to the inter-digitating processes reported by Biava and West (115) between human JG cells. There is no readily available evidence of this in the literature, perhaps due to the fact that aligned serial EM sections are required to visualise it. It is possible that these processes further facilitate coordinated communication between different cell types in the JGA.

Chronic administration of an ACE inhibitor and a low NaCl diet enhanced expres-

sion of COX2 in the JGA of Ren1d$^{-/-}$ mice compared to C57Bl/6 controls. This could be due, in part, to the lack of PGE-mediated renin release in Ren1d$^{-/-}$ mice, normally initiated by COX2 expression. The feedback loop would therefore increase levels of COX2 to increase renin secretion (Figure 7.1). Although these experiments were not performed on huRen$^{+/-}$Ren1d$^{-/-}$ mice, the same increased expression of COX2 would be expected, since human renin does not cleave mouse angiotensinogen and thereby contribute to the murine RAAS. This could potentially account for the hyper-cellularity of the MD plaque; the constant deficiency in active renin secretion would instigate signalling to the MD to express more PGE2, eventually responding by recruiting surrounding pericytes or cTAL cells to differentiate into MD cells.

Chronic administration of an ACE inhibitor alone, such as that given to both Ren1d$^{-/-}$ and huRen$^{+/-}$Ren1d$^{-/-}$ mice, acts on both the MD and JG cells (Figure 7.1). The ACE inhibitor blocks generation of AngII, reducing AngII availability at the AT1/2 receptors. Therefore AngII-mediated inhibition of renin synthesis and secretion through release of intracellular Ca^{2+} stores is significantly reduced within JG cells, leading to an increase in renin expression. This was shown using qPCR and 3D reconstructions of JG cell morphology, which also revealed that the expression level of renin was closely linked to the extent of granulation within JG cells.

7.2.1 Future Directions

The ability to image dynamic processes intracellularly within JG cells is crucial if we are to further our understanding of granulopoiesis and secretory mechanisms. Therefore the continued attempt to derive a cell line which correctly packages renin into dense core granules and releases active renin on a regulated secretory pathway would be highly de-

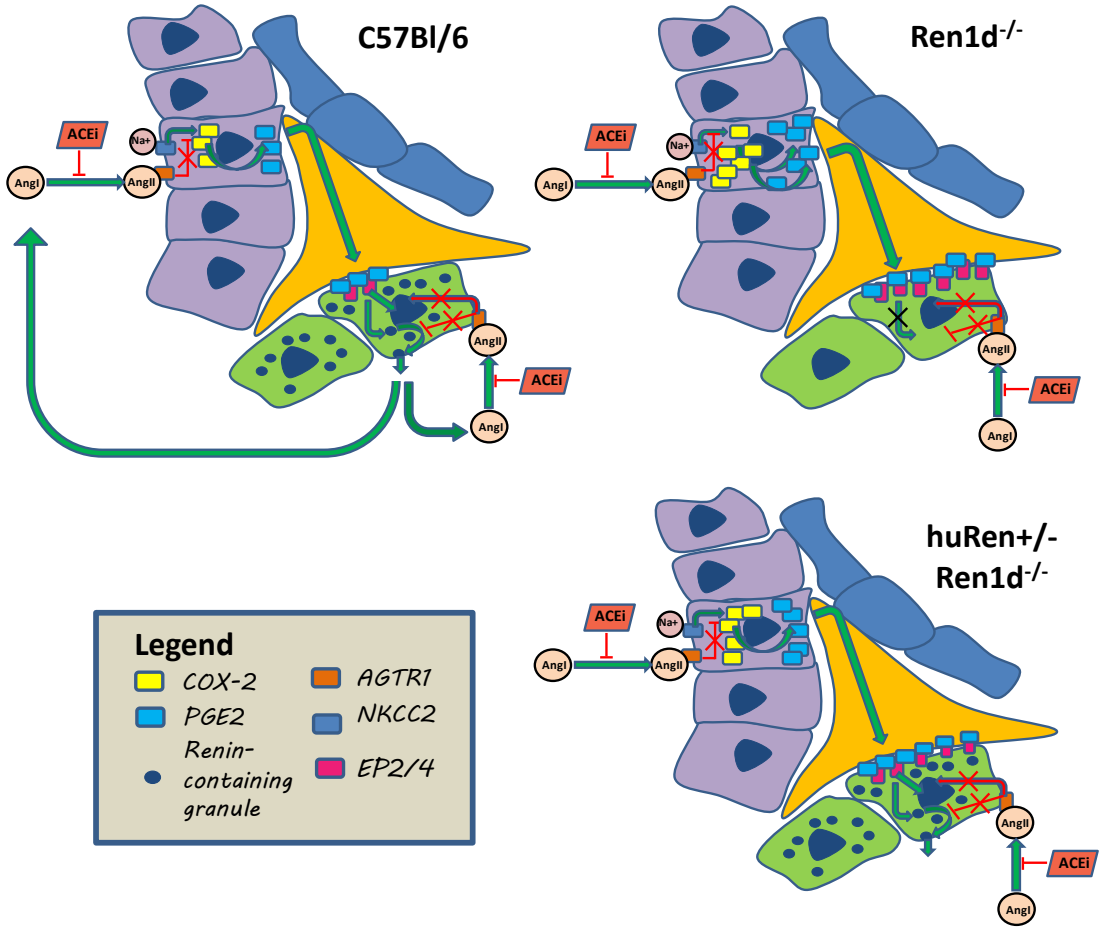

Figure 7.1: Hypothesised model of action for chronic low salt and ACE inhibitor stimulation in C57Bl/6, *Ren*1-knockout and *huRen* − *Ren*1*d* mice. - Mechanisms involved in MD stimulation via low salt and ACE inhibition. Increases in MD COX2 expression arise through low salt-NKCC2 stimulation and the ACE inhibitor removal of AngII-mediated inhibition of COX2 activation. Increased COX2 activations stimulated PGE2 generation, which translocates across the mesangial cells region to bind to EP2/4 receptors on JG cells. These lead to increased synthesis and secretion of renin, which is enhanced by the removal of AngII-mediated inhibition of renin synthesis and secretion. These processes are further enhanced in the Ren1d$^{-/-}$ system; basal levels of MD COX2 are higher due to the lack of active renin, which is therefore unable to lead to AngII generation. With less AngII, there is a reduction of AngII-mediated inhibition of COX2 generation. SImilarly, although granules containing human renin are present in huRen$^{+/-}$Ren1d$^{-/-}$ mice, the active renin released cannot lead to the generation of AngI, potentially causing the same increase in COX2 expression. Cell types: blue = glomerulus, purple = MD, green = JG, orange = mesangial.

sirable. The present study showed that the ability to proliferate as an immortalised cell line is insufficient on its own for JG cells to retain their native phenotype. By culturing primary isolated JG cells on endothelial cells or under flow conditions similar to those found *in vivo*, the environmental and chemical factors necessary for granulopoeisis may be further teased apart. Embryonic kidney culture could be a useful model in which to study this, since the native cellular architecture is intact, vascular development is retained and fluorescence from endogenous reporters can be easily visualised.

The accurate identification of renin-containing granules *in vitro* is also important. Since transfection of renin fusion constructs into these cells is not possible due to the sensitivity and low number of primary cells in culture, a more effective identification method would be through the generation of a Ren1d fusion mouse using GFP or a far red fluorescent protein, such as E2-Crimson. The experimental design established in the current study could then be used for isolating and imaging JG cells from these mice. Tracking would again be possible, as would co-staining for another intracellular organelle since the 591 nm excitation laser would be available. By crossing these mice with other genetically modified animals, such as Ren1d$^{-/-}$ mice, granules on the regulated and constitutive release pathway could be more clearly identified and their dynamics fully characterised. Time lapse imaging of JG cells from such mice could also facilitate the capture of granule formation through fusion events.

Initial experiments have been performed investigating whole-JG cell Ca^{2+} signalling in high spatial and temporal resolution; using this technique, it is possible to investigate the role of many different signalling molecules. Furthermore, by using photolabile chelators and FRAP (fluorescent recovery after photobleaching), different signalling molecules can be uncaged in precisely defined regions of the cell, and the effects on

granule transport and exocytosis analysed.

Whilst I was able to establish that TGF functioned effectively in $huRen^{+/-}Ren1d^{-/-}$ mice despite the altered MD morphology and non-granulated JG cells, I was not able to look directly at the renin content of JG cells due to the calcium indicator dyes I used. It would be advantageous to image the secretion of renin from the JG cells in isolated perfused JGA preparations. This could be performed on C57Bl/6, $Ren1d^{-/-}$ and the granulated hu$Ren^{+/-}Ren1d^{-/-}$ mice, to test whether signalling between MD and JG cells is affected by altered MD morphology.

Compared to C57Bl/6 controls, $Ren1d^{-/-}$ mice exhibited increased expression of Cox-2 and NG2 within the JGA as well as increased numbers of Ki67-positive proliferating cells, at baseline as well as after chronic MD stimulation. To elucidate the mechanisms involved further, co-localisation studies for COX2, NG2 and Ki67 would clarify whether the proliferating cells are also the NG2-positive, immature progenitor cells. To help characterize further the MD cells under baseline and stimulated conditions it would also be beneficial to stain with a marker such as nNOS or NADPH enabling the change in MD cell number and volume to be quantified (253).

Performing 3D reconstructions of JG cells from untreated 1446 animals was an effective way of quantifying granulation in JG cells. Due to time constraints it was not possible to perform more reconstructions, however advances in the field mean that it is now possible to automate 3D EM sectioning, hugely speeding up the acquisition process. It would therefore be advantageous to quantify granulation in JG cells from 1446 male and female $huRen^{+/-}Ren1d^{-/-}$ mice after treatment with captopril using this sectioning method. This would strengthen the observation that renin expression levels dictate the extent of granulation within JG cells. Immunogold labelling to determine

whether *hRen* was still present within granules of ranging electron lucency would also be particularly interesting.

References

[1] Schnermann J and Briggs JP. **Synthesis and secretion of renin in mice with induced genetic mutations.** *Kidney International*, **81**(6):529–538, 2012. 1

[2] Click RL, Joyner WL, and Gilmore JP. **Reactivity of glomerular afferent and efferent arterioles in renal hypertension.** *Kidney International*, **15**(2):109–115, (1979). 4

[3] Dhanaraj V, Dealwis CG, Frazao C, Badasso M, Sibanda BL, Tickle IJ, Cooper JB, Driessen HPC, Newman M, Aguilar C, Wood SP, Blundell TL, Hobart OM, Geoghegan KF, Ammirati MJ, Danley DE, O'Connor BA, and Hoover DJ. **X-ray analyses of peptide–inhibitor complexes define the structural basis of specificity for human and mouse renins.** *Nature*, **357**:466–472, (1992). 4

[4] Belova LA. **Angiotensin II-generating enzymes.** *Biochemistry (Moscow)*, **65**(12):1337–1345, (2000). 4

[5] Friis UG, Madsen K, Stubbe J, Hansen PBL, Svenningsen P, Bie P, Skøtt O, and Jensen BL. **Regulation of renin secretion by renal juxtaglomerular cells.** *Pflügers Archiv : European Journal of Physiology*, **465**(1):25–37, (2013). 4

[6] Müller MW, Todorov V, Krämer BK, and Kurtz A. **Angiotensin II inhibits renin gene transcription via the protein kinase C pathway.** *Pflügers Archiv*, **444**(4):499–505, (2002). 4, 35

[7] Scholz H, Kaissling B, Inagami T, and Kurtz A. **Differential response of renin secretion to vasoconstrictors in the isolated perfused rat kidney.** *The Journal of Physiology*, **441**(1):453–468, (1991). 4, 35

[8] Ackermann M, Ritthaler T, Riegger G, Kurtz A, and Krämer BK. **Endothelin inhibits cAMP-induced renin release from isolated renal juxtaglomerular cells.** *Journal of Cardiovascular Pharmacology*, **26**:S135–7, (1994). 4, 35

[9] Gomez RA, Lynch KR, Chevalier RL, Everett AD, Johns DW, Wilfong N, Peach MJ, and Carey RM. **Renin and angiotensinogen gene expression and intrarenal renin distribution during ACE inhibition.** *American Journal of Physiology*, **254**(6 Pt 2):F900–F906, (1988). 4, 45

[10] Taugner R and Metz R. **Development and fate of the secretory granules of juxtaglomerular epithelioid cells.** *Cell and Tissue Research*, **246**(3):595–606, (1986). 4, 13, 23, 25, 27

[11] Jones CA, Hurley MI, Black TA, Kane CM, Pan L, Pruitt SC, and Gross KW. **Expression of a renin/GFP transgene in mouse embryonic, extra-embryonic, and adult tissues.** *Physiological Genomics*, **4**(1):75–81, (2000). 4, 44, 45, 108

[12] Berka JLA, Alcorn D, Ryan GB, and Skinner SL. **Renin processing studied by immunogold localization of prorenin and renin in granular juxtaglomerular cells in mice treated with enalapril.** *Cell and Tissue Research*, **268**(1):141–148, (1992). 4, 196

[13] Kurtz A. **Renin release: sites, mechanisms, and control.** *Annual Review of Physiology*, **73**:377–399, (2011). 5, 8, 19, 88, 109, 196

[14] Gomez RA, Chevalier RL, Everett AD, Elwood JP, Peach MJ, Lynch KR, and Carey RM. **Recruitment of renin gene-expressing cells in adult rat kidneys.** *American Journal of Physiology-Renal Physiology*, **259**(4):F660–F665, (1990). 5, 13

[15] Schnermann J. **Juxtaglomerular cell complex in the regulation of renal salt excretion.** *American Journal of Physiology-Regulatory, Integrative and Comparative Physiology*, **274**(2):R263–R279, (1998). 5

[16] Skøtt O and Briggs JP. **Direct demonstration of macula densa-mediated renin secretion.** *Science*, **237**(4822):1618–1620, (1987). 5, 144, 165

[17] Deen WM, Robertson CR, and Brenner BM. **A model of glomerular ultrafiltration in the rat.** *American Journal of Physiology–Legacy Content*, **223**(5):1178–1183, (1972). 6

[18] Stevens LA, Coresh J, Greene T, and Levey AS. **Assessing kidney functionmeasured and estimated glomerular filtration rate.** *New England Journal of Medicine*, **354**(23):2473–2483, (2006). 6

[19] Castrop H and Schiessl IM. **Physiology and pathophysiology of the renal Na-K-2Cl cotransporter (NKCC2).** *American Journal of Physiology-Renal Physiology*, **307**(9):F991–F1002, (2014). 7

[20] Peti-Peterdi J and Harris RC. **Macula densa sensing and signaling mechanisms of renin release.** *Journal of the American Society of Nephrology*, **21**(7):1093–1096, (2010). 7

[21] Greenberg SG, Lorenz JN, He XR, Schnermann JB, and Briggs JP. **Effect of prostaglandin synthesis inhibition on macula densa-stimulated renin secretion.** *American Journal of Physiology*, **265**(4):F578–F583, (1993). 7, 145

[22] Peti-Peterdi J, Komlosi P, Fuson AL, Guan Y, Schneider A, Qi Z, Redha R, Rosivall L, Breyer MD, and Bell PD. **Luminal NaCl delivery regulates basolateral PGE_2 release from macula densa cells.** *Journal of Clinical Investigation*, **112**(1):76–82, (2003). 7, 145

[23] Yang T, Parks JM, Arend L, Huang Y, Topaloglu R, and Schnermann J. **Low chloride stimuation of prostaglandin E_2 release and cycooxygenase-2 expression in a mouse macula densa cell line.** *Journal of Biological Chemistry*, **275**(48):37922–37929, (2000). 7, 145

[24] Friis UG, Stubbe J, Uhrenholt TR, Svenningsen P, Nüsing RM, Skøtt O, and Jensen BL. **Prostaglandin E2 EP2 and EP4 receptor activation mediates cAMP-dependent hyperpolarization and exocytosis of renin in juxtaglomerular cells.** *American Journal of Physiology-Renal Physiology*, **289**(5):F989–F997, (2005). 7, 18, 33, 145

[25] Bell PD, Lapointe JY, and Peti-Peterdi J. **Macula densa cell signaling**. *Annual Review of Physiology*, **65**(1):481–500, (2003). 7, 8

[26] Inscho EW, Cook AK, Imig JD, Vial C, and Evans RJ. **Physiological role for P2X1 receptors in renal microvascular autoregulatory behavior.** *The Journal of Clinical Investigation*, **112**(12):1895–1905, (2003). 7

[27] Sun D, Samuelson LC, Yang T, Huang Y, Paliege A, Saunders T, Briggs J, and Schnermann J. **Mediation of tubuloglomerular feedback by adenosine: evidence from mice lacking adenosine 1 receptors.** *Proceedings of the National Academy of Sciences*, **98**(17):9983–9988, (2001). 7

[28] Sipos A, Vargas S, and Peti-Peterdi J. **Direct demonstration of tubular fluid flow sensing by macula densa cells.** *American Journal of Physiology-Renal Physiology*, **299**(5):F1087–F1093, (2010). 7, 10, 61, 145, 162

[29] Bell PD, Lapointe J-Y, and Cardinal J. **Direct measurement of basolateral membrane potentials from cells of the macula densa**. *American Journal of Physiology Renal Fluid Electrolyte Physiology*, **257**(3):F463–F468, (1989). 7

[30] Uchida S and Sasaki S. **Function of chloride channels in the kidney.** *Annual Review of Physiology*, **67**:759–778, (2005). 7

[31] Kim SM, Mizel D, Huang YG, Briggs JP, and Schnermann J. **Adenosine as a mediator of macula densa-dependent inhibition of renin secretion.** *American Journal of Physiology-Renal Physiology*, **290**(5):F1016–F1023, (2006). 8

[32] Peti-Peterdi J. **Calcium wave of tubuloglomerular feedback.** *American Journal of Physiology-Renal Physiology*, **291**(2):F473–F480, (2006). 8, 10, 61, 62, 63, 64, 72, 77, 162, 164, 197

[33] Peti-Peterdi J, Morishima S, Bell PD, and Okada Y. **Two-photon excitation fluorescence imaging of the living juxtaglomerular apparatus.** *American Journal of Physiology-Renal Physiology*, **283**(1):F197–F201, (2002). 8, 10, 162

[34] Kang JJ, Toma I, Sipos A, McCulloch F, and Peti-Peterdi J. **Quantitative imaging of basic functions in renal (patho) physiology.** *American Journal of Physiology-Renal Physiology*, **291**(2):F495–F502, (2006). 9, 134

[35] Peti-Peterdi J, Toma I, Sipos A, and Vargas SL. **Multiphoton imaging of renal regulatory mechanisms.** *Physiology*, **24**(2):88–96, (2009). 9, 161

[36] Peti-Peterdi J, Fintha A, Fuson AL, Tousson A, and Chow RH. **Real-time imaging of renin release in vitro.** *American Journal of Physiology-Renal Physiology*, **287**(2):F329–F335, (2004). 9, 25, 36, 37, 134, 135, 201

[37] Hanner F, Chambrey R, Bourgeois S, Meer E, Mucsi I, Rosivall L, Shull GE, Lorenz JN, Eladari D, and Peti-Peterdi J. **Increased renal renin content in mice lacking the Na+/H+ exchanger NHE2**. *American Journal of Physiology-Renal Physiology*, **294**(4):F937–F944, (2008). 10

[38] Bell PD and Navar LG. **Relationship between tubulo-glomerular feedback responses and perfusae hypotonicity.** *Kidney International*, **22**(3):234–239, (1982). 10

[39] Briggs J, Schubert G, and Schnermann J. **Further evidence for an inverse relationship between macula densa NaCl concentration and filtration rate.** *Pflügers Archive*, **392**(4):372–378, (1982). 10

[40] Marsh DJ, Toma I, Sosnovtseva OV, Peti-Peterdi J, and Holstein-Rathlou N-H. **Electrotonic vascular signal conduction and nephron synchronization.** *American Journal of Physiology-Renal Physiology*, **296**(4):F751–F761, (2009). 10

[41] Komlosi P, Banizs B, Fintha A, Steele S, Zhang Z-R, and Bell PD. **Oscillating cortical thick ascending limb cells at the juxtaglomerular apparatus.** *Journal of the American Society of Nephrology*, **19**(10):1940–1946, (2008). 10

[42] Sauter A, Machura K, Neubauer B, Kurtz A, and Wagner C. **Development of renin expression in the mouse kidney.** *Kidney International*, **73**(1):43–51, (2007). 10, 11, 12, 45, 104, 109, 112

[43] Tufro A, Norwood VF, Carey RM, and Gomez RA. **Vascular Endothelial Growth Factor induces nephrogenesis and vasculogenesis.** *Journal of the American Society of Nephrology*, **84**(10):2125–2134, (1999). 10

[44] Hellstrom M, Kalen M, Lindahl P, Abramsson A, and Betsholtz C. **Role of PDGF-B and PDGFR-β in recruitment of vascular smooth muscle cells and pericytes during embryonic blood vessel formation in the mouse.** *Development*, **126**(14):3047–3055, (1999). 11

[45] Stefańska AM, Péault B, and Mullins JJ. **Renal pericytes: multifunctional cells of the kidneys.** *Pflügers Archiv-European Journal of Physiology*, **465**(6):767–773, (2013). 11, 17, 18, 110

[46] Brühl U, Taugner R, and Forssmann WG. **Studies on the juxtaglomerular apparatus.** *Cell and Tissue Research*, **151**(4):433–456, (1974). 13

[47] Egerer G, Taugner R, and Tiedemann K. **Renin immunohistochemistry in the mesonephros and metanephros of the pig embryo.** *Histochemistry*, **81**(4):385–390, (1984). 13

[48] Ljungvist A and Wågermark J. **Renal juxtaglomerular granulation in the human foetus and infant.** *Acta Pathologica et Microbiologica Scandinavica*, **67**(2):257–266, (1965). 13

[49] Lopez MLSS, Pentz ES, Nomasa T, Smithis O, and Gomez RA. **Renin cells are precursors for multiple cell types that switch to the renin phenotype when homeostasis is threatened.** *Developmental Cell*, **6**(5):719–728, (2004). 13, 14

[50] Capin M, Araujo-Nascimento MDF, Benchimol S, and Desormeaux Y. **Metaplasia of smooth muscle cells into juxtaglomerular cells in the juxtaglomerular apparatus, arteries, and arterioles of the ischemic (endocrine) kidney.** *American Journal of Pathology*, **198**(??):661–667, (1977). 13

[51] Lopez MLSS, Pentz ES, Robert B, Abrahamson DR, and Gomez RA. **Embryonic origin and lineage of juxtaglomerular cells.** *American Journal of Physiology*, **281**(2):F345–F356, (2001). 14

[52] Brunskill EW, Sequeira-Lopez MLS, Pentz ES, Lin E, Yu J, Aronow BJ, Potter SS, and Gomez RA. **Genes that confer the identity of the renin cell.** *Journal of the American Society of Nephrology*, **22**(12):2213–2225, (2011). 14, 15, 19, 88, 108, 110

[53] Chang DF, Belaguli NS, Iyer D, Roberts WB, Wu S-P, Dong X-R, Marx JG, Moore MS, Beckerle MC, Majesky MW, and Schwartz RJ. **Cysteine-rich LIM-only proteins CRP1 and CRP2 are potent smooth muscle differentiation cofactors**. *Developmental Cell*, **4**(1):107–118, (2003). 14

[54] Latonen L, Järvinen PM, and Laiho M. **Cytoskeleton-interacting LIM-domain protein CRP1 suppresses cell proliferation and protects from stress-induced cell death.** *Experimental Cell Research*, **314**(4):738–747, (2008). 14

[55] Biava CG and West M. **Fine structure of normal human juxtaglomerular cells. I. General structure adn intercellular relationships.** *The American Journal of Pathology*, **49**(5):679–721, (1966). 14, 15, 26, 27

[56] Bondjers C, Kalén M, Hellström M, Scheidl SJ, Abramsson A, Renner O, Lindahl P, Cho H, Kehrl J, and Betsholtz C. **Transcription profiling of platelet-derived growth factor-B-deficient mouse embryos identifies RGS5 as a novel marker for pericytes and vascular smooth muscle cells.** *The American Journal of Pathology*, **162**(3):721–729, (2003). 15

[57] Kurtz L, Schweda F, de Wit C, Kriz W, Witzgall R, Warth R, Sauter A, Kurtz A, and Wagner C. **Lack of connexin 40 causes displacement of renin-producing cells from afferent arterioles to the extraglomerular mesangium.** *Journal of the American Society of Nephrology*, **18**(4):1103–1111, (2007). 15, 16, 111

[58] Wagner C and Kurtz A. **Distribution and functional relevance of connexins in renin-producing cells.** *Pflügers Archiv-European Journal of Physiology*, **465**(1):71–77, (2013). 15, 16

[59] Hanner F, Sorensen CM, Holstein-Rathlou N-H, and Peti-Peterdi J. **Connexins and the kidney.** *American Journal of Physiology-Regulatory, Integrative and Comparative Physiology*, **298**(5):R1143–R1155, (2010). 15

[60] Firouzi M, Kok B, Spiering W, Busjahn A, Bezzina CR, Ruijter JM, Koeleman BPC, Schipper M, Groenewegen WA, Jongsma HJ, and deLeeuw PW. **Polymorphisms in human connexin40 gene promoter are associated with increased risk of hypertension in men.** *Journal of Hypertension*, **24**(2):325–330, (2006). 16

[61] de Wit C, Roos F, Bolz S-S, and Pohl U. **Lack of vascular connexin 40 is associated with hypertension and irregular arteriolar vasomotion.** *Physiological Genomics*, **13**(2):169–177, (2003). 16

[62] Armulik A, Abramsson A, and Betsholtz C. **Endothelial/pericyte interactions.** *Circulation Research*, **97**(6):512–523, (2005). 17, 18

[63] Smith SW, Chand S, and Savage COS. **Biology of the renal pericyte.** *Nephrology Dialysis Transplantation*, **27**(6):2149–2155, (2012). 17, 18

[64] Humphreys BD, Lin S-L, Kobayashi A, Hudson TE, Nowlin BT, Bonventre JV, Valerius MT, McMahon AP, and Duffield JS. **Fate tracing reveals the pericyte and not epithelial origin of myofibroblasts in kidney fibrosis.** *The American Journal of Pathology*, **176**(1):85–97, (2010). 17

[65] Crisan M, Yap S, Casteilla L, Chen C-W, Corselli M, Park TS, Andriolo G, Sun B, Zheng B, Zhang L, Norotte C, Pang-Ning T, Traas J, Schugar R adn Deasy BM, Sadylak S, Hans-Jörg B, Giacobino J-P, Lazzari L, Huard J, and Péalt B. **A perivascular origin for mesenchymal stem cells in multiple human organs.** *Cell Stem Cell*, **3**(3):301–313, (2008). 17

[66] Lin S-L, Kisseleva T, Brenner DA, and Duffield JS. **Pericytes and perivascular fibroblasts are the primary source of collagen-producing cells in obstructive fibrosis of the kidney.** *The American Journal of Pathology*, **173**(6):1617–1627, (2008). 17

[67] Díaz-Flores L, Gutiérrez R, Madrid JF, Varela H, Valladares F, Acosta E, Martin-Vasallo P, et al. **Pericytes. Morphofunction, interactions and pathology in a quiescent and activated mesenchymal cell niche.** (2009). 17

[68] Smith SW, Schrimpf C, Parekh DJ, Venkatachalam M, and Duffield JS. **Kidney pericytes: A novel therapeutic target in interstitial fibrosis.** *Histology and Histopathology*, **27**(12):1503–1514, (2012). 17

[69] Nehls V and Drenckhahn D. **The versatility of microvascular pericytes: from mesenchyme to smooth muscle?** *Histochemistry*, **99**(1):1–12, (1993). 17

[70] Courtoy PJ and Boyles J. **Fibronectin in the microvasculature: localization in the pericyte-endothelial interstitium.** *Journal of Ultrastructure Research*, **83**(3):258–273, (1983). 18

[71] Lindahl P, Hellstrom M, Kalén M, Karlsson L, Pekny M, Pekna M, Soriano P, and Betsholtz C. **Paracrine PDGF-B/PDGF-Rbeta signaling controls mesangial cell development in kidney glomeruli.** *Development*, **125**(17):3313–3322, (1998). 18

[72] Friis UG, Jensen BL, Sethi S, Andreasen D, Hansen PB, and Skøtt O. **Control of renin secretion from rat juxtaglomerular cells by cAMP-specific phosphodiesterases.** *Circulation Research*, **90**(9):996–1003, (2002). 18, 34, 36

[73] Ortiz-Capisano MC, Ortiz PA, Harding P, Garvin JL, and Beierwaltes WH. **Adenylyl cyclase isoform v mediates renin release from juxtaglomerular cells.** *Hypertension*, **49**(3):618–624, (2007). 18, 19, 53, 89, 106, 107

[74] Chen L, Kim SM, Oppermann M, Faulhaber-Walter R, Huang Y, Mizel D, Chen M, Lopez MLS, Weinstein LS, Gomez RA, Briggs JP, and Schnermann J. **Regulation of renin in mice with Cre recombinase-mediated deletion of G protein Gsα in juxtaglomerular cells.** *American Journal of Physiology-Renal Physiology*, **292**(1):F27–F37, (2007). 19, 33

[75] Ortiz-Capisano MC, Reddy M, Mendez M, Garvin JL, and Beierwaltes WH. **Juxtaglomerular cell CaSR stimulation decreases renin release via activation of the PLC/IP3 pathway and the ryanodine receptor.** *American Journal of Physiology-Renal Physiology*, **304**(3):F248–F256, (2013). 19, 107

[76] Mendez M, Gross KW, Glenn ST, Garvin JL, and Carretero OA. **Vesicle-associated membrane protein-2 (VAMP2) mediates cAMP-stimulated renin release in mouse juxtaglomerular cells.** *Journal of Biological Chemistry*, **286**(32):28608–28618, (2011). 19, 39, 106, 107, 108

[77] Friis UG, Madsen K, Svenningsen P, Hansen PBL, Gulaveerasingam A, Jørgensen F, Aalkjær C, Skøtt O, and Jensen BL. **Hypotonicity-induced Renin exocytosis from juxtaglomerular cells requires aquaporin-1 and cyclooxygenase-2.** *Journal of the American Society of Nephrology*, **20**(10):2154–2161, (2009). 19

[78] Kirchhoff C, Araki Y, Huhtaniemi I, Matusik RJ, Osterhoff C, Poutanen M, Samalecos A, Sipilä P, Suzuki K, and Orgebin-Crist M-C. **Immortalization by large T-antigen of the adult epididymal duct epithelium.** *Molecular and Cellular Endocrinology*, **216**(1):83–94, (2004). 19, 20

[79] Dyson N and Balmain A. **Oncogenes and cell proliferation.** *Current Opinion in Genetics & Development*, **9**(1):11–14, (1999). 19

[80] Lee KM, Choi KH, and Ouellette MM. **Use of exogenous hTERT to immortalize primary human cells.** *Cytotechnology*, **45**(1):33–38, (2004). 20

[81] Jha KK, Banga S, Palejwala V, and Ozer HL. **SV40-mediated immortalization.** *Experimental Cell Research*, **245**(1):1–7, (1998). 20

[82] Jat PS, Noble MD, Ataliotis P, Tanaka Y, Yannoutsos N, Larsen L, and Kioussis D. **Direct derivation of conditionally immortal cell lines from an H-2Kb-tsA58 transgenic mouse.** *Proceedings of the National Academy of Sciences*, **88**(12):5096–5100, (1991). 21, 44, 108

[83] Whitehead RH, VanEeden PE, Noble MD, Ataliotis P, and Jat PS. **Establishment of conditionally immortalized epithelial cell lines from both colon and small intestine of adult H-2Kb-tsA58 transgenic mice.** *Proceedings of the National Academy of Sciences*, **90**(2):587–591, (1993). 21, 44, 89, 108

[84] Holley MC and Lawlor PW. **Production of conditionally immortalised cell lines from a transgenic mouse.** *Audiology and Neurotology*, **2**(1-2):25–35, (1997). 21

[85] Lang JA, Ying LH, Morris BJ, and Sigmund CD. **Transcriptional and posttranscriptional mechanisms regulate human renin gene expression in Calu-6 cells.** *American Journal of Physiology-Renal Physiology*, **271**(1):F94–F100, (1996). 21

[86] Ying L, Morris BJ, and Sigmund CD. **Transactivation of the human renin promoter by the cyclic AMP/protein kinase A pathway is mediated by both cAMP-responsive element binding protein-1 (CREB)-dependent and CREB-independent mechanisms in Calu-6 cells.** *Journal of Biological Chemistry*, **272**(4):2412–2420, (1997). 21

[87] Sigmund CD, Okuyama K, Ingelfinger J, Jones CA, Mullins JJ, Kane C, Kim U, Wu CZ, Kenny L, and Rustum Y. **Isolation and characterization of renin-expressing cell lines from transgenic mice containing a renin-promoter viral oncogene fusion construct.** *Journal of Biological Chemistry*, **265**(32):19916–19922, (1990). 22

[88] Sigmund CD, Jones CA, Fabian JR, Mullins JJ, and Gross KW. **Tissue and cell specific expression of a renin promoter-reporter gene construct in transgenic mice.** *Biochemical and Biophysical Research Communications*, **170**(1):344–350, (1990). 22

[89] Jones CA, Petrovic N, Novak EK, Swank RT, Sigmund CD, and Gross KW. **Biosynthesis of renin in mouse kidney tumor As4. 1 cells.** *European Journal of Biochemistry*, **243**(1-2):181–190, (1997). 22, 89

[90] Desch M, Hackmeyer G, and Todorov VT. **Identification of ATF2 as a transcriptional regulator of renin gene.** *Biological Chemistry*, **393**(1):93–100, (2012). 22, 89

[91] Weatherford ET, Liu X, and Sigmund CD. **Regulation of renin expression by the orphan nuclear receptors Nr2f2 and Nr2f6.** *American Journal of Physiology-Renal Physiology*, **302**(8):F1025–F1033, (2012). 22, 89

[92] Klar J, Sigl M, Obermayer B, Schweda F, Krämer BK, and Kurtz A. **Calcium inhibits renin gene expression by transcriptional and posttranscriptional mechanisms.** *Hypertension*, **46**(6):1340–1346, (2005). 22, 89

[93] Beierwaltes WH. **Hydrogen sulfide, renin, and regulating the second messenger cAMP. Focus on Hydrogen sulfide regulates camp homeostasis and renin degranulation in as4. 1 and rat renin-rich kidney cell.**. *Americal Journal of Physiology: Cell Physiology*, **302**:C21–C23, (2011). 22

[94] Lu M, Liu Y-H, Ho CY, Tiong CX, and Bian J-S. **Hydrogen sulfide regulates cAMP homeostasis and renin degranulation in As4. 1 and rat renin-rich kidney cells.** *American Journal of Physiology-Cell Physiology*, **302**(1):C59–C66, (2012). 22

[95] Cohen S, Taylor JM, Murakami K, Michelakis AM, and Inagami T. **Isolation and characterization of renin-like enzymes from mouse submaxillary glands.** *Biochemistry*, **11**(23):4286–4293, (1972). 22

[96] Ganten D, Hutchinson JS, Schelling P, Ganten U, and Fischer H. **The iso-renin angiotensin systems in extrarenal tissue.** *Clinical and Experimental Pharmacology and Physiology*, **3**(2):103–126, (1976). 22

[97] Dzau VJ, Ingelfinger J, Pratt RE, and Ellison KE. **Identification of renin and angiotensinogen messenger RNA sequences in mouse and rat brains.** *Hypertension*, **8**(6):544–548, (1986). 22

[98] Schweda F Friis U Wagner C Skott O Kurtz A. **Renin release**. *Physiology*, **22**(5):310–319, 2007. 23

[99] Pratt RE, Carleton JE, Richie JP, Heusser C, and Dzau VJ. **Human renin biosynthesis and secretion in normal and ischemic kidneys.** *Proceedings of the National Academy of Sciences*, **84**(22):7837–7840, (1987). 22, 24

[100] Sigmund CD, Jones CA, Jacob HJ, Ingelfinger J, Kim U, Gamble D, Dzau VJ, and Gross KW. **Pathophysiology of vascular smooth muscle in renin promoter-T-antigen transgenic mice.** *American Journal of Physiology*, **260**(2 Pt 2):F249–F257, (1991). 24, 28, 30

[101] Hackenthal EMDR, Paul M, Ganten D, and Taugner R. **Morphology, physiology, and molecular biology of renin secretion.** *Physiological Reviews*, **70**(4):1067–1116, (1990). 24, 25, 33, 34, 38, 139, 195

[102] Jensen BL and Kurtz A. **Differential regulation of renal cyclooxygenase mRNA by dietary salt intake.** *Kidney International*, **52**(5):1242–1249, (1997). 24, 25, 38, 166

[103] Mellman I, Fuchs R, and Helenius A. **Acidification of the endocytic and exocytic pathways.** *Annual Review of Biochemistry*, **55**(1):663–700, (1986). 25

[104] Ålund M. **Juxtaglomerular cell activity during hemorrhage and ischemia as revealed by quinacrine histofluorescence.** *Acta Physiologica Scandinavica*, **110**(2):113–121, (1980). 25, 37, 134

[105] Mercure C, Jutras I, Day R, Seidah NG, and Reudelhuber TL. **Prohormone convertase PC5 is a candidate processing enzyme for prorenin in the human adrenal cortex.** *Hypertension*, **28**(5):840–846, (1996). 25

[106] Soltesz BM, Gomba Sz, and Szokol M. **Lysosomal enzymes in the juxtaglomerular cell granules.** *Experientia*, **35**(4):533–534, (1979). 25, 38, 196

[107] Neves FAR, Duncan KG, and Baxter JD. **Cathepsin B is a prorenin processing enzyme.** *Hypertension*, **27**(3):514–517, (1996). 25

[108] Mercure C, Lacombe M-J, Khazaie K, and Reudelhuber TL. **Cathepsin B is not the processing enzyme for mouse prorenin.** *American Journal of Physiology-Regulatory, Integrative and Comparative Physiology*, **298**(5):R1212–R1216, (2010). 25

[109] Almeida PC, Oliveira V, Chagas JR, Meldal M, Juliano MA, and Juliano L. **Hydrolysis by cathepsin B of fluorescent peptides derived from human prorenin.** *Hypertension*, **35**(6):1278–1283, (2000). 25

[110] Gross KW, Gomez RA, and Sigmund CD. **Twists and turns in the search for the elusive renin processing enzyme: focus on Cathepsin B is not the processing enzyme for mouse prorenin.** *American Journal of Physiology-Regulatory, Integrative and Comparative Physiology*, **298**(5):R1209–R1211, (2010). 25

[111] Wurfer K, Hackenthal E, Metz R, Nobiling R, Simon Th, and Taugner R. **Interzonal and intrazonal heterogeneities in the renin status of the preglomerular arterioles in five species.** *Histochemistry*, **89**(3):283–287, (1988). 25

[112] Ogawa K, Yamasato M, and Taniguchi K. **Exocytosis of secretory granules in the juxtaglomerular granular cells of kidneys.** *The Anatomical Record*, **243**(3):336–346, (1995). 25, 27, 137, 140, 195, 196, 202

[113] Steppan D, Zügner A, Rachel R, and Kurtz A. **Structural analysis suggests that renin is released by compound exocytosis.** *Kidney International*, **83**(2):233–241, (2012). 25, 27, 38, 69, 136, 195, 196, 201, 202

[114] Clark AF, Sharp MGF, Morley SD, Fleming S, Peters J, and Mullins JJ. **Renin-1 is essential for normal renal juxtaglomerular cell granulation and macula densa morphology.** *Journal of Biological Chemistry*, **272**(29):18185–18190, (1997). 27, 29, 44, 45, 144, 162, 165, 167, 168, 170, 193, 195, 200, 204, 205

[115] Biava CG and West M. **Fine structure of normal human juxtaglomerular cells. II. Specific and nonspecific cytoplasmic granules.** *The American Journal of Pathology*, **49**(5):955–979, (1966). 26, 27, 205

[116] Mullins JJ, Burt DW, Windass JD, McTurk P, George H, and Brammar WJ. **Molecular cloning of two distinct renin genes from the DBA/2 mouse.** *The EMBO Journal*, **1**(11):1461, (1982). 28

[117] Dickinson DP, Gross KW, Piccini N, and Wilson CM. **Evolution and variation of renin genes in mice.** *Genetics*, **108**(3):651–667, (1984). 28

[118] Abel KJ and Gross KW. **Physical characterization of genetic rearrangements at the mouse renin loci.** *Genetics*, **124**(4):937–947, (1990). 29

[119] Sharp MGF, Fettes D, Brooker G, Clark AF, Peters J, Fleming S, and Mullins JJ. **Targeted inactivation of the Ren-2 gene in mice.** *Hypertension*, **28**(6):1126–1131, (1996). 29

[120] Mullins LJ, Payne CM, Kotelevtseva N, Brooker G, Fleming S, Harris S, and Mullins JJ. **Granulation rescue and developmental marking of juxtaglomerular cells using Piggy-BAC recombination of the mouse Ren locus.** *Journal of Biological Chemistry*, **275**(51):40378–40384, (2000). 30, 165, 170, 195

[121] V Rothwell, Kosowski S, Hadjilambris O, Baska R, and Norman J. **Glycosylation of active human renin is necessary for secretion: effect of targeted modifications of Asn-5 and Asn-75.** *DNA and Cell Biology*, **12**(4):291–298, (1993). 30

[122] WJ Oliver and F Gross. **Unique specificity of mouse angiotensinogen to homologous renin.** *Experimental Biology and Medicine*, **122**(3):923–926, (1966). 31, 171, 192, 198

[123] Yan Y, Chen R, Pitarresi T, Sigmund CD, Gross KW, Sealey JE, Laragh JH, and Catanzaro DF. **Kidney is the only source of human plasma renin in 45-kb human renin transgenic mice.** *Circulation Research*, **83**(12):1279–1288, (1998). 31, 171, 192

[124] Raza S, McDerment N, Lacaze PA, Robertson K, Watterson S, Chen Y, Chisholm M, Eleftheriadis G, Monk S, O'Sullivan M, Turnbull A, Roy D, Theocharidis A, Ghazal P, and Freeman TC. **Construction of a large scale integrated map of macrophage pathogen recognition and effector systems.** *BMC Systems Biology*, **4**(1):63, (2010). 32

[125] Freeman TC and Ghazal P Raza S, Theocharidis A. **The mEPN scheme: an intuitive and flexible graphical system for rendering biological pathways.** *BMC Systems Biology*, **4**(65):1–16, (2010). 32

[126] Hautmann M, Friis UG, Desch M, Todorov V, Castrop H, Segerer F, Otto C, Schütz G, and Schweda F. **Pituitary adenylate cyclase–activating polypeptide stimulates renin secretion via activation of PAC1 receptors.** *Journal of the American Society of Nephrology*, **18**(4):1150–1156, (2007). 33

[127] Holmer SR, Kaissling B, Putnik K, Pfeifer M, Krämer BK, Riegger GAJ, and Kurtz A. **Beta-adrenergic stimulation of renin expression in vivo.** *Journal of Hypertension*, **15**(12):1471–1479, (1997). 33

[128] Vandongen R, Peart WS, and Boyd GW. **Adrenergic stimulation of renin secretion in the isolated perfused rat kidney.** *Circulation Research*, **32**(2):290–296, (1973). 33, 161

[129] Weinberger MH, Aoi W, and Henry DP. **Direct effect of beta-adrenergic stimulation on renin release by the rat kidney slice in vitro.** *Circulation Research*, **37**(3):318–324, (1975). 33, 161

[130] Kim SM, Chen L, Faulhaber-Walter R, Oppermann M, Huang Y, Mizel D, Briggs JP, and Schnermann J. **Regulation of renin secretion and expression in mice deficient in β1-and β2-adrenergic receptors.** *Hypertension*, **50**(1):103–109, (2007). 33

[131] Cooper D. **Regulation and organization of adenylyl cyclases and cAMP.** *Journal of Biochemistry*, **375**:517–529, (2003). 33, 34

[132] Aldehni F, Tang T, Madsen K, Plattner M, Schreiber A, Friis UG, Hammond HK, Han PL, and Schweda F. **Stimulation of renin secretion by catecholamines is dependent on adenylyl cyclases 5 and 6.** *Hypertension*, **57**(3):460–468, (2011). 33, 134, 135

[133] Kurtz A, Bruna RD, Pratz J, and Cavero I. **Rat juxtaglomerular cells are endowed with DA-1 dopamine receptors mediating renin release.** *Journal of Cardiovascular Pharmacology*, **12**(6):658–663, (1988). 33

[134] Sunahara RK, Guan H-C, O'Dowd BF, Seeman P, Laurier LG, Ng G, George SR, Torchia J, Van Tol HHM, and Niznik HB. **Cloning of the gene for a human dopamine D5 receptor with higher affinity for dopamine than D1.** *Nature*, **350**(6319):614–619, (1991). 33

[135] Yamaguchi I, Yao L, Sanada H, Ozono R, Mouradian MM, Jose PA, Carey RM, and Felder RA. **Dopamine D1A receptors and renin release in rat juxtaglomerular cells.** *Hypertension*, **29**(4):962–968, (1997). 33

[136] Pan L, Black TA, Shi Q, Jones CA, Petrovic N, Loudon J, Kane C, Sigmund CD, and Gross KW. **Critical roles of a cyclic AMP responsive element and an E-box in regulation of mouse renin gene expression.** *Journal of Biological Chemistry*, **276**(49):45530–45538, (2001). 34

[137] Klar J, Sandner P, Müller MW, and Kurtz A. **Cyclic AMP stimulates renin gene transcription in juxtaglomerular cells.** *Pflügers Archiv*, **444**(3):335–344, (2002). 34, 107

[138] Asico LD, Ladines C, Fuchs S, Accili D, Carey RM, Semeraro C, Pocchiari F, Felder RA, Eisner GM, and Jose PA. **Disruption of the dopamine D3 receptor gene produces renin-dependent hypertension.** *Journal of Clinical Investigation*, **102**(3):493–498, (1998). 34

[139] Ortiz-Capisano MC, Atchison DK, Harding P, Lasley RD, and Beierwaltes WH. **Adenosine inhibits renin release from juxtaglomerular cells via an A1 receptor-TRPC-mediated pathway.** *American Journal of Physiology-Renal Physiology*, **305**(8):F1209–F1219, (2013). 34

[140] Burgoyne RD and Morgan A. **Secretory granule exocytosis.** *Physiological Reviews*, **83**(2):581–632, (2003). 34, 36, 39, 40, 202

[141] Grünberger C, Obermayer B, Klar J, Kurtz A, and Schweda F. **The calcium paradoxon of renin release calcium suppresses renin exocytosis by inhibition of calcium-dependent adenylate cyclases AC5 and AC6.** *Circulation Research*, **99**(11):1197–1206, (2006). 35, 107, 135

[142] Ortiz-Capisano MC, Reddy M, Mendez M, Garvin JL, and Beierwaltes WH. **Juxtaglomerular cell CaSR stimulation decreases renin release via activation of**

the PLC/IP3 pathway and the ryanodine receptor. *American Journal of Physiology-Renal Physiology*, **304**(3):F248–F256, (2013). 35

[143] Kurtz A, Pfeilschifter J, Hutter A, Buhrle C, Nobiling R, Taugner R, Hackenthal E, and Bauer C. **Role of protein kinase C in inhibition of renin release caused by vasoconstrictors.** *American Journal of Physiology-Cell Physiology*, **250**(4):C563–C571, (1986). 35

[144] Della Bruna R, Pinet F, Corvol P, and Kurtz A. **Calmodulin antagonists stimulate renin secretion and inhibit renin synthesis in vitro.** *American Journal of Physiology*, **262**(3):F397–F402, (1992). 35, 40, 106

[145] Madsen K, Friis UG, Gooch JL, Hansen PB, Holmgaard L, Skøtt O, and Jensen BL. **Inhibition of calcineurin phosphatase promotes exocytosis of renin from juxtaglomerular cells.** *Kidney International*, **77**(2):110–117, (2010). 35, 40

[146] Shoback DM, Thatcher J, Leombruno R, and Brown EM. **Relationship between parathyroid hormone secretion and cytosolic calcium concentration in dispersed bovine parathyroid cells.** *Proceedings of the National Academy of Sciences*, **81**(10):3113–3117, (1984). 36

[147] Fuchs S, Philippe J, Corvol P, and Pinet F. **Implication of Ref-1 in the repression of renin gene transcription by intracellular calcium.** *Journal of hypertension*, **21**(2):327–335, (2003). 36

[148] Dousa TP. **Cyclic-3, 5-nucleotide phosphodiesterase isozymes in cell biology and pathophysiology of the kidney.** *Kidney International*, **55**(1):29–62, (1999). 36

[149] Chiu N, Park I, and Reid IA. **Stimulation of renin secretion by the phosphodiesterase IV inhibitor rolipram.** *Journal of Pharmacology and Experimental Therapeutics*, **276**(3):1073–1077, (1996). 36

[150] Kurtz A, Götz K-H, Hamann M, and Wagner C. **Stimulation of renin secretion by nitric oxide is mediated by phosphodiesterase 3.** *Proceedings of the National Academy of Sciences*, **95**(8):4743–4747, (1998). 36

[151] Chiu YJ, Hu S-H, and Reid IA. **Inhibition of phosphodiesterase III with milrinone increases renin secretion in human subjects.** *Journal of Pharmacology and Experimental Therapeutics*, **290**(1):16–19, (1999). 36

[152] Ortiz-Capisano MC, Liao T-D, Ortiz PA, and Beierwaltes WH. **Calcium-dependent phosphodiesterase 1C inhibits renin release from isolated juxtaglomerular cells.** *American Journal of Physiology-Regulatory, Integrative and Comparative Physiology*, **297**(5):R1469–R1476, (2009). 36

[153] Taugner R, Bührle CP, and Nobiling R. **Ultrastructural changes associated with renin secretion from the juxtaglomerular apparatus of mice.** *Cell and Tissue Research*, **237**(3):459–472, (1984). 37, 38, 195, 201, 202

[154] Skøtt O. **Episodic release of renin from single isolated superfused rat afferent arterioles.** *Pflügers Archiv*, **407**(1):41–45, (1986). 37

[155] Friis UG, Jensen BL, Aas JK, and Skøtt O. **Direct demonstration of exocytosis and endocytosis in single mouse juxtaglomerular cells.** *Circulation Research*, **84**(8):929–936, (1999). 37, 135, 137

[156] Chow RH, Klingauf J, Heinemann C, Zucker RS, and Neher E. **Mechanisms determining the time course of secretion in neuroendocrine cells.** *Neuron*, **16**(2):369–376, (1996). 38

[157] Peter S. **Ultrastructural studies on the secretory process in the epithelioid cells of the juxtaglomerular apparatus.** *Cell and Tissue Research*, **168**(1):45–53, (1976). 38

[158] Toonen RF, Kochubey O, de Wit H, Gulyas-Kovacs A, Konijnenburg B, Sørensen JB, Klingauf J, and Verhage M. **Dissecting docking and tethering of secretory vesicles at the target membrane.** *The EMBO Journal*, **25**(16):3725–3737, (2006). 39

[159] McNew JA, Parlati F, Fukuda R, Johnston RJ, Paz K, Paumet F, Söllner TH, and Rothman JE. **Compartmental specificity of cellular membrane fusion encoded in SNARE proteins.** *Nature*, **407**(6801):153–159, (2000). 39

[160] Mendez M and Gaisano HY. **Role of the SNARE protein SNAP23 on cAMP-stimulated renin release in mouse juxtaglomerular cells.** *American Journal of Physiology-Renal Physiology*, **304**(5):F498–F504, (2013). 39, 107

[161] Nagy G, Reim K, Matti U, Brose N, Binz T, Rettig J, Neher E, and Sørensen JB. **Regulation of releasable vesicle pool sizes by protein kinase A-dependent phosphorylation of SNAP-25.** *Neuron*, **41**(3):417–429, (2004). 40

[162] Hepp R, Puri N, Hohenstein AC, Crawford GL, Whiteheart SW, and Roche PA. **Phosphorylation of SNAP-23 regulates exocytosis from mast cells.** *Journal of Biological Chemistry*, **280**(8):6610–6620, (2005). 40

[163] Glenn ST, Jones CA, Pan L, and Gross KW. **In vivo analysis of key elements within the renin regulatory region.** *Physiological Genomics*, **35**(3):243–253, (2008). 43, 44

[164] Wilson CM, Erdös EG, Wilson JD, and Taylor BA. **Location on chromosome 1 of Rnr, a gene that regulates renin in the submaxillary gland of the mouse.** *Proceedings of the National Academy of Sciences*, **75**(11):5623–5626, (1978). 45

[165] Huerta-Ocampo I, Christian HC, Thompson NM, El-Kasti MM, and Wells T. **The 'intermediate' lactotroph: a morphologically distinct, ghrelin-responsive pituitary cell in the dwarf (dw/dw) rat.** *Endocrinology*, **146**(11):5012–5023, (2005). 70

[166] Abel MH, Charlton HM, Huhtaniemi I, Pakarinen P, Kumar TR, and Christian HC. **An investigation into pituitary gonadotrophic hormone synthesis, secretion, subunit gene expression and cell structure in normal and mutant male mice.** *Journal of Neuroendocrinology*, **25**(10):863–875, (2013). 70

[167] Lipp P and Niggli E. **Ratiometric confocal Ca^{2+} measurements with visible wavelength indicators in isolated cardiac myocytes.** *Cell Calcium*, **14**(5):359–372, (1993). 77

[168] Peti-Peterdi J and Bell PD. **Cytosolic Ca^{2+} signaling pathway in macula densa cells.** *American Journal of Physiology-Renal Physiology*, **277**(3):F472–F476, (1999). 77, 164

[169] Peti-Peterdi J, Bebok Z, Lapointe J-Y, and Bell PD. **Novel regulation of cell Na^+ in macula densa cells: apical Na^+ recycling by HK-ATPase.** *American Journal of Physiology-Renal Physiology*, **282**(2):F324–F329, (2002). 77

[170] Della Bruna R, Pinet F, Corvol P, and Kurtz A. **Regulation of renin secretion and renin synthesis by second messengers in isolated mouse juxtaglomerular cells.** *Cellular Physiology and Biochemistry*, **1**(2):98–110, (1991). 89

[171] Tai G, Hohenstein P, and Davies JA. **Making immortalized cell lines from embryonic mouse kidney.** *Kidney Development*, pages 165–171, (2012). 103, 104, 108, 112

[172] Della Bruna R, Pinet F, Corvol P, and Kurtz A. **Regulation of renin secretion and renin synthesis by second messengers in isolated mouse juxtaglomerular cells.** *Cellular Physiology and Biochemistry*, **1**(2):98–110, (1991). 106

[173] Ortiz-Capisano MC, Ortiz PA, Harding P, Garvin JL, and Beierwaltes WH. **Decreased intracellular calcium stimulates renin release via calcium-inhibitable adenylyl cyclase.** *Hypertension*, **49**(1):162–169, (2007). 106

[174] Ortiz-Capisano MC, Ortiz PA, Garvin JL, Harding P, and Beierwaltes WH. **Expression and function of the calcium-sensing receptor in juxtaglomerular cells.** *Hypertension*, **50**(4):737–743, (2007). 106

[175] Blanc-Brunat N, Mutin M, and Peyrol S. **Immunohistochemical localization of type IV collagen fibronectin and laminin in the juxtaglomerular apparatus of the rat kidney.** *Cellular and Molecular Biology*, **35**(4):469–484, (1988). 107

[176] Churchill PC and Churchill MC. **Isoproterenol-stimulated renin secretion in the rat: second messenger roles of Ca and cyclic AMP.** *Life Sciences*, **30**(15):1313–1319, (1982). 107, 134

[177] Della Bruna R, Kurtz A, Corvol P, and Pinet F. **Renin mRNA quantification using polymerase chain reaction in cultured juxtaglomerular cells. Short-term effects of cAMP on renin mRNA and secretion.** *Circulation Research*, **73**(4):639–648, (1993). 107

[178] Castrop H, Höcherl K, Kurtz A, Schweda F, Todorov V, and Wagner C. **Physiology of kidney renin.** *Physiological Reviews*, **90**(2):607–673, (2010). 108, 110, 137

[179] Jikihara H, Poisner AM, and Handwerger S. **Interferon-γ inhibits the synthesis and release of renin from human decidual cells.** *Biology of Reproduction*, **54**(6):1311–1316, (1996). 110

[180] Kaneko K, Nishiyama H, Ohba K, Shibasaki A, Hirose T, Totsune, Furuyama K, and Takahashi K. **Expression of (pro) renin receptor in human erythroid cell lines and its increased protein accumulation by interferon-γ.** *Peptides*, **37**(2):285–289, (2012). 110

[181] Navis AR. **Hanging Drop Tissue Culture**. *Embryo Project Encyclopedia*, 2012. 111

[182] Axelrod D. **Cell-substrate contacts illuminated by total internal reflection fluorescence.** *The Journal of Cell Biology*, **89**(1):141–145, (1981). 113

[183] Steyer JA and Almers W. **A real-time view of life within 100 nm of the plasma membrane.** *Nature Reviews Molecular Cell Biology*, **2**(4):268–275, (2001). 114

[184] Casellas D, Dupont M, Kaskel FJ, Inagami T, and Moore LC. **Direct visualization of renin-cell distribution in preglomerular vascular trees dissected from rat kidney.** *American Journal of Physiology*, **265**(1):F151–F151, (1993). 134

[185] Peti-Peterdi J. **Multiphoton imaging of renal tissues in vitro.** *American Journal of Physiology-Renal Physiology*, **288**(6):F1079–F1083, (2005). 134

[186] Vargas SL, Toma I, Kang JJ, Meer EJ, and Peti-Peterdi J. **Activation of the succinate receptor GPR91 in macula densa cells causes renin release.** *Journal of the American Society of Nephrology*, **20**(5):1002–1011, (2009). 134

[187] Duncan RR, Greaves J, Wiegand UK, Matskevich I, Bodammer G, Apps DK, Shipston MJ, and Chow RH. **Functional and spatial segregation of secretory vesicle pools according to vesicle age.** *Nature*, **422**(6928):176–180, (2003). 134

[188] Schweda F, Klar J, Narumiya S, Nüsing RM, and Kurtz A. **Stimulation of renin release by prostaglandin E2 is mediated by EP2 and EP4 receptors in mouse kidneys.** *American Journal of Physiology-Renal Physiology*, **287**(3):F427–F433, (2004). 135

[189] Kurt B, Karger C, Wagner C, and Kurtz A. **Control of renin secretion from kidneys with renin cell hyperplasia.** *American Journal of Physiology-Renal Physiology*, **306**(3):F327–F332, (2014). 135

[190] Skøtt O and Taugner R. **Effects of extracellular osmolality on renin release and on the ultrastructure of the juxtaglomerular epithelioid cell granules.** *Cell and tissue research*, **249**(2):325–329, (1987). 135

[191] Ravier MA, Tsuboi T, and Rutter GA. **Imaging a target of Ca^{2+} signalling: Dense core granule exocytosis viewed by total internal reflection fluorescence microscopy**. *Methods*, **46**(3):233–238, (2008). 136

[192] Allersma MW, Bittner MA, Axelrod D, and Holz RW. **Motion matters: secretory granule motion adjacent to the plasma membrane and exocytosis.** *Molecular Biology of the Cell*, **17**(5):2424–2438, (2006). 136, 142, 143

[193] Rasch R, Jensen BL, Nyengaard JR, and Skøtt O. **Quantitative changes in rat renin secretory granules after acute and chronic stimulation of the renin system.** *Cell and Tissue Research*, **292**(3):563–571, (1998). 136, 165, 195

[194] Blank U. **The mechanisms of exocytosis in mast cells.** *Mast Cell Biology: Contemporary and Emerging Topics*, pages 107–122, (2011). 137

[195] Liu D, Meckel T, and Long EO. **Distinct role of rab27a in granule movement at the plasma membrane and in the cytosol of NK cells.** *PLoS One*, **5**(9):e12870–e12870, (2010). 139

[196] Johnson JL, Monfregola J, Napolitano G, Kiosses WB, and Catz SD. **Vesicular trafficking through cortical actin during exocytosis is regulated by the Rab27a effector JFC1/Slp1 and the RhoA-GTPase–activating protein Gem-interacting protein.** *Molecular Biology of the Cell*, **23**(10):1902–1916, (2012). 139

[197] Kapitein LC, van Bergeijk P, Lipka J, Keijzer N, Wulf PS, Katrukha EA, Akhmanova A, and Hoogenraad CC. **Myosin-V opposes microtubule-based cargo transport and drives directional motility on cortical actin.** *Current Biology*, **23**(9):828–834, (2013). 140, 142

[198] Mattila PK and Lappalainen P. **Filopodia: molecular architecture and cellular functions.** *Nature Reviews Molecular Cell Biology*, **9**(6):446–454, (2008). 140

[199] Pollard TD and Korn ED. **Acanthamoeba myosin I. Isolation from Acanthamoeba castellanii of an enzyme similar to muscle myosin.** *Journal of Biological Chemistry*, **248**(13):4682–4690, (1973). 141

[200] Dicou E and Brachet P. **Precursors of the nerve growth factor gamma subunit and renin bind to microtubules.** *European Journal of Biochemistry*, **143**(2):381–387, (1984). 141

[201] Toffelmire EB, Slater K, Corvol P, Menard J, and Schambelan M. **Response of plasma prorenin and active renin to chronic and acute alterations of renin secretion in normal humans. Studies using a direct immunoradiometric assay.** *Journal of Clinical Investigation*, **83**(2):679–687, (1989). 141, 193

[202] Aschenbrenner L, Naccache SN, and Hasson T. **Uncoated endocytic vesicles require the unconventional myosin, Myo6, for rapid transport through actin barriers.** *Molecular Biology of the Cell*, **15**(5):2253–2263, (2004). 141

[203] Caspi A, Granek R, and Elbaum M. **Diffusion and directed motion in cellular transport.** *Physical Review E*, **66**(1):011916, (2002). 142

[204] Toba S, Watanabe TM, Yamaguchi-Okimoto L, Toyoshima YY, and Higuchi H. **Overlapping hand-over-hand**

mechanism of single molecular motility of cytoplasmic dynein. *Proceedings of the National Academy of Sciences*, **103**(15):5741–5745, (2006). 142

[205] Svoboda K and Block SM. **Force and velocity measured for single kinesin molecules.** *Cell*, **77**(5):773–784, (1994). 142

[206] Ng Y-K, Lu X, Gulacsi A, Han W, Saxton MJ, and Levitan ES. **Unexpected mobility variation among individual secretory vesicles produces an apparent refractory neuropeptide pool.** *Biophysical Journal*, **84**(6):4127–4134, (2003). 142

[207] Huet S, Karatekin E, Tran VS, Fanget I, Cribier S, and Henry J-P. **Analysis of transient behavior in complex trajectories: application to secretory vesicle dynamics.** *Biophysical Journal*, **91**(9):3542–3559, (2006). 143

[208] Laamarti MA and Lapointe J-Y. **Determination of NH_4^+/NH_3 fluxes across apical membrane of macula densa cells: a quantitative analysis.** *American Journal of Physiology-Renal Physiology*, **273**(5):F817–F824, (1997). 145

[209] Schnermann J, Ploth DW, and Hermle M. **Activation of tubulo-glomerular feedback by chloride transport.** *Pflügers Archive*, **362**(3):229–240, (1976). 145

[210] Wolf K, Castrop H, Hartner A, Goppelt-Strübe M, Hilgers KF, and Kurtz A. **Inhibition of the renin-angiotensin system upregulates cyclooxygenase-2 expression in the macula densa.** *Hypertension*, **34**(3):503–507, (1999). 145, 166

[211] Grönhagen-Riska C. **Effects of ACE inhibition on renal regulation of salt and water.** *Acta Medica Scandinavica*, **219**(S707):95–99, (1986). 145

[212] Peti-Peterdi J, Kidokoro K, and Riquier-Brison A. **Novel in vivo techniques to visualize kidney anatomy and function**. *Kidney International*, (2015). 161

[213] Ucero AC, Benito-Martin A, Izquierdo MC, Sanchez-Niño MD, Sanz AB, Ramos AM, Berzal S, Ruiz-Ortega M, Egido J, and Ortiz A. **Unilateral ureteral obstruction: beyond obstruction**. *International Urology and Nephrology*, **46**(4):765–776, (2014). 161

[214] Leybaert, Sneyd J, and Sanderson MJ. **A simple method for high temporal resolution calcium imaging with dual excitation dyes.** *Biophysical Journal*, **75**(4):2025–2029, (1998). 162

[215] Lattarulo C, Thyssen D, Kuchibholta KV, Hyman BT, and Bacskaig BJ. **Microscopic imaging of intracellular calcium in live cells using lifetime-based ratiometric measurements of Oregon Green BAPTA-1.** *Methods in Molecular Biology*, pages 377–389, (2011). 162

[216] Moore LC, Casellas D, Persson AE, Müller-Suur R, and Morsing P. **Renal hemodynamic regulation by the renin-secreting segment of the afferent arteriole.** *Kidney International. Supplement*, **30**:S65–8, (1990). 162

[217] Taugner R, Schiller A, Kaissling B, and Kriz W. **Gap junctional coupling between the JGA and the glomerular tuft.** *Cell and Tissue Research*, **186**(2):279–285, (1978). 162

[218] Xiong J, Wang Y, Zhu Z, Liu J, Wang Y, Zhang C, Hammes H-P, Lang F, and Feng Y. **NG2 proteoglycan increases mesangial cell proliferation and extracellular matrix production.** *Biochemical and Biophysical Research Communications*, **361**(4):960–967, (2007). 163

[219] Bell PD, Komlosi P, and Zhang Z-R. **ATP as a mediator of macula densa cell signalling.** *Purinergic Signalling*, **5**(4):461–471, (2009). 164

[220] Seidel S, Neymeyer H, Kahl T, Roeschel T, Mutig K, Flower R, Schnermann J, and Bachmann Sand Paliege A. **Annexin A1 modulates macula densa function by inhibiting cyclooxygenase 2.** *American Journal of Physiology-Renal Physiology*, **303**(6):F845–F854, (2012). 164

[221] Salomonsson M, Gonzalez E, Westerlund P, and Persson AEG. **Intracellular cytosolic free calcium concentration in the macula densa and in ascending limb cells at different luminal concentrations of sodium chloride and with added furosemide.** *Acta Physiologica Scandinavica*, **142**(2):283–290, (1991). 164

[222] Gunter TE, Yule DI, Gunter KK, Eliseev RA, and Salter JD. **Calcium and mitochondria.** *FEBS letters*, **567**(1):96–102, (2004). 164

[223] Harris RC, Zhang M-Z, and Cheng H-F. **Cyclooxygenase-2 and the renal renin–angiotensin system.** *Acta Physiologica Scandinavica*, **181**(4):543–547, (2004). 165

[224] Schnermann J. **Cyclooxygenase-2 and macula densa control of renin secretion.** *Nephrology Dialysis Transplantation*, **16**(9):1735–1738, (2001). 165

[225] Crofford LJ. **COX-1 and COX-2 tissue expression: implications and predictions.** *The Journal of Rheumatology. Supplement*, **49**:15–19, (1997). 165

[226] Harris RC and Breyer MD. **Physiological regulation of cyclooxygenase-2 in the kidney.** *American Journal of Physiology-Renal Physiology*, **281**(1):F1–F11, (2001). 165

[227] Harris RC, McKanna JA, Akai Y, Jacobson HR, Dubois RN, and Breyer MD. **Cyclooxygenase-2 is associated with the macula densa of rat kidney and increases with salt restriction.** *Journal of Clinical Investigation*, **94**(6):543–547, (1994). 166

[228] Burford J, Villanueva K, Riquier-Brison A, Kumar S, Liu J, McMahon A, and Peti-Peterdi J. **The macula densa controls glomerular remodelling.** *American Society of Nephrology, Annual Meeting*, (2013). 166

[229] Razga Z and Nyengaard JR. **The effect of angiotensin II on the number of macula densa cells through the AT1 receptor.** *Nephron Physiology*, **112**(2):p37–p43, (2009). 167, 168, 205

[230] Castrop H, Schweda F, Schumacher K, Wolf K, and Kurtz A. **Role of renocortical cyclooxygenase-2 for renal vascular resistance and macula densa control of renin secretion.** *Journal of the American Society of Nephrology*, **12**(5):867–874, (2001). 167

[231] Castrop H, Klar J, Wagner C, Höcherl K, and Kurtz A. **General inhibition of renocortical cyclooxygenase-2 expression by the renin-angiotensin system.** *American Journal of Physiology-Renal Physiology*, **284**(3):F518–F524, (2003). 167

[232] Scholzen T and Gerdes J. **The Ki-67 protein: from the known and the unknown.** *Journal of Cellular Physiology*, **182**(3):311–322, (2000). 168

[233] Dr. Robert Nelson. **Doctoral Thesis: Complementation of the mouse Ren1-^{d} knockout with human renin**. *University of Edinburgh*, (2003). 171, 194, 197, 198, 204

[234] Sigmund CD, Jones CA, Kane CM, Wu C, Lang JA, and Gross KW. **Regulated tissue-and cell-specific expression of the human renin gene in transgenic mice.** *Circulation Research*, **70**(5):1070–1079, (1992). 192, 198

[235] Yan Y, Hu L, Chen R, Sealey JE, Laragh JH, and Catanzaro DF. **Appropriate regulation of human renin gene expression and secretion in 45-kb human renin transgenic mice.** *Hypertension*, **32**(2):205–214, (1998). 192, 193, 194

[236] Goldstone R, Horton R, Carlson EJ, and Hsueh WA. **Reciprocal Changes in Active and Inactive Renin after Converting Enzyme Inhibition in Normal Man.** *The Journal of Clinical Endocrinology & Metabolism*, **56**(2):264–268, (1983). 193

[237] Bing J, Poulsen K, Hackenthal E, Rix E, and Taugner R. **Renin in the submaxillary gland: a review.** *Journal of Histochemistry & Cytochemistry*, **28**(8):874–880, (1980). 193

[238] Morris JF and Pow DV. **Capturing and quantifying the exocytotic event.** *Journal of Experimental Biology*, **139**(1):81–103, (1988). 195

[239] Berka JLA, Alcorn D, Coghlan JP, Fernley RT, Morgan TO, Ryan GB, Skinner SL, and Weaver DA. **Granular juxtaglomerular cells and prorenin synthesis in mice treated with enalapril.** *Journal of Hypertension*, **8**(3):229–238, (1990). 196

[240] Ren Y, Liu R, Carretero OA, and Garvin JL. **Increased intracellular Ca^{++} in the macula densa regulates tubuloglomerular feedback.** *Kidney International*, **64**(4):1348–1355, (2003). 198

[241] Liu R and Persson AEG. **Simultaneous changes of cell volume and cytosolic calcium concentration in macula densa cells caused by alterations of luminal NaCl concentration.** *The Journal of Physiology*, **563**(3):895–901, (2005). 198

[242] Fukamizu A, Sugimura Kand Takimoto E, Sugiyama F, Seo M-S, Takahashi S, Hatae T, Kajiwara N, Yagami K-I, and Murakami K. **Chimeric renin-angiotensin system demonstrates sustained increase in blood pressure of transgenic mice carrying both human renin and human angiotensinogen genes.** *Journal of Biological Chemistry*, **268**(16):11617–11621, (1993). 198

[243] Park CS, Sigmon DH, Han DS, Honeyman TW, and Fray JC. **Control of renin secretion by Ca^{2+} and cyclic AMP through two parallel mechanisms.** *American Journal of Physiology-Regulatory, Integrative and Comparative Physiology*, **251**(3):R531–R536, (1986). 202

[244] Plattner H. **Regulation of membrane fusion during exocytosis.** *International Review of Cytology*, **119**:197–286, (1990). 202

[245] Brown MJ. **Renin: friend or foe?** *Heart*, **93**(9):1026–1033, (2007). 204

[246] Persson PB. **Renin: origin, secretion and synthesis.** *The Journal of Physiology*, **552**(3):667–671, (2003). 204

[247] Azizi M, Guyene T-T, Chatellier G, Wargon M, and Ménard J. **Additive effects of losartan and enalapril on blood pressure and plasma active renin.** *Hypertension*, **29**(2):634–640, (1997). 204

[248] Mann B, Hartner A, Jensen BL, Kammerl M, Krämer BK, and Kurtz A. **Furosemide stimulates macula densa cyclooxygenase-2 expression in rats.** *Kidney International*, **59**(1):62–68, (2001). 204

[249] Dickerson JEC, Hingorani AD, Ashby MJ, Palmer CR, and Brown MJ. **Optimisation of antihypertensive treatment by crossover rotation of four major classes.** *The Lancet*, **353**(9169):2008–2013, (1999). 204

[250] Christensen JA, Bader H, Bohle A, and Meyer DS. **The structure of the juxtaglomerular apparatus in Addison's disease, Bartter's syndrome, and in Conn's syndrome.** *Virchows Archive A*, **370**(2):103–112, (1976). 204

[251] Schnermann JB, Traynor T, Yang T, Huang YG, Oliverio MI, Coffman T, and Briggs JP. **Absence of tubuloglomerular feedback responses in AT1A receptor-deficient mice.** *American Journal of Physiology-Renal Physiology*, **273**(2):F315–F320, (1997). 205

[252] Yao J, Oite T, and Kitamura M. **Gap junctional intercellular communication in the juxtaglomerular apparatus.** *American Journal of Physiology-Renal Physiology*, **296**(5):F939–F946, (2009). 205

[253] Tojo A, Onozato ML, and Fujita T. **Role of macula densa neuronal nitric oxide synthase in renal diseases.** *Medical Molecular Morphology*, **39**(1):2–7, (2006). 209

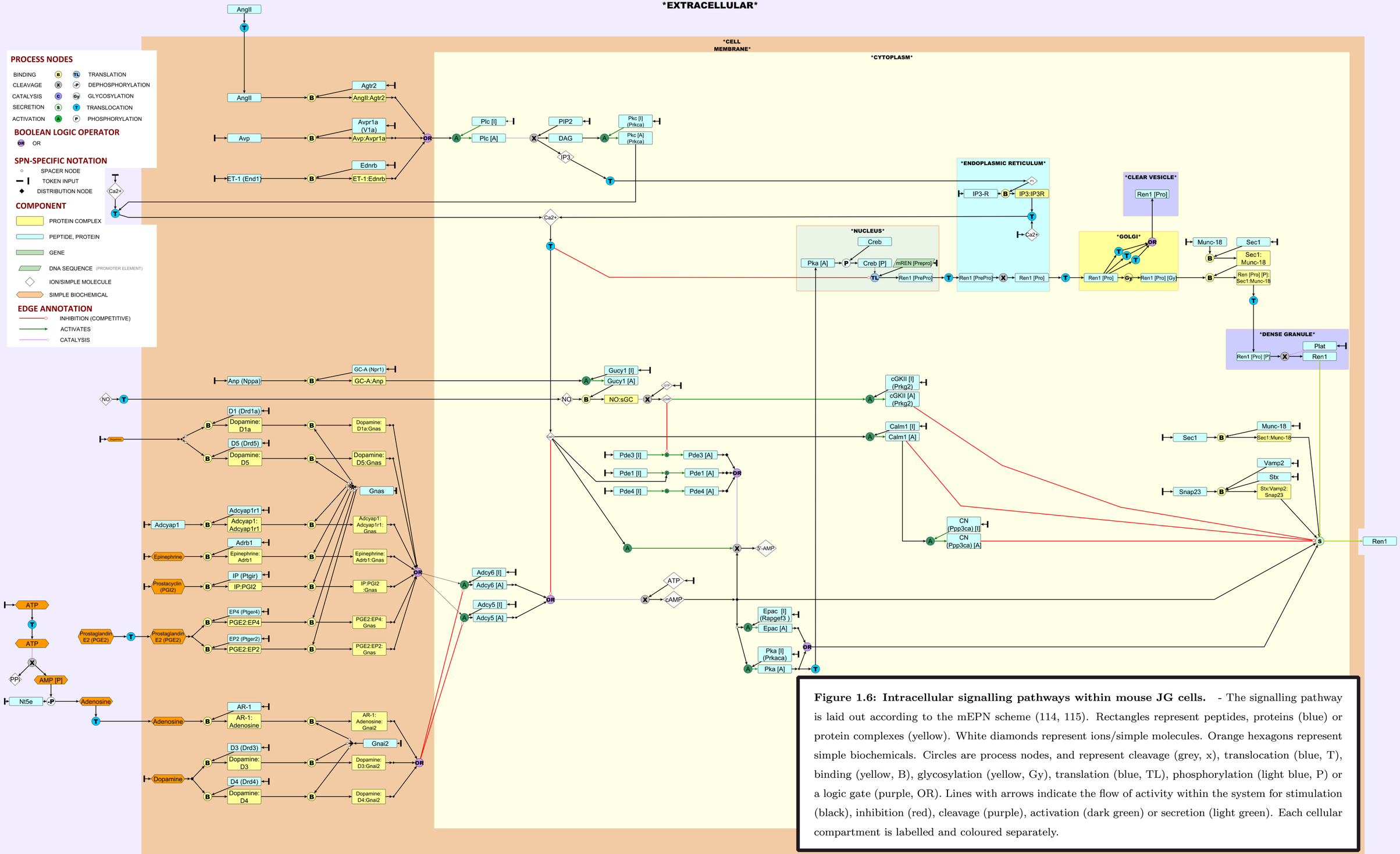

Figure 1.6: Intracellular signalling pathways within mouse JG cells. - The signalling pathway is laid out according to the mEPN scheme (114, 115). Rectangles represent peptides, proteins (blue) or protein complexes (yellow). White diamonds represent ions/simple molecules. Orange hexagons represent simple biochemicals. Circles are process nodes, and represent cleavage (grey, x), translocation (blue, T), binding (yellow, B), glycosylation (yellow, Gy), translation (blue, TL), phosphorylation (light blue, P) or a logic gate (purple, OR). Lines with arrows indicate the flow of activity within the system for stimulation (black), inhibition (red), cleavage (purple), activation (dark green) or secretion (light green). Each cellular compartment is labelled and coloured separately.